UNIVERSITY OF CALIFORNIA, SAN DIEGO

Electron Transport, Energy Transfer, and Optical Response in Single Molecule Junctions

A dissertation submitted in partial satisfaction of the
requirements for the degree
Doctor of Philosophy

in

Chemistry

by

Alexander James White

Committee in charge:

Professor Michael Galperin, Chair
Professor Henry Abarbanel
Professor Francesco Paesani
Professor William Trogler
Professor John Weare

2014

The dissertation of Alexander James White is approved, and it is acceptable in quality and form for publication on microfilm and electronically:

_____

_____

_____

_____

_____

Chair

University of California, San Diego

2014

DEDICATION

To All my Family and Friends

TABLE OF CONTENTS

LIST OF FIGURES

LIST OF TABLES

ACKNOWLEDGEMENTS

I would like to acknowledge Prof. Misha Galperin for his support as my Ph.D. advisor. Thank you for giving me the opportunity to work with you and for sharing your expertise.

I would like to thank those with whom I have collaborated on this work: Prof. Abraham Nitzan, Prof. Boris Fainberg, Dr. Agostino Migliore, Prof. Maxim Sukharev, Prof. Uri Peskin, and Dr. Sergei Tretiak.

Chapter 2, in full, is a reprint of the material as it appears in Physical Chemistry Chemical Physics 2012. White, Alexander J.; Galperin, Michael, The Owner Societies 2012. The dissertation author was the primary investigator and author of the paper.

Chapter 3, in full, is a reprint of the material as it appears in The Journal of Chemical Physics 2013. White, Alexander J.; Migliore, Agostino; Galperin, Michael; and Nitzam, Abraham, AIP Publishing LLC 2013. The dissertation author was the primary investigator and author of the paper.

Chapter 4, in full, is a reprint of the material as it appears in Physical Review B 2013. White, Alexander J.; Psekin, Uri; Galperin, Michael, American Physical Society 2013. The dissertation author was the primary investigator and author of the paper.

Chapter 5, in full, is a reprint of the material as it appears in Physical Review B 2012. White, Alexander J.; Sukharev, Maxim; Galperin, Michael, American Physical Society 2012. The dissertation author was the primary investigator and author of the paper.

Chapter 6, in full, is a reprint of the material as it appears in The Journal of Physical Chemistry Letters 2012. White, Alexander J.; Fainberg, Boris D.; Galperin, Michael, American Chemical Society 2012. The dissertation author was the primary investigator and author of the paper.

Chapter 7, in full, is a reprint of the material as it appears in Nano Letters, 2014. White, Alexander J.; Tretiak, Sergei; Galperin, Michael, American Chemical Society 2014. The dissertation author was the primary investigator and author of the paper.

VITA

2008	Bachelor of Science in Chemistry, California Polytechnic State University, San Luis Obispo
2008-2009	Chemist, Materia Inc., Pasadena, CA
2009-2010	Graduate Teaching Assistant, University of California, San Diego
2009-2014	Research Assistant, University of California, San Diego
2011	Master of Science in Chemistry, University of California, San Diego
2014	Doctor of Philosophy in Chemistry, University of California, San Diego

PUBLICATIONS

A.J.White and M.Galperin. Inelastic transport: a pseudoparticle approach. *Phys. Chem. Chem. Phys.* **14**, 13809-13819 (2012).

A.J.White, B.D.Fainberg, and M.Galperin. Collective plasmon-molecule excitations in nanojunctions: Quantum consideration. *J. Phys. Chem. Lett.* **3**, 2738-2743 (2012).

A.J.White, M.Sukharev, and M.Galperin. Molecular nanoplasmonics: Self-consistent electrodynamics in current-carrying junctions. *Phys. Rev. B* **86**, 205324 (2012).

A.J.White, A.Migliore, M.Galperin, and A.Nitzan. Quantum transport with two interacting conduction channels. *J. Chem. Phys.* **138**, 174111 (2013).

A.J.White, M.Galperin, B.Apter, and B.D.Fainberg. Non-Markovian theory of collective plasmon-molecule excitations in nanojunctions combined with classical electrodynamic simulations. *Proc. SPIE* **8827**, 88270C (2013).

A.J.White, U.Peskin, and M.Galperin. Coherence in charge and energy transfer in molecular junctions. *Phys. Rev. B* **88**, 205424 (2013).

A.J.White, S.Tretiak, and M.Galperin. Raman Scattering in Molecular Junctions: A Pseudoparticle Formulation. *Nano Lett.* DOI: 10.1021/nl4039532 (2014).

ABSTRACT OF THE DISSERTATION

Electron Transport, Energy Transfer, and Optical Response in Single Molecule Junctions

by

Alexander James White

Doctor of Philosophy in Chemistry

University of California, San Diego, 2014

Professor Michael Galperin, Chair

The last decade has seen incredible growth in the quality of experiments being done on single molecule junctions. Contemporary experimental measurements have expanded far beyond simple electron transport. Measurement of vibronic effects, quantum interference and decoherence effects, molecular optical response (Raman spectroscopy), and molecular spintronics are just some of the continuing areas of research in single molecule junctions. Experimental advancements demand advanced theoretical treatments, which can be used accurately within appropriate physical regimes, in order to understand measured phenomena and predict interesting directions for future study. In this dissertation we will study systems with strong intra-system interactions using a many-body states based approach.

We will be focused on three related processes in molecular junctions: electron transport, electronic energy transfer, and molecular excitation. Inelastic electron transport in the regime of strong and nonlinear electron-vibration coupling within and outside of the Born-Oppenheimer regime will be investigated. To understand their appropriateness, we will compare simple semi-classical approximations in molecular redox junctions and electron-counting devices to fully quantum calculations based on many-body system states. The role of coherence and quantum interference in energy and electron transfer in molecular junctions is explored.

Experiments that simultaneously measure surface enhanced Raman scattering and electron conduction have revealed a strong interaction between conducting electrons and molecular excitation. We investigate the role of the molecular response to a classical surface plasmon enhanced electric field considering the back action of the oscillating molecular dipole. Raman scattering is quantum mechanical by nature and involves strong interaction between surface plasmons in the contacts and the molecular excitation. We develop a scheme for treating strong plasmon-molecular excitation interactions quantum mechanically within nonequilibrium molecular junctions. Finally we perform preliminary calculations of the Raman spectrum of a three-ring oligophenylene vinylene terminating in amine functional groups molecule in a molecular junction and compare our results to experimental measurements. This work is the first steps towards full calculations of the optical response of current-carrying molecular junction, which should combine classical calculations of the plasmon enhanced electric field with quantum calculations for the plasmon-molecular exciton interaction and nonequilibrium Raman scattering.

Chapter 1

Introduction

1.1 Background

The use of molecules in electronic devices was first proposed by Aviram and Ratner in 1974.[1] This was the beginning of the theoretical field of molecular electronics. Not until 1997 were the first measurements in single molecule junctions, electronic conductance as a function of source-drain bias, reported.[2] The single molecule junction is a device in which a single molecule bridges two metallic electrodes. Since then, great progress in experimental techniques at the nanoscale has driven the molecular electronics field. Endeavours in the field were originally, and continue to be, motivated by the desire to miniturize electronics components such as transistors, switches, and rectifiers. Today the field has become a playground for fundamental studies, and the possibilities for novel molecule characterization at the single molecule level can change the way we approach problems in solar-energy harvesting, thermoelectrics, catalysis, and sensing.[3]

While early molecular electronics experiments were focused on elastic electron tunneling,[4] current research in the field has branched in many directions, often probing the interaction of conducting electrons with other degrees of freedom of the molecule.[5,6] Some of these directions include measurement of thermoelectric properties of molecular devices[7–9] and heat transport,[10–13] molecular mechanics measurements,[14,15] atomic-scale molecular imaging,[16,17] molecular spintronics,[18–22] inelastic[23–25] and resonant inelastic[26–28] electron tunneling spectroscopy and the measurement of noise.[29,30] Additionally, people measure the consequencies of quantum interference effects in transport.[31–33]

Theoretical methods capable of simulating these nonequilibrium systems efficiently and accurately are required to complement experimental measurement, both to explain measurements and to propose new interesting systems for study. Much theoretical work involves applying quantum chemistry methods with nonequilibrium transport calculations to achieve realistic "first-principle" simulations of molecular junctions, usually based on heavy approximations. Alternatively one may apply nonequilibrium techniques to toy models in an attempt to understand the fundamental physics of transport in molecules and to develop methods for future "first-principle" simulations.

Realistic simulations for single molecule junctions require quantum chemistry calculations combined with nonequilibrium methodologies for calculating transport. The large size of the molecular junction system (with the partial inclusion of metallic leads) and the development of hybrid-functionals capable of accurate calculations of electronic structure of organic molecules,[34] made the efficient density functional theory (DFT),[35,36] and its time-dependent version (TD-DFT),[37,38] a clear choice for electronic structure calculations of single molecule junctions. The nonequilibrium Green function (NEGF)[39,40] method had already been well established for quantum transport in mesoscopic (e.g. quantum dots) scale systems.[41,42] The NEGF method is based on "quasi-particle"[43] excitations, elementry excitations which exist on top of the ground state of a large many-body system. DFT is similarly based on effectively independent single particle Kohn-Sham orbitals.[44] Both methods work in the same language of these elementary excitations and their combination into the NEGF-DFT(TDDFT) formalism was natural.[45–47] This language is convenient when the elementary excitations are non- or weakly interacting (as would be the case if the exchange correlation functional used was exact). In this regime, the complex many-body problem is effectively reduced to a problem of non- or weakly interacting single particle picture. The NEGF-DFT method has successfully been applied to quantum chemistry calculations of elastic[48–51] and inelastic[52–55] transport. Though NEGF-DFT is inconvenient for calculation of inelastic transport in the resonant tunneling regime or when intra-system interaction is not weak (where perturbation theory is inappropriate).[56] Additionally toy model calculations based on NEGF methods have improved our understanding of inelastic effects in transport in the off-resonant (inelastic electron tunneling spectroscopy, IETS) and resonant (RIETS)

tunneling regimes.[23,24,26,56]

While the NEGF-DFT method has been, and will continue to be, very useful in simulation of electron transport in the off-resonant and/or weak intramolecular interaction regime, it is not convenient in the physically important situation of strong intramolecular interaction and resonant tunneling. Note that a large molecular response to an external stimuli (e.g. current induced chemistry,[57] hysteresis and switching[58–60] or negative differential resistance[61–64]) is required of a useful molecular electronics device. Within this regime multiple degrees of freedom of the molecule, e.g. vibrational and electronic, are mixed. For example, when the Born-Oppenheimer approximations breaks down, e.g. when mixing between electronic and vibrational degrees of freedom couples quasi-degenerate electronic orbitals,[65] or when the vibrational structure of a molecule is dependent on the charge or electronic state of the molecule,[27,66] it is especially convenient to represent the Hamiltonian in terms of the many-body, vibronic, states.

Interaction with light has great potential for the characterization and control of molecular junctions. The field of molecular optoelectronics[67–69] has developed due to great advancements in laser technology and in fabrication techniques which have made the production of nanoscale gaps possible. These nanoscale gaps form "hot spots" of strong electromagnetic field enhancement allowing for the measurement of the optical response of current carrying molecular junctions.[70–73] In particular, over the past five years surface enhanced Raman spectroscopy[74] has become an important tool for characterizing vibrational and electronic heating,[75–77] molecule orientation,[78,79] and structure[80–83] of single molecule junctions. Additionally correlations between electrical conductance and Raman signal, which reveal information on the dynamics of the molecular junction, have been observed.[70,76,84]

Theoretical treatment of optical response in current carrying molecular junctions is complicated by the interaction of current and light scattering. Attemping to understand this interaction, much work has been done at the simple model level[85–90] Steady-state and time dependent non-equilibrium Green function methods have been applied to the Raman problem for model systems.[86,91–93] These model systems consider the optical driving of either a two-level (HOMO-LUMO type) system (intramolecular Raman process)[86,89,90] , or between the molecule and metal (charge transfer Raman),[93]

with linear coupling between the molecular electrons and vibrations. These methods have been used to analyze the relationship between the electronic conductance and the Raman signal. Like NEGF-DFT, these studies have used a "quasiparticle" approach.

Interaction between molecules and surface plasmon-polariton (SPP) modes is critical to the single-molecule optical response. The field of molecular nanoplasmonics studies this interaction. Interacting SPP-molecule systems are usually modeled using quantum mechanics for the molecule part[94–100] and numerical integration of Maxwell's equations[101–105] for the SPP part. Usually the electromagnetic field is assumed to be an external driving force. The NEGF technique has been used to study charge transport and optical response of a molecular junction which is subjected to such an electromagnetic field, taking into account the SPP modes specific to the junction geometry.[106,107] However, a semi-classical description of the interaction of the SPP-molecular excitation is not always appropriate. Quantum effects observed in strongly-hybridized plasmonic nanostructures,[108] and in systems of hybridized molecule-plasmon excitations,[109,110] motivated a quantum description of the interaction.[111–114] Recently a mean-field equilibrium Green function based formalism was utilized to study the plasmon absorption spectrum of a, molecule like, quantum emitter between a pair of metallic nanoparticles.[115]

Charge and electronic energy transfer processes occur simultaneously in molecular optoelectronic devices. A many-body representation has many advantages in the theoretical treatment of these processes. An orbital-based representation is complicated by the non-quadratic form of the energy transfer matrix elements, which necessitates an approximate treatment, while this issue does not exist in a many-body state representation. Rigorous treatment of the radiationless energy transfer between surface plasmon-polaritons in the contacts and molecule excitations is required for the theoretical description of single-molecule optical response,[85,106] where enhancement of electromagnetic field is critical[116,117] and where strongly interacting plasmonic and molecular excitations give rise to a new "quasiparticle" - polariton.[109,110,115] Additionally, molecular spectroscopy and most quantum chemistry methods are naturally formulated in the language of many-body states. Thus, a many-body state formulation is more convenient for quantum chemistry based calculations and analysis of optical response and transport properties in molecular electronics.

As we have discussed, a many-body state based representation is desirable for theoretical treament of both electron transport and optical response in molecular junctions. Multiple methodologies based on many-body states are used in nonequilibrium transport calculations. Scattering theory is often used when working at the wavefunction level. In transport calculations,[118–124] the full many-body problem is often reduced to single-particle scattering problem (as the full many-body wavefunction may intractable) including in the Landauer-Buttiker formalism,[125] and is exact and convenient when elastic scattering in a non-interacting system is considered.[126] The exact mapping method[127] can be used to represent inelastic transport in junctions as a single-particle scattering problem in the space of many-body states. This can be useful in describing systems with strong intra-system interactions, though it is not completely rigorous. Single-particle scattering theory, including exact mapping, generally misses the blocking of scattering channels due to the Pauli principle (Fermi distribution in the contacts).[128,129]

Generalization of the wavefunction based formalism to a density matrix approach, which takes into account spatial correlations, is a natural step when using a reduced description in which the bath degree of freedom is traced out. While a formally exact equation of motion for the density matrix, a quantum master equation (QME), can be written,[130,131] in practical applications a perturbation theory in system-bath coupling is applied.[132–134] The second order perturbation, the Redfield QME, is only appropriate in the very high temperature regime, $k_b T \gg \Gamma$,[135] where Γ is the electron escape rate or contact coupling strength, T is the temperature and k_B is the Boltzmann constant, and when there are no degeneracies in the system.[136] Additionally, the Redfield QME neglects hybridization of the molecular orbitals with those in the contacts (broadening of the molecular levels)[137] which may lead to qualitative failure.[107,138] Higher order, usually fourth order, perturbation theories[135,139,140] are available in the literature, but may not resolve these issues. Additionally, a nonperturbative generalized quantum master equation (GQME) approach has been developed in the Galperin group.[137,138] The formulations starts from an exact equation of motion, which is part of an infinite chain of equations of motion with increasingly complicated multi-time correlation functions. The chain is truncated by expressing two-time correlation functions in terms of the reduced density matrix. Formulating the truncations on either the Keldysh contour, or the

anti-contour, yields a time-nonlocal or time-local version of the GQME respectively. The effective second order in the system bath coupling applied in Ref. [137,138] recovers the broadening and resolves the low temperature limit. However, going beyond effective second order coupling is required to resolve the problem of degeneracies. Alternative QME variations which recover broadening are also available in the literature,[141–143] though they have their own limitations.[137] Additionally, a sophisticated method involving the use of the real-time renormalization group in the framework of a quantum master equation was reported recently, though it is numerically expensive.[144]

The time locality of the density matrix makes it suitable for the evaluation of time local quantities. Green functions are nonlocal in space and time, which makes treatment of system-bath hybridization and non-Markovian effects easier. The closest approach to the usual nonequilibrium Green function that utilizes the basis of many-body states is the Hubbard Green function approach. A spectral decomposition of the "quasiparticle" creation operator, $\hat{d}^\dagger_m = \sum_{M_1,M_2} \langle M_1|\hat{d}^\dagger_m|M_2\rangle \hat{X}_{M_1,M_2}$, shows that an elementary excitation is equivalent to a weighted mixture of transitions between many-body states, $|M\rangle$, (which differ by a single electron) defined by the Hubbard projection operator, X_{M_1,M_2}. An exact equation of motion can be written for the Hubbard operator by introducing auxiliary fields and using the technique of functional derivatives.[40,145–149] However to use the equations of motion in practice, the auxiliary fields must be eliminated in some approximate way. The lowest order approximation, dropping the auxiliary fields entirely, constitutes the Hubbard one approximation (H1A). The approach has been used to simulate transport in molecular junctions,[145,150,151] including quantum chemistry based simulations.[152] However, straightforward application of the Hubbard GF to a system with degeneracies does not guarantee Hermiticiy of the resulting density matrix (DM is the expectation value of the transpose of the Hubbard operator).[151] Systematic improvement of approximations, beyond H1A, has been called into question in Ref [153] Note that the failure of the H1A approximation is due to symmetry breaking due to truncation of the infinite EOM chain. The problem exists even in eqyilibrium formulations of the GF EOM method.[154] This issue has attracted recent attention in transport junctions.[155,156]

In Sec 1.4 we describe a pseudoparticle non-equilibrium Green function approach, which we use through most of the chapters of this dissertation. The method was originally

developed in condensed matter physics to describe strongly correlated systems, and is based on the language of many-body states of the system.[157–159] It is a generalization of the nonequilibrium slave-boson technique to include multiple electronic levels and other system components, such as molecular vibrations[160] and plasmon excitations.[161] Interest in the methodology was renewed[162,163] due to development of the dynamical mean field theory approach.[164,165] The method is based on pseudoparticle operators with canonical commutation relations, thus there is no problem with symmetry breaking. The method is conceptually simple and it is straightforward to introduce systematic improvements to the concerving approximations, based on standard diagrammatic techniques. Already in the simplest implementation, the non-crossing approximation, the approach goes far beyond Redfield QME, as it accounts for time non-local effects and hybridization of molecular and contact levels, while remaining relatively inexpensive numerically. However, as is explained further in Sec 1.4, the pseudoparticle approach requires one to work in an extended Hilbert space, and projections must be taken restricting the final expressions to the physical subspace.

1.2 Dissertation Overview

We are interested in the theoretical treatment of electron transport, energy transfer and molecular excitation in single molecule junctions. These processes are not independent, and their proper description is critical to the underlying physics of single molecule junction optical response (absorption, emission, or Raman spectra) and conductance measurements. Such treatment is epecially important when intra-molecular interactions are strong relative to the coupling to the electronic reservoirs. This is also the physically relevant regime for many of the most interesting single molecule junction experiments mentioned in the previous section.

As mentioned in the previous section the NEGF-DFT/TDDFT method is the dominant tool for conductance simulations in molecular junctions, but this method is inconvenient in the regime of strong intramolecular interactions. We utilize a pseudoparticle nonequilibrium Green function (PP-NEGF) approach that is exact in the strong inter-system interactions. The formulation of the methodology is explained in Sec. 1.4

(see also the appendices of chapter 2). This methodology is based on the language of the many-body system state, which allows us to explore strong intra-system interactions of any form. The pseudoparticle method is a generalization of the nonequilibrium slave-boson method of Meir and Wingreen,[159] to include multiple electronic levels and other system components, such as molecular vibrations[160] and plasmon excitations.[161]

In chapters 2-4 we analyze the role of energy transfer and electron-electron interaction on electronic conductance measurements, utilizing the PP-NEGF approach. We investigate inelastic electron transport within simple toy models, where transfer of energy between conducting electrons and molecular vibrations is visible in the conductance measurements. While approaches to resonant inelastic transport simulation utilize linear electron-vibration coupling, this is not necessarily appropriate for single molecules. We demonstrate that the PP-NEGF approach to calculating inelastic electron transport and resonant inelastic electron transport is applicable to any electron-vibration coupling strength or form (Figs. 2.2, 2.3, 2.6). Additionally, quantum interference effects are shown in current at large bias in a two-level bridge model (Fig. 2.4). The application of the PP-NEGF approach to inelastic transport can be thought of as a generalization of the exact mapping method of Bonča and Trugman,[127] which includes information of the Fermi-Dirac distribution of electrons in the leads and the Pauli-exclusion principle.

Electron-electron interaction between two conducting channels, which strongly differ in their coupling to the contacts, is investigated. The channel with strong coupling to the leads dominates the electronic conduction, but is affected through capacitive coupling to the weakly coupled channel, which models a molecular redox center. In a mixed quantum-classical approach, where the strongly coupled channel is treated quantum mechanically, via the nonequilibrium Green's function method and the weakly coupled channel is treated classically via rate equations, the electron-electron interaction can be approximately treated by an averaged charge transfer rate (Model A) or an averaged level energy (model B). We compare these two approximate schemes to the fully quantum treatment using PP-NEGF which treats the electron-electron interaction exactly. Two timescales have to be considered, the characteristic timescale of the bath, τ_B, and the dynamics of the redox level, $\varepsilon_r(t)$. The dynamics of the weakly coupled channel is controled by the rate of population change of the strongly coupled channel, which is pro-

portional to the inverse of the strong coupling to the contacts, Γ_s^{-1}. In our consideration of the wideband limit, small τ_B, For steady state current we find that the averaged rates approximation works well for voltage well above or below the resonance for charging the weakly coupled channel (Figs. 3.2-3.5). When renormalization of the level is slow relative to the bath dynamics, $\tau_B \ll \Gamma_s^{-1}$ the exact electron escape rate reduces to a set of two rates for different energies of the redox level (Model A). When renormalization of the level is fast relative to the bath dynamics, $\tau_B \gg \Gamma_s^{-1}$ the escape rate reduces to a single rate, calculated at the average energy of the redox level (Model B). Only the fully quantum calculation can correctly resolve the voltage threshold for charging the weakly coupled level.

The interaction between field-induced electron and electronic energy transfer is investigated in two models, 1) a system of two interacting pathways which leads to quantum interference effects (Fig. 4.1a), and 2) a three terminal system in which charge and energy transport can be separated through coherent control (Fig. 4.1b). In the first model we consider the effect of dephasing on a "two-slit" junction, where initially electron flux is surpressed due to destructive quantum interference between the paths, while constructive interference promotes energy transfer. As expected, dephasing results in an increase of current and reduction of energy transfer in the system. Surprisingly the behavior of the energy flow is non-monotonic with dephasing rate. This effect is due to interaction between the electron and energy transfer processes (Fig. 4.2). In the second model we suggest the possibility of coherent control of energy transfer in single molecule junctions. We demonstrate the possibility of spatial separation between electron and energy fluxes in the junction. Moreover, we show that the direction of the two fluxes can be controlled by varying the amplitude or frequency of the pumping electric field (Fig. 4.3). The theoretical demonstration of charge-energy separation in a molecular junction is a first step in the direction of engineering low-heating stable molecular nano-scale devices.

Chapters 5-7 are investigations of the component parts of the electromagnetic field - metallic plasmons - molecular excitation interaction that controls the optical response of molecular junctions. We consider a biased junction subject to a time-dependent electromagnetic field. The local field felt by the molecule is amplified by surface plasmon-

polariton excitations in the gold contacts. We demonstrate that the molecular response, due to the oscillating polarization of the molecule, strongly affects the local field (Figs. 5.2-5.3) and thus the electron transport characteristics of the junction (Figs. 5.4-5.6). The finite difference time domain method is used to propagate a classical electromagnetic pulse using Maxwell's equations. The molecular response is calculated quantum mechanically using NEGF. The nonequilibrium Green function method for a system subject to a general time-dependent electric field is described in Sec. 1.3.

When the interaction between the surface plasmon-polariton excitations and the molecular excitation is strong, it must be treated quantum mechanically. We utilize the PP-NEGF method in which the plasmon excitations are taken as part of the system, and the plasmon-molecular excitation interaction is treated exactly. Combined energy-electron transfer plays an important role in the plasmonic absorption spectrum in such a system (Fig. 6.1). We demonstrate the sensitivity of the Fano resonance,[166] due to the molecule-plasmon interaction, to junction bias and intramolecular interaction, including Coulomb repulsion (Fig. 6.1) and energy exchange (Figs. 6.3 and 6.4). We propose that measurement of the absorption spectrum of such a system, under bias, could provide direct measurement of intramolecular exciton coupling strength. We compare our prediction for non-linear optical response to previous studies based on a mean-field approximation.[167]

Recent experimental measurements of the optical response of junctions are focused on single molecule Raman spectroscopy. The latter is only feasible due to surface enhancement of the electromagnetic field by the surface plasmon-polariton excitations discussed in chapters 5 and 6. We present a formulation of Raman scattering in molecular junctions based on the PP-NEGF approach. This provides convenient way to incorporate quantum chemistry calculations, proven for equilibrium molecular spectroscopy, into calculations for optical spectroscopy of nonequilibrium molecular junctions, while also going beyond previous effective single particle formalisms.[86,91,92] We present quantum chemistry simulations of Raman scattering of a three ring oligophenylene vinylene terminating in amine functional groups (OPV3) junction (Fig. 7.1). The Raman spectrum of this molecule, in a junction under bias, has been experimentally measured.[77] We propose that observed shifts in Stokes frequencies may be caused by an increased con-

tribution from the cation OPV3 species at nonzero bias, and that the direction of the shift depends on the renormalization of the normal modes (Fig 7.2). Additionally, we demonstrate that the vibrational heating can be calculated and is in agreement with experimental measurements (Fig 7.3). This developed method constitutes an important step towards full *ab initio* calculations of the optical response of molecular junctions. In the future this method should be combined with a quantum treatment of the interaction between the molecule and plasmonic excitations and classical generation and propagation of the plasmon enhanced electromagnetic field described in chapters 5 and 6.

1.3 Nonequilibrium Green function method for a system subject to a general time-dependent electric field

1.3.1 Model

In Chapter 5 we consider a junction with a molecular bridge (M) connecting two metallic leads (L and R). This molecular bridge consists of D two-level systems with the levels representing ground (g) and excited (x) states of the molecule. Each two-level system is subject to a classical time dependent electromagnetic field ($\vec{E}(t)$). The contacts are assumed to be free electron reservoirs, each at their own equilibrium with a chemical potential, $\mu_{L/R}$. The total time dependent Hamiltonian reads (atomic units):

$$\hat{H}(t) = \hat{H}_M(t) + \sum_{K=L,R} \left(\hat{H}_K + \hat{V}_K \right) \tag{1.1}$$

$$\begin{aligned} \hat{H}_M(t) = & \sum_{s=g,x} \left[\sum_{m=1}^{D} \varepsilon_s \hat{d}_{ms}^{\dagger} \hat{d}_{ms} - \sum_{m=1}^{D-1} t_s \left(\hat{d}_{m+1s}^{\dagger} \hat{d}_{ms} + H.c. \right) \right] \\ & - \sum_{m=1}^{D} \left(\vec{\mu}_{mg,mx} \hat{d}_{mg}^{\dagger} \hat{d}_{mx} + H.c. \right) \vec{E}_m(t) \end{aligned} \tag{1.2}$$

$$\hat{H}_K = \sum_{k \in K} \varepsilon_k \hat{c}_k^{\dagger} \hat{c}_k \tag{1.3}$$

$$\hat{V}_K = \sum_{k \in K} \sum_{s=g,x} \left(V_{k,ms} \hat{c}_k^{\dagger} \hat{d}_{ms} + H.c \right) \tag{1.4}$$

$\hat{H}_M(t)$ and $\hat{H}_K$ are the Hamiltonians of the molecular bridge (M) and the contacts ($K = L, R$), and $\hat{V}_K$ is coupling between them. $\hat{d}^\dagger_{ms}$ ($\hat{d}_{ms}$) and $\hat{c}^\dagger_k$ ($\hat{c}_k$) are creation (annihilation) operators for an electron on the level s of the molecular bridge site m and state k of the contact, respectively. $\vec{\mu}_{ms,ms'} = \langle ms|\hat{\vec{\mu}}|ms'\rangle$ is the matrix element of the transition molecular (vector) dipole operator between states $|ms\rangle$ and $|ms'\rangle$ and $\vec{E}_m(t)$ is the local time-dependent field at bridge site m. t_s ($s = g, x$) and $V_{k,m_K s}$ are matrix elements for electron transfer in the molecular bridge and between molecule and contacts, respectively. Note that treating the external field classically allows us to account for arbitrary time dependence exactly (i.e. beyond perturbation theory).[107]

1.3.2 Time-dependent current

We are interested in calculating time-dependent current of the junction. The current at the interface between the molecular bridge and the contact, $K = L/R$ is:[42]

$$I_K(t) = \int_{-\infty}^{t} dt_1 \mathrm{Tr}[\mathbf{\Sigma}^<_K(t,t_1)\mathbf{G}^>(t_1,t) + \mathbf{G}^>(t,t_1)\mathbf{\Sigma}^<_K(t_1,t) - \mathbf{\Sigma}^>_K(t,t_1)\mathbf{G}^<(t_1,t) - \mathbf{G}^<(t,t_1)\mathbf{\Sigma}^>_K(t_1,t)] \tag{1.5}$$

The $\mathbf{G}^{>/<}(t,t')$ matrix is the greater/lesser projection of the contour ordered single-electron Green function in the molecular subspace,

$$G_{ms,m's'}(\tau,\tau') = \langle T_c \hat{d}_{ms}(\tau)\hat{d}^\dagger_{m's'}(\tau')\rangle \tag{1.6}$$

where T_c is the contour-ordering operator and τ is the contour time variable.[42] $\mathbf{\Sigma}^{>/<}_K(t,t')$ matrix is the greater/lesser projection of the self-energy due to coupling to the contact, K,

$$\Sigma_{K;ms,m's'}(\tau,\tau') = \sum_{k\in K} V^*_{m's',k} V_{k,ms} g_k(\tau,\tau') \tag{1.7}$$

where g_k is the free contact electron Green function. The real time projections of the self-energy are given by:

$$\Sigma^{>}_{K;ms,m's'}(t,t') = \int \frac{dE}{2\pi}[1 - f_K(E)]\Gamma_{K;ms,m's'}(E)e^{-iE(t-t')} \tag{1.8}$$

$$\Sigma^{<}_{K;ms,m's'}(t,t') = \int \frac{dE}{2\pi} f_K(E)\Gamma_{K;ms,m's'}(E)e^{-iE(t-t')}$$

$$\Sigma^{r/a}_{K;ms,m's'}(t,t') = \pm\Theta(\pm t \mp t')[\Sigma^{>}_{K;ms,m's'}(t,t') - \Sigma^{<}_{K;ms,m's'}(t,t')] \tag{1.9}$$

with the electronic escape rate,

$$\Gamma_{K;ms,m's'}(E) = 2\pi \sum_{k\in K} V^{*}_{m's',k} V_{k,ms}\delta(E - \varepsilon_k) \tag{1.10}$$

, where $f_K(E)$ is the Fermi-Dirac distribution function, $f_K(E) = 1/[1 - e^{(\mu_K - E_f)/(K_B T)}]$, defined by the chemical potential, μ_K, the Fermi level, E_f, the Boltzmann constant, K_B, and the temperature, T, of the contact K. We assume the wideband limit, where Γ is assumed to be energy independent and disregard the real part of the retarded/advanced self-energy, Eq.1.9. When the time-dependence of the total Hamiltonian is limited to the system subspace the time-dependent current reduces to:[168]

$$I_K(t) = I^{in}_K(t) - I^{out}_k(t) \tag{1.11}$$

$$I^{in}_K(t) = -\int \frac{dE}{\pi} f_K(E)\text{Im Tr}[\mathbf{\Gamma}_K \mathbf{G^r}(\mathbf{t},\mathbf{E})] \tag{1.12}$$

$$I^{out}_K(t) = \int \text{Tr}[\mathbf{\Gamma}_K \mathbf{G}^{<}(\mathbf{t},\mathbf{t})] \tag{1.13}$$

where $\mathbf{G^r}(t,E)$ is the time-dependent one-sided Fourier transfrom of the retarded Greens function matrix,

$$G^r_{ms,m's'}(t,t') = \Theta(t-t')[G^{>}_{ms,m's'}(t,t') - G^{<}_{ms,m's'}(t,t')] \tag{1.14}$$

$$G^r_{ms,m's'}(t,E) = \int dt' e^{iE(t-t')} G^r_{ms,m's'}(t,t') \tag{1.15}$$

.

1.3.3 Equations of Motion

The retarded and lesser Green functions in Eqs.1.12-1.13 can be obtained from a Keldysh-contour based equation of motion approach.[42]

$$i\frac{\delta}{\delta\tau}\mathbf{G}(\tau,\tau') = \mathbf{I}\times\delta(\tau,\tau') + \mathbf{H}_M(\tau)\mathbf{G}(\tau,\tau') + \sum_K \int_C d\tau_1 \mathbf{\Sigma}_K(\tau,\tau_1)\mathbf{G}(\tau_1,\tau') \tag{1.16}$$

where $\mathbf{I}$ is the unitary matrix and $\mathbf{H}_M$ is representation of the bridge Hamiltonian operator, Eq.1.2, in the single electron basis. From Eq.1.16 and the similar equation of motion $i\frac{\delta}{\delta\tau'}\mathbf{G}(\tau,\tau')$, and using Eqs.1.8-1.9, we can obtain a system of equations for the Greens functions in Eqs.1.12-1.13:

$$i\frac{\delta}{\delta t}\mathbf{G}^{\mathbf{r}}(t,E) = \mathbf{I} - (E\mathbf{I} - \mathbf{H}_M(t) + \frac{i}{2}\mathbf{\Gamma})\mathbf{G}^{\mathbf{r}}(t,E) \tag{1.17}$$

$$\begin{aligned} i\frac{\delta}{\delta t}\mathbf{G}^{<}(t,t) =& [\mathbf{H}_M(t);\mathbf{G}^{<}(t,t)] - \frac{i}{2}\{\mathbf{\Gamma};\mathbf{G}^{<}(t,t)\} \\ &+ i\sum_K \int \frac{dE}{2\pi} f_K(E)(\mathbf{\Gamma}_K\mathbf{G}^{\mathbf{a}}(E,t) - \mathbf{G}^{\mathbf{r}}(t,E)\mathbf{\Gamma}_K) \end{aligned} \tag{1.18}$$

where $\mathbf{\Gamma} = \mathbf{\Gamma}_L + \mathbf{\Gamma}_R$, $[...;...]$ and $\{...;...\}$ are the commutator and anti-commutator and $\mathbf{G}^{\mathbf{a}}(E,t) = [\mathbf{G}^{\mathbf{r}}(t,E)]^\dagger$. The first order differential equations, Eqs. 1.17-1.18, are solved numerically using the initial condition of the biased junction at steady-state in the absense of an external electric field ($E(0) = 0$).

$$\mathbf{G}^{\mathbf{r}}(0,E) = [\mathbf{I} - (E\mathbf{I} - \mathbf{H}_M(0) + \frac{i}{2}\mathbf{\Gamma}]^{-1} \tag{1.19}$$

$$\mathbf{G}^{<}(0,0) = \sum_K \int \frac{dE}{2\pi}\mathbf{G}^{\mathbf{r}}(0,E)\mathbf{\Gamma}_K\mathbf{G}^{\mathbf{a}}(E,0). \tag{1.20}$$

.

1.4 Pseudoparticle Nonequilibrium Green Functions Method

1.4.1 System and Bath Hamiltonians

Throughout this dissertation we will consider total Hamiltonians, $\hat{H}$, which are separated into system, a set of baths (optical, thermal, electronic) and system-bath

interactions.

$$\hat{H} = \hat{H}_{\text{sys}} + \hat{B}_{\text{op}} + \hat{B}_{\text{th}} + \hat{B}_{\text{el}} + \hat{I}_{\text{sys-op}} + \hat{I}_{\text{sys-th}} + \hat{I}_{\text{sys-el}} \tag{1.21}$$

Where

$$\hat{B}_{\text{op}} = \sum_{\alpha \in \text{op}} \omega_\alpha \hat{a}^\dagger_\alpha \hat{a}_\alpha \tag{1.22}$$

$$\hat{B}_{\text{th}} = \sum_{\nu \in \text{th}} \omega_\nu \hat{b}^\dagger_\nu \hat{b}_\nu \tag{1.23}$$

$$\hat{B}_{\text{el}} = \sum_{\kappa \in K=L,R} \varepsilon_\kappa \hat{c}^\dagger_\kappa \hat{c}_\kappa \tag{1.24}$$

$$\hat{I}_{\text{sys-op}} = \sum_{\substack{\alpha \in \text{op} \\ m,m' \in \text{sys}}} W^\alpha_{m,m'} \hat{D}^\dagger_{m,m'} \hat{a}_\alpha \; + \; h.c. \tag{1.25}$$

$$\hat{I}_{\text{sys-th}} = \sum_{\substack{\nu \in \text{th} \\ v \in \text{sys}}} X_{v\nu} \hat{b}^\dagger_v \hat{b}_\nu \; + \; h.c. \tag{1.26}$$

$$\hat{I}_{\text{sys-el}} = \sum_{\substack{\kappa \in L,R \\ m \in \text{sys}}} V_{m\kappa} \hat{c}^\dagger_m \hat{c}_\kappa \; + \; h.c. \tag{1.27}$$

$\hat{a}^\dagger_\alpha(\hat{a}_\alpha)$, $\hat{b}^\dagger_\nu(\hat{b}_\nu)$, $\hat{c}^\dagger_\kappa(\hat{c}_\kappa)$, create (destroy) the bath photon, α, phonon, ν, and electron, κ respectively. $\hat{c}^\dagger_m$ creates an electron in system molecular or atomic orbital m, $\hat{D}^\dagger_{m,m'} \equiv \hat{c}^\dagger_m \hat{c}_{m'}$ excites an electron from orbital m' to m, and $\hat{b}^\dagger_v$ creates a molecular vibron, v. $\hat{H}_{\text{sys}}$ may be either a model system Hamiltonian, or the Hamiltonian defined by any quantum chemistry technique.

1.4.2 Pseudoparticle Non-Equilibrium Green Functions

The basis of the pseudoparticle non-equilibrium Green functions (PPNEGF) is defined by the many-body states of the molecular subsystem $|M\rangle$. $\hat{d}^\dagger_M$ ($\hat{d}_M$) are the pseudoparticle creation(annihilation) operators for the many-body molecular state M. The pseudoparticle creation and annihilation operators are related to the effective single-

particle orbital creation operators through:

$$\hat{c}_m^\dagger = \sum_{M,M' \in \text{sys}} \xi_{M,M'}^m \; \hat{d}_M^\dagger \hat{d}_{M'} \tag{1.28}$$

Where $\xi_{M,M'}^m$ is the overlap of the states, M and M', which have N_M and $N_M + 1$ electrons in the molecular subsystem.

$$\xi_{M,M'}^m \equiv \langle M | \hat{c}_m^\dagger | M' \rangle \tag{1.29}$$

Similarly, the creation operators of molecular vibration and excitation "quasipariticles" can be expressed in terms of the pseudoparticle operators.

$$\hat{b}_v^\dagger = \sum_{M,M' \in \text{sys}} \chi_{M,M'}^v \; \hat{d}_M^\dagger \hat{d}_{M'} \tag{1.30}$$

$$\hat{D}^\dagger{}_{m_2,m_1} \equiv \hat{c}_{m_1}^\dagger \hat{c}_{m_2} = \sum_{M,M' \in \text{sys}} \Delta_{M,M'}^{m_1,m_2} \; \hat{d}_M^\dagger \hat{d}_{M'} \tag{1.31}$$

Both $\chi_{M,M'}^\nu$ and $\Delta_{M,M'}^{m_1,m_2}$ are overlap tensors for states with the same molecular charge. $\Delta_{M,M'}^{m_1,m_2}$ is an element of the transition density matrix. The pseudoparticle operators satisfy the usual fermion and boson commutation relations, within an extended Hilbert space, depending on the electron count of the molecular state. The physical subspace of this extended Hilbert space is defined by:

$$\hat{Q} \equiv \sum_{M \in \text{sys}} \hat{d}_M^\dagger \hat{d}_M = 1 \tag{1.32}$$

The single-pseudoparticle GF is defined on the Keldysh contour as:

$$G_{M,M'}(\tau_1, \tau_2) = -i \langle T_c \, \hat{d}_M^\dagger(\tau_1) \hat{d}_{M'}(\tau_1) \rangle \tag{1.33}$$

where τ_1 and τ_1 are contour variables and T_c is the contour time ordering operator. Within the extended Hilbert space, these single-pseudoparticle GFs satisfies the usual

Dyson equation:

$$\mathbf{G} = \mathbf{g} + \mathbf{g}\mathbf{\Sigma}\mathbf{G} \tag{1.34}$$

where $\mathbf{g}$ is the pseudoparticle GF matrix in the absence of system-bath coupling. $\mathbf{\Sigma}$ is the pseudoparticle self-energy, which includes contributions from coupling to the electronic, thermal and optical baths. Using the Dyson and Keldysh equations for the pseudoparticles we solve for the retarded, advanced, greater and lesser Green functions. At steady state this leads to:

$$\mathbf{G^r}(E) = \mathbf{G^{a\dagger}}(E) = [\mathbf{I}E - \mathbf{H} - \mathbf{\Sigma^r}(E)]^{-1} \tag{1.35}$$

$$\mathbf{G}^{>/<}(E) = \mathbf{G^r}(E)\mathbf{\Sigma}^{>/<}(E)\mathbf{G^a}(E) \tag{1.36}$$

Projection from the extended Hilbert space to the physical $Q = 1$ subspace, Eq. 1.32, is, in part, accomplished by normalizing such that:

$$\sum_{M\in\text{sys}} \frac{i\zeta_M}{2\pi} \int_{-\infty}^{\infty} dE\, G^<_{M,M}(E) \equiv 1 \tag{1.37}$$

where ζ_M is 1(-1) if M has an even(odd) number of electrons in the system.

Luttinger-Ward functional in the PPNEGF: Derivation of Pseudoparticle Self-Energies and quasiparticle/single-particle Green functions

We follow the path integral formulation of Ref. [163] with the goal of deriving the pseudoparticle self-energies and the usual non-equilibrium Green functions for the electron, phonons, and excitons in the system. We introduce the grand canonical partition function, Z, as a path integral over the Keldysh contour.

$$Z = \int_C \mathbf{D}[\bar{d}, d, \bar{a}, a, \bar{b}, b, \bar{c}, c] \exp(iS) \tag{1.38}$$

The measure D is defined as:

$$\mathbf{D}[\bar{d},d,\bar{a},a,\bar{b},b,\bar{c},c] \equiv \prod_{m\in\text{sys}} \frac{1}{\Theta_m} d\bar{d}_m dd_m \times \prod_{\alpha\in\text{op}} \frac{-i}{2\pi} d\bar{a}_\alpha da_\alpha \tag{1.39}$$

$$\times \prod_{\nu\in\text{th}} \frac{-i}{2\pi} d\bar{b}_\nu db_\nu \times \prod_{\kappa\in\text{el}} d\bar{c}_\kappa dc_\kappa \tag{1.40}$$

$$\Theta_m \equiv \left\{ \begin{array}{l} (1) \text{ for } m = \text{Fermion} \\ (i2\pi) \text{ for } m = \text{Boson} \end{array} \right\}$$

With the contour action give by:

$$\begin{aligned} S = \int_C d\tau \Bigg\{ & \sum_{M,M'\in\text{sys}} \bar{d}_M(\tau)\hat{g}^{-1}_{M,M'} d_{M'}(\tau) \\ & + \sum_{\alpha\in\text{op}} \bar{a}_\alpha(\tau) p_\alpha^{-1} a_\alpha(\tau) + \sum_{\nu\in\text{th}} \bar{b}_\nu(\tau) o_\nu^{-1} b_\nu(\tau) + \sum_{\kappa\in\text{el}} \bar{c}_\kappa(\tau) l_\kappa^{-1} c_\kappa(\tau) \\ & - \sum_{\substack{\alpha\in\text{op} \\ m_1,m_2\in\text{sys}}} \left(W^{\alpha}_{m_1,m_2} \bar{a}_\alpha(\tau) D_{m_1,m_2}[\eta(\tau),\bar{\eta}(\tau)] + W^{\alpha *}_{m_1,m_2} \bar{D}_{m_1,m_2}[\eta(\tau),\bar{\eta}(\tau)] a_\alpha(\tau) \right) \\ & - \sum_{\substack{\nu\in\text{th} \\ v\in\text{sys}}} \left(X_{\nu,v} \bar{b}_\nu(\tau) b_v[\eta(\tau),\bar{\eta}(\tau)] + X_{v,\nu} \bar{b}_v[\eta(\tau),\bar{\eta}(\tau)] b_\nu(\tau) \right) \\ & - \sum_{\substack{\kappa\in\text{el} \\ m\in\text{sys}}} \left(V_{\kappa,m} \bar{c}_\kappa(\tau) c_m[\eta(\tau),\bar{\eta}(\tau)] + V_{m,\kappa} \bar{c}_m[\eta(\tau),\bar{\eta}(\tau)] c_\kappa(\tau) \right) \\ & - \sum_{m\in\text{sys}} \left(\bar{\eta}_m(\tau) d_m(\tau) + \bar{d}_m(\tau) \eta_m(\tau) \right) \Bigg\} \end{aligned} \tag{1.41}$$

d,a,b, and c, are the Grassman variable for Fermions and complex numbers for Bosons representing the pseudoparticle, photon in the optical bath, phonon in the thermal bath, and electron in the contact, respectively. $\bar{d}$ is the conjugate of d. $g^{-1}_{M,M'}$, p_α^{-1},o_ν^{-1},l_κ^{-1} are the matrix inverse, of the corresponding free, *i.e.* no system-bath coupling, system pseudoparticle and bath photon, phonon and electron Green functions, respectively. The Grassman variables/complex numbers for the system operators are expressed in terms

of functional derivatives of the auxiliary fields, η.

$$\bar{D}_{m,m'}[\eta(\tau),\bar{\eta}(\tau)] \equiv \sum_{M,M'\in \mathrm{sys}} \Delta^{m,m'}_{M,M'}\zeta_M \frac{\delta}{\delta\eta_M(\tau)}\frac{\delta}{\delta\bar{\eta}_{M'}(\tau)} \tag{1.42}$$

$$\bar{b}_{v}[\eta(\tau),\bar{\eta}(\tau)] \equiv \sum_{M,M'\in \mathrm{sys}} \chi^{v}_{M,M'}\zeta_M \frac{\delta}{\delta\eta_M(\tau)}\frac{\delta}{\delta\bar{\eta}_{M'}(\tau)} \tag{1.43}$$

$$\bar{c}_{m}[\eta(\tau),\bar{\eta}(\tau)] \equiv \sum_{M,M'\in \mathrm{sys}} \xi^{m}_{M,M'}\zeta_M \frac{\delta}{\delta\eta_M(\tau)}\frac{\delta}{\delta\bar{\eta}_{M'}(\tau)} \tag{1.44}$$

Taking the integral over the system pseudoparticles, and bath electrons, phonons, and photons in Eq. 1.38 leads to:

$$\begin{aligned} Z = Z_0 \exp\Bigg(-i \iint_c d\tau d\tau' \Bigg\{ & \\ & \sum_{\substack{m_1,m_2\in \mathrm{sys}\\ m_3,m_4\in \mathrm{sys}}} \bar{D}_{m_1,m_2}[\eta(\tau),\bar{\eta}(\tau)]\,\pi^{m_1,m_2}_{m_3,m_4}(\tau,\tau')\,D_{m_3,m_4}[\eta(\tau'),\bar{\eta}(\tau')] \\ & + \sum_{v,v'\in \mathrm{sys}} \bar{b}_{v}[\eta(\tau),\bar{\eta}(\tau)]\,\omega_{v,v'}(\tau,\tau')\,b_{v'}[\eta(\tau'),\bar{\eta}(\tau')] \\ & + \sum_{\substack{m,m'\in \mathrm{sys}\\ K=L,R}} \bar{c}_{m}[\eta(\tau),\bar{\eta}(\tau)]\,\lambda^{K}_{m,m'}(\tau,\tau')\,c_{m'}[\eta(\tau'),\bar{\eta}(\tau')] \Bigg\}\Bigg) \\ & \times \exp\left(i \sum_{M,M'\in \mathrm{sys}} \iint_c d\tau d\tau' \bar{\eta}_M(\tau) g_{m,m'}(\tau,\tau')\eta_{m'}(\tau') \right) \end{aligned} \tag{1.45}$$

where $\boldsymbol{\lambda}$, $\boldsymbol{\pi}$, and $\boldsymbol{\omega}$ are the standard contact, photon, and phonon self-energy matricies due to Eq 1.25-1.27:

$$\lambda^{K}_{m,m'}(\tau,\tau') \equiv \sum_{\kappa,\in K} V_{m,\kappa}\,l_{\kappa}(\tau,\tau')\,V^{*}_{\kappa,m'} \tag{1.46}$$

$$\pi^{m_1 m_2}_{m_3 m_4}(\tau,\tau') \equiv \sum_{\alpha,\in K} W^{\alpha}_{m_1,m_2}\,p_{\alpha}(\tau,\tau')\,W^{\alpha\,*}_{m_3,m_4} \tag{1.47}$$

$$\omega_{v,v'}(\tau,\tau') \equiv \sum_{\nu,\in th} X_{v,\nu}\,o_{\nu}(\tau,\tau')\,X^{*}_{\nu,v'} \tag{1.48}$$

and Z_0 is the zero-order Grand canonical partition function, which neglects system-bath coupling.

To arive at a useful expression, the first exponent in Eq. 1.45 is expanded in a

power series, and Eq. 1.42-1.44 are inserted into Eq. 1.45. The derivatives with respect to the auxiliary fields are taken, and the fields are set to zero. The resulting connected diagrams are collected into cumulant expansions, which leads to:

$$Z = Z_0 \exp(-iY) \tag{1.49}$$

Where

$$\begin{aligned} Y = Y' + \sum_N \zeta_N Tr[\ln(-G^{-1}) + \mathbf{\Sigma G}] + Tr[\ln(-\Pi^{-1}) + \mathbf{\Sigma^{\Pi}\Pi}] \\ + Tr[\ln(-\Omega^{-1}) + \mathbf{\Sigma^{\Omega}\Omega}] - \sum_{K\in L,R} Tr[\ln(-\Lambda^{K\,-1}) + \mathbf{\Sigma^{\Lambda}\Lambda^{K}}] \end{aligned} \tag{1.50}$$

Y' is a collection of all closed skeleton diagrams, *i.e.* diagrams with no self-energy insertions that describe system-bath interaction. $\mathbf{\Sigma}$ ($\mathbf{\Sigma^{\Pi}}$, $\mathbf{\Sigma^{\Omega}}$, $\mathbf{\Sigma^{\Lambda}}$) is the pseudoparicle (photon, phonon, contact electron) self-energy and G (Π, Ω, Λ) is the full pseudoparticle (photon, phonon, contact electron) Green function . N indicates a block of the system Hamiltonian with the N electrons in the system. The Trace is taken over both contour variable and states. Dressing the skeleton diagrams with the full pseudoparticle Greens functions collects all skeleton diagrams with the same number of self-energy crossings. This results in a systematic inclusion of all diagrams of higher order that include the same number of crossings and indistinguishable self-energy directions. Y' expressed in terms of the dressed diagrams is known as the Luttinger-Ward functional.[169] Y is stationary with respect to the Green functions, $\boldsymbol{G}$, $\mathbf{\Pi}$, $\mathbf{\Omega}$,$\mathbf{\Lambda}$. Therefore the self-energies immediatly follow from Eq. 1.50 as:

$$\Sigma_{M,M'} = \zeta_M \frac{\delta\, Y'}{\delta\, G_{M',M}} \delta_{N_M,N_{M'}} \tag{1.51}$$

$$\Sigma^{\Pi\, m_1,m_2}_{\quad m_3,m_4} = + \frac{\delta\, Y'}{\delta\, \Pi^{m_3,m_4}_{m_1,m_2}} \tag{1.52}$$

$$\Sigma^{\Omega}_{v,v'} = + \frac{\delta\, Y'}{\delta\, \Omega_{v',v}} \tag{1.53}$$

$$\tag{1.54}$$

$$\Sigma^{\Lambda}_{m,m'} = - \frac{\delta\, Y'}{\delta\, \Lambda_{m',m}} \tag{1.55}$$

NCA-Pseudoparticle Self Energies

The pseudoparticle self-energy, $\mathbf{\Sigma}$ Eq. 1.51, is approximated to the dressed second-order, the noncrossing approximation. At steady state:

$$\begin{aligned}\Sigma^{r/<}_{M,M'}(E) = \frac{i}{2\pi}\sum_{M_1,M_2\in\text{sys}}\int_{-\infty}^{\infty} dE'\, G^{r/<}_{M_1,M_2}(E') \\ [\lambda^{>/<}_{MM_1,M'M_2}(E-E') - \lambda^{</>}_{M_2M',M_1M}(E'-E) \\ \pm\pi^{>/<}_{MM_1,M'M_2}(E-E') \pm \pi^{</>}_{M_2M',M_1M}(E'-E) \\ \pm\omega^{>/<}_{MM_1,M'M_2}(E-E') \pm \omega^{</>}_{M_2M',M_1M}(E'-E)]\end{aligned} \tag{1.56}$$

is the retarded(lesser) pseudoparticle self energy. Note that within the physical $Q = 1$ subspace, $\mathbf{\Sigma}^{>} = \mathbf{\Sigma}^{r} - \mathbf{\Sigma}^{a}$ and $\mathbf{\Sigma}^{a} = \mathbf{\Sigma}^{r\,\dagger}$ The self-energies due to coupling to the electronic, photon, and phonon baths, respectively, in the many-body state basis are given by:

$$\lambda^{>/<}_{M_1M_2,M_3M_4}(E) = \sum_{\substack{K=L,R\\ m,m'\in\text{sys}}} \xi^{m}_{M_1M_2}\xi^{m'\dagger}_{M_3M_4}\,\lambda^{K\,>/<}_{m,m'}(E) \tag{1.57}$$

$$\pi^{>/<}_{M_1M_2,M_3M_4}(E) = \sum_{\substack{m_1,m_2\in\text{sys}\\ m_3,m_4\in\text{sys}}} \Delta^{m_1,m_2}_{M_1M_2}\Delta^{m_3,m_4\dagger}_{M_3M_4}\,\pi^{m_1m_2\,>/<}_{m_3m_4}(E) \tag{1.58}$$

$$\omega^{>/<}_{M_1M_2,M_3M_4}(E) = \sum_{v,v'\in\text{sys}} \chi^{v}_{M_1M_2}\chi^{v'\dagger}_{M_3M_4}\,\omega^{>/<}_{v,v'}(E) \tag{1.59}$$

where $\boldsymbol{\lambda}^{>/<}(E)$, $\boldsymbol{\pi}^{>/<}(E)$, and $\boldsymbol{\omega}^{>/<}(E)$ are the steady state Fourier transforms of the greater/lesser projections of Eq. 1.46-1.48.

$$\lambda^{K\,>/<}_{m,m'}(E) = \Gamma^{K}_{m,m'}(E)\,\{[1-f_K(E)]\,/\,f_K(E)\} \tag{1.60}$$

$$\pi^{m_1m_2\,>/<}_{m_3m_4}(E) = \gamma^{m_1m_2}_{m_3m_4}(E)\,\{[1+N_{\omega_0}(E)]\,/\,N_{\omega_0}(E)\} \tag{1.61}$$

$$\omega^{>/<}_{v,v'}(E) = \rho_{v,v'}(E)\,\{[1+N_{\omega_\beta}(E)]\,/\,N_{\omega_\beta}(E)\} \tag{1.62}$$

$$\Gamma^{K}_{m,m'}(E) = 2\pi \sum_{\kappa \in K} V_{m\kappa} V^{*}_{\kappa m'} \delta(E - \varepsilon_k) \tag{1.63}$$

$$\gamma^{m_1 m_2}_{m_3 m_4}(E) = 2\pi \sum_{\alpha \in \mathrm{op}} W^{\alpha}_{m_1,m_2} W^{\alpha\,*}_{m_3 m_4} \delta(E - \omega_\alpha) \tag{1.64}$$

$$\rho_{v,v'}(E) = 2\pi \sum_{\nu \in \mathrm{th}} X_{v\nu} X^{*}_{\nu v'} \delta(E - \omega_\nu) \tag{1.65}$$

$\boldsymbol{\Gamma^K}$,$\boldsymbol{\gamma}$, and $\boldsymbol{\rho}$ are the electron, photon, and phonon dissipation matricies. $f_K(E) = [\exp(\frac{E-\mu_K}{k_B T}) + 1]^{-1}$ is the Fermi-Dirac distribution function, where μ_K is the equilibrium chemical potential of the contact K. $N_{\omega_\beta}(E) = [\exp(\frac{E}{k_B T}) - 1]^{-1}$ is the Bose-Einstein distribution function, and $N_{\omega_0}(E) = N_0 \frac{\delta^2}{(E-\omega_0)^2+\delta^2}$ is the population distribution function of the bath created by the laser with frequency, ω_0, and an energy bandwidth, δ. The thermal bath is assumed to contain phonons of a single mode, ω_β , and the phonon dissipation function is given by $\rho_{v,v'}(E) = \rho_{v,v'} \frac{\omega^2}{\omega^2_\beta} \exp(2 - \frac{2\omega}{\omega_\beta})$. $\boldsymbol{\Gamma^K}$ and $\boldsymbol{\gamma}$ are assumed to be in the wide-band limit, *i.e.* energy independent.

1.4.3 Electrical Current in the NCA

Current through the junction is defined as the rate of change of the number of electrons in the contact K.

$$I_K = -\frac{d}{dt} \sum_{\kappa \in K} \langle \hat{c}^{\dagger}_{\kappa} \hat{c}_{\kappa} \rangle \tag{1.66}$$

Following Ref .[160] At steady state this leads to

$$I_K = \int_{-\infty}^{\infty} \frac{dE}{2\pi} \mathrm{Tr}[\boldsymbol{\lambda}^{K<}(E)\, \boldsymbol{\Sigma}^{\boldsymbol{\Lambda}>}(E) - \boldsymbol{\lambda}^{K>}(E)\, \boldsymbol{\Sigma}^{\boldsymbol{\Lambda}<}(E)] \tag{1.67}$$

The trace is over the single particle electronic orbitals of the system. $\lambda^{K\,(>/<)}(E)$ is defined in Eq.1.60. $\Sigma^{\Lambda\,(>/<)}_{m,m'}(E)$ is the Fourier transform of the greater/lesser projecton of the electronic Green function $-i\langle T_c\, \hat{c}_m(\tau) \hat{c}^{\dagger}_{m'}(\tau') \rangle$. Within the NCA, $\Sigma^{\Lambda\,(>/<)}_{m,m'}(E)$ is

determined, through Eq.1.54, to be:

$$\Sigma^{\Lambda\,(>/<)}_{m,m'}(E) = \sum_{\substack{M_1,M_2\in \mathrm{sys}\\ M_1',M_2'\in \mathrm{sys}}} i\zeta_{M_1}\xi^{m}_{M_1',M_2'}\xi^{m'\,*}_{M_1,M_2}\int_{-\infty}^{\infty}\frac{dE'}{2\pi}G^{>/<}_{M_1,M_1'}(E+E')\,G^{>/<}_{M_2',M_2}(E') \tag{1.68}$$

1.4.4 Absorption and Emission in the NCA

Absorption and emission are described by the flux of photons into and out of the system, respectively. This photon current is obtained as the time derivative of the average number of bath photons.

$$I_{ph} = -\frac{d}{dt}\sum_{\alpha}\langle \hat{a}^{\dagger}_{\alpha}\hat{a}_{\alpha}\rangle \tag{1.69}$$

Simillarly to Eq. 1.67, the photon current at steady state is given by

$$\begin{aligned} I_{ph} &= -\int_{-\infty}^{\infty} d(t-t')\mathrm{Tr}[\boldsymbol{\pi}^{<}(t-t')\,\boldsymbol{\Sigma}^{\boldsymbol{\Pi}\,>}(t'-t) - \boldsymbol{\pi}^{>}(t'-t)\,\boldsymbol{\Sigma}^{\boldsymbol{\Pi}\,<}(t-t')] \\ &= \int_{-\infty}^{\infty}\frac{dE}{2\pi}\mathrm{Tr}[\boldsymbol{\pi}^{<}(E)\,\boldsymbol{\Sigma}^{\boldsymbol{\Pi}\,>}(E) - \boldsymbol{\pi}^{>}(E)\,\boldsymbol{\Sigma}^{\boldsymbol{\Pi}\,<}(E)] \end{aligned} \tag{1.70}$$

The trace in Eq. 1.70 is taken over the allowed electronic transitions (two orbitals per matrix index). $\pi^{(>/<)}(E)$ is defined in Eq.1.61. $\Sigma^{m_1,m_2\,\Pi\,(>/<)}_{m_3,m_4}(E)$ is the Fourier transform of the greater/lesser projection of the electronic Green function $-i\langle T_c\,\hat{D}_{m_1,m_2}(\tau)\hat{D}^{\dagger}_{m_3,m_4}(\tau')\rangle$. The first term inside the trace in Eq.1.70 describes the flux of photons into the system, and is proportional to the measured absorption spectrum. The second term accounts for the flux of photons from the system to the bath, and is proportional to the emission spectrum. To calculate the absorption/emission spectrum we use the NCA expression for $\Sigma^{\Pi\,(>/<)}(E)$.

$$\Sigma^{m_1,m_2\Pi\,(>/<)}_{m_3,m_4}(E) = \sum_{\substack{M_1,M_2\in \mathrm{sys}\\ M_1',M_2'\in \mathrm{sys}}} i\zeta_{M_1}\Delta^{m_1,m_2}_{M_1',M_2'}\Delta^{m_3,m_4\,*}_{M_1,M_2}\int_{-\infty}^{\infty}\frac{dE'}{2\pi}G^{>/<}_{M_1,M_1'}(E+E')\,G^{>/<}_{M_2',M_2}(E') \tag{1.71}$$

1.4.5 Raman Scattering in the NCA

In deriving an expression for Nonequilibrium Raman Scattering we first consider the flux of photons out of the system into the bath (second term inside the trace in Eq. 1.70).[91] This term accounts for coupling of the system to the empty modes of the optical bath. The diagram representing this emission flux is shown in Fig. 1.1a. Fig. 1.1.

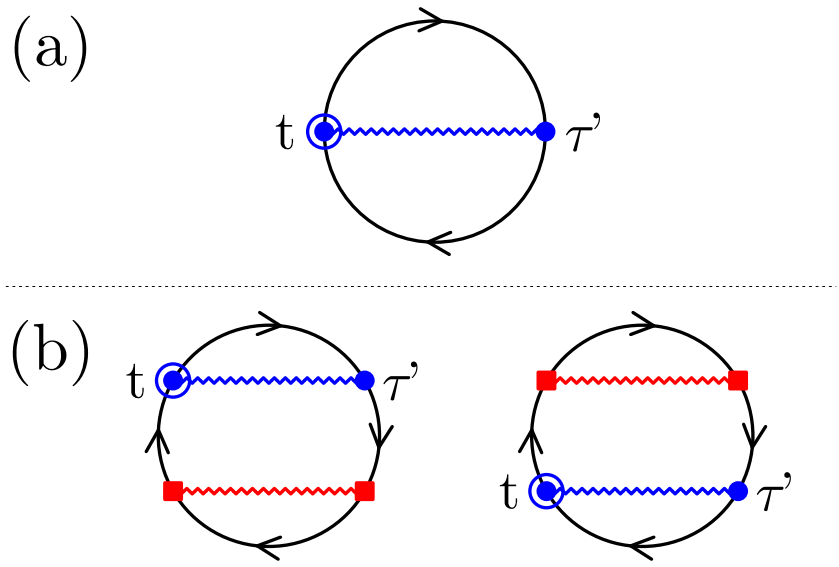

Figure 1.1: Flux diagrams. Shown are (a) general flux diagram and (b) possible flux diagrams in the fourth order perturbation theory in coupling to the radiation bath within the non-crossing approximation. Directed solid line (black) represents dressed pseudoparticle Green function, Eq.(6) of the paper. Non-directed zigzag lines stand for the self-energy due to coupling to radiation bath, Eq.(8) of the paper. Both directions have to be considered for the non-directed zigzag lines. We distinguish interactions with filled initial (red line, squares) and empty final (blue line, circles) modes of the field. Reprinted with permission from *Nano Lett.* ,DOI:10.1021/nl4039532 (2014). Copyright 2014 American Chemical Society.

Next we condsider a second order perturbation in coupling to the optical bath and consider only flux into the system (coupling to filled modes of optical bath). Fig 1.1b. shows the two possible diagrams within the non-crossing approximation. Self-energies due to interactions with the contacts and the thermal bath are not shown explicitly. However, the pseudoparticle Green functions are assumed to be dressed in these interactions (within NCA). As usual, summation over all state indices and integration over contour variables is assumed at every intersection in the diagram, with the exception of

the circled connection, where the assigned time, t, is the time that the outgoing flux is calculated.

We are interested in the "normal" Raman flux, the Raman scattering process which begins in the ground state of the system, proceeds through the excited states, and returns to the ground state. Ground and excited states here are defined by the isolated molecule (since PP-NEGF is defined in the language of the many-body states of the isolated molecule). In molecular junctions at low bias, where the excited states do not become significantly populated due to electron transfer, this is the main contribution to total Raman scattering. Fig. 8a of Ref [91] shows the contour projection relevant to the process. Though we stress that the PP-NEGF and "quasiparticle" approach of Ref [91] are fundamentally different.

As described in Ref [162] and Ref ,[163] when taking real time projections, within the physical $Q = 1$ subspace, we must consider only contributions with a single lesser pseudoparticle Green functions. Projecting the diagrams in Fig 1.1 within the physical subspace and keeping only lesser projection for the self-energy due to coupling to initial modes (red line), and greater projections for the self-energy due to coupling to final modes (blue line) leads to:

$$\begin{aligned} J(t) = 2\mathrm{Re} \sum_{\substack{g_i,x_1,x_2,g_f \\ \bar{g}_i,\bar{x}_1\bar{x}_2,\bar{g}_f}} \zeta_{g_i} \int_{-\infty}^{t} dt' \int_{-\infty}^{t} dt_1 \int_{-\infty}^{t'} dt_2 \\ \pi^{<}_{g_i x_1,\bar{g}_i\bar{x}_1}(t_1 - t_2)\, \pi^{>}_{g_f x_2,\bar{g}_f\bar{x}_2}(t' - t) \\ G^{>}_{\bar{x}_1\bar{x}_2}(t_2,t')\, G^{>}_{\bar{g}_f g_f}(t',t)\, G^{>}_{x_2 x_1}(t,t_1)\, G^{<}_{g_i\bar{g}_i}(t_1,t_2) \end{aligned} \tag{1.72}$$

Chapter 1 References

[1] Aviram, A. and Ratner, M.A. Chemical Physics Letters **29**, 277 (1974)

[2] Reed, M.; Zhou, C.; Muller, C.; Burgin, T. and Tour, J. Science **278**, 252 (1997)

[3] Nature Nanotechnology **8**, 377 (2013)

[4] Nitzan, A. and Ratner, M.A. Science **300**, 1384 (2003)

[5] Ratner, M.A. Nature Nanotechnology **8**, 378 (2013)

[6] Aradhya, S.V. and Venkataraman, L. Nature Nanotechnology **8**, 399 (2013)

[7] Reddy, P.; Jang, S.Y.; Segalman, R.A. and Majumdar, A. Science **315**, 1568 (2007)

[8] Ludoph, B. and van Ruitenbeek, J.M. Physical Review B **59**, 12290 (1999)

[9] Widawsky, J.R.; Darancet, P.; Neaton, J.B. and Venkataraman. Nano Letters **12**, 354 (2012)

[10] Carter, J.A.; Wang, Z.; Fujiwara, H. and Dlott, D.D. The Journal of Physical Chemistry A **113**, 12105 (2009)

[11] Wang, Z.; Carter, J.A.; Lagutchev, A.; Koh, Y.K.; Seong, N.H.; Cahill, D.G. and Dlott, D.D. Science **317**, 787 (2007)

[12] Nitzan, A. Science **317**, 759 (2007)

[13] Lee, W.; Kim, K.; Jeong, W.; Zotti, L.A.; Pauly, F.; Cuevas, J.C. and Reddy, P. Nature **498**, 209 (2013)

[14] Frei, M.; Aradhya, S.V.; Koentopp, M.; Hybertsen, M.S. and Venkataraman, L. Nano Letters **11**, 1518 (2011)

[15] Xu, B.Q.; Xiao, X.Y. and Tao, N.J. The Journal of the American Chemical Society **125**, 16164 (2003)

[16] Gross, L.; Mohn, F.; Liljeroth, P.; Repp, J.; Giessibl, F.J. and Meyer, G. Science **324**, 1428 (2009)

[17] Gross, L.; Moll, N.; Mohn, F.; Curioni, A.; Meyer, G.; Hanke, F. and Persson, M. Physical Review Letters **107**, 086101 (2011)

[18] Bogani, L. and Wernsdorfer, W. Nature Materials **7**, 179 (2008)

[19] Chen, X.; Fu, Y.S.; Ji, S.H.; Zhang, T.; Cheng, P.; Ma, X.C.; Zou, X.L.; Duan, W.H.; Jia, J.F. and Xue, Q.K. Physical Review Letters **191**, 197208 (2008)

[20] Jo, M.H.; Grose, J.E.; Baheti, K.; Deshmukh, M.M.; Sokol, J.J.; Rumberger, E.M.; Hendrickson, D.N.; Long, J.R.; Park, H. and Ralph, D.C. Nano Letters 2014–2020 (2006)

[21] Petta, J.R.; Slater, S.K. and Ralph, D.C. Physical Review Letters **93**, 136601 (2004)

[22] Sanvito, S. Nature Materials **10**, 484 (2011)

[23] Galperin, M.; Ratner, M.A.; Nitzan, A. and Troisi, A. Science **22**, 1056 (2008)

[24] Galperin, M.; Ratner, M.A. and Nitzan, A. Journal of Physics: Condensed Matter **19**, 103201 (2007)

[25] Reed, M.A. Materials Today **11**, 46 (2008)

[26] Galperin, M.; Nitzan, A. and Ratner, M.A. Physical Review B **73**, 045314 (2006)

[27] Park, H.; Park, J.; Lim, A.K.L.; Anderson, E.H.; Alivisatos, A.P. and McEuen, P.L. Nature **407**, 57 (2000)

[28] Song, H.; Kim, Y.; Jang, Y.H.; Jeong, H.; Reed, M.A. and Lee, T. Nature **462**, 1039 (2009)

[29] Tsutsui, M.; Taniguchi, M. and Kawai, T. Nature Communications **1**, 138 (2010)

[30] Djukic, D. and van Ruitenbeek, J.M. Nano Letters **6**, 789 (2006)

[31] Ballmann, S.; Härtle, R.; Coto, P.B.; Elbing, M.; Mayor, M.; Bryce, M.R.; Thoss, M. and Weber, H.B. Physical Review Letters **109**, 056801 (2012)

[32] Mayor, M.; Weber, H.B.; Reichert, J.; Elbing, M.; von Hänisch, C.; Beckmann, D. and Fischer, M. Angewandte Chimie International Edition **47**, 5834 (2003)

[33] Vazquez, H.; Skouta, R.; Schneebeli, S.; Kamenetska, M.; Breslow, R.; Venkataraman, L. and Hybertsen, M. Nature Nanotechnology **7**, 663 (2012)

[34] Becke, A. Journal of Chemical Physics **98**, 5648 (1993)

[35] R.M.Dreizler and E.K.U.Gross. *Density Functional Theory* (Springer-Verlag, 1990) (1990)

[36] Parr, R.G. and Yang, W. *Density-Functional Theory of Atoms and Molecules* (Oxford University Press, 1989) (1989)

[37] Marques, M.; C.A.Ullrich; F.Noguiera; A.Rubio; K.Burke and E.K.U.Gross, editors. *Time-dependent Density Functional Theory* (Springer, Heidelberg, 2006) (2006)

[38] Ullrich, C.A. *Time-Dependent Density Functional Theory. Concepts and Applications.* (Oxford University Press, 2012) (2012)

[39] Keldysh, L.V. Soviet Physics JETP **20**, 1018 (1965)

[40] Kadanoff, L.P.; Baym, G. and Pines, D. *Quantum Statistical Mechanics: Green's Function Methods in Equilibrium and Nonequilibrium Problems* (W. A. Benjamin, Inc., 1962) (1962)

[41] Rammer, J. and Smith, H. Review of Modern Physics **58**, 323 (1986)

[42] Haug, H. and Jauho, A.P. *Quantum Kinetics in Transport and Optics of Semiconductors.* Springer Series in Solid-State Sciences (Springer-Verlag, Berlin Heidelberg, 1996) (1996)

[43] Abrikosov, A.A.; Gorkov, L.P. and Dzyaloshinski, E.I. *Methods of Quantum Field Theory in Statistical Physics* (Dover Publications, Inc., 1975) (1975)

[44] Kohn, W. and Sham, L.J. Physical Review **140**, A1133 (1965)

[45] Brandbyge, M.; Mozos, J.L.; Ordejón, P.; Taylor, J. and Stokbro, K. Physical Review B **65**, 165401 (2002)

[46] Damle, P.; Ghosh, A.W. and Datta, S. Chemical Physics **281**, 171 (2002)

[47] Xue, Y.; Datta, S. and Ratner, M.A. Chemical Physics **281**, 151 (2002)

[48] Cheng, Z.L.; Skouta, R.; Vazquez, H.; Widawsky, J.R.; Schneebeli, S.; Chen, W.; Hybertsen, M.S.; Breslow, R. and Venkataraman, L. Nature Nanotechnology **6**, 353 (2011)

[49] Hybertsen, M.S.; Venkataraman, L.; Klare, J.E.; Whalley, A.C.; Steigerwald, M.L. and Nuckolls, C. Journal of Physics: Condensed Matter **20**, 374115 (2008)

[50] Schull, G.; Frederiksen, T.; Brandbyge, M. and Berndt, R. Physical Review Letters **103**, 206803 (2009)

[51] Stokbro, K. Journal of Physics: Condensed Matter **20**, 064216 (2008)

[52] Frederiksen, T.; Paulsson, M.; Brandbyge, M. and Jauho, A.P. Physical Review B **75**, 205413 (2007)

[53] Kim, Y.; Garcia-Lekue, A.; Sysoiev, D.; Frederiksen, T.; Groth, U. and Scheer, E. Physical Review Letters **109**, 226801 (2012)

[54] Sergueev, N.; Roubtsov, D. and Guo, H. Physical Review Letters **95**, 146803 (2005)

[55] Sergueev, N.; Demkov, A.A. and Guo, H. Physical Review B **75**, 233418 (2007)

[56] Galperin, M.; Ratner, M.A. and Nitzan, A. Journal of Chemical Physics **121**, 11965 (2004)

[57] Ho, W. The Journal of Chemical Physics **117**, 11033 (2002)

[58] Lortscher, E.; Ciszek, J.W.; Tour, J. and Riel, H. Small **2**, 973 (2006)

[59] Wei, J.H.; Xie, S.J.; Mei, L.M.; Berakdar, J. and Yan, Y. Organic electronics **8**, 487 (2007)

[60] Wu, S.W.; Ogawa, N.; Nazin, G.V. and Ho, W. The Journal of Physical Chemistry C **112**, 5241 (2008)

[61] Blum, A.S.; Kushmerick, J.G.; Long, D.P.; Patterson, C.H.; Yang, J.C.; Henderson, J.C.; Yao, Y.; Tour, J.M.; Shashidhar, R. and Ratna, B.R. Nature Materials **4** (2005)

[62] Chen, J.; Reed, M.A.; Rawlett, A.M. and Tour, J.M. Science **286**, 1550 (1999)

[63] Kiehl, R.A.; Le, J.D.; Candra, P.; Hoye, R.C. and Hoye, T.R. Applied Physics Letters **88**, 172102 (2006)

[64] Rinkio, M.; Johansson, A.; Kotimaki, V. and Torma, P. ACS Nano **4**, 3356 (2010)

[65] Repp, J.; Liljeroth, P. and Meyer, G. Nature Physics **6**, 975 (2010)

[66] Seldenthuis, J.S.; van der Zant, H.S.J.; Ratner, M.A. and Thijssen, J.M. ACS Nano **2**, 1445 (2008)

[67] Galperin, M. and Nitzan, A. Physical Chemistry Chemical Physics **14**, 9421 (2012)

[68] Natelson, D.; Li, Y. and Herzog, J.B. Physical Chemistry Chemical Physics **15**, 5262 (2013)

[69] Shamai, T. and Selzer, Y. Chemical Society Reviews **40**, 2293 (2011)

[70] Banik, M.; Nag, A.; El-Khoury, P.Z.; Rodriguez Perez, A.; Guarrotxena, N.; Bazan, G.C. and Apkarian, V.A. The Journal of Physical Chemistry C **116**, 10415 (2012)

[71] Kleinman, S.L.; Frontiera, R.R.; Henry, A.I.; Dieringer, J.A. and Van Duyne, R.P. Physical Chemistry Chemical Physics **15**, 21 (2013)

[72] Michaels, A.M.; Jiang, J. and Brus, L. The Journal of Physical Chemistry B **104**, 11965 (2000)

[73] Ward, D.R.; Grady, N.K.; Levin, C.S.; Halas, N.J.; Wu, Y.; Nordlander, P. and Natelson, D. Nano Letters **7**, 1396 (2007)

[74] Sharma, B.; Frontiera, R.R.; Henry, A.I.; Ringe, E. and Duyne, R.P.V. Materials Today **15**, 16 (2012)

[75] Ioffe, Z.; Shamai, T.; Ophir, A.; Noy, G.; Yutsis, I.; Kfir, K.; Cheshnovsky, O. and Selzer, Y. Nature Nanotechnology **3**, 727 (2008)

[76] Ward, D.R.; Halas, N.J.; Ciszek, J.W.; Tour, J.M.; Wu, Y.; Nordlander, P. and Natelson, D. Nano Letters **8**, 919 (2008)

[77] Ward, D.R.; Corley, D.A.; Tour, J.M. and Natelson, D. Nature Nanotechnology **6**, 33 (2011)

[78] Banik, M.; El-Khoury, P.Z.; Nag, A.; Rodriguez-Perez, A.; Guarrottxena, N.; Bazan, G.C. and Apkarian, V.A. ACS Nano **6**, 10343 (2012)

[79] Zhang, R.; Zhang, Y.; Dong, Z.C.; Jiang, S.; Zhang, C.; Chen, L.G.; Zhang, L.; Liao, Y.; Aizpurua, J.; Luo, Y.; Yang, J.L. and Hou, J.G. Nature **498**, 82 (2013)

[80] El-Khoury, P.Z.; Hu, D.; Apkarian, V.A. and Hess, W.P. Nano Lett. **13**, 1858 (2013)

[81] Matsuhita, R.; Horikawa, M.; Naitoh, Y.; Nakamura, H. and Kiguchi, M. The Journal of Physical Chemistry C **117**, 1791 (2013)

[82] Jiang, N.; Foley, E.T.; Klingsporn, J.M.; Sonntag, M.D.; Valley, N.A.; Dieringer, J.A.; Seideman, T.; Schatz, G.C.; Hersam, M.C. and Van Duyne, R.P. Nano Lett. **12**, 5061 (2012)

[83] Liu, Z.; Ding, S.Y.; Chen, Z.B.; Wang, X.; Tian, J.H.; Anema, J.R.; Zhou, X.S.; Wu, D.Y.; Mao, B.W.; Xu, X.; Ren, B. and Tian, Z.Q. Nat. Commun. **2**, 305 (2011)

[84] Konishi, T.; Kiguchi, M.; Takase, M.; Nagasawa, F.; Nabika, H.; Ikeda, K.; Uosaki, K.; Ueno, K.; Misawa, H. and Murakoshi, K. J. Am. Chem. Soc. **135**, 1009 (2013)

[85] Galperin, M. and Nitzan, A. The Journal of Chemical Physics **124**, 234709 (2006)

[86] Galperin, M. and Nitzan, A. The Journal of Physical Chemistry Letters **2**, 2110 (2011)

[87] Galperin, M. and Nitzan, A. Phys. Chem. Chem. Phys. **14**, 9421 (2012)

[88] Galperin, M. and Nitzan, A. Phys. Rev. B **84**, 195325 (2011)

[89] Galperin, M.; Ratner, M.A. and Nitzan, A. J. Chem. Phys. **130**, 144109 (2009)

[90] Galperin, M.; Ratner, M.A. and Nitzan, A. Nano Lett. **9**, 758 (2009)

[91] Galperin, M.; Nitzan, A. and Ratner, M.A. The Journal of Chemical Physics **130**, 144109 (2009)

[92] Galperin, M.; Nitzan, A. and Ratner, M. Nano Letters **9**, 758 (2009)

[93] Park, T.H. and Galperin, M. Europhysics Letters **95**, 27001 (2011)

[94] Arntsen, C.; Lopata, K.; Wall, M.R.; Bartell, L. and Neuhauser, D. The Journal of Chemical Physics **134**, 084101 (2011)

[95] Gao, Y. and Neuhauser, D. The Journal of Chemical Physics **137**, 074113 (2012)

[96] Lopata, K. and Neuhauser, D. The Journal of Chemical Physics **131**, 014701 (2009)

[97] Lopata, K. and Neuhauser, D. The Journal of Chemical Physics **130**, 104707 (2009)

[98] Mullin, J. and Schatz, G. The Journal of Physical Chemistry A **116**, 1931 (2012)

[99] Salomon, A.; Gordon, R.J.; Prior, Y.; Seideman, T. and Sukharev, M. Physical Review Letters **109**, 073002 (2012)

[100] Sukharev, M. and Nitzan, A. Physical Review A **84**, 043802 (2011)

[101] Coomar, A.; Arntsen, C.; Lopata, K.A.; Pistinner, S. and Neuhauser, D. The Journal of Chemical Physics **135**, 084121 (2011)

[102] Gray, S.K. and Kupka, T. Physical Review B **68**, 045415 (2003)

[103] Henry, A.I.; Bingham, J.M.; Ringe, E.; Marks, L.D.; Schatz, G.C. and Duyne, R.P.V. The Journal of Physical Chemistry C **115**, 9291 (2011)

[104] McMahon, J.M.; Li, S.; Ausman, L.K. and Schatz, G.C. The Journal of Physical Chemistry C **116**, 1627 (2012)

[105] Yelk, J.; Sukharev, M. and Seideman, T. The Journal of Chemical Physics **129**, 064706 (2008)

[106] Fainberg, B.D.; Sukharev, M.; Park, T.H. and Galperin, M. Physical Review B **83**, 205425 (2011)

[107] Sukharev, M. and Galperin, M. Physical Review BP **81**, 165307 (2010)

[108] Luk'yanchuk, B.; Zheludev, N.I.; Maier, S.A.; Halas, N.J.; Nordlander, P.; Giessen, H. and Chong, C.T. Nat Mater **9**, 707 (2010)

[109] Wiederrecht, G.P.; Wurtz, G.A. and Hranisavljevic, J. Nano Letters **4**, 2121 (2004)

[110] Wurtz, G.A.; Evans, P.R.; Hendren, W.; Atkinson, R.; Dickson, W.; Pollard, R.J.; Zayats, A.V.; Harrison, W. and Bower, C. Nano Letters **7**, 1297 (2007)

[111] Artuso, R.D. and Bryant, G.W. Nano Lett. **8**, 2106 (2008). PMID: 18558787

[112] Ridolfo, A.; Di Stefano, O.; Fina, N.; Saija, R. and Savasta, S. Phys. Rev. Lett. **105**, 263601 (2010)

[113] Zhang, W.; Govorov, A.O. and Bryant, G.W. Phys. Rev. Lett. **97**, 146804 (2006)

[114] Artuso, R.D. and Bryant, G.W. Phys. Rev. B **82**, 195419 (2010)

[115] Manjavacas, A.; García de Abajo, F.J. and Nordlander, P. Nano Letters **11**, 2318 (2011)

[116] Nie, S. and Emory, S.R. Science **275**, 1102 (1997)

[117] Zhang, J.; Fu, Y.; Chowdhury, M.H. and Lakowicz, J.R. Nano Letters **7**, 2101 (2007)

[118] Chen, Y.C.; Zwolak, M. and Di Ventra, M. Nano Letters **4**, 1709 (2004)

[119] Chen, Y.C. and Di Ventra, M. Physical Review Letters **95**, 166802 (2005)

[120] Jorn, R. and Seideman, T. The Journal of Chemical Physics **131**, 244114 (2009)

[121] Jorn, R. and Seideman, T. Accounts of Chemical Research **43**, 1186 (2010)

[122] Lorente, N. and Gauyacq, J.P. Physical Review Letters **103**, 176601 (2009)

[123] Montgomery, M.; Todorov, T. and Sutton, A. Journal of Physics: Condensed Matter **14**, 5377 (2002)

[124] Nitzan, A. Annual Review of Physical Chemistry **52**, 681 (2001)

[125] Landauer, R. Philosophical Magazine **21**, 863 (1970)

[126] Datta, S. *Electronic Transport in Mescoscopic Systems* (Cambridge University Press, 1995) (1995)

[127] Bonca, J. and Trugman, S.A. Physical Review Letters **75**, 2566 (1995)

[128] Galperin, M.; Nitzan, A. and Ratner, M.A. Physical Review B **73**, 045314 (2006)

[129] Mitra, A.; Aleiner, I. and Millis, A.J. Physical Review B **69**, 245302 (2004)

[130] Breuer, H.P. and Petruccione, F. *The Theory of Open Quantum Systems* (Oxford University Press, 2006) (2006)

[131] Nitzan, A. *Chemical Dynamics in Condensed Phases* (Oxford University Press, 2006) (2006)

[132] Harbola, U.; Esposito, M. and Mukamel, S. Physical Review B **74**, 235309 (2006)

[133] Selzer, Y. and Peskin, U. The Journal of Physical Chemistry C **117**, 22369 (2013)

[134] Zelinskyy, Y. and May, V. Nano Letters **12**, 446 (2012)

[135] Leijnse, M. and Wegewijs, M.R. Physical Review B **78**, 235424 (2008)

[136] Schultz, M.G. and von Oppen, F. Physical Review B **80**, 033302 (2009)

[137] Esposito, M. and Galperin, M. Physical Review B **79**, 205303 (2009)

[138] Esposito, M. and Galperin, M. The Journal of Physical Chemistry C **114**, 20362 (2010)

[139] Jang, S.; Cao, J. and Silbey, R.J. The Journal of Chemical Physics **116**, 2705 (2002)

[140] Koller, S.; Grifoni, M.; Leijnse, M. and Wegewijs, M.R. Physical Review B **82**, 235307 (2010)

[141] Karlström, O.; Emary, C.; Zedler, P.; Pedersen, J.N.; Bergenfeldt, C.; Samuelsson, P.; Brandes, T. and Wacker, A. Journal of Physics A: Mathematical and Theoretical **46**, 065301 (2013)

[142] Ovchinnikov, I.V. and Neuhauser, D. Journal of Chemical Physics **122**, 024707 (2005)

[143] Pedersen, J.N. and Wacker, A. Physical Review B **72**, 195330 (2005)

[144] Saptsov, R.B. and Wegewijs, M.R. Physical Review B **86**, 235432 (2012)

[145] Fransson, J. Physical Review B **72**, 075314 (2005)

[146] Izyumov, Y.A.; Chaschin, N.I.; Alexeev, D.S. and Mancini, F. The European Physical Journal B - Condensed Matter and Complex Systems **45**, 69 (2005)

[147] Ruckenstein, A.E. and Schmitt-Rink, S. Physical Review B **38**, 7188 (1988)

[148] Sandalov, I.; Johansson, B. and Eriksson, O. International Journal of Quantum Chemistry **94**, 113 (2003)

[149] Shastry, B.S. Physical Review B **81** (2010)

[150] Fransson, J.; Eriksson, O. and Sandalov, I. Physical Review B **66**, 195319 (2002)

[151] Galperin, M.; Nitzan, A. and Ratner, M.A. Physical Review B **78**, 125320 (2008)

[152] Yeganeh, S.; Ratner, M.A.; Galperin, M. and Nitzan, A. Nano Letters **9**, 1770 (2009)

[153] Pedersen, J.N.; Bohr, D.; Wacker, A.; Novotný, T.; Schmitteckert, P. and Flensberg, K. Physical Review B **79**, 125403 (2009)

[154] Bonch-Bruevich, V.L. and Tyablikov, S.V. *The Green Function method in Statistical Mechanics* (North-Holland Publishing Company, 1962) (1962)

[155] Levy, T.J. and Rabani, E. Journal of Physics: Condensed Matter **25**, 115302 (2013)

[156] Levy, T.J. and Rabani, E. The Journal of Chemical Physics **138**, 164125 (2013)

[157] Meir, Y. and Golub, A. Physical Review Letters **88**, 116802 (2002)

[158] Sivan, N. and Wingreen, N.S. Physical Review B **54**, 11622 (1996)

[159] Wingreen, N.S. and Meir, Y. Physical Review B **49**, 40 (1994)

[160] White, A.J. and Galperin, M. Physical Chemistry Chemical Physics **14**, 13809 (2012)

[161] White, A.J.; Fainberg, B.D. and Galperin, M. The Journal of Physical Chemistry Letters **3**, 2738 (2012)

[162] Eckstein, M. and Werner, P. Physical Review B **82**, 115115 (2010)

[163] Oh, J.H.; Ahn, D. and Bubanja, V. Physical Review B **83**, 205302 (2011)

[164] Anisimov, V. and Izyumov, Y. *Electronic Structure of Strongly Correlated Materials* (Springer, 2010) (2010)

[165] Kotliar, G.; Savrasov, S.Y.; Haule, K.; Oudovenko, V.S.; Parcollet, O. and Marianetti, C.A. Review of Modern Physics **78**, 865 (2006)

[166] Fano, U. Phys. Rev. **124**, 1866 (1961)

[167] Manjavacas, A.; Abajo, F.J.G.D. and Nordlander, P. Nano Lett. **11**, 2318 (2011)

[168] Jauho, A.P.; Wingreen, N.S. and Meir, Y. Phys. Rev. B **50**, 5528 (1994)

[169] Luttinger, J.M. and Ward, J. Physical Review **118**, 1417 (1960)

Chapter 2

Inelastic transport: a pseudoparticle approach

Alexander J. White[1] **and Michael Galperin**[1]

[1] Department of Chemistry and Biochemsitry, University of California at San Diego, La Jolla CA 92093, USA

Physical Chemistry Chemical Physics **14**, 13809-13819 (2012). Reproduced by permission of the PCCP Owner Societies.

We discuss a pseudoparticle NEGF approach as a tool to describe transport in molecular junctions in the language of many-body states of the molecule. A method developed by Oh et al. [Phys. Rev. B **83**, 205302 (2011)] is applied to inelastic transport in the case of strong electron-vibron interaction. The approach can be seen as a generalization of the exact mapping developed by Bŏnca and Trugman [Phys. Rev. Lett. **75**, 2566 (1995)] which includes information on the Pauli exclusion principle and Fermi electron distribution in the leads. Within simple model calculations of inelastic transport in junctions, we compare the pseudoparticle approach to other approximate NEGF schemes.

2.1 Introduction

Electron transfer is a fundamental process behind all oxidation-reduction reactions. Thus, the theoretical description of electron transfer rates, Marcus theory,[1–7] is widely used in chemistry[8–13] and biology[14–19] for the description of a variety of phenomena ranging from electrochemistry and processes controlling corrosion, to photosynthesis, to vision and the sense of smell (for reviews see *e.g.* Refs.[20–22]).

While electron transfer theory is focused on donor-bridge-acceptor (DBA) systems, molecular electronics[23] studies electron transfer in metal-molecule-metal (and similar) junctions. Similar to Marcus's expression for the DBA electron transfer rate, the expression for the (elastic) current voltage characteristic of a molecular junction, the Landauer formula,[24–29] utilizes scattering theory considerations. A relationship between electron transfer rates and molecular conduction was discussed in the literature[30] (see Ref.[31] for a comprehensive review).

Inelastic electron and phonon (energy) transfer play an important role in transport characteristics of molecular junctions due to the flexibility of the molecular species. Since scattering theory was shown to be inadequate for the description of inelastic processes in junctions,[32,33] alternative theoretical schemes were utilized. In particular, a common approach is the nonequilibrium Green function (NEGF) technique.[34–38] This quantum field theory method, together with density functional theory (NEGF-DFT), provided an *ab initio* methodology for analysis of molecular conduction using quantum chemistry software.[39–44] While far from being rigorous[45] the NEGF-DFT methodology appeared to be quite accurate in predicting off-resonant transport characteristics.

NEGF-DFT (and similar methods) becomes inconvenient in the resonant tunneling regime when oxidation/reduction of a molecule leads to a significant change in its electronic and vibrational structure,[46] or when the Born-Oppenheimer approximation fails.[47] In such situations, a description of transport utilizing a basis of many-body molecular states (rather than single-particle molecular orbitals) is desirable. The latter is an alternative way to introduce quantum chemistry methods into molecular transport simulations.

Our recent attempt to simulate transport in molecular junctions in the language of many-body states[48] utilizes the Hubbard NEGF methodology. While this is a vi-

able alternative to the standard NEGF methods, several problems[49,50] related to the approximations involved are yet to be resolved. In particular, Ref.[50] indicates that the Hubbard-I approximation may violate the Hermiticity of a reduced density matrix.

Another popular state oriented approach to transport simulations uses a reduced density matrix description.[51–54] Usually quantum master equations (QME) account for system-bath coupling at a finite order of perturbation theory. Such formulations (at least partially) miss information on the hybridization of the molecular states with the metal states of the contacts, which may lead to inadequate prediction of junction characteristics.[55,56] Degeneracies in the molecular spectrum require special care within the QME scheme.[57] Finally, sometimes the standard QME treatment may lead to unphysical results.[58–62] Note that more involved QME formulations are available in the literature. For example, Ref.[63] utilizes an inifinite hierarchy of equations-of-motion, while Ref.[64] is based on a coarse graining procedure.

A state based approach to transport is also useful for the description of inelastic effects in junctions. Initially, a consistent treatment of inelastic transport in molecular junctions was available only for weak (relative to molecule-contact) interactions between electronic and vibrational degrees of freedom. A standard perturbation theory within NEGF, mostly in the form of the self-consistent Born approximation (SCBA), was employed.[65,66] Later, stronger electron-vibron interaction in junctions was treated either with rate equations[32,67,68] or approximate NEGF schemes.[33,69–71] The first shares advantages and limitations of the QME approaches, the latter is able to account for linear electron-vibron coupling of moderate strength. An approach capable of treating inelastic interaction of arbitrary type and strength was formulated in Ref.[72] for zero temperature, and later generalized to finite temperatures in Ref.[73] The formalism of Ref.[72] is based on single-electron scattering consideration, which limits its ability to describe junction transport, where inelastic scattering has to be treated as a many-body process. Attempts to complement the formalism of Ref.[72] include a self-consistent inelastic scattering scheme[74] and expansion in the molecule-contact coupling performed for the retarded GF.[75]

Here we want to attract the attention of the molecular electronics community to another field theory method – the pseudoparticle NEGF (the auxiliary operator repre-

sentation in the NEGF).[76–80] Originally the method was developed to describe strongly correlated systems (*e.g.* the Kondo effect). However, it can also be applied to a simpler problem of describing transport in the molecular states language all the way down to the Kondo temperature, T_K. The pseudoparticle NEGF has several advantages: 1. The method is conceptually simple; 2. Its practical implementations rely on a set of controlled approximations (standard diagrammatic perturbation theory techniques can be applied); 3. Already in its simplest implementation, the non-crossing approximation (NCA), the pseudoparticle NEGF goes beyond standard QME approaches by accounting for both non-Markovian effects and hybridization of molecular states; 4. The method is capable of treating transport in the language of many-body states of the isolated molecule, exactly accounting for all the on-the-molecule interactions. As with any approximate scheme, the pseudoparticle NEGF has its own limitations,[81] however those are important mostly for the low-temperature region $T \ll T_K$. We rely on the pseudoparticle NEGF technique as an effective way to combine generality of the scattering formalism of Refs.[72,73] with many-body character of transport in molecular junctions. Note that the applicability of state-base approaches to realistic calculations has been demonstrated in a number of papers (see *e.g.* Ref.[48]). Here we focus on demonstrating the capabilities of the pseudoparticle NEGF within generic models.

The structure of the paper is as follows. After introducing the model in Section 2.2, we present details of the pseudoparticle NEGF approach in Section 2.3. Numerical examples are discussed in Section 2.4. Section 2.5 concludes.

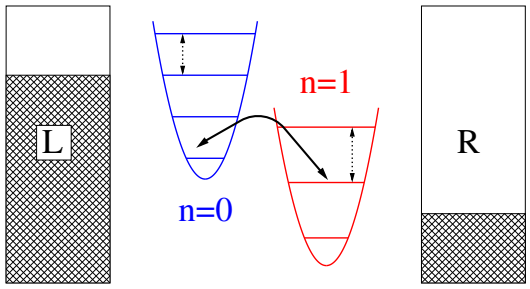

Figure 2.1: Sketch of the model. Electron transfer between the molecule and contacts, L and R, induces transitions between vibronic states of empty ($n = 0$) and charged ($n = 1$) molecule (solid line). Energy transfer between the molecule and thermal bath B induces transitions within the two vibronic manifolds (dashed lines).

2.2 Model

We consider a molecule, M, coupled to two metallic contacts, L and R, and to a thermal bath, B. The molecule has electronic and vibrational degrees of freedom, which are coupled to each other. The contacts L and R are assumed to be free electron reservoirs, each at its own equilibrium. The bath B represents vibrational degrees of freedom interacting with the molecular vibrations, but not with its electronic degrees of freedom. For example, these may be phonons in the contacts or vibrational modes of other molecules. The bath B is modeled as a set of free harmonic oscillators. Difference in the contacts' chemical potentials, μ_L and μ_R, causes charge flow through the molecule and defines a nonequilibrium distribution of electron population on the molecule. Molecular vibrations are heated by the electron flux, and dissipate the energy to the thermal bath. Competition between these two processes defines a nonequilibrium distribution of the molecular vibration. The system Hamiltonian in the second quantized form is (here and below $\hbar = 1$)

$$\hat{H} = \hat{H}_M + \sum_{K=L,R,B} \left(\hat{H}_K + \hat{V}_K \right) \tag{2.1}$$

where $\hat{H}_M$ is the molecular Hamiltonian (we discuss it below),

$$\hat{H}_{L(R)} = \sum_{\kappa \in L(R)} \varepsilon_\kappa \hat{c}_\kappa^\dagger \hat{c}_\kappa \tag{2.2}$$

$$\hat{H}_B = \sum_{\beta \in B} \omega_\beta \hat{b}_\beta^\dagger \hat{b}_\beta \tag{2.3}$$

are the Hamiltonians of the baths,

$$\hat{V}_{L(R)} = \sum_{\substack{\nu \in M \\ \kappa \in L(R)}} \left(V_{\kappa,\nu} \hat{c}_\kappa^\dagger \hat{c}_\nu + H.c. \right) \tag{2.4}$$

$$\hat{V}_B = \sum_{\substack{\alpha \in M \\ \beta \in B}} \left(W_{\alpha\beta} \hat{a}_\alpha^\dagger \hat{b}_\beta + H.c. \right) \tag{2.5}$$

describes electron and phonon (or vibrational excitation) transfer between the molecule and corresponding bath, respectively. Here and below greek subscripts indicate effective single-particle orbitals, latin subscripts will be used for molecular many-body states.

In Eqs. (2.1)-(2.5) $\hat{c}_\nu^\dagger$ ($\hat{c}_\nu$) and $\hat{c}_\kappa^\dagger$ ($\hat{c}_\kappa$) are electron creation (annihilation) operators on the molecule and contacts, respectively. $\hat{a}_\alpha^\dagger$ ($\hat{a}_\alpha$) and $\hat{b}_\beta^\dagger$ ($\hat{b}_\beta$) are creation (annihilation) operators for molecular vibration and phonon in the thermal bath.

The form of the molecular Hamiltonian $\hat{H}_M$ can, in principle, be as general as desired. For example, it can include electron-electron, electron-vibron, or spin-exchange interactions of any type and strength as long as they are confined to the molecular subspace only. In our inelastic transport calculations below, we consider three different models:

1. A simple model of single-level ($\nu = 0$) linearly coupled to a single molecular vibration ($\alpha = 0$)

$$\hat{H}_M = \varepsilon_0 \hat{c}_0^\dagger \hat{c}_0 + \omega_0 \hat{a}_0^\dagger \hat{a}_0 + M(\hat{a}_0 + \hat{a}_0^\dagger)\hat{c}_0^\dagger \hat{c}_0 \tag{2.6}$$

2. A two-level bridge ($\nu = 1, 2$) with non-local electron coupling to a single molecular vibration ($\alpha = 0$)

$$\begin{aligned} \hat{H}_M = &\sum_{\nu=1,2} \varepsilon_\nu \hat{c}_\nu^\dagger \hat{c}_\nu + \omega_0 \hat{a}_0^\dagger \hat{a}_0 \\ &+ \left[t + M(\hat{a}_0 + \hat{a}_0^\dagger) \right] (\hat{c}_1^\dagger \hat{c}_2 + \hat{c}_2^\dagger \hat{c}_1) \end{aligned} \tag{2.7}$$

3. A simple model of a molecule (represented by a quantum dot) with molecular charging state dependent vibrational frequency. The molecular Hamiltonian is represented in terms of vibronic states $\{|ev\rangle\}$ as

$$\hat{H}_M = \sum_{e=0,\uparrow,\downarrow,2} \sum_{v=0}^{\infty} |ev\rangle \, E_{ev} \, \langle ev| \tag{2.8}$$

where

$$E_{0v} = \omega^{(0)}(v + \frac{1}{2}) \tag{2.9}$$

$$E_{\nu v} = \varepsilon_\nu + \omega^{(1)}(v + \frac{1}{2}) \quad (\nu = \uparrow, \downarrow) \tag{2.10}$$

$$E_{2v} = \varepsilon_\uparrow + \varepsilon_\downarrow + U + \omega^{(2)}(v + \frac{1}{2}) \tag{2.11}$$

Here ε_ν is on-site energy of single-particle orbital ν and U is the on-site Coulomb repul-

sion.

The first model, Eq.(2.6), allows us to compare the pseudoparticle NEGF calculations to results presented for the model within the standard NEGF scheme referenced earlier.[33] The second and third models, Eqs. (2.7) and (2.8), are examples where consideration within standard NEGF schemes is non-trivial. Note that, contrary to the usual NEGF treatment, where electronic and vibrational degrees of freedom are described by their own quantum fields, our goal here is a scheme describing the molecule in a basis of its vibronic states $\{|m>\}$ (see Fig. 2.1 for a sketch).

2.3 Pseudoparticle approach to transport

A set of molecular many-body states, $\{|m>\}$, defines the set of pseudoparticles to be considered. This set may be eigenstates obtained by diagonalizing the molecular Hamiltonian, $\hat{H}_M$, or any other molecular state basis. Let $\hat{d}_m^\dagger$ ($\hat{d}_m$) be the creation (annihilation) operator for the state $|m>$. These operators satisfy usual commutation relations (Fermi or Bose - depending on the type of the state) within an extended Hilbert space. The physical subspace of the total pseudoparticle Hilbert space is defined by the constraint

$$\hat{Q} = \sum_m \hat{d}_m^\dagger \hat{d}_m = 1 \tag{2.12}$$

This constraint can be implemented *e.g.* by introducing a Lagrange multiplier[80,82] or an operator delta function leading to the appearance of a complex chemical potential.[76,83]

The electron and vibron operators in the molecular subspace can be represented in terms of pseudoparticles as

$$\hat{c}_\nu^\dagger \equiv \sum_{m_1,m_2} \xi_{m_1 m_2}^\nu \hat{d}_{m_1}^\dagger \hat{d}_{m_2} \tag{2.13}$$

$$\hat{a}_\alpha^\dagger \equiv \sum_{m_1,m_2} \chi_{m_1 m_2}^\alpha \hat{d}_{m_1}^\dagger \hat{d}_{m_2} \tag{2.14}$$

where

$$\xi^{\nu}_{m_1 m_2} \equiv \langle m_1 | \hat{c}^{\dagger}_{\nu} | m_2 \rangle \tag{2.15}$$

$$\chi^{\alpha}_{m_1 m_2} \equiv \langle m_1 | \hat{a}^{\dagger}_{\alpha} | m_2 \rangle \tag{2.16}$$

are the electron- and vibron-pseudoparticle overlap tensors.

The quantities of interest are dressed single-particle Green functions (GFs) for the pseudoparticles, G, electrons in the contacts, C^K $(K = L, R)$, and phonons in the thermal bath, F^B, defined in the molecular subspace as

$$G_{m_1 m_2}(\tau_1, \tau_2) = -i \langle T_c \, \hat{d}_{m_1}(\tau_1) \, \hat{d}^{\dagger}_{m_2}(\tau_2) \rangle \tag{2.17}$$

$$C^K_{\nu_1 \nu_2}(\tau_1, \tau_2) = \sum_{\kappa_1, \kappa_2 \in K} V_{\nu_1 \kappa_1} C_{\kappa_1 \kappa_2}(\tau_1, \tau_2) V_{\kappa_2 \nu_2} \tag{2.18}$$

$$F^B_{\alpha_1 \alpha_2}(\tau_1, \tau_2) = \sum_{\beta_1, \beta_2 \in B} W_{\alpha_1 \beta_1} F_{\beta_1, \beta_2}(\tau_1, \tau_2) W_{\beta_2 \alpha_2} \tag{2.19}$$

where T_c is the contour ordering operator, $\tau_{1,2}$ are contour variables, and

$$C_{\kappa_1 \kappa_2}(\tau_1, \tau_2) = -i \langle T_c \, \hat{c}_{\kappa_1}(\tau_1) \, \hat{c}^{\dagger}_{\kappa_2}(\tau_2) \rangle \tag{2.20}$$

$$F_{\beta_1, \beta_2}(\tau_1, \tau_2) = -i \langle T_c \, \hat{b}_{\beta_1}(\tau_1) \, \hat{b}^{\dagger}_{\beta_2}(\tau_2) \rangle \tag{2.21}$$

are GFs for electrons in the contacts and phonons in the thermal bath, defined in subspaces of the corresponding baths. Note that the Green functions C and F, Eqs. (2.20) and (2.21), differ from the free particle GFs in the baths, which are routinely introduced within the standard NEGF scheme, since they are dressed by interaction with the molecular pseudoparticles. Below we will use capital letters to indicate dressed GFs, while lower case letters will be utilized for the bare (non-interacting) GFs.

In the extended Hilbert space the single-psudoparticle GF G, Eq.(2.17), satisfies the usual Dyson equation

$$\mathbf{G} = \mathbf{g} + \mathbf{g}\boldsymbol{\Sigma}\mathbf{G} \tag{2.22}$$

where $\mathbf{g}$ is the bare GF, i.e. the GF in the absence of molecule-baths couplings, Eqs. (2.4)-(2.5), and $\boldsymbol{\Sigma}$ is the pseudoparticles self-energy due to coupling to the contacts and thermal bath, Eq.(2.44) (see Appndexes A and B for details). Similar expressions can be written

for the GFs C^K, Eq.(2.18), and F^B, Eq.(2.19). Eq.(2.22) is written for the pseudoparticle GF (2.17) defined on the Keldysh contour.

In practice, one first formulates a standard set of equations for the GFs (2.17)-(2.19) (i.e. Eq.(2.22) and similar to it for the other GFs) in the full pseudoparticle Hilbert space, and then projects these expressions onto the physical subspace, so that contributions to physical observables come from the subspace $Q = 1$ (see *e.g.* Ref.[76] for details). As a result we solve equations for retarded and lesser projections of the GF. At steady state these equations are

$$\mathbf{G}^r(E) = [E\mathbf{I} - \mathbf{H}_M - \mathbf{\Sigma}^r(E)]^{-1} \tag{2.23}$$

$$\mathbf{G}^<(E) = \mathbf{G}^r(E)\,\mathbf{\Sigma}^<(E)\,\mathbf{G}^a(E) \tag{2.24}$$

Here the molecular Hamiltonian, pseudoparticle GFs and self-energies are presented as matrices in the many-body basis of the molecule. Note that Eq.(2.23) belongs to the $Q = 0$ subspace, while Eq.(2.24) is projected onto the $Q = 1$ subspace of the total pseudoparticle Hilbert space. Thus self-consistent solutions for the two equations are decoupled with Eq.(2.23) solved first. Also, projection to the $Q = 1$ subspace requires normalization (see *e.g.* Ref.[76] for details)

$$\sum_m i\zeta_m \int_{-\infty}^{+\infty} \frac{dE}{2\pi} G^<_{mm}(E) = 1 \tag{2.25}$$

In the calculations we enforce normalization (2.25) at each step of the self-consistent cycle.

Eqs. (2.23) and (2.24) have to be solved self-consistently, since the self-energies, Σ^r and $\Sigma^<$, in these equations depend on the pseudoparticle GFs, G^r and $G^<$, as well as the bare GFs for electrons in the contacts and phonons in the thermal bath (see Appendix B for details). An initial guess for the pseudoparticle GFs may be based, for example, on the isolated molecule limit and the thermal distribution for the many-body molecular states or taken from a QME solution for the junction.

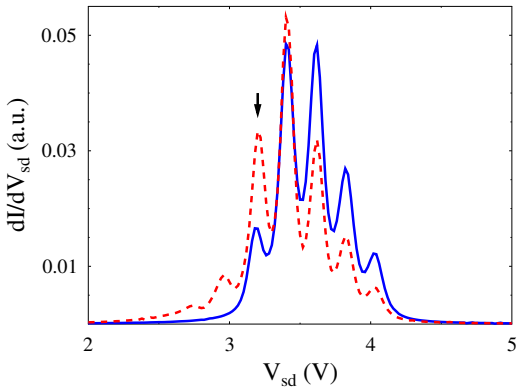

Figure 2.2: Conductance vs. applied bias calculated for the single-level model (2.1)-(2.6) within the pseudoparticle NEGF approach. Shown are results for thermalized (solid line, blue) and non-equilibirum (dashed line, red) molecular vibration. Arrow indicates position of the elastic peak. See text for parameters.

Current at the interface K ($= L, R$) is given by[38]

$$I_K(t) \equiv \langle \hat{I}_K(t) \rangle = -\frac{d}{dt} \left\langle \sum_{\kappa \in K} \hat{c}^\dagger_\kappa(t) \hat{c}_\kappa(t) \right\rangle \tag{2.26}$$

where $\hat{I}_K(t)$ is the current operator

$$\hat{I}_K \equiv i \sum_{\kappa \in K} \sum_{\nu \in M} \left(V_{\kappa\nu} \hat{c}^\dagger_\kappa \hat{c}_\nu - V_{\nu\kappa} \hat{c}^\dagger_\nu \hat{c}_\kappa \right) \tag{2.27}$$

in the Heisenberg picture. Eq.(2.26) can be expressed in terms of the GF (2.18) and SE (2.42) as (see Appendix C for the derivation)

$$\begin{aligned} I_K(t) = & \sum_{\nu,\nu_1 \in M} \int_{-\infty}^{t} dt_1 \\ & \Big(\; c^{K<}_{\nu\nu_1}(t,t_1)\, \Sigma^{K>}_{\nu_1\nu}(t_1,t) + \Sigma^{K>}_{\nu\nu_1}(t,t_1)\, c^{K<}_{\nu_1\nu}(t_1,t) \\ & - c^{K>}_{\nu\nu_1}(t,t_1)\, \Sigma^{K<}_{\nu_1\nu}(t_1,t) - \Sigma^{K<}_{\nu\nu_1}(t,t_1)\, c^{K>}_{\nu_1\nu}(t_1,t) \; \Big) \end{aligned} \tag{2.28}$$

Note that while the expression (2.28) is formally exact, our calculations are performed within the non-crossing approximation (NCA). The corresponding diagram is shown in Fig. 2.7b.

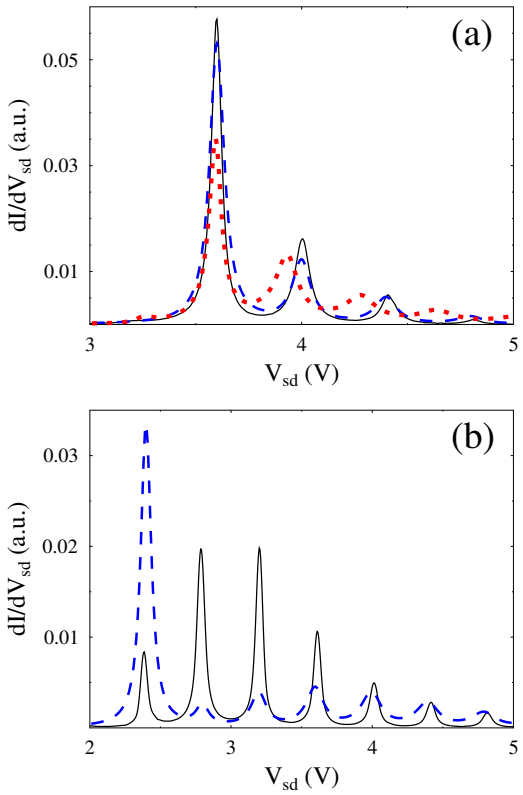

Figure 2.3: Comparison between the pseudoparticle NEGF (solid line, black) and the standard NEGF-based approach of Ref.[33] (dashed line, blue - zero order; dashed line red in panel (a) - self-consistent calculation). Conductance vs. applied bias is calculated for the single-level model (2.1)-(2.6). Shown are results for $\frac{M}{\omega_0} = 1$ (a) and 2 (b). See text for parameters.

At steady state the current does not depend on time, the corresponding GFs and SEs can be transformed to energy domain, which yields

$$I_K = \sum_{\nu_1,\nu_2} \int_{-\infty}^{+\infty} \frac{dE}{2\pi} \tag{2.29}$$
$$\left(c^{K<}_{\nu_1\nu_2}(E)\,\Sigma^{K>}_{\nu_2\nu_1}(E) - c^{K>}_{\nu_1\nu_2}(E)\,\Sigma^{K<}_{\nu_2\nu_1}(E)\right)$$

where explicit expressions for the bare GFs for electrons in contacts, $c^{K<}(E)$ and $c^{K>}(E)$, are given in Eqs. (2.47)-(2.48).

2.4 Numerical results

Here we demonstrate the capabilities of the pseudoparticle NEGF approach discussed in Section 2.3 in simulations of inelastic transport for the models introduced in Section 2.2.

Single level linearly coupled to molecular vibration.

This model, Eqs. (2.1)-(2.6), is a popular test case for approaches to transport in molecular junctions with strong electron-vibron interactions. The Lang-Firsov (or small polaron) transformation,[84] resolving the atomic limit of the model, in the case of junctions, shifts information on the electron-vibron interaction into the molecule-lead electron transfer matrix elements. A subsequent approximation based on the separation of the electron and vibration timescales allows introduction of Frank-Condon factors in a way similar to the Marcus theory of electron transfer. Several NEGF based approaches were formulated for this model by us[33] and others.[69] The approach of Ref.[33] was later generalized to multiple vibrational modes.[70,71]

Figure 2.2 shows conductance vs. applied bias calculated within the pseudoparticle NEGF approach. Parameters of the calculation are $T = 100K$, $\varepsilon_0 = 2\text{eV}$, $\Gamma_L = \Gamma_R = 0.05\text{eV}$, $\omega_0 = 0.1\text{eV}$ and $M = 0.2\text{eV}$. Fermi energy is taken to be at the origin, $E_F = 0$, and bias is applied symmetrically, $\mu_{L,R} = E_F \pm V_{sd}/2$. Calculations are performed on an adaptive grid. We present calculations with ($\gamma = 0.05\text{eV}$, solid line) and without ($\gamma = 0\text{eV}$, dashed line) coupling to thermal bath. The former case results in equilibrium vibrational population, while the latter corresponds to heated molecular vibration. This nonequilibrium vibrational population results in additional peaks in conductance to the left from the elastic tunneling feature (indicated by the arrow). The peaks correspond to the absoprtion of vibrational quanta by tunneling electron. Such heating of vibration by charge flux has been observed in experiments (see *e.g.* Ref.[85]). Figure 2.2 is an analog of Fig. 4 in Ref.[33] calculated for stronger electron-vibration coupling. Note that (as is discussed below) the latter method is not capable of treating strong electron-vibron interaction properly.

A comparison between the pseudoparticle and standard NEGF methods is demon-

strated in Figure 2.3. Here $\Gamma_L = \Gamma_R = 0.02$eV, $\omega_0 = 0.2$eV and $\gamma = 0.01$eV. Other parameters are as in Fig.2.2. Fig. 2.3a compares pseudoparticle NEGF calculation (solid line) with results of the approach presented in Ref.[33] (dashed line - zero-order; dotted line - self-consistent calculation) for moderate electron-vibration coupling $M/\omega_0 = 1$. It is interesting that the zero-order approximation of the latter coincides with the pseudoparticle NEGF calculation, while the more advanced self-consistent treatment deviates from it considerably. The effect can be explained as follows. Since the small polaron transformation utilized in Ref.[33] is exact in the atomic limit and since molecule-contact coupling is relatively weak, error introduced by considering electron transport in the junction as a hopping process (similar to the Marcus theory of electron transfer) is small. However, even this small error may sum up to a substantial deviation in a self-consistent procedure. For stronger electron-vibron coupling $M/\omega_0 = 2$ (see Fig. 2.3b) difference between the two approaches is evident already in comparison to zero-order result. This results from failure of the second cumulant approximation used to introduce a nonequilibrium version of Frank-Condon factor in Ref.[33] While this approximation becomes exact when $\Gamma \to 0$, it fails with increasing M/ω_0 at finite Γ.

Note that the pseudoparticle NEGF is free from approximation related to the introduction of Frank-Condon factors, providing a nonequilibrium scheme more stable for stronger electron-vibron coupling than the approach introduced in Ref.[33] Note also that strong electron-vibron interaction was proposed in a number of publications as as possible mechanism for negative differential resistance in several molecular junctions (see *e.g.* Ref.[86] and references therein). Finally, within the NCA approximation employed here, pseudoparticle NEGF is constrained to relatively weak molecule-contact couplings. This may be considered a less important restriction (compared to restriction on strength of electron-vibron coupling) since, for strong Γ, usual perturbation theory (*e.g.* the self-consistent Born approximation) is applicable.

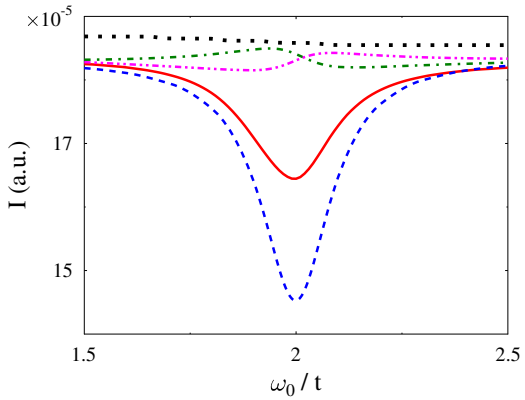

Figure 2.4: A two-level bridge model with non-diagonal electron-phonon coupling, Eqs. (2.1)-(2.5) and (2.7). Current at bias $V_{sd} = 4$V is plotted vs. ratio of the frequency of molecular vibration ω_0 to intra-molecular elastic hopping parameter t. Shown are results of calculations within the pseudoparticle NEGF approach (solid line, red), the exact mapping scheme of Ref.[72] with oscillator initially in its ground (dashed line, blue), third (dash-dotted line, green) and fourth (dash-double-dotted line, magenta) excited states, and the equation of motion NEGF method of Ref.[87] (dotted line, black). See text for parameters.

Two-level bridge with non-local electron-vibron coupling.

A two-level bridge with off-diagonal coupling to a molecular vibration, Eqs. (2.1)-(2.5) and (2.7), is a simple example where two timescales exist on the molecule: one is related to intra-molecular electronic dynamics (the elastic hopping parameter t), the other is due to the molecular vibration (the frequency, ω_0). Note that the pseudoparticle NEGF method does not rely on the Born-Oppenheimer approximation to separate electronic and vibrational dynamics with respect to intra-molecular processes. Thus it is an appropriate tool to apply in a regime, where timescale speration arguments do not apply. This issue is relevant for the cases when several electronic states are coupled to a molecular vibration(s) are considered (see *e.g.* Ref.[70]).

Figure. 2.4 shows current at $V_{sd} = 4$V as a function of the ratio of the frequency of the molecular vibration ω_0 to the intra-molecular elastic hopping parameter t. Parameters of the calculations are $\varepsilon_1 = \varepsilon_2 = 0.5$eV, $t = 0.1$eV, $\Gamma_L = \Gamma_R = 0.01$eV, $M = 0.1$eV, $\gamma = 0$. Other parameters are as in Fig. 2.2.

The pseudoparticle NEGF result (solid line) demonstrates a destructive interference feature at resonance $\omega_0 = \Omega_{Rabi}$, where $\Omega_{Rabi} \equiv \sqrt{(\varepsilon_1 - \varepsilon_2)^2 + 4|t|^2}$ is the Rabi

frequency due to elastic hopping.

Result of the exact mapping scheme[72] calculation (see dashed line in Fig. 2.4) shows qualitatively similar behavior. Note that difference between the two results (solid and dashed lines in Fig. 2.4) is due to the fact that for the exact mapping approach we calculated current within an assumption of the oscillator being in the ground state, which disregards heating of the molecular vibration. Scattering theory results with the oscillator initially in an excited state have different qualitative behavior (see dash-dotted and dash-double-dotted lines in Fig. 2.4). Note that the heating should be essential at high biases, and is included in the pseudoparticle NEGF calculation.

Approaches based on the Born-Oppenheimer approximation introduce nonequilibrium analogs of Franck-Condon factors, decoupling electronic and vibrational dynamics (see *e.g.* Refs.[33,87]). This results in qualitatively wrong behavior at resonance, where the timescale separation argument is not applicable (compare dotted line to solid and dashed lines in Fig. 2.4). Note that experimental evidence for a breakdown of the Born-Oppenheimer approximation was reported for junctions when electronic levels in a molecule are coupled by a molecular vibration.[47]

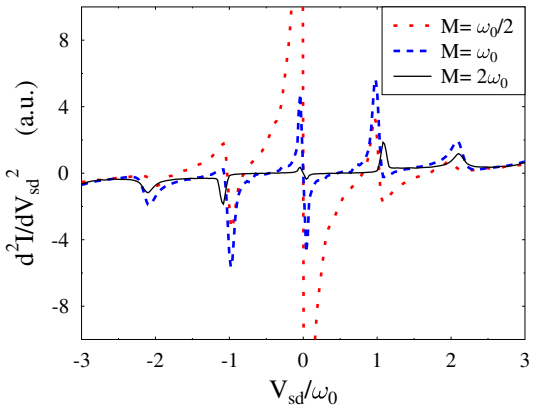

Figure 2.5: d^2I/dV_{sd}^2 vs. bias for inelastic transport through a quantum dot model, Eqs. (2.1)-(2.5) and (2.8), in the Kondo regime. Shown are results for $M = \omega_0/2$ (dotted line, red), ω_0 (dashed line, blue), and $2\omega_0$ (solid line, black). See text for the parameters.

Inelastic transport in the Coulomb blockade and Kondo regimes.

The pseudoparticle NEGF approach is capable of qualitative description of the Kondo regime in the limit of large Coulomb repulsion $U \to \infty$,[88] although at least the

one-crossing approximation is needed to get quantitative predictions for finite U.[89]

Figure 2.5 demonstrates the vibrational sidebands of the Kondo peak in the limit of $U \to \infty$ for the quantum dot model, Eqs. (2.1)-(2.5) and (2.8). Parameters of the calculation are $\varepsilon_\nu = -2\text{eV}$ ($\nu = \uparrow, \downarrow$), $\Gamma_L = \Gamma_R = 0.5\text{eV}$, $\omega^{(0)} = \omega^{(1)} \equiv \omega_0 = 0.5\text{eV}$, and $\gamma = 0$. We assume linear coupling to the vibrational degree of freedom, $M(\hat{a}_0 + \hat{a}_0^\dagger) \sum_{\nu=\uparrow,\downarrow} \hat{c}_\nu^\dagger \hat{c}_\nu$. Other parameters are as in Fig. 2.2. As expected strong electron-vibron coupling destroys the Kondo peak. This result is similar to the one obtained for the same model within an equation-of-motion approach;[87] however, it is free from restrictions imposed by the Franck-Condon factors in the latter consideration.

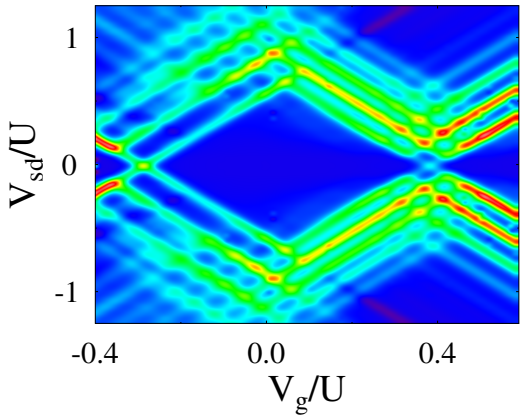

Figure 2.6: Conductance map for inelastic transport through a quantum dot with charge state dependent frequencies, Eqs. (2.1)-(2.5) and (2.8). See text for the parameters.

Finally, we demonstrate an example of simulating state-specific properties in transport. Experimental data on molecular charging state dependent vibrational sidebands in the Coulomb blockade regime is available in the literature. Simulation of such behavior within standard NEGF methodology poses a challenge to theory. At the same time any scheme utilizing many-body states of the system as a basis can easily treat the problem. Here we use a quantum dot coupled to a vibrational degree of freedom with state-specific (more precisely - molecular charge specific) frequency as a model for a molecular junction in the Coulomb blockade regime, Eqs. (2.1)-(2.5) and (2.8). The transport is described in the language of vibronic states of the molecular system. Note that contrary to our previous consideration,[49] we do not rely on the small polaron trans-

formation in our calculations. Also the pseudoparticle NEGF approach is capable of calculating both nonequilibrium populations and coherences within the system.

Figure 2.6 shows a conductance map of the model with vibrational sidebands clearly indicating change in vibrational frequency for different charging states of the molecule. Parameters of the calculation are $\varepsilon_\nu = 0$ ($\nu = \uparrow, \downarrow$), $U = 1$eV, $\Gamma_L = \Gamma_R = 0.02$eV, $\omega^{(0)} = 0.08$eV, $\omega^{(1)} = 0.1$eV, and $\omega^{(2)} = 0.14$eV, $\gamma = 0$. Other parameters as in Fig. 2.2. In realistic simulations, overlap matrices between wavefunctions of the state-specific vibrational mode should be evaluated taking into account the Duschinsky mixing effect.[90,91] Since our calculation is for demonstration purposes only, for simplicity, we assign different vibrational frequencies to different charging states keeping the same form of linear coupling as in (2.6) with $M = 0.2$eV. Results are similar to those presented earlier,[49] however the approach itself is more general. Note that realistic calculations on state specific frequencies in molecular junctions were reported recently[92] within a rate equation approach. It is straightforward to incorporate the pseudoparticle NEGF method into the framework of Ref.[92] Note that rate equation based description will become inadequate the moment two molecular levels are close in energy so that interference effects become pronounced.

2.5 Conclusion

We discuss a pseudoparticle NEGF approach as a tool to describe transport in molecular junctions in the language of many-body states of an isolated molecule. In particular, we focus on inelastic transport in the regime of strong electron-vibron interaction on the molecule with relatively weak molecular coupling to leads. The pseudoparticle NEGF approach is compared to alternative formulations. These include scattering theory,[72] generalized quantum master equation schemes,,[54–56,68] standard[33,69] and Hubbard[48,49] NEGF techniques.

The Hubbard NEGF is a viable scheme, whose application is complicated by absence of well defined rules for formulation of a conserving approximation. Since usual (Fermi or Bose) commutation relations are fulfilled by the pseudoparticle creation and annihilation operators, formulation of such an approximation in the pseudoparti-

cle NEGF technique follows standard diagrammatic rules (although formulated in an extended Hilbert space).

The pseudoparticle NEGF is more general than the GQME schemes: the perturbation theory in Green function schemes is formulated for a self-energy. Thus, resummation of an infinite series of diagrams entering in the form of the retarded SE in the denominator of the GF assures accounting for broadening of molecular level due to coupling to continuum of states in the contacts. This effect is (at least partially) missed in the GQME, while it may play an important role (see Ref.[56] for discussion). Note that the GF technique has a well defined procedure for extending the consideration to any desired order in the system-bath coupling. Such extension is not trivial in the QME scheme (see *e.g.* Ref.[54] for discussion). Note also that the GQME is not capable, *e.g.*, of reproducing the Kondo regime (see Fig. 2.5) even qualitatively.

Consideration of inelastic transport in junctions in the regime of strong electron-vibron coupling within standard NEGF approaches usually relies upon the Lang-Firsov transformation with subsequent introduction of nonequilibrium analogs of the Frank-Condon factors. Thus restrictions of these techniques are related to either inadequacy of schemes based on small polaron transformation in the the regime of strong electron-vibron coupling (see Fig. 2.3b), or inapplicability of the Born-Oppenheimer approximation (see Fig. 2.4). Note also that these considerations are restricted to linear electron-vibron coupling, making *e.g.* description of state specific vibrational effects nontrivial. We compare the pseudoparticle NEGF results to those of the previous NEGF formulations, and demonstrate stability of the former in the strong electron-vibron coupling regime.

The superiority of the pseudoparticle NEGF lies in its ability to treat an open molecular system in the language of many-body (vibronic) states, which eliminates the need to separate electronic and vibrational dynamics within the molecule. The same idea is at the heart of the "exact mapping" approach introduced in Ref.[72] However the latter technique is a strictly single-particle scattering theory, which makes it ill-posed to describe inelastic transport in junctions (see *e.g.* Ref.[32]). Thus the pseudoparticle NEGF method can be seen as a generalization of the "exact mapping" approach, which includes information on the Pauli exclusion principle and Fermi electron distribution

in the leads. Note that the ability to describe inelastic transport in the language of vibronic states is also important when state-specific characteristics of the molecule reveal themselves in transport measurements (see Fig. 2.6). Incorporating the pseudoparticle NEGF methodology into an *ab initio* calculation scheme (such as *e.g.* presented in Ref.[92]) is straightforward.

Finally, we note that effects considered in this paper within simple model calculations are representative of experimental observations. In particular, state-specific frequencies have been measured in experiments on resonant inelastic tunneling spectroscopy,[46] non-Born-Oppenheimer behavior was observed in molecular junctions with strong electron-vibron coupling,[47] and vibrational sidebands of the Kondo peak were reported in experiments on conduction in C_{60} junction.[93]

Acknowledgments

We gratefully acknowledge support by the Department of Energy (Early Career Award, DE-SC0006422) and the Hellmann Family Foundation. Chapter 2, in full, is a reprint of the material as it appears in Physical Chemistry Chemical Physics 2012. White, Alexander J.; Galperin, Michael, The Owner Societies 2012. The dissertation author was the primary investigator and author of the paper.

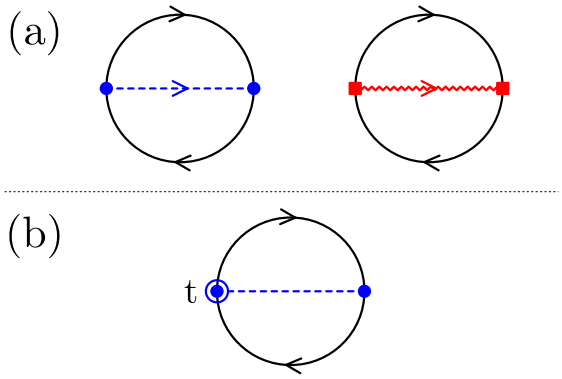

Figure 2.7: (a) Skeleton diagrams of the generating functional Y', Eq.(2.40) and (b) the current $I_K(t)$, Eq.(2.29). Directed solid line (black) represents dressed pseudoparticle propagator G, Eq.(2.17), directed dashed line (blue) inidicates electron Green function of the contacts C^K, Eq.(2.18), directed zigzag line (red) stands for the phonon Green function of the thermal bath F^B, Eq.(2.19). Non-directed dashed line in (b) indicates both possible directions. Circle (blue) and square (red) represents electron- and vibron-pseudoparticle overlap tensors, Eqs. (2.15) and (2.16), respectively. Summation over all indices and integration over contour variables is assumes for every connection in the diagrams except the circled connection where an assigned time is indicated in the plot. The diagrams are presented within the non-crossing approximation (NCA).

2.6 Appendix A: Luttinger-Ward functional in the pseudoparticle NEGF

In order to identify self-energies of the GFs (2.17)-(2.19) induced by interactions (2.4)-(2.5), we follow the path integral formulation of Ref.[801]

For future reference we also introduce the GFs for electrons in the contacts, C^K ($K = L, R$), and phonons in the thermal bath, F^B, defined in the space of transitions between many-body states of the molecule

$$C^K_{m_1m_2,m_3m_4}(\tau_1,\tau_2) = \sum_{\nu_1,\nu_2\in M} \xi^{\nu_1}_{m_1m_2}\, C^K_{\nu_1\nu_2}(\tau_1,\tau_2)\, \overset{*}{\xi}{}^{\nu_2}_{m_3m_4} \tag{2.30}$$

$$F^B_{m_1m_2,m_3m_4}(\tau_1,\tau_2) = \sum_{\alpha_1,\alpha_2\in M} \chi^{\alpha_1}_{m_1m_2}\, F^B_{\alpha_1\alpha_2}(\tau_1,\tau_2)\, \overset{*}{\chi}{}^{\alpha_2}_{m_3m_4} \tag{2.31}$$

We believe that the presence of single greek, as in Eqs. (2.18) and (2.19), or double

[1] Note that an equivalent alternative derivation is the linked cluster expansion.[84]

latin, as in Eqs. (2.30) and (2.31), index is enough to avoid confusion between the two representations.

The partition function, Z, is introduced as a path integral over the Keldysh contour[94]

$$Z = \int_c \mathbf{D}[\bar{d}, d, \bar{c}, c, \bar{b}, b]\, e^{iS} \tag{2.32}$$

where S is the action

$$\begin{aligned} S = \int_c d\tau \Bigg[& \sum_{m,m' \in M} \bar{d}_m(\tau) \hat{g}^{-1}_{mm'} d_{m'}(\tau) \\ & + \sum_{\kappa \in \{L,R\}} \bar{c}_\kappa(\tau) \hat{c}^{-1}_\kappa c_\kappa(\tau) + \sum_{\beta \in B} \bar{b}_\beta(\tau) \hat{f}^{-1}_\beta b_\beta(\tau) \\ & - \sum_{\substack{\nu \in M \\ \kappa \in \{L,R\}}} \Big(V_{\kappa\nu}\, \bar{c}_\kappa(\tau)\, c_\nu[\eta(\tau), \bar{\eta}(\tau)] + V_{\nu\kappa}\, \bar{c}_\nu[\eta(\tau), \bar{\eta}(\tau)]\, c_\kappa(\tau) \Big) \\ & - \sum_{\substack{\alpha \in M \\ \beta \in B}} \Big(W_{\beta\alpha}\, \bar{b}_\beta(\tau)\, a_\alpha[\eta(\tau), \bar{\eta}(\tau)] + W_{\alpha\beta}\, \bar{a}_\alpha[\eta(\tau), \bar{\eta}(\tau)]\, b_\beta(\tau) \Big) \\ & - \sum_{m \in M} \Big(\bar{\eta}_m(\tau)\, d_m(\tau) + \bar{d}_m(\tau)\, \eta_m(\tau) \Big) \Bigg] \end{aligned} \tag{2.33}$$

Here d (c, b) is the Grassman variable for Fermions and complex number for Bosons representing a pseudoparticle (electron in the contacts, phonon in the thermal bath), $\bar{d}$ ($\bar{c}$, $\bar{b}$) is the corresponding conjugate, and $\hat{g}^{-1}_{mm'}$ ($\hat{c}^{-1}_\kappa$, $\hat{f}^{-1}_\beta$) is the inverse (in both state and contour variable space) of the free Green function (i.e. when the system-bath coupling is disregarded). Note that Grassman variables representing electrons on the molecule, c_ν ($\bar{c}_\nu$), and molecular vibrations, a_α ($\bar{a}_\alpha$), are expressed in Eq.(2.33) as functional derivatives in auxiliary fields η of the last term in Eq.(2.33) (compare with Eqs. (2.13)-(2.14))

$$\bar{c}_\nu[\eta(\tau), \bar{\eta}(\tau)] \equiv \sum_{m_1, m_2 \in M} \xi^\nu_{m_1 m_2} \zeta_{m_1} \frac{\delta}{\delta \eta_{m_1}(\tau)} \frac{\delta}{\delta \bar{\eta}_{m_2}(\tau)} \tag{2.34}$$

$$\bar{a}_\alpha[\eta(\tau), \bar{\eta}(\tau)] \equiv \sum_{m_1, m_2 \in M} \chi^\alpha_{m_1 m_2} \zeta_{m_1} \frac{\delta}{\delta \eta_{m_1}(\tau)} \frac{\delta}{\delta \bar{\eta}_{m_2}(\tau)} \tag{2.35}$$

The measure in (2.32) is

$$\mathbf{D}[\bar{d}, d, \bar{c}, c, \bar{b}, b] \equiv \prod_{m\in M} \frac{1}{\mathcal{N}_m} d\bar{d}_m \, dd_m \times \prod_{\kappa\in\{L,R\}} d\bar{c}_\kappa \, dc_\kappa \times \frac{1}{2\pi i} \prod_{\beta\in B} d\bar{b}_\beta \, db_\beta \tag{2.36}$$

where $\mathcal{N}_m = 1$ $(2\pi i)$ for Fermi (Bose) pseudoparticle.

Performing the integration in (2.33) over the pseudoparticles, electrons in the contacts, and phonons in the thermal bath yields[95]

$$\begin{aligned} Z =& Z_0 \exp\Bigg(-i \int_c d\tau \int_c d\tau' \\ & \Bigg\{ \sum_{\substack{\nu,\nu'\in M \\ K=L,R}} \bar{c}_\nu[\eta(\tau), \bar{\eta}(\tau)] \, c^K_{\nu\nu'}(\tau,\tau') \, c_{\nu'}[\eta(\tau'), \bar{\eta}(\tau')] \\ & + \sum_{\alpha,\alpha'\in M} \bar{a}_\alpha[\eta(\tau), \bar{\eta}(\tau)] \, f^B_{\alpha\alpha'}(\tau,\tau') \, a_{\alpha'}[\eta(\tau'), \bar{\eta}(\tau')] \Bigg\} \Bigg) \\ & \times \exp\Bigg(i \sum_{m,m'\in M} \int_c d\tau \int_c d\tau' \bar{\eta}_m(\tau) g_{mm'}(\tau,\tau') \eta_{m'}(\tau') \Bigg) \end{aligned} \tag{2.37}$$

Expanding the first exponent on the right side of (2.37), taking auxiliary field derivatives, setting the fields to zero, and collecting terms of the connected diagrams into cumulant expansion leads to

$$Z = Z_0 \, e^{-Y} \tag{2.38}$$

where Z_0 is the partition function of the model in the absence of the system-baths couplings and Y is the collection of all of the connected diagrams.

The final expression is obtained by dressing these diagrams, i.e. substituting full GFs in place of the bare ones. This yields[96]

$$\begin{aligned} Y =& Y' + \sum_{M_m} \zeta_m \mathrm{Tr}[\log \hat{G}^{-1} + \mathbf{\Sigma}\, \mathbf{G}] + \mathrm{Tr}[\log \hat{F}_B^{-1} + \mathbf{\Pi}^B \, \mathbf{F}^B] \\ & - \sum_{K=L,R} \mathrm{Tr}[\log \hat{C}_K^{-1} + \mathbf{\Sigma}^K \mathbf{C}^K] \end{aligned} \tag{2.39}$$

Here the Tr[...] is a trace over both states and contour variables, M_m indicates a block of molecular states $|m>$ with the same number of electrons, and $\zeta_m = -1$ $(+1)$ for a Fermi (Bose) state. $\mathbf{G}$, $\mathbf{C}^K$, and $\mathbf{F}^B$ are the dressed GFs defined in Eqs. (2.17), (2.18), and (2.19), respectively. $\mathbf{\Sigma}$, $\mathbf{\Sigma}^K$, and $\mathbf{\Pi}^B$ are the corresponding self-energies and $\hat{G}^{-1}$, $\hat{C}_K^{-1}$, and $\hat{F}_B^{-1}$ are inverses of the corresponding GFs (in the sense of both states and contour variables).

Y' is the Luttinger-Ward functional – the collection of all connected skeleton diagrams (i.e. diagrams that have no self-energy insertions). Fig. 2.7a shows such diagrams for the lowest non-zero (second) order in the sytem-baths interactions - the non-crossing approximation (NCA). The explicit expression for the model (2.1)-(2.5) is

$$\begin{aligned} Y'_{NCA} = & -i \sum_{\substack{m_1,m_2 \\ m'_1,m'_2 \in M}} \zeta_{m_1} \int_c d\tau \int_c d\tau' \\ & G_{m'_1 m_1}(\tau',\tau)\, G_{m_2 m'_2}(\tau,\tau') \\ & \Bigg[\sum_{\substack{\nu,\nu' \in M \\ K=L,R}} \xi^{\nu}_{m_1 m_2} \overset{*}{\xi}{}^{\nu'}_{m'_1 m'_2} C^K_{\nu\nu'}(\tau,\tau') \\ & + \sum_{\alpha,\alpha' \in M} \chi^{\alpha}_{m_1 m_2} \overset{*}{\chi}{}^{\alpha'}_{m'_1 m'_2} F^B_{\alpha\alpha'}(\tau,\tau') \Bigg] \end{aligned} \tag{2.40}$$

2.7 Appendix B: Expressions for the self-energies

Since Y is stationary with respect to changes of the GFs,[96] expressions for the self-energies follow immediately from Eq.(2.39) as

$$\Sigma_{m_1 m_2}(\tau_1,\tau_2) = -\zeta_{m_1} \frac{\delta Y'}{\delta G_{m_2 m_1}(\tau_2,\tau_1)} \tag{2.41}$$

$$\Sigma^K_{\nu_1\nu_2}(\tau_1,\tau_2) = +\frac{\delta Y'}{\delta C^K_{\nu_2\nu_1}(\tau_2,\tau_1)} \tag{2.42}$$

$$\Pi^B_{\alpha_1\alpha_2}(\tau_1,\tau_2) = -\frac{\delta Y'}{\delta F^B_{\alpha_2\alpha_1}(\tau_2,\tau_1)} \tag{2.43}$$

Using (2.40) in (2.41)-(2.43) and projecting onto the physical subspace (see *e.g.*

Ref.[80] for details) yields NCA expressions for the pseudoparticles SE

$$\begin{aligned}\Sigma_{mm'}(\tau,\tau') = i \sum_{m_1,m_2\in M} & G_{m_1m_2}(\tau,\tau') \\ \Big[\sum_{K=L,R} & c^K_{mm_1,m'm_2}(\tau,\tau') - c^K_{m_2m',m_1m}(\tau',\tau) \\ & + f^B_{mm_1,m'm_2}(\tau,\tau') + f^B_{m_2m',m_1m}(\tau',\tau)\Big],\end{aligned} \tag{2.44}$$

SE for the electrons in the contacts

$$\begin{aligned}\Sigma^K_{\nu\nu'}(\tau,\tau') = -i \sum_{\substack{m_1,m_2\in M \\ m_1',m_2'\in M}} & \zeta_{m_1}\xi^{\nu'}_{m_1'm_2'}\overset{*}{\xi}{}^{\nu}_{m_1m_2} \\ & \times G_{m_1m_1'}(\tau,\tau')\, G_{m_2'm_2}(\tau',\tau),\end{aligned} \tag{2.45}$$

and SE for the phonons in the thermal bath

$$\begin{aligned}\Pi^B_{\alpha\alpha'}(\tau,\tau') = i \sum_{\substack{m_1,m_2\in M \\ m_1',m_2'\in M}} & \zeta_{m_1}\chi^{\alpha'}_{m_1'm_2'}\overset{*}{\chi}{}^{\alpha}_{m_1m_2} \\ & \times G_{m_1m_1'}(\tau,\tau')\, G_{m_2'm_2}(\tau',\tau).\end{aligned} \tag{2.46}$$

Standard Langreth rules should be employed at this point to obtain Keldysh contour projections.

At steady state self-energies can be Fourier transformed to energy space. Corresponding expressions for the self-energies (2.44)-(2.46) contain Fourier transforms of the GFs (2.17)-(2.19).

The bare GF for the electrons in contacts c^K is given by the usual expression for electron self-energy within NEGF. The Fourier transform of its lesser and greater projections is precisely

$$c^{K<}_{\nu_1\nu_2}(E) = i\Gamma^K_{\nu_1\nu_2}(E)\, f_K(E) \tag{2.47}$$

$$c^{K>}_{\nu_1\nu_2}(E) = -i\Gamma^K_{\nu_1\nu_2}(E)\,[1 - f_K(E)] \tag{2.48}$$

where $K = L, R$, $\Gamma^K_{\nu_1\nu_2}(E) \equiv 2\pi \sum_{\kappa\in K} V_{\nu_1\kappa}V_{\kappa\nu_2}\delta(E-\varepsilon_\kappa)$ is the electron dissipation

matrix and $f_K(E) = [\exp(\frac{E-\mu_K}{k_BT}) + 1]^{-1}$ is the Fermi-Dirac thermal distribution.

The corresponding non-interacting GF for the phonons in the thermal bath comes from the phonon self-energy within NEGF. The Fourier transform of its lesser and greater projections is ($\omega > 0$)

$$f^{B<}_{\alpha_1\alpha_2}(\omega) = -\, i\gamma^B_{\alpha_1\alpha_2}(\omega)\, N_B(\omega) \tag{2.49}$$

$$f^{B>}_{\alpha_1\alpha_2}(\omega) = -\, i\gamma^B_{\alpha_1\alpha_2}(\omega)\, [1 + N_B(\omega)] \tag{2.50}$$

where $\gamma^B_{\alpha_1\alpha_2}(\omega) = \sum_{\beta\in B} W_{\alpha_1\beta}W_{\beta\alpha_2}\delta(\omega-\omega_\beta)$ is the phonon damping matrix and $N_B(\omega) = [\exp(\frac{\omega}{k_BT}) - 1]^{-1}$ is the Bose-Einstein thermal distribution. Specificly, in the case of a single phonon mode with a frequency ω_0, we model the phonon damping function as

$$\gamma^B(\omega) = \gamma\frac{\omega^2}{\omega_0^2}\exp\left(2\left[1 - \frac{\omega}{\omega_0}\right]\right) \tag{2.51}$$

2.8 Appendix C: Expression for the current, Eq.(2.28)

Following Ref.[38] we define current at the molecule-contact interface K as

$$I_K(t) = -\frac{d}{dt}\sum_{\kappa\in K}\langle \hat{c}^\dagger_\kappa(t)\, \hat{c}_\kappa(t)\rangle \equiv -i\frac{d}{dt}C^{K<}_{\kappa\kappa}(t,t) \tag{2.52}$$

where $C^{K<}_{\kappa\kappa}(t,t)$ is the equal time lesser projection of the dressed electron Green function in a state $|k>$ of the contact K, Eq.(2.20). In order to perform the derivative in (2.52) we write left and right equations-of-motion for the lesser projection of the GF

$$\left[i\frac{\partial}{\partial t_1} - \varepsilon_{\kappa_1}\delta_{\kappa_1,\kappa_2}\right] C^{K<}_{\kappa_1\kappa_2}(t_1,t_2) = \sum_{\kappa'\in K}\int_{-\infty}^{+\infty} dt' \tag{2.53}$$

$$\left[\Sigma^{K<}_{\kappa_1\kappa'}(t_1,t')\, C^{K\,a}_{\kappa'\kappa_2}(t',t_2) + \Sigma^{K\,r}_{\kappa_1\kappa'}(t_1,t')\, C^{K<}_{\kappa'\kappa_2}(t',t_2)\right]$$

$$\left[-i\frac{\partial}{\partial t_2} - \varepsilon_{\kappa_2}\delta_{\kappa_1,\kappa_2}\right] C^{K<}_{\kappa_1\kappa_2}(t_1,t_2) = \sum_{\kappa'\in K}\int_{-\infty}^{+\infty} dt' \tag{2.54}$$

$$\left[C^{K<}_{\kappa_1\kappa'}(t_1,t')\, \Sigma^{K\,a}_{\kappa'\kappa_2}(t',t_2) + C^{K\,r}_{\kappa_1\kappa'}(t_1,t')\, \Sigma^{K<}_{\kappa'\kappa_2}(t',t_2)\right]$$

Here $\Sigma^K_{\kappa_1\kappa_2}$ is a self-energy analogous to $\Sigma^K_{\nu_1\nu_2}$, Eq.(2.42), defined in the subspace of the contact K

$$\Sigma^K_{\kappa_1\kappa_2}(\tau_1,\tau_2) = \sum_{\nu_1,\nu_2\in M} V_{\kappa_1\nu_1}\,\Sigma^{(K)}_{\nu_1\nu_2}(\tau_1,\tau_2)V_{\nu_2\kappa_2} \tag{2.55}$$

Subtracting (2.53) from (2.54) at $t_1 = t_2 = t$, and using (2.18) and (2.55) in (2.52) yields

$$\begin{aligned} I_K(t) = \sum_{\nu,\nu_1\in M}\int_{-\infty}^{t} dt_1 \qquad\qquad (2.56)\\ \Big(\; C^{K<}_{\nu\nu_1}(t,t_1)\,\Sigma^{K>}_{\nu_1\nu}(t_1,t) + \Sigma^{K>}_{\nu\nu_1}(t,t_1)\,C^{K<}_{\nu_1\nu}(t_1,t) \\ - C^{K>}_{\nu\nu_1}(t,t_1)\,\Sigma^{K<}_{\nu_1\nu}(t_1,t) - \Sigma^{K<}_{\nu\nu_1}(t,t_1)\,C^{K>}_{\nu_1\nu}(t_1,t)\;\Big) \end{aligned}$$

This expression should be projected onto physical subspace of the full Hilbert space. Taking into account that expressions for $\Sigma^{(K)>,<}$ contain the lesser projection of the pseudoparticle GF $G^<$, the only physical contribution in Eq.(2.56) comes from the free term in the Dyson equation for the GF C^K. This leads to Eq.(2.28).

Chapter 2 References

[1] Marcus, R.A. J. Chem. Phys. **24**, 966 (1956)

[2] Marcus, R.A. J. Chem. Phys. **24**, 979 (1956)

[3] Levich, V.G. and Dogonadze, R.R. Doklady Akad. Nauk SSSR **124**, 123 (1959)

[4] Levich, V.G. and Dogonadze, R.R. Doklady Akad. Nauk SSSR **133**, 159 (1960)

[5] Hush, N.S. Trans. Faraday Soc. **57**, 557 (1961)

[6] Hush, N.S. Electrochimica Acta **13**, 1005 (1968)

[7] Jortner, J. J. Chem. Phys. **64**, 4860 (1976)

[8] Miller, J.R.; Calcaterra, L.T. and Closs, G.L. J. Am. Chem. Soc. **106**, 3047 (1984)

[9] Miller, J.R.; Beitz, J.V. and Huddleston, R.K. J. Am. Chem. Soc. **106**, 5057 (1984)

[10] Kuharski, R.A.; Bader, J.S.; Chandler, D.; Sprik, M.; Klein, M.L. and Impey. J. Chem. Phys. **89**, 3248 (1988)

[11] Barbara, P.F.; Meyer, T.J. and Ratner, M.A. J. Phys. Chem. **100**, 13148 (1996)

[12] Rosso, K.M. and Dupuis, M. J. Chem. Phys. **120**, 7050 (2004)

[13] Nitzan, A. *Chemical Dynamics in Condensed Phases* (Oxford University Press, 2006) (2006)

[14] Kuki, A. and Wolynes, P. Science **236**, 1647 (1987)

[15] Beratan, D.N.; Betts, J.N. and Onuchic, J.N. Science **252**, 1285 (1991)

[16] Beratan, D.N.; Onuchic, J.N.; Winkler, J.R. and Gray, H.B. Science **258**, 1740 (1992)

[17] Stuchebrukhov, A.A. The Journal of Chemical Physics **104**, 8424 (1996)

[18] Stuchebrukhov, A.A. The Journal of Chemical Physics **105**, 10819 (1996)

[19] Brookes, J.C.; Hartoutsiou, F.; Horsfield, A.P. and Stoneham, A.M. Phys. Rev. Lett. **98**, 038101 (2007)

[20] Newton, M.D. and Sutin, N. Ann. Rev. Phys. Chem. **35**, 437 (1984)

[21] Kuznetsov, A.M. *Charge Transfer in Physics, Chemistry and Biology: Physical Mechanisms of Elementary Processes and an Introduction to the Theory* (Gordon & Breach, 1995) (1995)

[22] Jortner, J. and Bixon, M. *Electron transfer - from isolated molecules to biomolecules* (John Wiley, 1999) (1999)

[23] Aviram, A. and Ratner, M.A. Chem. Phys. Lett. **29**, 277 (1974)

[24] Landauer, R. IBM J. Res. Develop. **1**, 223 (1957)

[25] Landauer, R. Phil. Mag. **21**, 863 (1970)

[26] Stone, A.D. and Szafer, A. IBM J. Res. Dev. **32**, 384 (1988)

[27] Engquist, H.L. and Anderson, P.W. Phys. Rev. B **24**, 1151 (1981)

[28] Büttiker, M.; Imry, Y.; Landauer, R. and Pinhas, S. Phys. Rev. B **31**, 6207 (1985)

[29] Büttiker, M. Phys. Rev. Lett. **57**, 1761 (1986)

[30] Nitzan, A. J. Phys. Chem. A **105**, 2677 (2001)

[31] Nitzan, A. Ann. Rev. Phys. Chem. **52**, 681 (2001)

[32] Mitra, A.; Aleiner, I. and Millis, A.J. Phys. Rev. B **69**, 245302 (2004)

[33] Galperin, M.; Nitzan, A. and Ratner, M.A. Phys. Rev. B **73**, 045314 (2006)

[34] Kadanoff, L.P. and Baym, G. *Quantum Statistical Mechanics*. Frontiers in Physics (W. A. Benjamin, Inc., New York, 1962) (1962)

[35] Keldysh, L.V. Sov. Phys. JETP **20**, 1018 (1965)

[36] Danielewicz, P. Ann. Phys. **152**, 239 (1984)

[37] Rammer, J. and Smith, H. Rev. Mod. Phys. **58**, 323 (1986)

[38] Haug, H. and Jauho, A.P. *Quantum Kinetics in Transport and Optics of Semiconductors*, vol. 123 of *Springer Series in Solid-State Sciences* (Springer-Verlag, Berlin Heidelberg, 1996) (1996)

[39] Xue, Y.; Datta, S. and Ratner, M.A. Chem. Phys. **281**, 151 (2002)

[40] Damle, P.; Ghosh, A.W. and Datta, S. Chem. Phys. **281**, 171 (2002)

[41] Brandbyge, M.; Mozos, J.L.; Ordejón, P.; Taylor, J. and Stokbro, K. Phys. Rev. B **65**, 165401 (2002)

[42] Frederiksen, T.; Paulsson, M.; Brandbyge, M. and Jauho, A.P. Phys. Rev. B **75**, 205413 (2007)

[43] Sergueev, N.; Demkov, A.A. and Guo, H. Phys. Rev. B **75**, 233418 (2007)

[44] Frederiksen, T.; Lorente, N.; Paulsson, M. and Brandbyge, M. Phys. Rev. B **75**, 235441 (2007)

[45] Galperin, M. and Tretiak, S. J. Chem. Phys. **128**, 124705 (2008)

[46] Chae, D.H.; Berry, J.F.; Jung, S.; Cotton, F.A.; Murillo, C.A. and Yao, Z. Nano Letters **6**, 165 (2006)

[47] Repp, J.; Liljeroth, P. and Meyer, G. Nature Physics **6**, 975 (2010)

[48] Yeganeh, S.; Ratner, M.A.; Galperin, M. and Nitzan, A. Nano Letters **9**, 1770 (2009)

[49] Galperin, M.; Nitzan, A. and Ratner, M.A. Phys. Rev. B **78**, 125320 (2008)

[50] Pedersen, J.N.; Bohr, D.; Wacker, A.; Novotný, T.; Schmitteckert, P. and Flensberg, K. Phys. Rev. B **79**, 125403 (2009)

[51] Breuer, H.P. and Petruccione, F. *The Theory of Open Quantum Systems* (Oxford University Press, 2003) (2003)

[52] Harbola, U.; Esposito, M. and Mukamel, S. Phys. Rev. B **74**, 235309 (2006)

[53] Timm, C. Phys. Rev. B **77**, 195416 (2008)

[54] Koller, S.; Grifoni, M.; Leijnse, M. and Wegewijs, M.R. Phys. Rev. B **82**, 235307 (2010)

[55] Esposito, M. and Galperin, M. Phys. Rev. B **79**, 205303 (2009)

[56] Esposito, M. and Galperin, M. J. Phys. Chem. C **114**, 20362 (2010)

[57] Schultz, M.G. and von Oppen, F. Phys. Rev. B **80**, 033302 (2009)

[58] Ungar, L.W. and Cina, J.A. J. Phys. Chem. A **102**, 7382 (1998)

[59] Cheng, Y.C.; Engel, G.S. and Fleming, G.R. Chem. Phys. **341**, 285 (2007)

[60] Ishizaki, A. and Fleming, G.R. J. Chem. Phys. **130**, 234110 (2009)

[61] Ishizaki, A. and Fleming, G.R. Proc. Nat. Acad. Sci. **106**, 17255 (2009)

[62] Rebentrost, P. and Aspuru-Guzik, A. J. Chem. Phys. **134**, 101103 (2011)

[63] Jin, J.; Zheng, X. and Yan, Y. J. Chem. Phys. **128**, 234703 (2008)

[64] Schaller, G.; Kießlich, G. and Brandes, T. Phys. Rev. B **80**, 245107 (2009)

[65] Galperin, M.; Ratner, M.A. and Nitzan, A. J. Chem. Phys. **121**, 11965 (2004)

[66] Galperin, M.; Nitzan, A. and Ratner, M.A. Phys. Rev. B **75**, 155312 (2007)

[67] Siddiqui, L.; Ghosh, A.W. and Datta, S. Phys. Rev. B **76**, 085433 (2007)

[68] Leijnse, M. and Wegewijs, M.R. Phys. Rev. B **78**, 235424 (2008)

[69] Zazunov, A. and Martin, T. Phys. Rev. B **76**, 033417 (2007)

[70] Härtle, R.; Benesch, C. and Thoss, M. Phys. Rev. B **77**, 205314 (2008)

[71] Härtle, R.; Benesch, C. and Thoss, M. Phys. Rev. Lett. **102**, 146801 (2009)

[72] Bonca, J. and Trugman, S.A. Phys. Rev. Lett. **75**, 2566 (1995)

[73] Haule, K. and Bonča, J. Phys. Rev. B **59**, 13087 (1999)

[74] Emberly, E.G. and Kirczenow, G. Phys. Rev. B **61**, 5740 (2000)

[75] Flensberg, K. Phys. Rev. B **68**, 205323 (2003)

[76] Wingreen, N.S. and Meir, Y. Phys. Rev. B **49**, 11040 (1994)

[77] Sivan, N. and Wingreen, N.S. Phys. Rev. B **54**, 11622 (1996)

[78] Hettler, M.H.; Kroha, J. and Hershfield, S. Phys. Rev. B **58**, 5649 (1998)

[79] Eckstein, M. and Werner, P. Phys. Rev. B **82**, 115115 (2010)

[80] Oh, J.H.; Ahn, D. and Bubanja, V. Phys. Rev. B **83**, 205302 (2011)

[81] Kotliar, G.; Savrasov, S.Y.; Haule, K.; Oudovenko, V.S.; Parcollet, O. and Marianetti, C.A. Rev. Mod. Phys. **78**, 865 (2006)

[82] Coleman, P. Phys. Rev. B **29**, 3035 (1984)

[83] Bickers, N.E. Rev. Mod. Phys. **59**, 845 (1987)

[84] Mahan, G.D. *Many-Particle Physics* (Plenum Press, 1990) (1990)

[85] LeRoy, B.J.; Lemay, S.G.; Kong, J. and Dekker, C. Nature **432**, 371 (2004)

[86] Galperin, M.; Ratner, M.A. and Nitzan, A. Nano Letters **5**, 125 (2005)

[87] Galperin, M.; Nitzan, A. and Ratner, M.A. Phys. Rev. B **76**, 035301 (2007)

[88] Costi, T.A.; Kroha, J. and Wölfle, P. Phys. Rev. B **53**, 1850 (1996)

[89] Grewe, N.; Schmitt, S.; Jabben, T. and Anders, F.B. Journal of Physics: Condensed Matter **20**, 365217 (2008)

[90] Ruhoff, P.T. Chem. Phys. **186**, 355 (1994)

[91] Ruhoff, P.T. and Ratner, M.A. Int. J. Quant. Chem. **77**, 383 (2000)

[92] Seldenthuis, J.S.; van der Zant, H.S.J.; Ratner, M.A. and Thijssen, J.M. ACS Nano **2**, 1445 (2008)

[93] Yu, L.H.; Keane, Z.K.; Ciszek, J.W.; Cheng, L.; Stewart, M.P.; Tour, J.M. and Natelson, D. Phys. Rev. Lett. **93**, 266802 (2004)

[94] Kamenev, A. and Levchenko, A. Advances in Physics **58**, 197 (2009)

[95] Negele, J.W. and Orland, H. *Quantum Many-Particle Systems*, vol. 68 of *Frontiers in Physics* (Addison-Wesley Publishing Company, Redwood City, California, 1988) (1988)

[96] Luttinger, J.M. and Ward, J.C. Phys. Rev. **118**, 1417 (1960)

Chapter 3

Quantum transport with two interacting conduction channels

Alexander J. White[1], Agostino Migliore[2,a)], Michael Galperin[1], and Abraham Nitzan[2]

[1]Department of Chemistry and Biochemsitry, University of California at San Diego, La Jolla CA 92093, USA

[2]School of Chemistry, Tel Aviv University, Tel Aviv 69978, Israel

[a)]Present address: Department of Chemistry, Duke University, Durham, North Carolina 27708, USA.

Reprinted with permission from *The Journal of Chemical Physics* **138**, 174111 (2012).

The transport properties of a conduction junction model characterized by two mutually coupled channels that strongly differ in their couplings to the leads are investigated. Models of this type describe molecular redox junctions (where a level that is weakly coupled to the leads controls the molecular charge, while a strongly coupled one dominates the molecular conduction), and electron counting devices in which the

current in a point contact is sensitive to the charging state of a nearby quantum dot. Here we consider the case where transport in the strongly coupled channel has to be described quantum mechanically (covering the full range between sequential tunneling and co-tunneling), while conduction through the weakly coupled channel is a sequential process that could by itself be described by a simple master equation. We compare the result of a full quantum calculation based on the pseudoparticle non-equilibrium Green function method to that obtained from an approximate mixed quantum-classical calculation, where correlations between the channels are taken into account through either the averaged rates or the averaged energy. We find, for the steady state current, that the approximation based on the averaged rates works well in most of the voltage regime, with marked deviations from the full quantum results only at the threshold for charging the weekly coupled level. These deviations are important for accurate description of the negative differential conduction behavior that often characterizes redox molecular junctions in the neighborhood of this threshold.

3.1 Introduction

Transport in mesoscopic and nanoscopic junctions is usually a multichannel phenomenon. Model studies of transport in junctions that comprise two, often interacting, conduction channels have been carried out in order to describe the essential features of different physical phenomena. Prominent examples are studies of interference effects in quantum conduction, analysis of single electron counting, where a highly transmitting junction (a point contact) is used to monitor the electronic state of a poorly transmitting one, and redox molecular junctions, where (transient) electron localization in one channel, stabilized by environmental polarization, determines the transition between redox states that are observed by the conduction properties of another channel. These three classes of phenomena are described by different flavors of the two-channel model. Interference is usually discussed as a single electron problem and interaction with the environment is minimized (often disregarded in model studies) so as to maintain phase coherent transport. Single electron counting with a point-contact detector is by definition a many electron problem, however environmental interactions are again minimized (and again often disregarded in theoretical analysis) by lowering the experimental temperature in order to obtain detectable signals. Conduction in redox junctions is usually observed in room temperature polar environments and is characterized by large solvent reorganization that accompanies the electron localization at the redox site.

In recent work[1–3,7] we have studied the conduction properties of junctions of the latter type. We first analyzed, for a model involving a single conduction channel, the consequence of large solvent reorganization in the limit where the coupling between the molecular bridge and the metal leads is large relative to the frequency of the phonon mode used to model the solvent dynamical response.[1–3] It was shown (using a mean field description essentially equivalent to the Born Oppenheimer approximation) that solvent induced stabilization of different charging states of the molecule can result in multistable operation of the junction, offering a possible rationalization of observations of negative differential resistance (NDR) and hysteretic response in molecular redox junctions. Such multistability was indeed observed recently in numerical simulations that avoid the mean field approximation.[8,9] Many redox junctions, however, operate in the opposite limit of relatively small molecule-lead coupling, where a single conduction

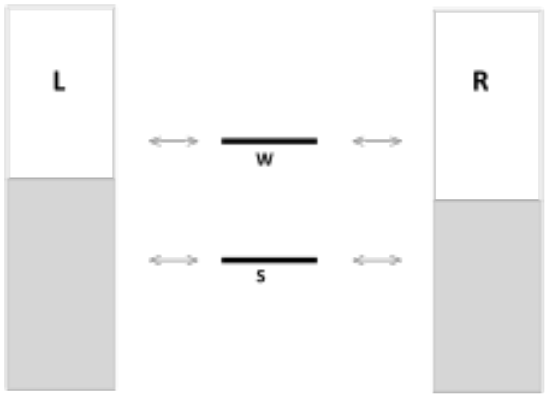

Figure 3.1: The two channel model discussed in the paper. Each channel comprises one level coupled to the left and right electrodes. W and S denote weakly and strongly coupled levels, respectively.

channel model cannot show multistable transport behavior. Two of us have recently advanced a two channel model that can account for such observations.[7] In the absence of electron-phonon interaction (solvent polarization) this model is given by the Hamiltonian (see Fig. 3.1)

$$\begin{aligned}\hat{H} = &\sum_{m=S,W} \varepsilon_m \hat{d}_m^\dagger \hat{d}_m + U\hat{n}_S\hat{n}_W + \sum_{k\in L,R} \varepsilon_k \hat{c}_k^\dagger \hat{c}_k \\ &+ \sum_{k\in L,R} \left(V_{kW}\hat{c}_k^\dagger \hat{d}_W + H.c. \right) \\ &+ \sum_{k\in L,R} \left(V_{kS}\hat{c}_k^\dagger \hat{d}_S + H.c. \right)\end{aligned} \tag{3.1}$$

where $\hat{d}_m^\dagger$ ($\hat{c}_k^\dagger$) creates electron in level m (state k of the contact), and $\hat{n}_m = \hat{d}_m^\dagger \hat{d}_m$, $m = S, W$. In this model, the two channels are coupled only capacitively (no inter-channel electron transfer). U represents the standard Coulomb interaction between them. Two coupled channel models such as (3.1) also characterize single electron counting devices,[10–15] where the current in a point contact (that can be represented by channel S) measures the charging state of a quantum dot used as a bridge in a nearby junction (channel W). The noise properties of such junctions have been studied extensively.[16–21]

In this model, supplemented by electron phonon coupling that represents the response of a polar environment to the electronic occupations in levels W and S, the

molecular redox site dominates the properties of one channel (addressed below as "weakly coupled" or "slow" and denoted by W), characterized by strong transient localization stabilized by large reorganization of the polar environment and weak coupling to the metal leads. Transport through this channel, that is, charging and discharging of the molecular redox site, was described by sequential kinetic processes. A second channel (addressed below as "strongly coupled" or "fast" and denoted by S) is more strongly coupled to the leads and is responsible for most or all of the observed current.[22] Switching between charging states of the slow channel amounts to molecular redox states that affect the transmission, therefore the observed current, through the fast channel. Bistability and hysteretic response on experimentally relevant timescales are endowed into the model in a trivial way[23] and, as was shown in Ref.[7] (see also Refs.[24–26]), NDR also appears naturally under suitable conditions.

Obviously, this behavior is generic and results from the timescale separation between the W and S channels together with the requirement that the observed current is dominated by the S channel. In Refs.[7] and,[27] we have described the expected phenomenology of such junction model in the limit where transport through both channels is described by simple kinetic equations with Marcus electron transfer rates. While, as indicated above, it is natural to model the slow dynamics (observed timescales $\sim 10^{-6}$ s) in this way, it is also of interest to consider fast channel transport on timescales where transport coherence is maintained. For example, one could envision a redox junction that switches between two conduction modes, which shows interference pattern associated with the structure of the fast channel. As a prelude for such considerations, we have studied in Ref.[27] also a model in which the weakly coupled channel W is described by Marcus kinetics, however conduction through the strongly coupled channel S is described as a coherent conduction process by means of the Landauer formula, assuming that the timescale of transport through this channel is fast enough to make it possible to ignore any interaction with the polar environment. As in any mixed quantum-classical dynamics, such description is not consistently derived from a system Hamiltonian, and ad-hoc assumptions about the way the quantum and classical subsystems interact with each other must be invoked, as described in Section 3.2.

In this paper we present a full quantum calculation of the current-voltage re-

sponse of the two channel model described above, and use it to assess the approximate solution obtained using Eqs. (3.2)-(3.6) with models A and B (see Section 3.2). The quantum calculation is done with the pseudoparticle non-equilibrium Green function (PP-NEGF) technique,[28–31] named the slave boson technique when applied to a 3-states system (Anderson problem at infinite U),[32–35] which was recently used by two of us to study effects of electron-phonon and exciton-plasmon interactions in molecular junctions.[36,37] We note that all the methods used in the paper have their own limitations. In particular, PP-NEGF is perturbative in the system-bath coupling. However, it accounts exactly for the intra-system interactions, and it is the role of these interactions (quantum correlations due to system channels interactions) which is missed by the mixed quantum classical approaches and is the focus of the present study.

In Section 3.2 we present our model, briefly review the master equation description and introduce two approximate descriptions of mixed classical-quantum dynamics. The PP-NEGF technique and other details of the fully quantum calculation are described in Section 3.3. Section 3.4 presents our results and discusses the validity of the approximate calculations. Section 3.5 concludes.

3.2 Mixed quantum classical approximations

To account for the current-voltage behavior of a junction characterized by the Hamiltonian (3.1), several workers[16–21] have used a master equation level of description, whereupon, for a given voltage, the dynamics of populating and de-populating the levels S and W is described by classical rate equations involving only their populations, with occupation and de-occupation rates given by standard expressions (see Eq. (3.4) below). Here, in order to focus on redox junction physics, the coupling of channel W to the contacts is assumed to be much smaller than that of channel S, so that in the absence of correlations channel W can be assumed to be classical and treated within such rate equations approach. At the same time channel S will be treated as quantum, as discussed in the previous section.

In Ref.,[27] we have assumed that on the timescale of interest the junction can be in two states: 1 and 0, where the weakly coupled channel, that is the molecular redox

site - is occupied or vacant, respectively. The probability $P_1 = 1 - P_0$ that the junction is in state 1 satisfies the kinetic equation

$$\frac{dP_1}{dt} = (1 - P_1)\, k_{0\to 1} - P_1 k_{1\to 0} \tag{3.2}$$

where the rates $k_{0\to 1}$ and $k_{1\to 0}$ are electron transfer rates between a molecule and an electrode, here the rates to occupy and vacate the redox molecular site, respectively. These rates are sums over contributions from the two electrodes

$$k_{i\to j} = k^{(L)}_{i\to j} + k^{(R)}_{i\to j}; \qquad i, j = 0, 1 \tag{3.3}$$

and depend on the position of the redox molecular orbital energy ε_r relative to the Fermi energy (electronic chemical potential) of the corresponding electrode. In Ref.[27] we have used Marcus heterogeneous electron transfer theory to calculate these rates, thus taking explicitly into account solvent reorganization modeled as electron-phonon coupling in the high temperature and strong coupling limit. For the purpose of the present work it is enough to use the simpler, phonon-less, model

$$\begin{aligned} k^{(K)}_{0\to 1}(\varepsilon_r) =& \Gamma^K_r f_K(\varepsilon_r) \\ k^{(K)}_{1\to 0}(\varepsilon_r) =& \Gamma^K_r \left[1 - f_K(\varepsilon_r)\right] \end{aligned} \tag{3.4}$$

where ε_r is the energy of the "redox level" (see below), $f_K(E) = \left[\exp\left((E - \mu_K)/T\right) + 1\right]^{-1}$ $(K = L, R)$ is the Fermi-Dirac function of the electrode K, μ_K is the corresponding electronic chemical potential and T is the temperature (in energy units). Γ^K_r, $K = L, R$ are the widths of the redox molecular level due to its electron transfer coupling to the electrodes.[38] In terms of the Hamiltonian, Eq. (3.1) above, these widths are given by $\Gamma^K_W = 2\pi \sum_{k\in K} |V_{Wk}|^2 \delta(E - \varepsilon_k)$. We have assumed that in the relevant energy regions these widths do not depend on energy.

From Eqs. (3.2) and (3.3), the steady state population of the redox site is $P_1 = 1 - P_0 = k_{0\to 1}/\left(k_{0\to 1} + k_{1\to 0}\right)$, and the current through the weakly coupled channel is $I_W = k^{(L)}_{0\to 1} P_0 - k^{(L)}_{1\to 0} P_1 = k^{(R)}_{1\to 0} P_1 - k^{(R)}_{0\to 1} P_0$. This current is however negligible relative to the contribution from the strongly coupled channel. In each of the states 0

and 1, the current I_S as well as the average bridge population $\langle n_S \rangle$ in this channel, are assumed to be given by the standard Landauer theory for a channel comprising one single electron orbital of energy ε_S bridging the leads, disregarding the effect of electron-phonon interaction,[39,40]

$$I_S\left(V;\varepsilon_S\right) = \frac{e}{\hbar}\int_{-\infty}^{+\infty}\frac{d\varepsilon}{2\pi}\,\frac{\Gamma_S^L\Gamma_S^R\left[f_L(E)-f_R(E)\right]}{\left(\varepsilon-\varepsilon_S\right)^2+\left(\Gamma_S/2\right)^2} \tag{3.5}$$

$$\langle n_S\left(V;\varepsilon_S\right)\rangle = \int_{-\infty}^{+\infty}\frac{d\varepsilon}{2\pi}\,\frac{\Gamma_S^L f_L(\varepsilon)+\Gamma_S^R f_R(\varepsilon)}{\left(\varepsilon-\varepsilon_S\right)^2+\left(\Gamma_S/2\right)^2} \tag{3.6}$$

where $\Gamma_S = \Gamma_S^L + \Gamma_S^R$ and where ε_S and Γ_S^K take the values $\varepsilon_S^{(0)}$, $\Gamma_S^{K(0)}$ in state 0, and $\varepsilon_S^{(1)} = \varepsilon_S^{(0)} + U$, $\Gamma_S^{K(1)} = \Gamma_S^{K(0)}$ in state 1. U is essentially a Coulomb energy term that measures the effect of electron occupation in channel W, i.e. at the redox site, on the energy of the bridging orbital in channel S. Γ_S^L, Γ_S^R, ε_S, and U are model parameters. The average population and current in channel S are given by $\langle n_S\rangle = P_0\langle n_S\rangle^{(0)} + P_1\langle n_S\rangle^{(1)}$; $\langle I_S\rangle = P_0 I_S^{(0)} + P_1 I_S^{(1)}$, where $I_S^{(0)}$ ($\langle n_S\rangle^{(0)}$) and $I_S^{(1)}$ ($\langle n_S\rangle^{(1)}$) are the values of I_S, Eq. (3.5) ($\langle n_S\rangle$, Eq. (3.6)) in system states 0 (redox level empty), and 1 (redox level populated). Finally, the total current at a given voltage is $I = I_S + I_W \approx I_S$.

It should be noted that the rates defined by Eq. (3.4) are not completely specified, because the "redox energy level" ε_r is not known: it is equal to ε_W only if the capacitive interaction between the S and W channels is disregarded. To take this interaction into account, two models were examined in Ref.:[27]

Model A. The rates are written as weighted averages over the populations 0 and 1 of channel S with respective weights $1-\langle n_S\rangle$ and $\langle n_S\rangle$:

$$\begin{aligned} k_{0\to1} &= \left(1-\langle n_S\rangle^{(0)}\right)k_{0\to1}^{(S0)} + \langle n_S\rangle^{(0)}k_{1\to0}^{(S0)} \\ k_{1\to0} &= \left(1-\langle n_S\rangle^{(1)}\right)k_{0\to1}^{(S1)} + \langle n_S\rangle^{(1)}k_{1\to0}^{(S1)} \end{aligned} \tag{3.7}$$

where $k_{0\to1}^{(S0)}$, $k_{0\to1}^{(S1)}$ are the rates to occupy and vacate, respectively, the redox site when the fast channel is not occupied, while $k_{0\to1}^{(S1)}$, $k_{1\to0}^{(S1)}$ are the corresponding rates when this channel is occupied. The dependence of these rates on the occupation of the fast channel is derived from the dependence of ε_r in Eq. (3.4) on the occupation of level S: $\varepsilon_r = \varepsilon_W$

when this level is not occupied, and $\varepsilon_r = \varepsilon_W + U$ when it is. That is,

$$\begin{aligned} k_{0\to1}^{(K,S0)} =& \Gamma_r^K f_K(\varepsilon_W) \\ k_{1\to0}^{(K,S0)} =& \Gamma_r^K \left[1 - f_K(\varepsilon_W)\right] \\ k_{0\to1}^{(K,S1)} =& \Gamma_r^K f_K(\varepsilon_W + U) \\ k_{1\to0}^{(K,S1)} =& \Gamma_r^K \left[1 - f_K(\varepsilon_W + U)\right] \end{aligned} \tag{3.8}$$

Here $K = L, R$.

Model B. The rates are given by Eq. (3.4), with ε_r calculated as the difference between the energies of two molecular states, one with the redox level populated, $E_1 = \left(\varepsilon_S^{(0)} + U\right)\langle n_S\rangle^{(1)} + \varepsilon_2^{(0)} = \varepsilon_S^{(1)}\langle n_S\rangle^{(1)} + \varepsilon_2^{(0)}$ and the other with the redox level empty, $E_0 = \varepsilon_S^{(0)}\langle n_S\rangle^{(0)}$:

$$\varepsilon_r = \left(\varepsilon_S^{(1)}\langle n_S\rangle^{(1)} + \varepsilon_2^{(0)}\right) - \varepsilon_S^{(0)}\langle n_S\rangle^{(0)} \tag{3.9}$$

These two models are associated with different physical pictures that reflect different assumptions about relative characteristic timescales. Model A assumes that the switching rates between states 0 and 1 follow the instantaneous population in channel S, while model B assumes that these switching rates are sensitive only to the average population $\langle n_S\rangle$. Model B results from a standard Hartree approximation that would be valid if the electronic dynamics in channel W is slow relative to that of channel S (see Appendix). From the discussion above it may appear at first glance to be the case, since transmission through channel W is small, implying that the rates $k_{0\to1}$ and $k_{1\to0}$ are small. However, the electronic process that determines the timescale on which these rates change is not determined by the magnitude of these rates but by the response of the electrodes to changes in ε_r following changes in the bridge level population of the strongly coupled channel. This characteristic time (or times), τ_B, which is bounded below by the inverse electrode bandwidth, may depend also on temperature and the energy dependence of the spectral density, and can be shorter than the timescale of order of Γ_S^{-1} on which population in channel S is changing (note that τ_B is vanishingly short in the wide band limit). In this case model A would provide a better approximation. For comparison, we also present below results for model C, in which the effect of the interaction between the two channels on the electron transfer kinetics in channel W is

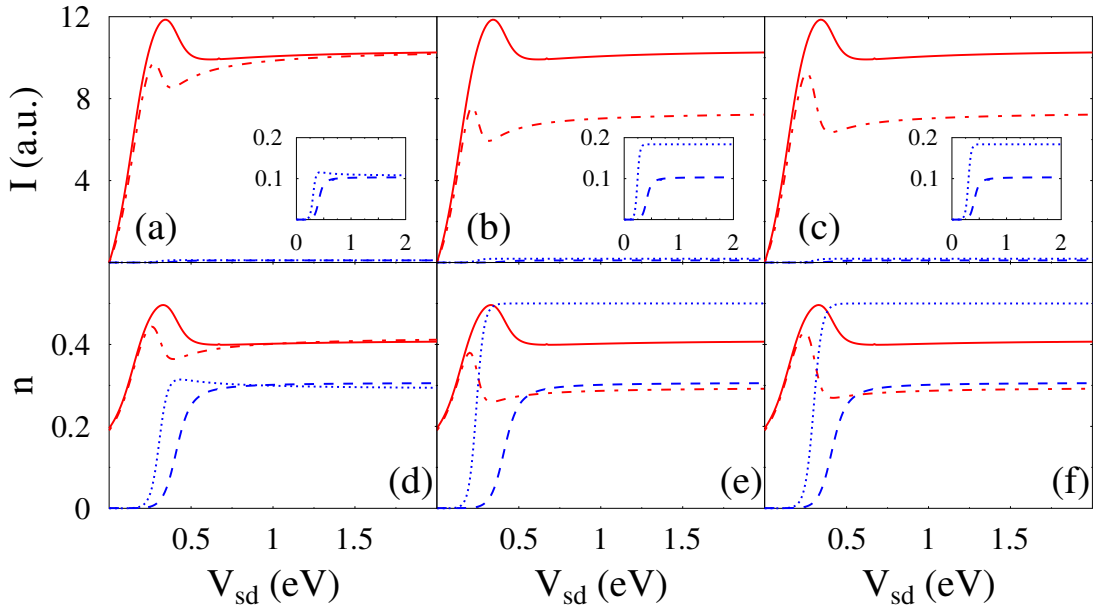

Figure 3.2: (Color online) Current (panels a-c) and populations of the channels (panels d-f). Results for the models A (panels a and d), B (panels b and e), and C (panels c and f) are shown for the channels S (dash-dotted line, red) and W (dotted line, blue), and compared to the PP-NEGF results for the same channels (solid, red and dashed, blue lines, respectively). Note, the PP-NEGF data is the same in panels a-c and d-f. See text for parameters.

disregarded so that

$$\begin{aligned} k^K_{0\to 1} =& \Gamma^K_W f_K(\varepsilon_W) \\ k^K_{1\to 0} =& \Gamma^K_W \left[1 - f_K(\varepsilon_W)\right] \end{aligned} \tag{3.10}$$

while the current through channel S continues to be sensitive to the difference between states 0 and 1, as before.

3.3 The pseudoparticle Green function method

Models A and B above represent attempts to partly account for the coupling between channels within the classical rate equations description of channel W. The existence of capacitive coupling between the channels makes such mixed quantum-classical description potentially invalid, since it misses quantum correlations between the two channels. To estimate the performance of these approximations we shall compare them

to a fully quantum calculation based on the pseudoparticle nonequilibrium Green function technique.[36]

In the PP-NEGF approach, a set of molecular many-body states, $\{|N\rangle\}$, defines the set of pseudoparticles to be considered, so that one pseudoparticle represents each state. In particular, for the model (3.1) the molecular subspace of the problem is represented by four many-body states: $|N\rangle = |n_W, n_S\rangle$, where $n_{W,S} = 0, 1$. Let $\hat{p}^\dagger_N$ ($\hat{p}_N$) be the creation (annihilation) operator for the state $|N\rangle$. These operators are assumed to satisfy the usual fermion or boson commutation relations depending on the type of the state. In our case the pseudoparticles associated with the states $|1, 0\rangle$ and $|0, 1\rangle$ are of Fermi type, while those corresponding to states $|0, 0\rangle$ and $|1, 1\rangle$ follow Bose statistics. The PP-NEGF is defined on the Keldysh contour as

$$G_{N_1,N_2}(\tau_1, \tau_2) \equiv -i\langle T_c\, \hat{p}_{N_1}(\tau_1)\, \hat{p}^\dagger_{N_2}(\tau_2)\rangle \tag{3.11}$$

In the extended Hilbert space it satisfies the usual Dyson equation, thereby providing a standard machinery for their evaluation. Reduction to the physically relevant subspace of the total pseudoparticle Hilbert space is achieved by imposing the constraint

$$\sum_N \hat{p}^\dagger_N \hat{p}_N = 1 \tag{3.12}$$

on the Dyson equation projections. The resulting system of equations for the Green function projections has to be solved self-consistently (see e.g. Ref.[36] for details). Finally, connections to Green functions of the standard NEGF formulation can be obtained by using relations between the electron operators in the molecular subspace of Eq. (3.1) and those of the pseudoparticles

$$\hat{d}^\dagger_m = \sum_{N_1,N_2} \langle N_1|\hat{d}^\dagger_m|N_2\rangle \hat{p}^\dagger_{N_1} \hat{p}_{N_2} \tag{3.13}$$

Thus the current through the junction can be obtained either by the usual NEGF expression,[40] or within its pseudoparticle analog.[36]

Results of calculations based on this procedure and on the kinetic schemes described in Section 3.1 are presented and discussed next.

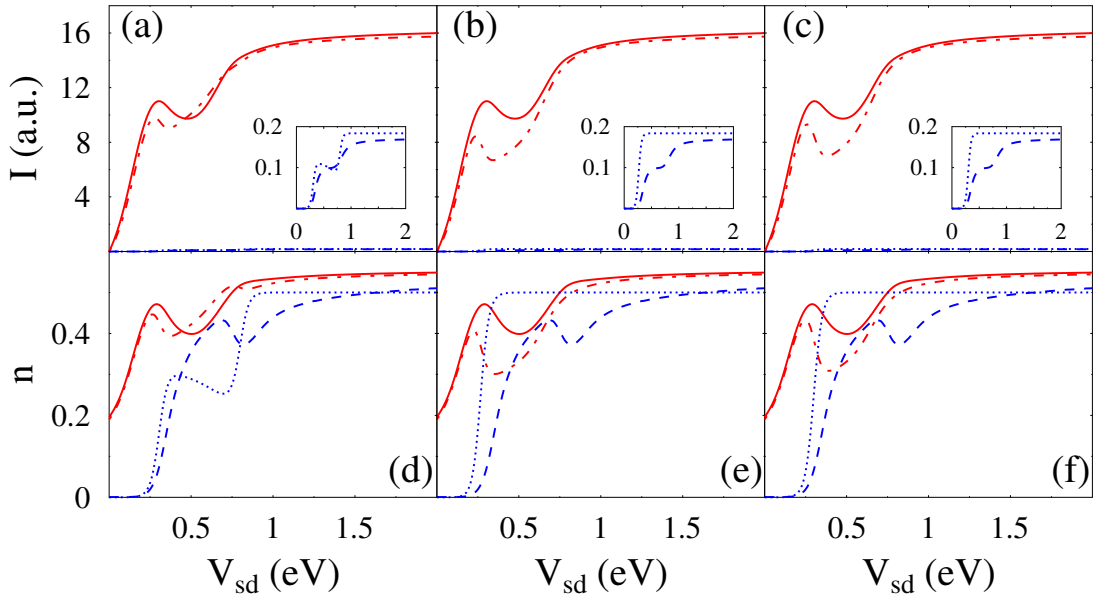

Figure 3.3: (Color online) Same as Fig. 3.2 except $U = 500$ meV

3.4 Results and discussion

In Figures 3.2 and 3.3 we compare results from the fully quantum calculation based on the PP-NEGF technique with those based on the kinetic approximations defined by models A-C of Section 3.1. Panels (a), (b) and (c) in Fig. 3.2 show the current through channels S (red) and W (blue) as function of voltage, while the corresponding panels (d), (e) and (f) show, with the same color and line-forms codes, the electronic populations in these channels. The full and dashed lines in these plots correspond to the PP-NEGF calculations for channels S and W, respectively, and are identical in the panels (a-c) and in panels (d-f). The dash-dotted and dotted lines show results based on models A (panels (a) and (d)), B (panels (b) and (e)) and C (panels (c) and (f)). The parameters used in these calculations are $E_F = 0$, $T = 300$ K, $\Gamma_W^L = \Gamma_W^R = 1$ meV, $\Gamma_S^L = \Gamma_S^R = 100$ meV, $\varepsilon_S = 150$ meV, $\varepsilon_W = 300$ meV, and $U = 10$ eV. For this choice of U states S and W cannot be populated simultaneously. The corresponding panels of Figs. 3.3 and 3.4 show similar results for the same choice of parameters, except that in Fig. 3.3 U is taken 500 meV while in Fig. 3.4 $\Gamma_W^L = 1.9$ meV and $\Gamma_W^R = 0.1$ meV (so $\Gamma_W = \Gamma_W^L + \Gamma_W^R = 2$ meV as before). The latter choice designates level W as a blocking level - current goes down considerably when the voltage bias exceeds the threshold

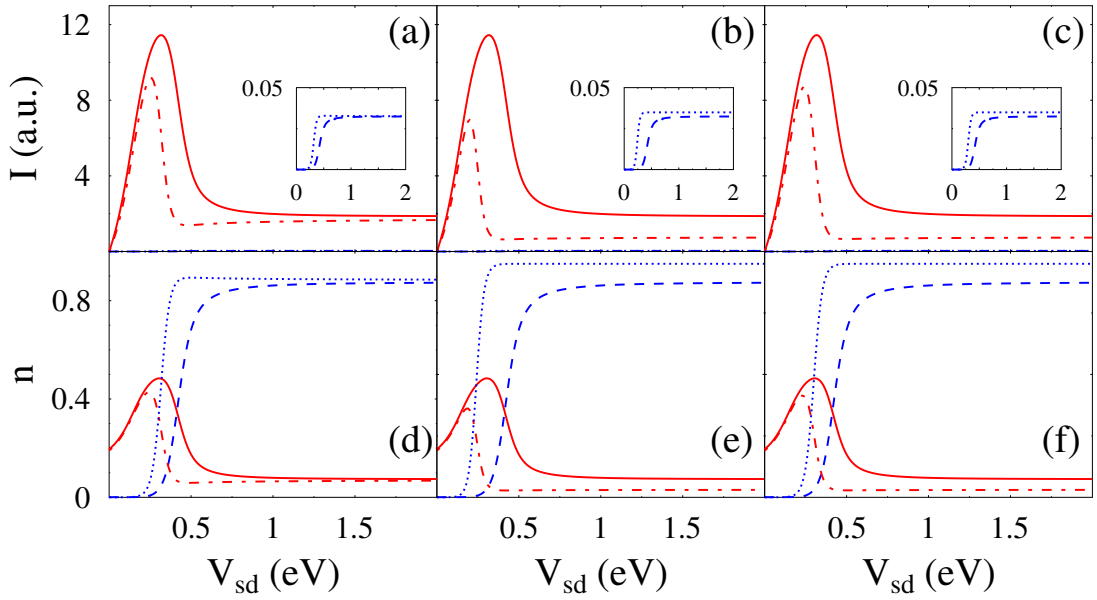

Figure 3.4: (Color online) Same as Fig. 3.2 except $\Gamma_W^L = 1.9$ meV and $\Gamma_W^R = 0.1$ meV.

(300 meV) needed to populate it), and has been suggested before[4–7] as a model for negative differential resistance in molecular junctions. Finally, in Fig. 3.5, the parameters are the same is in Fig. 3.2 except that $T = 0$ K. The voltage was changed by moving the Fermi level of the left electrode, keeping the right electrode static. The insets in the I/V plots show a closeup look at the contribution from channel W. The following observations are notable:

(a) In comparison with the full quantum calculation, Model A performs considerably better than model B and, not surprisingly, than model C. The failure of model B is notable in view of the common practice to use the timescale separation as an argument for applying mean field theory in such calculations; however, as argued above, it follows from the use of the wide band limit for the electrodes in the calculations.

(b) While model A seems to be quite successful in much of the voltage regime, it fails, as expected, near and around $V = 0.3$ V, the (bare) threshold to populate the W level. It is at this point of maximal fluctuations in the W population that electronic correlation is most pronounced, as this population is strongly correlated with that in S.

(c) The deviation of the kinetic approximation from the full quantum result is considerably larger for the current and population of channel W (the redox site) than for channel

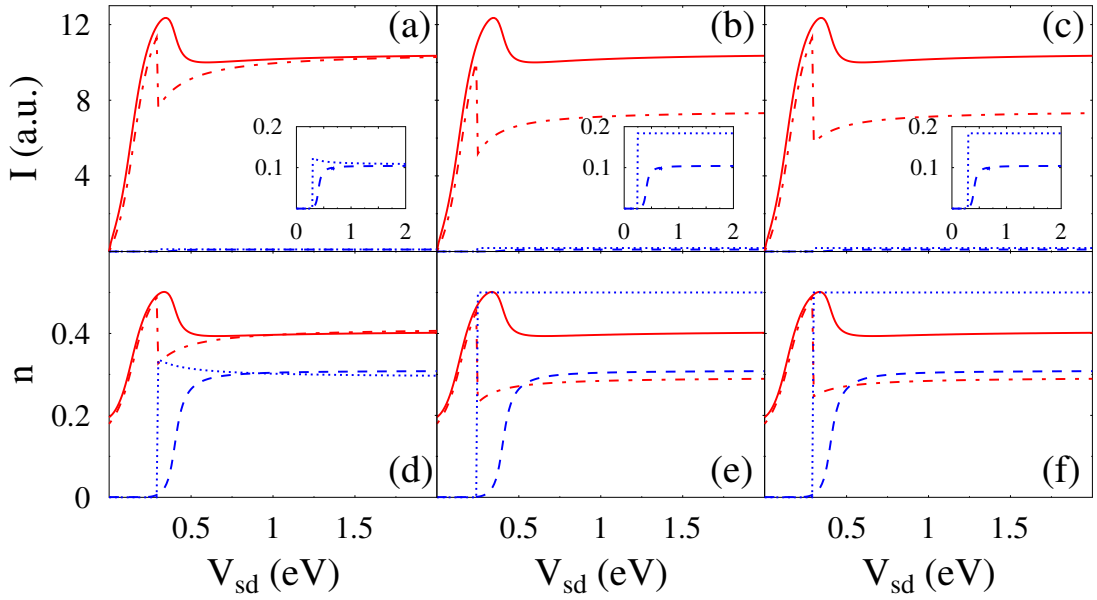

Figure 3.5: (Color online) Same as Fig. 3.2 except $T = 0$ K.

S. This reflects the fact that the rates of charging and discharging the redox site are sensitive to its correlation with the population on the strongly coupled level, while the dynamics of the latter responds most of the time just to the static population in W. Of course, these large deviations in the current carried by channel W have only an insignificant effect on the overall observed current. To see these important quantum correlation effects one would need to monitor directly the electronic population of the redox site, which is possible in principle using spectroscopy probes.

(d) As a model for negative differential resistance (Fig. 3.4), model A performs qualitatively well, however the full calculation sets the NDR threshold considerably higher than that predicated by the approximate calculation.

(e) As expected, the differences between the full quantum calculation and the results of model A become more pronounced at $T = 0$ K. While the results of model A display sharp threshold behavior, the full calculation is much less sensitive to temperature for the present choice of parameters because the width of the transition region is dominated by Γ_S that is substantially greater than the thermal energy.

3.5 Conclusion

We have examined the electronic transport behavior of a generic junction model that comprises a bridge characterized by two interacting transport channels whose couplings to the leads are vastly different from each other. This is a model for a molecular redox junction and also for a point contact detector interacting with a weakly coupled nanodot bridge. We have compared approximate kinetic schemes for the dynamics of this junction to a full quantum calculation based on the pseudoparticle NEGF methodology. We found that a kinetic model in which the electron transfer rates in the weakly coupled channel (redox site) respond instantaneously to occupation changes in the strongly coupled channel works relatively well in comparison with a mean field calculation. Still, this model fails quantitatively when the molecular level comes close to the electrochemical potential of the lead, reflecting the significance of electronic correlations in this voltage range.

This paper has focused on the steady state current. Correlations between the two channels are expected to become considerably more pronounced in the noise properties of such junctions and, most probably, would not be amenable to analysis using the kinetic approximation of model A. We defer this interesting issue to future work.

Acknowledgments

The research of AN is supported by the Israel Science Foundation, the Israel-US Binational Science Foundation and the European Research Council under the European Union's Seventh Framework Program (FP7/2007-2013; ERC grant agreement no 226628). MG gratefully aknowledges support by the Department of Energy (Early Career Award, DE-SC0006422) and the US-Israel Binational Science Foundation (grant no. 2008282). We thank Kristen Kaasbjerg for useful discussions. MG and AN thank the KITPC Beijing for hospitality and support during the time when this work was completed. Chapter 3, in full, is a reprint of the material as it appears in The Journal of Chemical Physics 2013. White, Alexander J.; Migliore, Agostino; Galperin, Michael; and Nitzam, Abraham, AIP Publishing LLC 2013. The dissertation author was the primary investigator and author of the paper.

3.6 Appendix: Timescale considerations leading to the models A and B

When it is reasonable to speak about rate of a channel, the formal expression for the W channel rate is[41]

$$\int_{-\infty}^{t} dt'\, e^{i\int_{t'}^{t} ds\, \varepsilon_r(s)} V(t)\, C(t-t')\, V(t') \tag{3.14}$$

where ϵ_r is the position of the redox level, $V(t)$ is the coupling between the channel W and the bath, and $C(t-t')$ is the bath correlation time.

At least two timescales have to be taken into account: one related to the dynamics of the redox level, $\varepsilon_r(t)$, the other representing characteristic timescale of the bath. Note, that in general the bath is characterized by several timescales (e.g. the bandwidth of the metal, temperature, and variation of spectral density). In our case the characteristic timescale for the dynamics of the level in the W channel is given by the rate of population change in the S channel. The latter is proportional to Γ_S^{-1} (Coulomb interaction is instantaneous). Let assume that the characteristic time of the bath is τ_B. The two extremes are $\tau_B \ll \Gamma_S^{-1}$ and $\tau_B \gg \Gamma_S^{-1}$. The former case corresponds to slow motion of the level relative to the bath dynamics, so that expression (3.14) yields a set of rates (2 in our case) for different positions of the redox level. This corresponds to the model A of the paper.

The other extreme, $\tau_B \gg \Gamma_S^{-1}$, corresponds to quick motion of the redox level position, which requires averaging of the exponential factor in (3.14). This leads to appearance of a single rate, calculated at the average position of the level, which is model B.

Chapter 3 References

[1] M. Galperin, M. A. Ratner, and A. Nitzan, Nano Letters **5**, 125-130 (2005).

[2] M. Galperin, A. Nitzan, and M. A. Ratner, The Journal of Physics: Condensed Matter **20**, 374107 (2008).

[3] M. Galperin, A. Nitzan, and M. A. Ratner, arXiv:0909.0915 (2009).

[4] M. H. Hettler, H. Schoeller, and W. Wenzel, Europhysics Letters **57**, 571 (2002).

[5] B. Muralidharan and S. Datta, Physical Review B **76**, 035432 (2007).

[6] R. Hartle and M. Thoss, Physical Review B **83**, 115414 (2011).

[7] A. Migliore and A. Nitzan, ACS Nano **5**, 6669 (2011).

[8] K. F. Albrecht, H. Wang, L. Mühlbacher, M. Thoss, and A. Komnik, Physical Review B **86**, 081412 (2012).

[9] It should be emphasized that the theory addresses only locally stable states that will not persist beyond some finite lifetime, and do not imply multistability in the thermodynamic sense.

[10] M. Field, C. G. Smith, M. Pepper, D. A. Ritchie, J. E. F. Frost, G. A. C. Jones, and D. G. Hasko, Physical Review Letters **70**, 1311 (1993).

[11] J. M. Elzerman, R. Hanson, L. H. W. v. Beveren, B. Witkamp, L. M. K. Vandersypen, and L. P. Kouwenhoven, Nature **430**, 431 (2004).

[12] L. M. K. Vandersypen, J. M. Elzerman, R. N. Schouten, L. H. W. v. Beveren, R. Hanson, and L. P. Kouwenhoven, Appied Physics Letters **85**, 4394 (2004).

[13] R. Schleser, E. Ruh, T. Ihn, K. Ensslin, D. C. Driscoll, and A. C. Gossard, Applied Physics Letters 85, 2005 (2004).

[14] T. Fujisawa, T. Hayashi, R. Tomita, and Y. Hirayama, Science **312**, 1634 (2006).

[15] S. Gustavsson, R. Leturcq, B. Simovic, R. Schleser, T. Ihn, P. Studerus, K. Ensslin, D. C. Driscoll, and A. C. Gossard, Physical Review Letters **96**, 076605 (2006).

[16] S. A. Gurvitz and Y. S. Prager, Physical Review B **53**, 15932 (1996).

[17] S. A. Gurvitz, Physical Review B **56**, 15215 (1997).

[18] G. Bulnes Cuetara, M. Esposito, and P. Gaspard, Physical Review B **84**, 165114 (2011).

[19] A. Carmi and Y. Oreg, Physical Review B **85**, 045325 (2012).

[20] G. Kiesslich, P. Samuelsson, A. Wacker, and E. Scholl, Physical Review B **73**, 033312 (2006).

[21] G. Kiesslich, E. Scholl, T. Brandes, F. Hohls, and R. J. Haug, Physical Review Letters **99**, 206602 (2007).

[22] The "fast" channel carries all the current if the "slow" channel is coupled only to one of the leads.

[23] A. Migliore, P. Schiff, and A. Nitzan, Physical Chemistry Chemical Physics **14**, 13746 (2012).

[24] B. Muralidharan and S. Datta, Physical Review B **76**, 035432 (2007).

[25] M. Leijnse, W. Sun, M. B. Nielsen, P. Hedegard, and K. Flensberg, The Journal of Chemical Physics **134**, 104107 (2011).

[26] K. Kaasbjerg and K. Flensberg, Physical Review B **84**, 115457 (2011).

[27] A. Migliore and A. Nitzan, to be published (2013).

[28] P. Coleman, Physical Review B **29**, 3035-3044 (1984).

[29] N. E. Bickers, Review Modern Physics **59**, 845-939 (1987).

[30] M. Eckstein and P. Werner, Physical Review B **82**, 115115 (2010).

[31] J. H. Oh, D. Ahn, V. Bubanja, Physical Review B **83**, 205302 (2011).

[32] M. H. Hettler, J. Kroha and S. Hershfield, Physical Review B **58**, 5649-5664 (1998).

[33] T. Schauerte, J. Kroha, and P. Wölfle, Physical Review B **62**, 4394-4402 (2000).

[34] N. S. Wingreen and Y. Meir, Physical Review B **49**, 11040-11052 (1994).

[35] N. Sivan and N. S. Wingreen, Physical Review B **54**, 11622-1629 (1996).

[36] A. J. White and M. Galperin, Physical Chemistry Chemical Physics **14**, 13809-13819 (2012).

[37] A. J. White, B. D. Fainberg, and M. Galperin, The Journal of Physical Chemistry Letters **3**, 2738-2743 (2012).

[38] Note that while in quantum mechanics damping rates and level widths are synonymous, it is exactly the energetic consequence of the finite lifetime, that is, the level broadening, which is disregarded in the kinetic approximation.

[39] S. Datta, *Electric transport in Mesoscopic Systems* (Cambridge University Press, Cambridge, 1995).

[40] H. Haug and A.-P. Jauho, *Quantum Kinetics in Transport and Optics of Semiconductors* (Springer, 2008).

[41] M. Esposito and M. Galperin, Physical Review B **79**, 205303 (2009).

Chapter 4

Coherence in charge and energy transfer in molecular junctions

Alexander J. White[1], Uri Peskin[2] and Michael Galperin[1]

[1] Department of Chemistry and Biochemsitry, University of California at San Diego, La Jolla CA 92093, USA

[2] Schulich Faculty of Chemistry and the Lise Meitner Center for Computational Quantum Chemistry, Technion-Israel Institute of Technology, Haifa 32000, Israel

Reprinted with permission from *Physical Review B* **88**, 205424 (2013).

We consider the effects of dephasing on field-induced coherent charge and energy transport in molecular junctions. Within generic models we show that dephasing controls the relative intensities of energy and charge fluxes, and that the dependence of the energy flux on the dephasing rate is non-monotonic. We further demonstrate the possibility for laser-controlled charge-energy separation in multi-terminal molecular junctions, a prerequisite for engineering low-heating stable nano-scale devices.

4.1 Introduction

Single molecules are promising candidates for integration into nano-scale devices. Based on the versatility in structural, electronic, optical and mechanical properties of molecules, molecular devices can be carefully designed and controlled. The small size of molecules implies the necessity of quantum mechanical treatment, and naturally poses questions on the role of coherences in the response properties of molecular devices. In molecular junctions experimental observations were attributed to interference effects in intra-molecular electron transfer[1] and elastic transport through single molecules,[2,3] or to vibrationally induced decoherence.[4]

Coherent control in molecules originated in studies of quantum dynamics in response to laser pulse excitations.[5,6] Advances in optics combined with molecular fabrication techniques in junctions resulted in a new field termed molecular optoelectronics.[7,8] Coherent control of transport in molecular junctions is one of the focuses of research in this field.[9–14] Another focus is the dynamics of energy transfer between plasmonic and molecular excitations.[15–19] The importance of quantum coherence in energy transfer was demonstrated recently in studies of the initial stages of photosynthesis.[20–24]

Theoretical studies in molecular electronics are mostly focused on the role of coherence in elastic transport. In particular, a molecular switch based on quantum interference was proposed in Refs.,[25,26] and molecular transistors utilizing coherence to control transport through single molecule junctions (usually containing a conjugated π system) were discussed in Refs.[27–33] Inelastic processes are usually considered as a source of decoherence, which can both destroy[34,35] or enhance[35–38] transport through molecular systems. Coherence induced by inelastic processes was observed experimentally[39] and discussed in several theoretical studies.[35,40,41] Finally, coherent and incoherent exciton transport in the Fenna-Matthews-Olson complex was studied in a number of theoretical publications.[42–46]

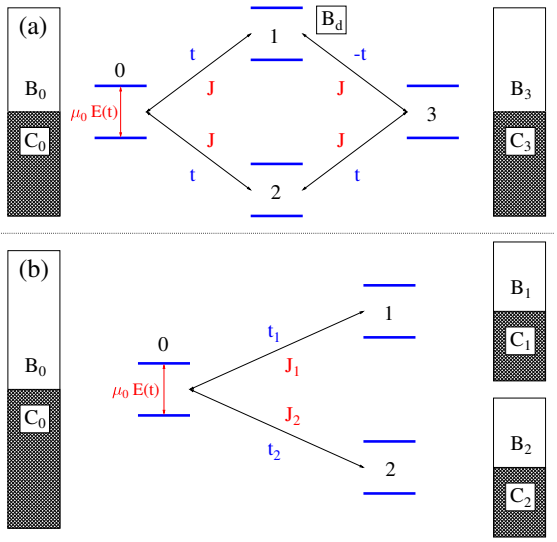

Figure 4.1: (Color online) A sketch of the models for coherently controlled charge-energy (a) pump and (b) switch.

In molecular optoelectronics[8] it is customary to distinguish between charge and energy transfer processes between the molecule and contacts (as well as inside the molecular complex). For example, elastic electron transport (single charges moving through the system) is at the heart of charge transfer - surface enhanced Raman spectroscopy (CT-SERS),[47,48] while pure energy transfer (transfer of excitation without charge transfer) accounts for coupling between molecular excitations and excitations of the leads (exciton-like or neutral pairings of electron-like and hole-like excitations).[17,49–53] Considering non-equilibrium transport through molecular junctions, charge and energy transport processes happen simultaneously, and a rigorous description must therefore account for this. The non-quadratic character of the energy transfer matrix elements complicates the theoretical description and the corresponding theoretical considerations usually rely on approximations.[54,55] Recently we proposed a pseudoparticle non-equilibrium Green's functions (PP-NEGF) method as a tool capable to treat the processes simultaneously and exactly.[52]

Contrary to previous studies where the effects of coherence in either charge or energy transfer were discussed, here we apply the PP-NEGF approach and consider the importance of coherences in simultaneous charge and energy transport through molecular junctions. In particular, we demonstrate possibilities for laser-induced coherent control

of the relative magnitude of energy and charge fluxes generated by a molecular pump. Inspired by the known effect of charge and spin separation in molecular systems[56–59] we also demonstrate a possibility to coherently control the spatial separation of charge and energy fluxes in properly designed multi-terminal molecular junctions.

The different response of charge and energy flows to an external field is derived from the different underlying laser-matter interactions. Energy transport is due to dipole coupling between molecular excitations to electron-hole or plasmon excitations in the leads (usually treated as dipole-dipole interactions), while charge transport is modeled as electron tunneling.[49] Therefore, matrix elements for energy and charge transport between given chromophores can differ in magnitude or phase. In simple cases the different matrix elements can be associated with different Rabi frequencies for charge and energy transfer through the molecule, and when one of these frequencies is in resonance with optically induced Rabi oscillations, the corresponding flux (energy or charge) is expected to be maximal. For realistic systems the task of optimizing the external field parameters for a selected process (amplitude and frequency) is more involved, but nevertheless, we still claim that conditions can be defined in which the field selectively enhances (or suppresses) charge flux along a given path and energy flux along another. As far as we know, this is the first time when the possibility of such separation between charge and energy fluxes is discussed.

In the following we consider explicitly only energy transfer within the molecule. Heat transfer between the molecule and the leads is not accounted for, assuming a constant junction temperature. Note that both charge transport (emission of energetic electrons) and energy transport (emission of electron-hole pairs) can induce heating in the leads, however these processes are external to the molecule, and take place far from the junction.[60] Thus, their effect on the transport at the molecular junction can be neglected. As a side note we mention that the description of molecular excitation (energy transfer) we consider is technically similar to modeling the propagation of vibrational excitation (phonon transport) when expressed in the language of vibronic states. Thus our findings may have implications also in the context of low heating stable nano-scale devices.

Below, after introducing two generic models for charge/energy pump and switch, we discuss a convenient methodology for treating the combined intra-molecular electron

and energy transfer. Our numerical simulations demonstrate different possibilities for laser control of coherent molecular energy and charge pumps, and for spatial separation of charge and energy fluxes in molecular junctions.

4.2 Model

We consider a network of N_m molecules, characterized by chromophores which are coupled to several reservoirs of electrons (or contacts, C) and thermal baths (B). The contacts are assumed to be in equilibrium (no bias), and the driving of the junctions is governed by a laser field $E(t)$ applied to one of the molecules. Each molecular chromophore is represented by its highest occupied (HOMO) and lowest unoccupied (LUMO) molecular orbitals (or ground, g, and excited, x, states). We consider electron and energy transfer between neighboring chromophores and between the chromophores and the baths. We emphasize that our models focus on energy transport through the molecule and does not account explicitly for the thermalization process of access energy in the leads, which happens far from the junction region.

Two systems are discussed: the first model corresponds to a molecular charge and energy pump ($N_m = 4$, see Fig. 4.1a), based on bridge-mediated (1 and 2) transfer between a donor (0) and an acceptor (3). The donor and acceptor are coupled to their own contacts and thermal baths, and the donor is driven by an external laser field. The bridge contains two molecules and the coherent transport reflects interference between the two possible pathways. In order to induce decoherence, one of the bridge molecules (1) is coupled to a local dephasing source (B_d). This type of model is frequently used in considerations of effects of decoherence on electron transfer.[34,36,40]

The second model ($N_m = 3$, see Fig. 4.1b) corresponds to a molecular switch with a donor (0) and two acceptors (1 and 2), each coupled to its own contact and thermal bath. As previously, the donor is driven by an external laser field. We used this model in our previous study[14] as a prototype of coherently controlled molecular switch. Here we extend the consideration to the case of simultaneous energy and charge transfer.

The Hamiltonian of the system(s) is

$$\hat{H}(t) = \hat{H}_M(t) + \sum_K \left(\hat{H}_K + \hat{V}_{MK} \right) \tag{4.1}$$

where $\hat{H}_M(t)$ and $\hat{H}_K$ describe the molecular system M and bath K (K is summed over all the baths in the model), and $\hat{V}_{MK}$ is the coupling between the two. The explicit expressions are

$$\begin{aligned} \hat{H}_M(t) = & \sum_{m=0}^{N_m} \sum_{\ell=g,x} \varepsilon_{m\ell} \hat{n}_{m\ell} - \mu_0 E_0 \left(\hat{d}_{0x}^\dagger \hat{d}_{0g} e^{-i\omega_0 t} + H.c. \right) \\ & + \sum_{m,m'=0}^{N_m} \left(\sum_{\ell=g,x} t_{m\ell,m'\ell} \hat{d}_{m\ell}^\dagger \hat{d}_{m'\ell} + J_{m,m'} \hat{D}_m^\dagger \hat{D}_{m'} + H.c. \right) \end{aligned} \tag{4.2}$$

$$\hat{H}_{C_m} = \sum_{\kappa \in C_m} \varepsilon_\kappa \hat{n}_\kappa; \qquad \hat{H}_{B_m} = \sum_{\alpha \in B_m} \omega_\alpha \hat{n}_\alpha \tag{4.3}$$

$$\begin{aligned} \hat{V}_{MC_m} &= \textstyle\sum_{\kappa \in C_m} \sum_{\ell=g,x} \left(V_{\kappa,m\ell} \hat{c}_\kappa^\dagger \hat{d}_{m\ell} + H.c. \right) \\ \hat{V}_{MB_m} &= \textstyle\sum_{\alpha \in B_m} \left(U_{\alpha,m} \hat{a}_\alpha^\dagger \hat{D}_m + H.c. \right) \end{aligned} \tag{4.4}$$

In the molecular pump model (Fig. 4.1a) local dephasing is introduced by coupling the LUMO of molecule 1 to the bath B_d

$$\hat{H}_{B_d} = \sum_\beta \omega_\beta \hat{n}_\beta; \quad \hat{V}_{MB_d} = M \sum_\beta \left(\hat{b}_\beta + \hat{b}_\beta^\dagger \right) \hat{n}_{1x} \tag{4.5}$$

In Eqs. (4.2)-(4.5) $\hat{d}_{m\ell}^\dagger$ and $\hat{c}_\kappa^\dagger$ create electrons in level ℓ of molecule m, and state κ of contacts $\{C_m\}$, respectively, and $\hat{a}_\alpha^\dagger$ and $\hat{b}_\beta^\dagger$ create phonons in the thermal baths $\{B_m\}$ and B_d, respectively. $\hat{n}_{m\ell} \equiv \hat{d}_{m\ell}^\dagger \hat{d}_{m\ell}$, $\hat{n}_\kappa \equiv \hat{c}_\kappa^\dagger \hat{c}_\kappa$, $\hat{n}_\alpha \equiv \hat{a}_\alpha^\dagger \hat{a}_\alpha$, and $\hat{n}_\beta \equiv \hat{b}_\beta^\dagger \hat{b}_\beta$ are population operators. $\hat{D}_m^\dagger \equiv \hat{d}_{mx}^\dagger \hat{d}_{mg}$ is the operator of molecular excitation. $\varepsilon_{m\ell}$ and ε_κ are on-site electronic energies of level $m\ell$ in the molecules and state k in the contacts. ω_α and ω_β are elementary excitations in the thermal baths $\{B_m\}$ and B_d, respectively. μ_0 is the transition dipole moment of the donor, and E_0 and ω_0 are the amplitude of the driving field and its frequency. $t_{m\ell,m'\ell}$ and $J_{m,m'}$ are the matrix elements of charge and

energy transfer between the chromophores m and m', where the pathways are indicated by lines in Fig. 4.1. Finally, $V_{\kappa,m\ell}$ and $U_{\alpha,m}$ represent electron and energy exchange between the chromophores and the baths. and M is the dephasing strength. We note that coupling to the driving field is written in the rotating wave approximation. Similar models for electron and energy (exciton) transport were considered in the literature previously.[49,54,55]

A transformation to the rotating frame of the field[14]

$$\hat{\tilde{H}} = i\left(\frac{\partial}{\partial t}e^{\hat{S}(t)}\right)e^{-\hat{S}(t)} + e^{\hat{S}(t)}\hat{H}e^{-\hat{S}(t)}, \tag{4.6}$$

where

$$\hat{S}(t) \equiv \frac{i\omega_0 t}{2}\sum_{m=1}^{N_m}\left(\hat{n}_{mx} - \hat{n}_{mg} + \sum_{\kappa\in C_m}\hat{n}_\kappa + \sum_{\alpha\in B_m}\hat{n}_\alpha\right) \tag{4.7}$$

represents the model in terms of effective time-independent Hamiltonian $\hat{\tilde{H}}$, which is given by Eqs. (4.2)-(4.5) with $\varepsilon_{mg} \to \varepsilon_{mg}+\omega_0/2$, $\varepsilon_{mx} \to \varepsilon_{mx}-\omega_0/2$, and $\mu_0 E_0 \exp(\pm i\omega_0 t) \to \mu_0 E_0$. As a result of the transformation one also has to consider different positions of the electrochemical potentials in the contacts for the x (shifted by $\omega_0/2$ downward) and the g (shifted by $\omega_0/2$ upward) molecular orbitals (see Appendix 4.5 for details). Note that the time-independent formulation is possible only in the case of relatively weak molecule-baths couplings, when effective second order is sufficient and bath-induced cross-correlations between ground and excited molecular levels can be disregarded.[56,61–63]

As discussed in our previous publication[52] the pseudoparticle nonequilibrium Green function (PP-NEGF) formalism is especially convenient for studies where combined electron and energy transfers play an important role. The PP-NEGF treats all the interactions in the molecule exactly, by representing the molecular part of the Hamiltonian in the basis of many-body states of an isolated molecule. Here we employ the PP-NEGF to the models (4.2)-(4.5). The pseudoparticles, introduced in an extended Hilbert space, correspond to the many-body states $\{|S\rangle\}$ of the molecular system. The physical subspace is defined by the constraint $\sum_S \hat{p}_S^\dagger \hat{p}_S = 1$, where $\hat{p}_S^\dagger$ ($\hat{p}_S$) is the operator of creation (annihilation) of the many-body state $|S\rangle$. In the extended Hilbert space the usual rules of quantum field theory are applicable. In particular, the pseudoparticle

Green function (GF) on the Keldysh contour

$$G_{SS'}(\tau,\tau') \equiv -i\langle T_c\, \hat{p}_S(\tau)\, \hat{p}_{S'}(\tau')\rangle \tag{4.8}$$

satisfies the Dyson equation. A self-consistent procedure for numerical evaluation of the projections of the GF can be formulated in the physical subspace (see e.g. Ref.[64] for details). After the procedure converges, the resulting projections of the GF can be used to calculate charge, I^c_m, and energy, I^E_m, currents at the interface between the molecular system and the baths C_m and B_m, respectively. Below we perform analysis within the non-crossing approximation (see e.g. Ref.[64] for details). The approximation works well for weak molecule-baths coupling, when the parameters describing coupling to the baths are small relative to all other relevant energy scales in the system. In our case the latter are the HOMO-LUMO gap and intra-molecular hopping parameters. Weak coupling to baths makes the processes of molecule-bath interactions rare, thus justifying a non-crossing approximation, i.e. treating the processes sequentially. At steady-state, this leads to the following explicit expressions for the fluxes (see Appendix 4.6 for the derivation)[52,64]

$$\begin{aligned} I^c_m = -\frac{e}{\pi h} \sum_{\substack{S_1,S_2\\S_3,S_4}} \mathrm{Re} \int_{-\infty}^{+\infty} dE \int_{-\infty}^{+\infty} d\epsilon\, \zeta_2\, G^<_{24}(E) \\ \Big(\Sigma^{C_m,<}_{12,34}(\epsilon) G^r_{31}(E+\epsilon) + \Sigma^{C_m,>}_{43,21}(\epsilon) G^r_{31}(E-\epsilon)\Big) \end{aligned} \tag{4.9}$$

$$\begin{aligned} I^E_m = \frac{1}{\pi h} \sum_{\substack{S_1,S_2\\S_3,S_4}} \mathrm{Re} \int_{-\infty}^{+\infty} dE \int_{0}^{\infty} d\omega\, \omega\, \zeta_2\, G^<_{24}(E) \\ \Big(\Pi^{B_m,<}_{12,34}(\omega) G^r_{31}(E+\omega) + \Pi^{B_m,>}_{43,21}(\omega) G^r_{31}(E-\omega)\Big) \end{aligned} \tag{4.10}$$

where $G^{r(<)}_{pq}(E) \equiv G^{r(<)}_{S_pS_q}(E)$ is the Fourier transform of the retarded (lesser) projection of the GF (4.8), $\zeta_p = 1$ (-1) for the bosonic (fermonic) state $|S_p\rangle$,[64] and $\Sigma^{C_m,\gtrless}$ $(\Pi^{B_m,\gtrless})$ are greater/lesser projections of the molecular system self-energy due to coupling to bath

C_m (B_m)

$$\Sigma^{C_m,\gtrless}_{12,34}(\epsilon) \equiv \mp i \sum_{m\ell,m'\ell'} \xi^{m\ell}_{12}\Gamma^{C_m}_{\ell}\overset{*}{\xi}{}^{m'\ell'}_{34} F^{\gtrless}_{C_m}(\epsilon) \tag{4.11}$$

$$\Pi^{B_m,\gtrless}_{12,34}(\omega) \equiv - i \sum_{m,m'} \chi^{m}_{12}\Omega^{B_m}\overset{*}{\chi}{}^{m'}_{34} F^{\gtrless}_{B_m}(\omega) \tag{4.12}$$

Here $F^{>}_{C_m}(\epsilon) \equiv 1 - f_{C_m}(\epsilon)$, $F^{<}_{C_m}(\epsilon) \equiv f_{C_m}(\epsilon)$, $F^{>}_{B_m}(\omega) \equiv 1 + N_{B_m}(\omega)$ $F^{<}_{B_m}(\omega) \equiv N_{B_m}(\omega)$; $f_{C_m}(\epsilon)$ and $N_{B_m}(\omega)$ are Fermi-Dirac and Bose-Einstein distributions,

$$\Gamma^{C_m}_{\ell} \equiv 2\pi \sum_{\kappa\in C_m} |V_{\kappa,m\ell}|^2 \delta(\epsilon - \epsilon_\kappa) \tag{4.13}$$

$$\Omega^{B_m} \equiv 2\pi \sum_{\alpha\in B_m} |U_{\alpha,m}|^2 \delta(\omega - \omega_\alpha) \tag{4.14}$$

are dissipation rates due to coupling to baths C_m and B_m, $\xi^{m\ell}_{pq} \equiv \langle S_p|\hat{d}^{\dagger}_{m\ell}|S_q\rangle$ and $\chi^{m}_{pq} \equiv \langle S_p|\hat{D}^{\dagger}_{m}|S_q\rangle$.

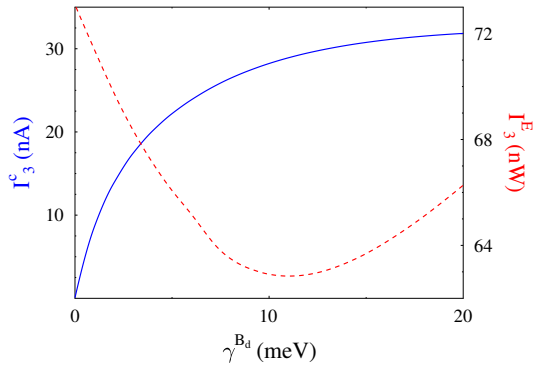

Figure 4.2: (Color online) Molecular pump (Fig. 4.1a). Shown are the charge (I^c_3, Eq.(4.9) - solid line, blue), and energy (I^E_3, Eq.(4.10) - dashed line, red) fluxes on the right interface as functions of dephasing rate γ^{B_d}, Eq.(4.15). See text for parameters.

4.3 Numerical results

Here we consider charge, Eq.(4.9), and energy, Eq.(4.10), fluxes in the molecular pump and switch models (Figs. 4.1a and b), Eqs. (4.2)-(4.5). Unless stated otherwise the calculations are performed for the following 'standard' set of parameters: $T = 300$ K,

$\varepsilon_{0g} = -1$ eV, $\varepsilon_{0x} = 1$ eV, $\omega_0 = 2$ eV, $t_{mg,m'g} = 0$, $t_{mx,m'x} = J_{m,m'} = 10$ meV, $\Gamma_\ell^{C_m} = \Omega^{B_m} = 2.5$ meV ($m, m' \in \{1, \ldots, N_m\}$). The Fermi energy is taken at the origin $E_F = 0$ and the calculations are performed on an adaptive energy grid.

We note that these model parameters are chosen to be in a physically relevant range. In particular, the molecular HOMO-LUMO gaps, $\varepsilon_{mx} - \varepsilon_{mg}$, are assigned typical values of 2 eV, which is accessible by lasers in the near infrared part of the spectrum. The escape rates Γ^{C_m} are chosen in accordance with experimental data on lifetime for the decay of an excess electron on molecule near metal surface.[65] These parameters lead to charge fluxes on the order of nA and heat fluxes on the order of nW, both are well within the measurable region (see e.g. Refs.[66] and[67] for measurable charge and heat flux estimates, respectively).

4.3.1 Molecular pump

First we consider the charge-energy pump model. In the absence of dephasing at the bridge the transport of both charge and energy through the molecule is coherent, and depends on interference between two independent paths from the donor (0) to the acceptor (3) through molecules 1 and 2 (see Fig. 4.1a). For the case of identical (degenerate) chromophores as considered here, the interference is controlled by the relative magnitudes and phases of the coupling matrix elements (the "J"s and the "t"s) along the different paths. In the particular design considered in Fig. 4.1a, destructive interference does not allow charge flux through the system, whereas energy flux is favored in this case due to constructive interference. The spatial separation between the two bridge chromophores allows one to selectively control the transport by coupling one of the chromophores to a local source of dephasing. The latter is introduced by coupling the LUMO of one of the bridge chromophores (1) to a bath (B_d, Eq.(4.5)) of harmonic oscillators, assumed to be in their ground state. To restrict the effect of this perturbation to pure dephasing, a limit of $\omega_\beta \to 0$ is taken (such that energy exchange with this particular bath is excluded). This results in a self-energy (see Appendix 4.7 for details)

$$\Sigma_{12,34}^{B_d,\gtrless} \equiv -i\eta_{12}^{1x}\,\gamma^{B_d}\,\overset{*}{\eta}{}_{34}^{1x} \tag{4.15}$$

where $\gamma^{B_d} \equiv 2\pi M^2 \rho_{B_d}$ is *the dephasing rate*, ρ_{B_d} is density of modes in the bath B_d, and $\eta_{pq}^{1x} \equiv \langle S_p|\hat{n}_{1x}|S_q\rangle$. Note that the resulting expression is similar to the Buttiker probe model, which is widely used for introducing dephasing.

Fig. 4.2 demonstrates the effect of increasing the dephasing rate on the two fluxes. As expected, the electric current (solid line) increases when destructive interference is suppressed. The energy flux (dashed line) shows a non-monotonic behavior. An initial decrease in the flux with increasing dephasing rate, related to the suppression of constructive interference, is followed by an unexpected increase at higher dephasing rates. We attribute this behavior to competition between energy and charge transfer processes at molecule 1 for the same electronic population of its LUMO. Indeed, for weak dephasing, the charge delocalization among the LUMOs of chromophores 0, 1, and 3, is expected to hinder energy transfer between those molecules. Transition from coherent to hopping mechanism of charge transfer takes place at rates of dephasing $\gamma^{B_d} \sim t_{1x,0x}$ ($t_{1x,3x}$), leading to localization of electronic population at the bridge site $1x$ and (as a result) to an increase in energy flux. It is interesting to note that controlling the dephasing can tune the molecular device between energy and charge pumping regimes.

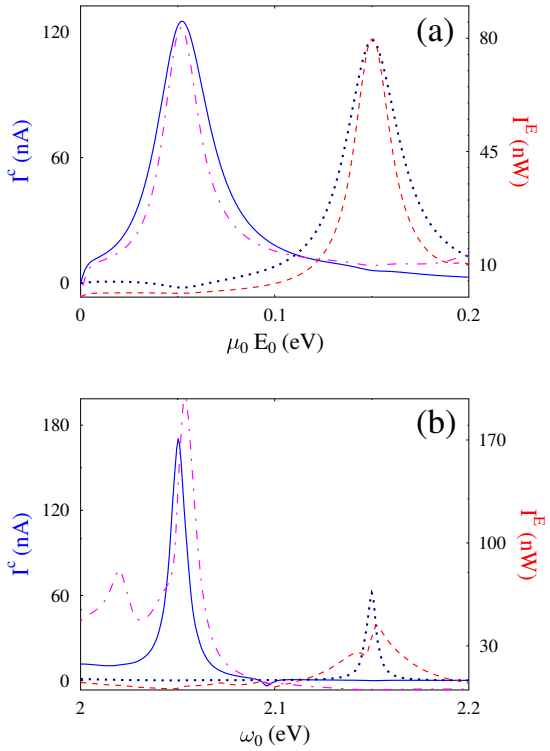

Figure 4.3: (Color online) Molecular switch (Fig. 4.1b). Shown are charge (I_1^c - solid line, blue; I_2^c - dotted line, dark blue; Eq.(4.9)), and energy (I_1^E - dashed line, red; I_2^E - dash-dotted line, magenta; Eq.(4.10)) fluxes as functions of (a) the driving amplitude $\mu_0 E_0$ and (b) frequency ω_0, Eq.(4.2). See text for parameters.

4.3.2 Molecular switch

Having introduced the possibility of control over charge and energy fluxes, which are present simultaneously, we turn to examine the possibility of charge-energy separation in coherent ransport through molecular devices. Note that effects of quantum coherence were observed experimentally (separately) for charge and energy (exciton) transport in molecular junctions. In some cases, such as in CT-SERS, charge and energy transfer are mixed coherently to define the overall optical response of a junction. Our consideration below suggests another possibility of observing coherence induced effects in charge and energy (exciton) transport in molecular junctions.

We consider a model of a molecular switch (4.1b), where a single donor, driven by an external field, is coupled to two different acceptors. The versatility of molecular chromophores allows the design of different acceptors with different orbital energies and

different coupling matrix elements to the donor. Therefore, coherent transport from the donor to each acceptor would be associated with characteristic Rabi frequencies, defined by the t and J hopping parameters for exchanging charge and energy with the donor. Our aim is to define conditions in which charge and energy fluxes are directed to different acceptors.

Fig. 4.3a demonstrates a possibility of charge-energy separation in a molecular switch. The calculation is performed for $T = 10$ K, $\varepsilon_{1g} = -1.25$ eV, $\varepsilon_{1x} = 1.05$ eV, $\varepsilon_{2g} = -0.95$ eV, $\varepsilon_{2x} = 1.15$ eV, and $\Omega^{B_m} = 10$ meV. For these parameters at $\mu_0 E_0 \sim 50$ meV charge flux is directed to acceptor 1 (solid line), while energy flux - to acceptor 2 (dash-dotted line). By tuning the amplitude of the laser field so that $\mu_0 E_0 \sim 150$ meV the direction of the fluxes is switched. Fig. 4.3b demonstrates the possibility of control by the driving field frequency. Here $\varepsilon_{1g} = -1.1$ eV, $\varepsilon_{1x} = 1.05$ eV, $\varepsilon_{2g} = -0.9$ eV, $\varepsilon_{2x} = 1.15$ eV, and $\mu_0 E_0 = 10$ meV. As one can see, also in this case charge and energy fluxes are picked at different field frequencies which facilitates their separation.

Notice that the results of Fig. 3, obtained by the PP-NEGF scheme can be regarded as a numerically exact solution of the simultaneous charge/energy transport problem. Indeed, the present calculation accounts exactly for the many-body problem within the molecular space, and given the (realistically) small molecule-contacts coupling parameters considered here, the non-crossing approximation yields the correct result for the effects of the molecule-leads interaction Note that simpler methodologies, such as Redfield-based quantum master equation techniques in principle can also account exactly for the many body problem within the molecular space, but may be inapplicable at the physically relevant low temperature regime ($k_B T \leq \Gamma$),[68–70] or when degenarate many-body eigenstates are present in the system.[71]

In order to gain a qualitative understanding of the physics behind the observed charge-energy separation, simpler methodologies may be useful. We refer to a reduced model of a molecular dimer, represented as two TLS connected by electron, t, and exciton, J, hopping matrix elements. One TLS represents the donor chromophor of the molecular switch and the other represents an acceptor, corresponding, e.g., to the lower pathway of Fig. 4.1b. The Fock space of this dimer is spanned by many-body states accounting for all possible populations of the four single particle levels. Within the scattering approach,

the total fluxes are obtained as integrals over energy-dependent transmission probabilities with weighting factors defined by populations in the baths. The scattering amplitudes for charge and energy (exciton) transport across the dimer are defined by sequences of electron transfer steps, as, e.g., the ones shown in Fig. 4.4a (relevant many-body states in the two-electron charging block of the system are enumerated in Fig. 4.4b), and the corresponding transfer probabilities at energy E are therefore proportional to $T^c(E) = |G^r_{16}(E)|^2$ for charge transfer and $T^E(E) = |G^r_{13}(E)|^2$ for energy transfer, respectively. Here $G^r_{S_1S_2}(E)$ is the matrix element of the retarded Green function. For simplicity we take the resolvent as a rough estimate of the corresponding retarded Green function $\mathbf{G}^r(E) = [E - \bar{\mathbf{H}}^{(2)}_M + i\eta]^{-1}$, with η taken as 1 meV. The dependence of the transfer probabilities on the energy and on the model parameters is therefore defined by the spectrum of the many body dimer Hamiltonian which defines the resolvent poles. Representation of the dimer Hamiltonian in the basis defined in Fig. 4.4a, reads,

$$\bar{\mathbf{H}}^{(2)}_M = \begin{bmatrix} \varepsilon_{0g}+\varepsilon_{2g}+\omega_0 & -\mu_0 E_0 & 0 & 0 & 0 & 0 \\ -\mu_0 E_0 & \varepsilon_{0x}+\varepsilon_{2g} & -J & 0 & 0 & t \\ 0 & -J & \varepsilon_{0g}+\varepsilon_{2x} & \mu_0 E_0 & t & 0 \\ 0 & 0 & \mu_0 E_0 & \varepsilon_{0x}+\varepsilon_{2x}-\omega_0 & 0 & 0 \\ 0 & 0 & t & 0 & \varepsilon_{0g}+\varepsilon_{0x} & 0 \\ 0 & t & 0 & 0 & 0 & \varepsilon_{2g}+\varepsilon_{2x} \end{bmatrix} \tag{4.16}$$

Maps of the charge, T^c, and energy (exciton), T^E, transmission coefficients as functions of the energy E and the external driving field parameters are shown in Fig. 4.4c for the driving field amplitude $\mu_0 E_0$, and Fig. 4.4d for the field frequency ω_0. The other parameters of the calculation are the same as in Fig. 4.3.

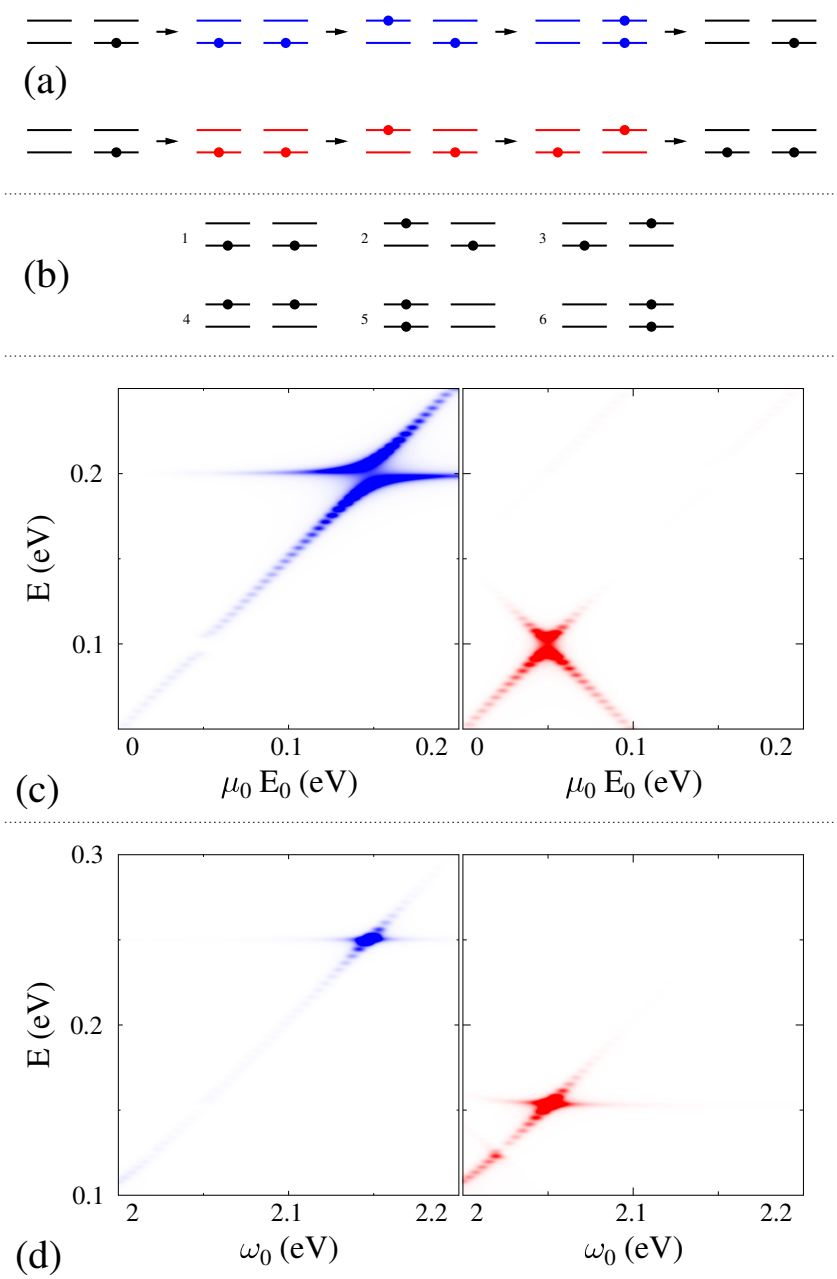

Figure 4.4: (Color online) Molecular dimer. Shown are (a) schemes for charge (top) and energy (bottom) transfer; (b) relevant many-body states of the molecule; charge $T^c(E)$ (left, blue) and energy $T^E(E)$ (right, red) transmission coefficients as functions of energy E and (c) the driving amplitude $\mu_0 E_0$ and (d) frequency ω_0. See text for details.

Two points are noteworthy: 1. T^c and T^E have their maxima at different values of the external driving parameters, which is the basis for the charge-energy separation

discussed above; 2. The energy transmission coefficient, T^E, has two maxima as a function of the driving field frequency ω_0 (see right panel in Fig. 4.4d), which is the reason for a multiple-peak structure of the energy flux presented in Fig. 4.3b. We reemphasize that such qualitative considerations are helpful, and are brought here as an interpretation to, but not instead of, the numerically exact results. Similarly, formulating conditions for maximal fluxes, based on resonances between Rabi frequencies in the field-free system and Rabi frequency induced by the field (as was discussed in Ref.[14] for charge transport) can support the numerical analysis, but provides only qualitative estimates.

4.4 Conclusion

We studied the effects of coherence on electron and energy fluxes in molecular junctions. First we discussed the effect of dephasing on coherent transport in a bridge model with two interfering pathways (see Fig. 4.1a). The molecular bridge was designed to minimize charge flux through the system due to destructive interference, and to maximize energy flux due to constructive interference between the different paths. Inducing dephasing destroys coherence in the system which leads to the appearance of charge flux and decrease in energy transfer. Further increase of the dephasing rate (to the order of inter-molecular electronic hopping parameter) unexpectedly results in an increase of the energy transfer. We argued that the effect is due to competition between charge and energy transport on the same electronic population in the LUMO of the bridge molecule. At strong dephasing, where the electron transport mechanism changes from coherent to hopping, charge localization at the molecular LUMO increases the efficiency of sequential energy transfer through the junction.

After demonstrating a possibility of coherent control over the two fluxes, we discussed the possibility of charge-energy separation in a molecular switch (see Fig 4.1b). In particular, we showed that by tuning the laser field parameters, the fluxes can be directed to different acceptors. Moreover, the directions of energy and charge fluxes can be reversed by adjusting the field amplitude and/or frequency.

The two different models demonstrate the controllability of charge and energy transport in junctions, in which coherences play a crucial role. The theoretical demon-

stration of charge-energy separation in a junction is a first step in the direction of engineering low-heating stable molecular nano-scale devices.

Acknowledgments

We gratefully acknowledge support by the Department of Energy (M.G., Early Career Award, DE-SC0006422), the German-Israeli Science Foundation (U.P.), and the US-Israel Binational Science Foundation (U.P. and M.G., Grant no. 2008282). Chapter 4, in full, is a reprint of the material as it appears in Physical Review B 2013. White, Alexander J.; Psekin, Uri; Galperin, Michael, American Physical Society 2013. The dissertation author was the primary investigator and author of the paper.

4.5 Appendix A: Transformation to the rotating frame of the field

Here we discuss the transformation to the rotating frame of the field, Eq. (4.6), and the formulation of the effective time-independent model. Applying the transformation to the rotating frame

$$\hat{A} \to e^{\hat{S}(t)} \hat{A} e^{-\hat{S}(t)}, \tag{4.17}$$

with $\hat{S}(t)$ defined in Eq. (4.7), to the quasi-particle excitation operators yields

$$\begin{aligned} &\hat{d}_{mg} \to \hat{d}_{mg} e^{-i\omega_0 t/2}, \quad \hat{d}_{mx} \to \hat{d}_{mx} e^{i\omega_0 t/2}, \\ &\hat{c}_\kappa \to \hat{c}_\kappa e^{i\omega_0 t/2}, \qquad\quad \hat{a}_\alpha \to \hat{a}_\alpha e^{-i\omega_0 t/2} \end{aligned} \tag{4.18}$$

Together with additional terms due to the time-dependent correction, (first term on the right side of Eq. (4.6))

$$\frac{\omega_0}{2} \sum_{m=1}^{N_m} \left[\hat{n}_{mg} - \hat{n}_{mx} - \sum_{\kappa \in C_m} \hat{n}_\kappa - \sum_{\alpha \in B_m} \hat{n}_\alpha \right] \tag{4.19}$$

this leads to the effective Hamiltonian of the form (compare with Eqs. (4.2)-(4.4))

$$\begin{aligned}\hat{\bar{H}}_M &= \sum_{m=0}^{N_m}\sum_{\ell=g,x}\bar{\varepsilon}_{m\ell}\hat{n}_{m\ell} - \mu_0 E_0\left(\hat{d}_{0x}^\dagger \hat{d}_{0g} + H.c.\right) \\ &+ \sum_{m,m'=0}^{N_m}\left(\sum_{\ell=g,x} t_{m\ell,m'\ell}\hat{d}_{m\ell}^\dagger \hat{d}_{m'\ell} + J_{m,m'}\hat{D}_m^\dagger \hat{D}_{m'} + H.c.\right)\end{aligned} \tag{4.20}$$

$$\begin{aligned}\hat{\bar{H}}_{C_m} &= \textstyle\sum_{\kappa\in C_m}\left(\varepsilon_\kappa - \frac{\omega_0}{2}\right)\hat{n}_\kappa \\ \hat{\bar{H}}_{B_m} &= \textstyle\sum_{\alpha\in B_m}\left(\omega_\alpha - \frac{\omega_0}{2}\right)\hat{n}_\alpha\end{aligned} \tag{4.21}$$

$$\begin{aligned}\hat{\bar{V}}_{MC_m} &= \textstyle\sum_{\kappa\in C_m}\left(V_{\kappa,mg}\hat{c}_\kappa^\dagger \hat{d}_{mg}e^{-i\omega_0 t} + \hat{c}_\kappa^\dagger \hat{d}_{mx} + H.c.\right) \\ \hat{\bar{V}}_{MB_m} &= \textstyle\sum_{\alpha\in B_m}\left(U_{\alpha,m}\hat{a}_\alpha^\dagger \hat{D}_m e^{i\omega_0 t/2} + H.c.\right)\end{aligned} \tag{4.22}$$

where $\bar{\varepsilon}_{mg} \equiv \varepsilon_{mg} + \omega_0/2$ and $\bar{\varepsilon}_{mx} \equiv \varepsilon_{mx} - \omega_0/2$.

Since coupling to the baths is treated within the effective second order, i.e. the irreducible self-energy is proportional to the second order in molecule-bath coupling, the time-dependent terms in the couplings, Eqs. (4.22), will (partially) compensate for the shift of excitation energies in the bath, Eqs. (4.21). In particular, the compensation will yield an unaltered expression for the self-energies due to the coupling to the bosonic baths B_m. Expressions for the self-energies due to the coupling to the fermonic baths C_m will have the state energies of the baths shifted by $\omega_0/2$ upwards (downwards) for the g (x) level of the molecule. If the HOMO-LUMO gap $\varepsilon_{mx} - \varepsilon_{mg}$ is big relative to the electron escape rate Γ (a common scenario in molecular junctions, where $\varepsilon_{mx} - \varepsilon_{mg} \sim 2$ eV and $\Gamma \sim 0.1$ eV), one can describe the molecule-contacts coupling at an interface C_m as coupling to two independent baths: one with the chemical potential $\mu_{C_m} + \omega_0/2$ representing coupling of the HOMO, the other with the chemical potential $\mu_{C_m} - \omega_0/2$ representing coupling of the LUMO. Such consideration results in an effective time-independent Hamiltonian for the originally time-dependent problem.

4.6 Appendix B: Charge and energy fluxes in the NCA within PP-NEGF

Here we discuss the derivation of Eqs. (4.9) and (4.10). The starting points are expressions for charge and energy (phonon-assisted) fluxes within the non-equilibrium Green functions (NEGF) technique. At steady-state the fluxes at the interface between molecule and baths C_m or B_m, respectively, are[72,73]

$$I_m^c = \frac{e}{\hbar}\int_{-\infty}^{+\infty}\frac{d\varepsilon}{2\pi}\sum_{m\ell,m'\ell'} \Big[\Sigma^{C_m,<}_{m\ell,m'\ell'}(\varepsilon)\, G^{>}_{m'\ell',m\ell}(\varepsilon) - \Sigma^{C_m,>}_{m\ell,m'\ell'}(\varepsilon)\, G^{<}_{m'\ell',m\ell}(\varepsilon)\Big] \tag{4.23}$$

$$I_m^E = -\frac{1}{\hbar}\int_0^{\infty}\frac{d\omega}{2\pi}\omega\sum_{m,m'} \Big[\Pi^{B_m,<}_{m,m'}(\omega)\, D^{>}_{m',m}(\omega) - \Pi^{B_m,>}_{m,m'}(\omega)\, D^{<}_{m',m}(\omega)\Big] \tag{4.24}$$

where $G^{\gtrless}$ and $D^{\gtrless}$ are the greater/lesser projections of the fermion and boson Green functions, respectively, defined on the Keldysh contour as

$$G_{m\ell,m'\ell'}(\tau,\tau') \equiv -i\langle T_c\, \hat{d}_{m\ell}(\tau)\, \hat{d}^{\dagger}_{m'\ell'}(\tau')\rangle \tag{4.25}$$

$$D_{m,m'}(\tau,\tau') \equiv -i\langle T_c\, \hat{D}_{m}(\tau)\, \hat{D}^{\dagger}_{m'}(\tau')\rangle \tag{4.26}$$

Here τ and τ' are the contour variables, T_c is the contour ordering operator, and operators $\hat{d}_{m\ell}$ and $\hat{D}_m$ are introduced below Eq. 4.5. Σ^{C_m} and Π^{B_m} are self-energies due to the coupling to fermonic bath C_m and bosonic bath B_m, respectively. Explicit expressions are[72,73]

$$\Sigma^{C_m,<}_{m\ell,m'\ell'}(\varepsilon) = i\Gamma^{C_m}_{m\ell,m'\ell'}(\varepsilon)\, f_{C_m}(\varepsilon) \tag{4.27}$$

$$\Sigma^{C_m,>}_{m\ell,m'\ell'}(\varepsilon) = -i\Gamma_{m\ell,m'\ell'}(\varepsilon)[1 - f_{C_m}(\varepsilon)] \tag{4.28}$$

$$\Pi^{B_m,<}_{m,m'}(\omega) = -i\Omega^{B_m}_{m,m'}(\omega)\, N_{B_m}(\omega) \tag{4.29}$$

$$\Pi^{B_m,>}_{m,m'}(\omega) = -i\Omega^{B_m}_{m,m'}(\omega)[1 + N_{B_m}(\omega)] \tag{4.30}$$

Here $f_{C_m}(\varepsilon)$ and $N_{B_m}(\omega)$ are the Fermi-Dirac and Bose-Einstein thermal distributions in the baths C_m and B_m, respectively, and

$$\Gamma^{C_m}_{m\ell,m'\ell'}(\varepsilon) \equiv \sum_{\kappa\in C_m} V_{m\ell,\kappa} V_{\kappa,m'\ell'} \delta(\varepsilon - \varepsilon_\kappa) \tag{4.31}$$

$$\Omega^{B_m}_{m,m'}(\omega) \equiv \sum_{\alpha\in B_m} U_{m,\alpha} U_{\alpha,m'} \delta(\omega - \omega_\alpha) \tag{4.32}$$

are the dephasing matrices due to coupling to the baths. Note that in the paper we assume the wide-band approximation for both matrices[74,75] (see Eqs. (4.13) and (4.14)).

Spectral decomposition of the quasi-particle Fermi, $\hat{d}^\dagger_{m\ell}$, and Bose, $\hat{D}^\dagger_m$, excitation operators yields the connection to the pseudoparticle creation and annihilation operators, $\hat{p}^\dagger_S$ and $\hat{p}_S$,

$$\hat{d}^\dagger_{m\ell} = \sum_{S_1,S_2} \xi^{m\ell}_{12} \hat{p}^\dagger_{S_1} \hat{p}_{S_2} \tag{4.33}$$

$$\hat{D}^\dagger_m = \sum_{S_1,S_2} \chi^m_{12} \hat{p}^\dagger_{S_1} \hat{p}_{S_2} \tag{4.34}$$

where $\xi^{m\ell}_{pq}$ and χ^m_{pq} are introduced below Eqs. (4.13) and (4.14), and $|S_1\rangle$ and $|S_2\rangle$ are molecular many-body states. Substituting Eqs. (4.33) and (4.34) into the lesser and greater projections of the definitions of the Green functions, Eqs. (4.25) and (4.26), and using properties of the non-crossing approximation,[76] leads to the connection between the quasi- and pseudo-particles Green functions

$$G^<_{m\ell,m'\ell'}(t,t') = -i \sum_{\substack{S_1,S_2\\S_3,S_4}} \zeta_2 \overset{*}{\xi}{}^{m\ell}_{21} \xi^{m'\ell'}_{43} G^>_{31}(t',t) G^<_{24}(t,t') \tag{4.35}$$

$$G^>_{m\ell,m'\ell'}(t,t') = i \sum_{\substack{S_1,S_2\\S_3,S_4}} \zeta_2 \overset{*}{\xi}{}^{m\ell}_{34} \xi^{m'\ell'}_{12} G^>_{31}(t,t') G^<_{24}(t',t) \tag{4.36}$$

$$D^<_{m,m'}(t,t') = i \sum_{\substack{S_1,S_2\\S_3,S_4}} \zeta_2 \overset{*}{\chi}{}^{m}_{21} \chi^{m'}_{43} G^>_{31}(t',t) G^<_{24}(t,t') \tag{4.37}$$

$$D^>_{m,m'}(t,t') = i \sum_{\substack{S_1,S_2\\S_3,S_4}} \zeta_2 \overset{*}{\chi}{}^{m}_{34} \chi^{m'}_{12} G^>_{31}(t,t') G^<_{24}(t',t) \tag{4.38}$$

where the PP-NEGF Green function is defined in Eq. (4.8), and ζ_p is introduced below Eq. (4.10).

Finally, using the connection between the greater and retarded pseudoparticle Green functions[76]

$$2i\,\mathrm{Im}G^r_{12}(t,t') = G^>_{12}(t,t'), \tag{4.39}$$

and substituting the Fourier transformed representations of the quasi-particles Green functions, Eqs. (4.35)-(4.38), into the NEGF expressions for the fluxes, Eqs. (4.23) and (4.24), leads to Eqs. (4.9) and (4.10).

4.7 Appendix C: Dephasing within the PP-NEGF formalism

It is customary to introduce dephasing via coupling to a bath of harmonic oscillators.[77] In the paper we utilize the bath B_d, coupled to the LUMO of molecule 1 in the molecular pump model (see Fig. 4.1a) as the source of dephasing in the system. The greater and lesser self-energies due to this coupling are given within the PP-NEGF formalism by the expression[64,75]

$$\Sigma^{B_d,<}_{12,34}(\omega) = -i\eta^{1x}_{12}\,\gamma^{B_d}\,\eta^{*1x}_{34} \tag{4.40}$$
$$(\theta(\omega)N_{B_d}(\omega) + \theta(-\omega)[1+N_{B_d}(-\omega)])$$
$$\Sigma^{B_d,>}_{12,34}(\omega) = -i\eta^{1x}_{12}\,\gamma^{B_d}\,\eta^{*1x}_{34} \tag{4.41}$$
$$(\theta(\omega)[1+N_{B_d}(\omega)] + \theta(-\omega)N_{B_d}(-\omega))$$

where $\theta(x)$ is the Heaviside step-function, and γ^{B_d} and η^{1x}_{pg} are introduced below Eq. (4.15).

Finite frequencies of the oscillators in the bath induce energy flow in the system. In addition to dephasing, this may cause inelastic effects in both charge and energy fluxes. To avoid this scenario we assume that the bath oscillators have zero frequency and all in the ground state. From the physical point of view, this assumption is valid when the relevant energy scales in the system (for example, the HOMO-LUMO gap) are much bigger than the frequencies of vibrations in the environment. Taking the limit of

$\omega_\alpha \to 0$ under the restriction $N_{B_d}(\omega) = 0$ leads to Eq. (4.15).

Chapter 4 References

[1] Patoux, C.; Coudret, C.; Launay, J.P.; Joachim, C. and Gourdon, A. Inorg. Chem. **36**, 5037 (1997)

[2] Mayor, M.; Weber, H.B.; Reichert, J.; Elbing, M.; von Hänisch, C.; Beckmann, D. and Fischer, M. Angew. Chem. Int. Edit. **47**, 5834 (2003)

[3] Vazquez, H.; Skouta, R.; Schneebeli, S.; Kamenetska, M.; Breslow, R.; Venkataraman, L. and Hybertsen, M. Nature Nanotech. **7**, 663 (2012)

[4] Ballmann, S.; Härtle, R.; Coto, P.B.; Elbing, M.; Mayor, M.; Bryce, M.R.; Thoss, M. and Weber, H.B. Phys. Rev. Lett. **109**, 056801 (2012)

[5] Assion, A.; Baumert, T.; Bergt, M.; Brixner, T.; Kiefer, B.; Seyfried, V.; Strehle, M. and Gerber, G. Science **282**, 919 (1998)

[6] Shapiro, M. and Brumer, P. *Principles of the Quantum Control of Molecular Processes* (Wiley, New York, 2003) (2003)

[7] Hornberger, K.; Gerlich, S.; Haslinger, P.; Nimmrichter, S. and Arndt, M. Rev. Mod. Phys. **84**, 157 (2012)

[8] Galperin, M. and Nitzan, A. Phys. Chem. Chem. Phys. **14**, 9421 (2012)

[9] Grifoni, M. and Hänggi, P. Physics Reports **304**, 229 (1998)

[10] Kohler, S.; Lehmann, J. and Hänggi, P. Superlattices Microstruct. **34**, 419 (2003)

[11] Kohler, S.; Lehmann, J. and Hänggi, P. Physics Reports **406**, 379 (2005)

[12] Pronin, K.A. and Bandrauk, A.D. Phys. Rev. B **69**, 195308 (2004)

[13] Li, G.; Schreiber, M. and Kleinekathöfer, U. New J. Phys. **10**, 085005 (2008)

[14] Peskin, U. and Galperin, M. J. Chem. Phys. **136**, 044107 (2012)

[15] Ridolfo, A.; Di Stefano, O.; Fina, N.; Saija, R. and Savasta, S. Phys. Rev. Lett. **105**, 263601 (2010)

[16] Morton, S.M. and Jensen, L. J. Chem. Phys. **135**, 134103 (2011)

[17] Manjavacas, A.; Abajo, F.J.G.d. and Nordlander, P. Nano Lett. **11**, 2318 (2011)

[18] Salomon, A.; Gordon, R.J.; Prior, Y.; Seideman, T. and Sukharev, M. Phys. Rev. Lett. **109**, 073002 (2012)

[19] Gao, Y. and Neuhauser, D. J. Chem. Phys. **137**, 074113 (2012)

[20] Lee, H.; Cheng, Y.C. and Fleming, G.R. Science **316**, 1462 (2007)

[21] Engel, G.S.; Calhoun, T.R.; Read, E.L.; Ahn, T.K.; Mancal, T.; Cheng, Y.C.; Blankenship, R.E. and Fleming, G.R. Nature **446**, 782 (2007)

[22] Panitchayangkoon, G.; Hayes, D.; Fransted, K.A.; Caram, J.R.; Harel, E.; Wen, J.; Blankenship, R.E. and Engel, G.S. Proc. Nat. Acad. Sci. **107**, 12766 (2010)

[23] Ishizaki, A.; Calhoun, T.R.; Schlau-Cohen, G.S. and Fleming, G.R. Phys. Chem. Chem. Phys. **12**, 7319 (2010)

[24] Hildner, R.; Brinks, D. and van Hulst, N.F. Nature Phys. **7**, 172 (2011)

[25] Baer, R. and Neuhauser, D. J. Am. Chem. Soc. **124**, 4200 (2002)

[26] Baer, R. and Neuhauser, D. Chem. Phys. **281**, 353 (2002)

[27] Cardamone, D.M.; Stafford, C.A. and Mazumdar, S. Nano Lett. **6**, 2422 (2006)

[28] Stafford, C.A.; Cardamone, D.M. and Mazumdar, S. Nanotechnology **18**, 424014 (2007)

[29] Brisker, D.; Cherkes, I.; Gnodtke, C.; Jarukanont, D.; Klaiman, S.; Koch, W.; Weissman, S.; Volkovich, R.; Toroker, M.C. and Peskin, U. Mol. Phys. **106**, 281 (2008)

[30] Qian, Z.; Li, R.; Zhao, X.; Hou, S. and Sanvito, S. Phys. Rev. B **78**, 113301 (2008)

[31] Ke, S.H.; Yang, W. and Baranger, H.U. Nano Lett. **8**, 3257 (2008)

[32] Hansen, T.; Solomon, G.C.; Andrews, D.Q. and Ratner, M.A. J. Chem. Phys. **131**, 194704 (2009)

[33] Sparks, R.E.; García-Suárez, V.M.; Manrique, D.Z. and Lambert, C.J. Phys. Rev. B **83**, 075437 (2011)

[34] Hod, O.; Baer, R. and Rabani, E. Phys. Rev. Lett. **97**, 266803 (2006)

[35] Volkovich, R.; Toroker, M.C. and Peskin, U. J. Chem. Phys. **129**, 034501 (2008)

[36] Skourtis, S.S.; Waldeck, D.H. and Beratan, D.N. J. Phys. Chem. B **108**, 15511 (2004)

[37] Härtle, R.; Butzin, M.; Rubio-Pons, O. and Thoss, M. Phys. Rev. Lett. **107**, 046802 (2011)

[38] Sinayskiy, I.; Marais, A.; Petruccione, F. and Ekert, A. Phys. Rev. Lett. **108**, 020602 (2012)

[39] Repp, J.; Liljeroth, P. and Meyer, G. Nature Phys. **6**, 975 (2010)

[40] Xiao, D.; Skourtis, S.S.; Rubtsov, I.V. and Beratan, D.N. Nano Lett. **9**, 1818 (2009)

[41] Galperin, M. and Nitzan, A. J. Phys. Chem. B **117**, 4449 (2013)

[42] Ishizaki, A. and Fleming, G.R. Proc. Nat. Acad. Sci. **106**, 17255 (2009)

[43] Ishizaki, A. and Fleming, G.R. J. Chem. Phys. **130**, 234111 (2009)

[44] Olbrich, C.; Jansen, T.L.C.; Liebers, J.; Aghtar, M.; Strümpfer, J.; Schulten, K.; Knoester, J. and Kleinekathöfer, U. J. Phys. Chem. B **115**, 8609 (2011)

[45] Renaud, N.; Ratner, M.A. and Mujica, V. J. Chem. Phys. **135**, 075102 (2011)

[46] Chin, A.W.; Prior, J.; Rosenbach, R.; Caycedo-Soler, F.; Huelga, S.F. and Plenio, M.B. Nature Phys. **9**, 113 (2013)

[47] Persson, B.N.J. Chem. Phys. Lett. **82**, 561 (1981)

[48] Oren, M.; Galperin, M. and Nitzan, A. Phys. Rev. B **85**, 115435 (2012)

[49] Galperin, M.; Nitzan, A. and Ratner, M.A. Phys. Rev. Lett. **96**, 166803 (2006)

[50] Galperin, M. and Nitzan, A. J. Chem. Phys. **124**, 234709 (2006)

[51] Fainberg, B.D.; Sukharev, M.; Park, T.H. and Galperin, M. Phys. Rev. B **83**, 205425 (2011)

[52] White, A.J.; Fainberg, B.D. and Galperin, M. J. Phys. Chem. Lett. **3**, 2738 (2012)

[53] Härtle, R.; Peskin, U. and Thoss, M. Phys. Stat. Sol. (b) 1–13 (2013)

[54] Li, G.Q.; Fainberg, B.D.; Nitzan, A.; Kohler, S. and Hänggi, P. Phys. Rev. B **81**, 165310 (2010)

[55] Li, G.; Shishodia, M.S.; Fainberg, B.D.; Apter, B.; Oren, M.; Nitzan, A. and Ratner, M.A. Nano Lett. **12**, 2228 (2012)

[56] Fransson, J. and Galperin, M. Phys. Rev. B **81**, 075311 (2010)

[57] Fransson, J. and Galperin, M. Phys. Chem. Chem. Phys. **13**, 14350 (2011)

[58] Rai, D. and Galperin, M. Phys. Rev. B **86**, 045420 (2012)

[59] Rai, D. and Galperin, M. The Journal of Physical Chemistry C **117**, 13730 (2013)

[60] Datta, S. *Electronic Transport in Mescoscopic Systems* (Cambridge University Press, 1995) (1995)

[61] Zhang, P.; Xue, Q.K. and Xie, X.C. Phys. Rev. Lett. **91**, 196602 (2003)

[62] Wang, B.; Wang, J. and Guo, H. Phy. Rev. B **67**, 092408 (2003)

[63] Fransson, J. and Zhu, J.X. Phys. Rev. B **78**, 113307 (2008)

[64] White, A.J. and Galperin, M. Phys. Chem. Chem. Phys. **14**, 13809 (2012)

[65] Kinoshita, I.; Misu, A. and Munakata, T. J. Chem. Phys. **102**, 2970 (1995)

[66] Porath, D.; Bezryadin, A.; de Vries, S. and Dekker, C. Nature **403**, 635 (2000)

[67] Schwab, K.; Henriksen, E.A.; Worlock, J.M. and Roukes, M.L. Nature **404**, 974 (2000)

[68] Leijnse, M. and Wegewijs, M.R. Phys. Rev. B **78**, 235424 (2008)

[69] Esposito, M. and Galperin, M. Phys. Rev. B **79**, 205303 (2009)

[70] Esposito, M. and Galperin, M. J. Phys. Chem. C **114**, 20362 (2010)

[71] Schultz, M.G. and von Oppen, F. Phys. Rev. B **80**, 033302 (2009)

[72] Haug, H. and Jauho, A.P. *Quantum Kinetics in Transport and Optics of Semiconductors*, vol. 123 of *Springer Series in Solid-State Sciences* (Springer, Berlin Heidelberg, 2008), second, substantially revised edition edn. (2008)

[73] Galperin, M.; Nitzan, A. and Ratner, M.A. Phys. Rev. B **75**, 155312 (2007)

[74] Mahan, G.D. *Many-Particle Physics* (Plenum Press, 1990) (1990)

[75] Galperin, M.; Ratner, M.A. and Nitzan, A. J. Chem. Phys. **121**, 11965 (2004)

[76] Wingreen, N.S. and Meir, Y. Phys. Rev. B **49**, 11040 (1994)

[77] Anantram, M.P. and Datta, S. Phys. Rev. B **51**, 7632 (1995)

Chapter 5

Molecular nanoplasmonics: self-consistent electrodynamics in current carrying junctions

Alexander J. White[1], Maxim Sukharev[2], and Michael Galperin[1]

[1]Department of Chemistry and Biochemistry, University of California at San Diego, La Jolla, California 92093, USA

[2]Department of Applied Sciences and Mathematics, Arizona State University, Mesa, Arizona 85212, USA

Reprinted with permission from *Physical Review B* **86**, 205324 (2012).

We consider a biased molecular junction subjected to external time-dependent electromagnetic field. We discuss local field formation due to both surface plasmon-polariton excitations in the contacts and the molecular response. Employing realistic parameters we demonstrate that such self-consistent treatment is crucial for proper description of the junction transport characteristics.

5.1 Introduction

Research in plasmonics is expanding its domains into several sub-fields due to significant advances in experimental techniques.[1–6] The unique optical properties of the surface plasmon-polariton (SPP) resonance, being the very foundation of plasmonics, find intriguing applications in optics of nano-materials,[7–9] materials with effective negative index of refraction,[10–12] direct visualization,[13,14] photovoltaics,[15–17] single molecule manipulation,[18–20] and biotechnology.[21–24] Theoretical modeling of the optical properties of metal nanostructures is conventionally based on numerical integration of Maxwell's equations,[25–29] although simulations within time-dependent density functional theory appeared recently for small atomic clusters.[30,31] Moreover, current theoretical models are quickly advancing toward self-consistent simulations of hybrid materials: metal/semiconductor nanostructures optically coupled to ensembles of quantum emitters.[32] This methodology, based on numerical integration of corresponding Maxwell-Bloch equations, brings new insights into nano-optics as it allows for the capture of collective effects.

The molecular optical response in a close proximity of plasmonic materials is greatly enhanced by SPP modes leading to the discovery of the single molecule spectroscopy.[33–35] Recently, experiments performed on current carrying molecular junctions started to appear.[36–40] Theoretical modeling of molecule-SPP systems utilizes the tools of quantum mechanics for the molecular part. In particular, studies of optical response of isolated molecules absorbed on metallic nanoparticles utilize Maxwell-Bloch (Maxwell-Schrödinger)[32,41–44] equations or near field-time dependent density functional theory formulations.[45,46]

Realistic molecular devices are open quantum systems exchanging energy and electrons with surrounding environment (baths). This is especially important in studies of molecules in current carrying junctions interacting with external fields.[47] Usually in such studies the electromagnetic (EM) field is assumed to be an external driving force.[51–62] Recently we utilized the nonequilibrium Green function technique to study the transport and optical response of a molecular junction subjected to external EM field taking into account near-fields driven by SPP local modes, specific for a particular junction geometry.[48,49] Although the formulation allows us to describe the molecular

junction with formation of the local field by SPP excitations in the contacts taken into account explicitly, the molecular influence on formation of the local EM field was disregarded in these studies. Note that such influence was shown to have measurable effects in plasmonic spectrum.[32,41,44,50]

When a molecule located near a metal surface is driven by a strong EM field, one can expect to observe significant changes in the total EM field due to radiation emitted by the molecule. Such radiation although quickly degrading with the distance from molecular position can nevertheless noticeably alter the local EM field. Since the latter is driving the molecule, transport characteristics of the junction may be significantly modified. This calls for a self-consistent treatment, where both SPP excitations and molecular response participate in formation of the local EM field.

Here we extend our previous considerations by taking into account complete electrodynamics and molecular junction response in a self-consistent manner combining Maxwell's equations with electron transport dynamics. The molecule is treated as a pointwise source in the Ampere law. We demonstrate the importance of the molecular response in the formation of the local field for an open molecular system far from equilibrium. The effect is shown to be important for proper description of the junction transport characteristics. The paper is organized as follows. Section 5.2 presents a transport model of the molecular junction. Section 5.3 describes the methodology of computing the EM field taking into account molecular response. The results are presented in section 5.4. Section 5.5 summarizes our work.

5.2 Molecular junction subjected to external EM field

We consider a junction with a molecular bridge (M) connecting between two contacts (L and R). The bridge is formed by D two-level systems with the levels representing ground (g) and excited (x) states of the molecule. Each of the two level systems is subjected to a classical local EM field $\vec{E}(t)$ (see section 5.3 for details of its calculation). Electron transfer is allowed along the chain of ground (excited) levels of the bridge. The contacts are taken in the form of bowtie antennas, and are assumed to be reservoirs of free electrons each in its own equilibrium with electrochemical potentials

μ_L and μ_R, respectively (see Fig. 5.1). The Hamiltonian of the system reads (here and below $e = \hbar = 1$)

$$\hat{H}(t) = \hat{H}_M(t) + \sum_{K=L,R} \left(\hat{H}_K + \hat{V}_K \right) \tag{5.1}$$

$$\hat{H}_M(t) = \sum_{s=g,x} \left[\sum_{m=1}^{D} \varepsilon_s \hat{d}_{ms}^\dagger \hat{d}_{ms} - \sum_{m=1}^{D-1} t_s \left(\hat{d}_{m+1s}^\dagger \hat{d}_{ms} + H.c. \right) \right] - \sum_{m=1}^{D} \left(\vec{\mu}_{mg,mx} \hat{d}_{mg}^\dagger \hat{d}_{mx} + H.c. \right) \vec{E}_m(t) \tag{5.2}$$

$$\hat{H}_K = \sum_{k \in K} \varepsilon_k \hat{c}_k^\dagger \hat{c}_k \tag{5.3}$$

$$\hat{V}_K = \sum_{k \in K} \sum_{s=g,x} \left(V_{k,m_K s} \hat{c}_k^\dagger \hat{d}_{m_K s} + H.c \right) \tag{5.4}$$

where $\hat{H}_M(t)$ and $\hat{H}_K$ are Hamiltonians of the molecular bridge (M) and the contacts ($K = L, R$), and $\hat{V}_K$ is coupling between them. In Eqs. (5.2)-(5.4) $\hat{d}_{ms}^\dagger$ ($\hat{d}_{ms}$) and $\hat{c}_k^\dagger$ ($\hat{c}_k$) are creation (annihilation) operators for an electron on the level s of the molecular bridge site m and state k of the contact, respectively. $\vec{E}_m(t)$ is the local time-dependent field at bridge site m, and $\vec{\mu}_{ms,ms'} = \langle ms|\hat{\vec{\mu}}|ms'\rangle$ is the matrix element of the transition molecular (vector) dipole operator between states $|ms\rangle$ and $|ms'\rangle$. For simplicity below we assume that the transition dipole moment is the same for all bridge sites and has only one non-zero component, $\mu_{mg,mx} \equiv \mu_{gx}$ for any m. t_s ($s = g, x$) and $V_{k,m_K s}$ are matrix elements for electron transfer in the molecular bridge and between molecule and contacts, respectively, and $m_K = 1$ (D) for $K = L$ (R). Note that treating the external field classically allows us to account for arbitrary time dependence exactly (i.e. beyond perturbation theory).[49]

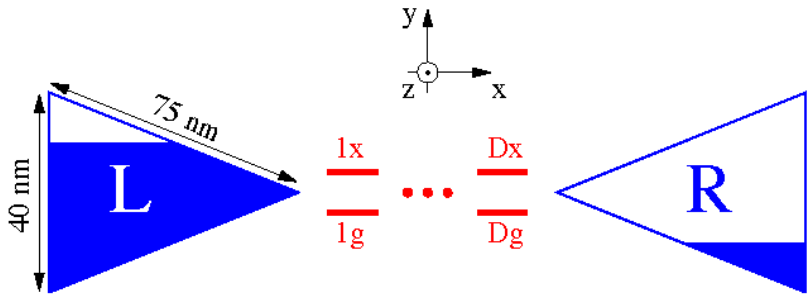

Figure 5.1: (Color online) A sketch of the junction.

We follow the formulation of Ref.[49] Time-dependent current at interface K (L or R) is[63]

$$I_K(t) = -\mathrm{Im}\,\mathrm{Tr}\left[\mathbf{\Gamma}^K\left(\mathbf{G}^<(t,t) + \int \frac{d\epsilon}{\pi}\, f_K(\epsilon)\,\mathbf{G}^r(t,\epsilon)\right)\right] \tag{5.5}$$

where $\mathrm{Tr}[\ldots]$ is a trace over the molecular subspace, $f_K(\epsilon) \equiv \left[e^{(\epsilon-\mu_K)/T}+1\right]^{-1}$ is the Fermi-Dirac distribution in contact K, $\mathbf{\Gamma}^K$ is the molecular dissipation matrix due to coupling to contact K

$$\Gamma^K_{m_1s_1,m_2s_2}(\epsilon) \equiv 2\pi \sum_{k\in K} V_{m_1s_1,k}V_{k,m_2s_2}\delta(\epsilon-\varepsilon_k), \tag{5.6}$$

and $\mathbf{G}^{<(r)}$ is a matrix in the molecular basis of the lesser (retarded) projection of the single particle Green function, defined on the Keldysh contour as[64]

$$G_{m_1s_1,m_2s_2}(\tau_1,\tau_2) \equiv -i\langle T_c\, \hat{d}_{m_1s_1}(\tau_1)\, \hat{d}^\dagger_{m_2s_2}(\tau_2)\rangle \tag{5.7}$$

Here T_c is the contour ordering operator and $\tau_{1,2}$ are the contour variables. In Eq.(5.5) $\mathbf{G}^r(t,\epsilon)$ is the right Fourier transform of the retarded projection of the Green function (5.7)

$$\mathbf{G}^r(t,\epsilon) \equiv \int dt'\, e^{i\epsilon(t-t')}\,\mathbf{G}^r(t,t') \tag{5.8}$$

Note that in Eq.(5.5) and below we assume the wide band limit[65] in the metallic contacts.

The Green functions in (5.5) satisfy the following set of equations of motions[48,66]

$$i\frac{\partial}{\partial t}\mathbf{G}^r(t,\epsilon) = \mathbf{I} - \left(\epsilon\mathbf{I} - \mathbf{H}_M(t) + \frac{i}{2}\mathbf{\Gamma}\right)\mathbf{G}^r(t,\epsilon) \tag{5.9}$$

$$\begin{aligned} i\frac{d}{dt}\mathbf{G}^<(t,t) &= \left[\mathbf{H}_M(t);\mathbf{G}^<(t,t)\right] - \frac{i}{2}\left\{\mathbf{\Gamma};\mathbf{G}^<(t,t)\right\} \\ &+ i\sum_{K=L,R}\int\frac{d\epsilon}{2\pi}f_K(\epsilon)\left(\mathbf{\Gamma}^K\mathbf{G}^a(\epsilon,t) - \mathbf{G}^r(t,\epsilon)\mathbf{\Gamma}^K\right) \end{aligned} \tag{5.10}$$

where $\mathbf{I}$ is the unity matrix, $\mathbf{H}_M(t)$ is a representation of the operator (5.2) in the molecular basis, $\mathbf{\Gamma} \equiv \sum_{K=L,R}\mathbf{\Gamma}^K$, $[\ldots;\ldots]$ and $\{\ldots;\ldots\}$ are the commutator and anti-commutator, and $\mathbf{G}^a(\epsilon,t) \equiv [\mathbf{G}^r(t,\epsilon)]^\dagger$. The first order differential equations (5.9) and (5.10) are solved starting from the initial condition of the biased junction steady-state in the absence of the optical pulse, $E(t=0)=0$

$$\mathbf{G}_0^r(\epsilon) \equiv \mathbf{G}^r(t=0,\epsilon) = \left[\epsilon\mathbf{I} - \mathbf{H}_M(t=0) + \frac{i}{2}\mathbf{\Gamma}\right]^{-1} \tag{5.11}$$

$$\begin{aligned} \mathbf{G}_0^< \equiv& \mathbf{G}^<(t=0,t=0) \\ =& i\sum_{K=L,R}\int\frac{d\epsilon}{2\pi}\,\mathbf{G}_0^r(\epsilon)\,\mathbf{\Gamma}^K f_K(\epsilon)\,\mathbf{G}_0^a(\epsilon) \end{aligned} \tag{5.12}$$

where $\mathbf{G}_0^a(\epsilon) \equiv [\mathbf{G}_0^r(\epsilon)]^\dagger$.

Below we calculate the charge pumped through the junction by the optical pulse

$$Q(t) \equiv \int_0^t dt'\,\frac{I_L(t') - I_R(t')}{2} - I_0\,t \tag{5.13}$$

where $I_{L,R}(t)$ are defined in Eq.(5.5), and I_0 is the steady-state current

$$I_0 \equiv \int\frac{d\epsilon}{2\pi}\,\mathrm{Tr}\Big[\mathbf{\Gamma}^L\,\mathbf{G}_0^r(\epsilon)\,\mathbf{\Gamma}^R\,\mathbf{G}_0^a(\epsilon)\Big]\Big(f_L(\epsilon) - f_R(\epsilon)\Big) \tag{5.14}$$

5.3 Self-consistent electrodynamics

The time evolution of electric, $\vec{E}$, and magnetic, $\vec{H}$, fields is considered according to the set of Maxwell's equations (written here in SI units)

$$\mu_0 \frac{\partial \vec{H}(\vec{r},t)}{\partial t} = -\vec{\nabla} \times \vec{E}(\vec{r},t), \tag{5.15a}$$

$$\epsilon_0 \frac{\partial \vec{E}(\vec{r},t)}{\partial t} = \vec{\nabla} \times \vec{H}(\vec{r},t) - \vec{J}(\vec{r},t), \tag{5.15b}$$

where μ_0 and ϵ_0 are the magnetic permiability and dielectric permittivity of the free space, respectively, and $\vec{J}(t)$ is the electric current density. Note that magnetization is disregarded in Eqs. (5.15a) and (5.15b), since we assume both molecule and contacts to be non-magnetic.

A molecule located at site m ($\equiv \vec{r}_m$) and driven by local electric field $\vec{E}(\vec{r}_m,t)$, yields time-dependent response, which enters Ampere's law as a polarization current density

$$\vec{J}(\vec{r}_m,t) = \frac{\partial \vec{P}_m(t)}{\partial t}\delta(\vec{r}_m), \tag{5.16}$$

where δ is the Dirac delta-function. The polarization depends on molecular characteristics through the molecular density matrix, which in turn is affected by the local field. In our model two-level systems of the molecular bridge (5.2) are assumed to occupy sites of the FDTD grid. Molecules contribute to the polarization at their site according to

$$\vec{P}_m(t) = 2\,\mathrm{Im}\left[\vec{\mu}_{mx,mg}\, G^{<}_{mg,mx}(t,t)\right] \tag{5.17}$$

The resulting system of coupled differential equations, Eqs (5.15)-(5.15b), is solved simultaneously with EOMs for the Green functions of the quantum system, Eqs. (5.9)-(5.10). The Maxwell's equations are discretized in time and space and propagated using the finite-difference time-domain approach (FDTD).[67] We employ three-dimensional FDTD calculations utilizing home-build parallel FORTRAN-MPI codes on a local multi-processor cluster.[68] In spatial regions occupied by a plasmonic nanostructure (a bowtie antenna in our case) we employ the auxiliary differential equation method to account for materials dispersion. The dielectric response of the metal is modeled using a

standard Drude formulation with the set of parameters describing silver.[48,49] The Green functions EOMs are propagated with the fourth order Runge-Kutta scheme.

Within described self-consistent model the local electric field $\vec{E}_m(t) \equiv \vec{E}(\vec{r}_m, t)$ in Eq.(5.2) driving a molecular junction is thus defined by both SPP excitations in the contacts and the local molecular response. In the next section we show that the molecular contribution changes the junction transport characteristics drastically, and in general can not be ignored.

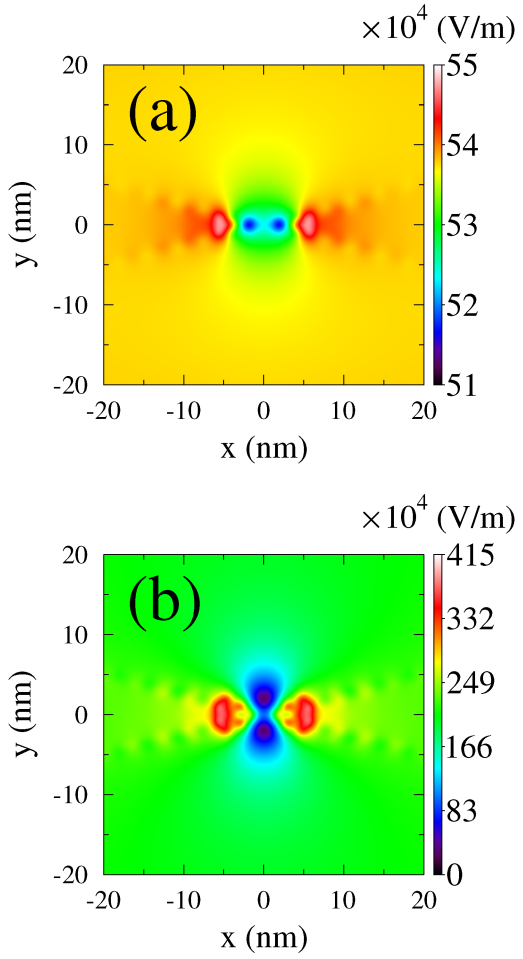

Figure 5.2: (Color online) Map of the instantaneous electric field strength, $[E_x^2(\vec{r},t) + E_y^2(\vec{r},t) + E_z^2(\vec{r},t)]^{1/2}$, at a distance of 10 nm from the molecule (the plane is parallel to xy) calculated (a) without and (b) with the molecular response. The distribution is shown for $t = 77.8$ fs and 81.7 fs for (a) and (b) respectively. See text for parameters.

5.4 Numerical results

Here we present results of numerical simulations demonstrating the importance of a self-consistent treatment of the local EM field dynamics. Previous studies considered the influence of an isolated molecule on plasmon transfer,[41,42,45] molecular features in absorption[32,50,69,70] and Raman[29,31,46] spectra of molecules attached to nanoparticles. Below we discuss how molecular junctions and electron transport are influenced by a local EM field and vice versa in a self-consistent manner.

Unless otherwise specified parameters of the calculations are $T = 300$ K, $\varepsilon_x = -\varepsilon_g = 1$ eV, $t_x = t_g = 0.05$ eV, $\mu_{gx} = 32$ D, $\Gamma^L_{1g,1g} = \Gamma^R_{Dx,Dx} = 0.1$ eV and $\Gamma^L_{1x,1x} = \Gamma^R_{Dg,Dg} = 0.01$ eV (other elements of the dissipation matrix are zero). The choice of parameters for the model was discussed in details in our previous considerations.[48,49] We note that according to the structure of the dissipation matrix, Eq.(5.6), and the characteristic HOMO-LUMO separation of $\sim 2-3$ eV, off-diagonal elements of the dissipation matrix (T_2 dissipation) are much smaller than its diagonal elements (T_1 dissipation), and thus can be ignored. Note also that the T_2 type of dephasing is present in the model through the molecular coupling to the external field. Asymmetry in the molecular coupling to the contacts represents a molecule with a strong charge-transfer transition (see Refs[59,61] for details). Such molecules are the primary candidates for construction of optically driven molecular charge pumps. The Fermi energy is taken at the origin, $E_F = 0$, and the bias is applied symmetrically, $\mu_L = -\mu_R = V_{sd}/2$.

Following Ref.,[48] the incoming incident field is taken in the form of a chirped pulse

$$E_{\rm inc}(t) = {\rm Re}\left[\mathcal{E}_0 \exp\left(-\frac{(\delta^2 - i\bar{\mu}^2)t^2}{2} - i\omega_0 t\right)\right] \tag{5.18}$$

where $\mathcal{E}_0$ is the incident peak amplitude, ω_0 is the incident frequency, and $\delta^2 \equiv 2\tau_0^2/(\tau_0^4 + 4\Phi''^2(\omega_0))$ and $\bar{\mu} \equiv -4\Phi''(\omega_0)/(\tau_0^4 + 4\Phi''^2(\omega_0))$ are parameters describing the incident chirped pulse (τ_0 is the characteristic time related to the pulse duration). In the calculations below we use $\mathcal{E}_0 = 10^7$ V/m, $\omega_0 = 2$ eV, $\tau_0 = 11$ fs, and $\Phi''(\omega_0) = 3000$ fs^2.

Figure 5.2 shows instantaneous electric field strength distributions in a plane shifted by $z = 10$ nm parallel to xy plane. The distribution is calculated for a junction formed by bowtie antennas with single molecule ($D = 1$) placed in the center of the gap.

Here $\varepsilon_x - \varepsilon_g = 1.75$ eV, $\Gamma^L_{1g,1g} = \Gamma^R_{Dx,Dx} = 0.01$ eV, $\Gamma^L_{1x,1x} = \Gamma^R_{Dg,Dg} = 0.001$ eV, and $V_{sd} = 0$. Fig. 5.2a presents simulations without molecular response. Fig. 5.2b shows the results of a calculation where both SPP excitations in the contacts and molecular response are taken into account. One can clearly see that even a single molecule drastically changes the local electric field distribution.

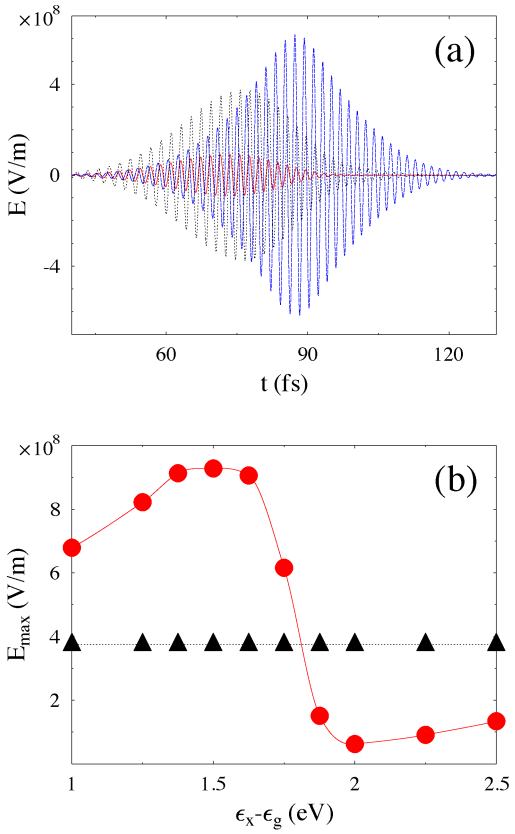

Figure 5.3: (Color online) Local EM field at the molecular position. (a) Pulse calculated without (dotted line, black) and with ($\varepsilon_x - \varepsilon_g > \omega_0$ - solid line, red; $\varepsilon_x - \varepsilon_g < \omega_0$ - dashed line, blue) molecular response. (b) Maximum local field during the pulse vs. molecular excitation energy calculated without (triangles, black) and with (circles, red) molecular response. See text for parameters.

Sensitivity of the pulse temporal behavior to the molecular response is presented in Figure 5.3a. Here a local field affected by only SPP modes (dotted line) is compared to pulses calculated when the molecular response is taken into account. The latter may result in both enhancement (dashed line) or quenching (solid line) of the local field depending on the ratio of the pulse frequency, ω_0, to the molecular excitation energy,

$\varepsilon_x - \varepsilon_g$. In particular, quenching is observed for the laser frequency being below the threshold ($\omega_0 < \varepsilon_x - \varepsilon_g = 2.25$ eV), while frequency above the threshold ($\omega_0 > \varepsilon_x - \varepsilon_g = 1.75$ eV) leads to enhancement of the field. To understand this behavior we perform a simple analysis treating coupling to the driving field as a perturbation, and neglecting the chirped character of the pulse. This leads to (see Appendix 5.6)

$$P_1(t) \approx -\mathcal{E}_0 \cos(\omega_0 t) \left|\mu_{gx}\right|^2 \int \frac{d\epsilon}{2\pi} \left(\mathrm{Im}\left[G^<_{1g,1g}(\epsilon)\right] \frac{\epsilon - (\varepsilon_x - \omega_0)}{[\epsilon - (\varepsilon_x - \omega_0)]^2 + [\Gamma_{1x,1x}/2]^2} + \mathrm{Im}\left[G^<_{1x,1x}(\epsilon)\right] \frac{\epsilon - (\varepsilon_g + \omega_0)}{[\epsilon - (\varepsilon_g + \omega_0)]^2 + [\Gamma_{1g,1g}/2]^2} \right) \tag{5.19}$$

where $\mathbf{G}^<$ is the lesser projection of the Green function (5.7). Taking into account that in the absence of the chirp $E_{\mathrm{inc}}(t) = \mathcal{E}_0 \cos(\omega_0 t)$, the first term in the right side of Eq.(5.19) suggests that for populated ground state, $G^<_{1g,1g}(\epsilon) \approx 1$, the molecular polarization oscillates in phase with the field for $\omega_0 < \varepsilon_x - \varepsilon_g$, and in anti-phase for $\omega_0 > \varepsilon_x - \varepsilon_g$. Thus according to Eqs. (5.15b) and (5.17) the molecular response quenches the field in the former case, and enhances it in the latter. Fig. 5.3b illustrates this finding within the exact calculation showing the maximum of the total field for different molecular excitation energies (circles) compared to the maximum of the EM field obtained without molecular response (triangles). Note that the contribution of the second term in the right side of Eq.(5.19) is exactly the opposite that of the first term; however, since the calculations presented in Fig. 5.3 are performed at zero bias, the molecular excited state is initially empty, $G^<_{1x,1x}(t = 0) \approx 0$.

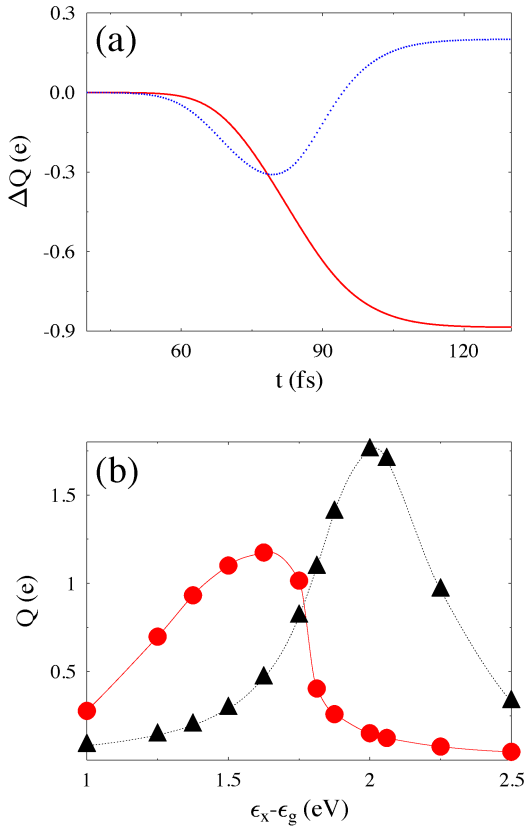

Figure 5.4: (Color online) Charge pumped through the junction. (a) Difference, $\Delta Q \equiv Q^{(sc)} - Q^{(nosc)}$, between results calculated with, $Q^{(sc)}$, and without, $Q^{(nosc)}$, molecular response vs. time for $\varepsilon_x - \varepsilon_g > \omega_0$ (solid line, red) and $\varepsilon_x - \varepsilon_g < \omega_0$ (dotted line, blue). (b) Total charge pumped during the pulse vs. molecular excitation energy calculated without (triangles, black) and with (circles, red) molecular response. See text for parameters.

While the local EM field cannot be measured directly, it is related to junction characteristics (in particular, its transport properties) detectable in experiments. Fig. 5.4a demonstrates the difference in the temporal buildup of the charge pumped through the junction, when the molecule is considered to be driven by the field obtained within the self-consistent model vs. model with only SPP excitations taken into account. The initial dip in the charge buildup (see dotted line) is related to a time delay of the molecule induced pulse for $\varepsilon_x - \varepsilon_g < \omega_0$ (compare solid and dashed lines to the dotted line in Fig. 5.3a). The delay is caused by the chirped nature of the incoming pulse, with initial pulse frequency being lower than the molecular excitation energy, which results in suppression of the local field at the start of the pulse. Eventually however the incom-

ing frequency becomes higher than the molecular transition energy. The corresponding enhancement of the local field leads to increase in the charge pumped through the junction. Note that for $\varepsilon_x - \varepsilon_g > \omega_0$ no delay is observed, and the local field is quenched throughout the pulse. Correspondingly effectiveness of the charge pump is lower in this case (see solid line in Fig. 5.4a).

Figure 5.4b shows the total charge pumped through the junction during the pulse at different molecular excitation energies. Clearly, the most effective EM field obtained without the molecular response taken into account corresponds to the resonance situation, $\omega_0 = \varepsilon_x - \varepsilon_g = 2$ eV. When molecular response is included in the model the situation is less straightforward. Since local field enhancement is expected for low molecular excitation energies, $\omega_0 > \varepsilon_x - \varepsilon_g$ (see Fig. 5.3b), the peak in the pumped charge distribution is shifted to the left. Note that the lower height of the shifted peak is related to the fact that, for a lower molecular gap, part of optical scattering channels is blocked due to partial population of the broadened excited and ground states of the molecule (see Ref.[49] for detailed discussion).

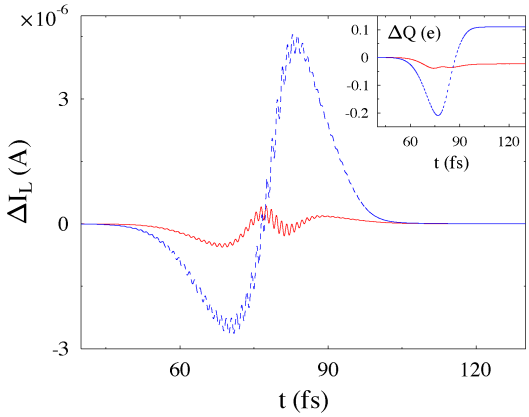

Figure 5.5: (Color online) Current at the left interface as a function of time. Shown are differences, $\Delta I_L \equiv I_L^{(sc)} - I_L^{(nosc)}$, between results calculated with $I_L^{(sc)}$, and without, $I_L^{(nosc)}$, molecular response. The calculations are performed for $V_{sd} = 1.5$ V (dashed line, blue) and 2 V (solid line, red). Inset shows corresponding difference in charge pumped through the junction. See text for parameters.

Note that the importance of the molecular response depends also on bias across the junction. Indeed, since high bias, $V_{sd} > \varepsilon_x - \varepsilon_g$, may inject holes into the molecular ground state and electrons into the excited state, and since populating these states has

opposite consequences for the local field enhancement (see Eq. (5.19) and the discussion following it), it is natural to expect that the molecular response is more important at low biases, $V_{sd} < \varepsilon_x - \varepsilon_g$. Figure 5.5 illustrates this conclusion with results of our calculations within the self-consistent model. Here $\Gamma^L_{1x,1x} = \Gamma^R_{1g,1g} = 0.05$ eV. We observe that both difference in optically induced current and charge pumped through the junction (see inset) is almost negligible at high biases. Similar reasoning indicates that the molecular response at strong incoming fields will be less important also due to population of the excited molecular state induced by external pulse.

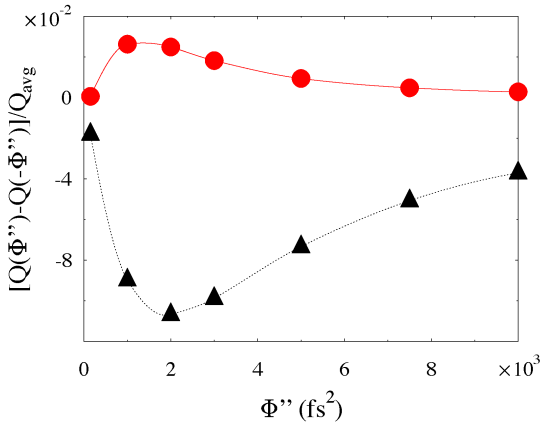

Figure 5.6: (Color online) Asymmetry in the charge transfer between positively and negatively chirped incoming laser pulses, $Q(\Phi'') - Q(-\Phi'')$, normalized by their average, $Q_{avg} \equiv (Q(\Phi'') + Q(-\Phi''))/2$. Shown are results calculated without (triangles, black) and with (circles, red) the molecular response. See text for parameters.

Asymmetry in the charge pumping relative to the sign of the chirp rate was discussed in our recent publication (see Fig. 4 in Ref.[48]). One of the reasons for the asymmetry is related to the time spent by the local pulse in the region of frequencies at and just below the resonance. This region provides the main contribution to charge transfer (see discussion of Fig. 3 in ref.[48]). Since time spent in this region by the positively chirped pulse is smaller than that by the pulse with equal negative chirp rate (the positively chirped local pulse is shorter), one expects to observe an asymmetry as represented by the result of calculations using local EM field influenced only by SPP modes driving the junction (see curve with triangles in Fig. 5.6). However as discussed above, it is this pre-resonance region where molecular response quenches local field, thus diminishing (or even overturning) the asymmetry relative to the chirp rate sign (see

curve with circles in Fig. 5.6).

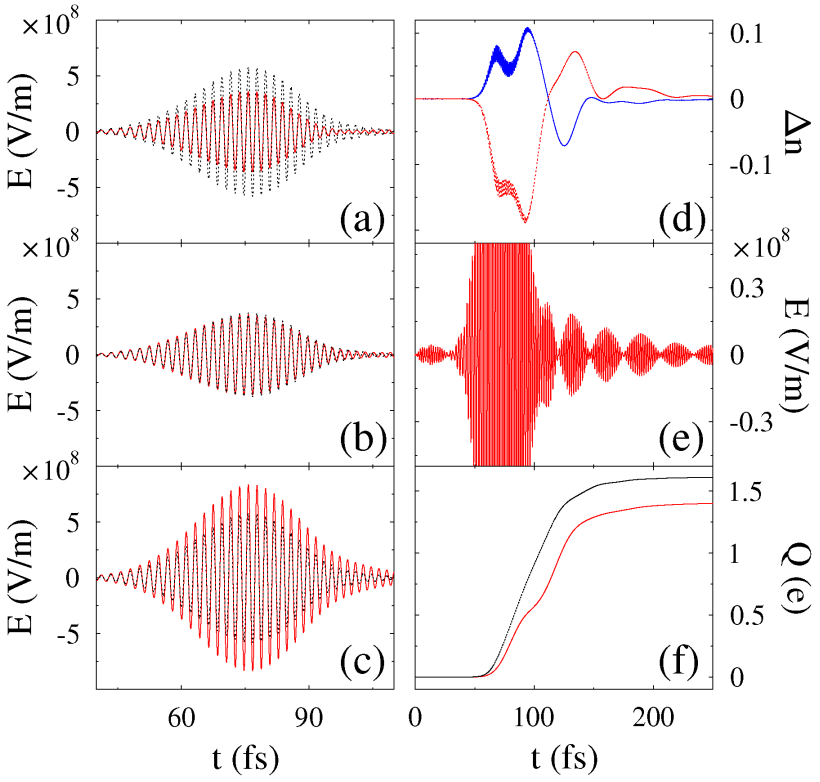

Figure 5.7: (Color online) Effect of the self-consistent treatment on local field and level population in a 3-sites molecular bridge ($D = 3$) as functions of time. Shown are (a)-(c) local field calculated without (dotted line, black) and with ($\varepsilon_x - \varepsilon_g > \omega_0$ - solid line, red) molecular response for the three molecular sites. Panel (d) shows the difference in population of the ground, $\Delta n_{1g} \equiv n_{1g}^{(sc)} - n_{1g}^{(nosc)}$ (solid line, blue) and excited, $\Delta n_{1x} \equiv n_{1x}^{(sc)} - n_{1x}^{(nosc)}$ (dotted line, red) states for the first molecular site ($m = 1$). Panel (e) shows the scaled plot of the field on the central site ($m = 2$) for a longer period of time. The charge pumped through the 3-sites molecular bridge vs. time is shown in panel (f). See text for parameters.

Finally, we consider a 3-site molecular bridge ($D = 3$) to model the spacial nonlocality of molecular polarization. Calculations are done for $\varepsilon_{mx} - \varepsilon_{mg} = 2.25$ eV, $\omega_0 = 2$ eV, and $V_{sd} = 0$. Panels (a)-(c) of Fig. 5.7 compare the pure plasmonic local field to the field calculated when the molecular response is taken into account for the three sites of the bridge. Molecular polarization decreases the local field amplitude on the first site, (a), and enhances it on the rightmost site, (c). The field at the middle site, (b), does not change. The effect can be understood following the discussion similar

to that of Fig. 5.3. We find that for $\varepsilon_x - \varepsilon_g > \omega_0$ increase in population in the ground (decrease in the excited) levels of the molecular sites quenches the local field. Change in the populations of the leftmost site, panel (a), resulting from self-consistent treatment is shown in Fig. 5.7d. We see that these changes are in agreement with the corresponding change in the local field. Similar considerations also hold for panels (b) and (c) (corresponding level population are not shown). We note in passing that several parameters of the model define behavior of the bridge population during and after the pulse. In particular, strength and frequency of the external field define efficiency of charge transfer between ground and excited states of the molecule: stronger coupling and resonant frequency usually result in stronger population of the excited state (at equilibrium the excited state is empty in the absence of the pulse). Strength of molecule-contacts coupling defines lifetime of the excess population on the molecule. After the end of the pulse it takes $\sim 1/\Gamma$ for populations of molecular states to return to their steady-state values. The latter are defined by the bias.

The self-consistently calculated electric field on a site in the bridge shows a visible beat at large timescale(see Fig. 5.7e). This behavior is related to the Rabi frequency due to the intersite coupling, t_s.

Finally, Fig 5.7f shows charge transferred through the 3-site junction as function of time. The decrease in the effectiveness of the pump is related to quenching of the local field on the first site of the bridge, where strong coupling to the left contact yields quick resupply of the ground level population. Decreased efficiency in pumping the charge between ground and excited levels at this site is the reason for the overall change in the effectiveness of the pump.

5.5 Conclusion

We consider a simple model of a molecular junction driven by external chirped laser pulses. The molecule is represented by a bridge of D two-level systems. The contacts geometry is taken in the form of a bowtie antenna. The FDTD technique is used to calculate the local field in the junction resulting from SPP excitations in the contacts. Simultaneously we solve time-dependent nonequilibrum Green functions

equations of motion to take into account the molecular contribution to the local field formation.

Note that many works on driven transport assume pure incident field to be a driving force acting on the molecule. In our recent publications[48,49] we considered effects of local field formation due to SPP excitations in the contacts on junction characteristics under external optical pumping. Here we make one more step by taking into account also the molecular response in the driving local field dynamics. Within a reasonable range of parameters we demonstrate that the latter is crucial for proper description of the junction transport. We compare our results with previously published predictions, and show that the molecular contribution may lead to measurable differences (both quantitative and qualitative) in characteristics of junctions. This contribution is especially important at low biases and relatively weak external fields in the presence of a strong molecular transition dipole. In particular, we show that for laser frequencies shorter (higher) than the molecular excitation energy the local SPP field is usually quenched (enhanced) by molecular response.

Extension of the approach to realistic *ab initio* calculations, taking into account time-dependent bias, and formulating a methodology for calculations in the language of molecular states are the goals for future research.

Acknowledgments

M.G. gratefully acknowledges support by the NSF (Grant No. CHE-1057930) and the BSF (Grant No. 2008282). Chapter 5, in full, is a reprint of the material as it appears in Physical Review B 2012. White, Alexander J.; Sukharev, Maxim; Galperin, Michael, American Physical Society 2012. The dissertation author was the primary investigator and author of the paper.

5.6 Appendix: Derivation of Eq.(5.19)

To understand trends observed in the exact calculations based on Eqs. (5.9)-(5.10) and (5.15a)-(5.15b), here we employ a simple consideration and derive an approximate expression for the molecular polarization, Eq.(5.17), given in Eq.(5.19). For simplicity

we assume that only one projection of the molecular dipole is non-zero, and consider a single molecule bridge ($D = 1$). Then the molecular polarization is

$$P_1(t) = -2\mathrm{Im}\left[\mu_{xg}\, G^{<}_{1g,1x}(t,t)\right] \tag{5.20}$$

Assuming the dissipation matrix, Eq.(5.6), is diagonal the lesser projection of the Green function in Eq.(5.20) is given by the Keldysh equation of the form

$$\begin{aligned} G^{<}_{1g,1x}(t,t) = \sum_{s=g,x} \int_{-\infty}^{t} dt_1 \int_{-\infty}^{t} dt_2\, G^{r}_{1g,1s}(t,t_1) \\ \times\, \Sigma^{<}_{1s,1s}(t_1-t_2)\, G^{a}_{1s,1x}(t_2,t) \end{aligned} \tag{5.21}$$

where

$$\Sigma^{<}_{1s,1s}(t_1-t_2) = i \sum_{K=L,R} \int \frac{d\epsilon}{2\pi}\, f_K(\epsilon) \Gamma^{K}_{1s,1s} e^{-i\epsilon(t_1-t_2)} \tag{5.22}$$

is the lesser self-energy due to coupling to the contacts.

We start by neglecting a chirp of the incoming field

$$E_{inc}(t) = \mathcal{E}_0 \cos(\omega_0 t) \tag{5.23}$$

and treat interaction between molecule and incoming field

$$V_{ss'}(t) \equiv -\delta_{s',\bar{s}}\, \mu_{s\bar{s}}\, E_{inc}(t) \tag{5.24}$$

within the first order of perturbation theory. Here $\bar{s}$ indicates the state opposite to s, i.e. for $s = g$ $\bar{s} = x$.

Within the approximations the retarded Green function in Eq.(5.21) can be expressed as (similar expression can be written for the advanced projection)

$$\begin{aligned} G^{r}_{1s,1s'}(t,t') \approx \delta_{s,s'} G^{(0)r}_{1s,1s}(t-t') \\ + \sum_{m,n=g,x} \int_{-\infty}^{+\infty} dt''\, G^{(0)r}_{1s,1s}(t-t'')\, V_{ss'}(t'')\, G^{(0)r}_{1s',1s'}(t''-t') \end{aligned} \tag{5.25}$$

Here $\mathbf{G}^{(0)r}$ is the retarded projection of the Green functions (5.7) in the absence of

external field

$$G^{(0)r}_{1s,1s}(t-t') = -i\theta(t-t')e^{-i(\varepsilon_s - i\Gamma_{1s,1s}/2)(t-t')} \tag{5.26}$$

and $\theta(\ldots)$ is the Heaviside step function.

Utilizing (5.23)-(5.26) in (5.20)-(5.22) leads to

$$P_1(t) \approx -\mathcal{E}_0 \left|\mu_{gx}\right|^2 \int \frac{d\epsilon}{2\pi} \left(\mathrm{Im}\left[G^{(0)<}_{1g,1g}(\epsilon)\right] \frac{[\epsilon - (\varepsilon_x - \omega_0)]\cos(\omega_0 t) - [\Gamma_{1x,1x}/2]\sin(\omega_0 t)}{[\epsilon - (\varepsilon_x - \omega_0)]^2 + [\Gamma_{1x,1x}/2]^2} \right. \tag{5.27}$$

$$\left. + \mathrm{Im}\left[G^{(0)<}_{1x,1x}(\epsilon)\right] \frac{[\epsilon - (\varepsilon_g + \omega_0)]\cos(\omega_0 t) + [\Gamma_{1g,1g}/2]\sin(\omega_0 t)}{[\epsilon - (\varepsilon_g + \omega_0)]^2 + [\Gamma_{1g,1g}/2]^2} \right)$$

where we have used the Keldysh equation for the steady state situation

$$G^{(0)<}_{1s,1s}(\epsilon) = \frac{\sum_{K=L,R} i f_K(\epsilon)\Gamma^K_{1s,1s}}{[\epsilon - \varepsilon_s]^2 + [\Gamma_{1s,1s}/2]^2} \tag{5.28}$$

Assuming that detuning is much bigger than levels broadenings, $|\omega_0 - (\varepsilon_x - \varepsilon_g)| \gg \Gamma_{1s,1s}$ $(s = g, x)$, the term with $\sin(\omega_0 t)$ in (5.27) can be ignored. Finally, dressing the Green functions in Eq. (5.27), i.e. taking into account diagrams related to population redistribution in the molecule due to presence of the driving field, leads to Eq.(5.19).

Chapter 5 References

[1] E. Hutter and J. H. Fendler, J. H., Advanced Materials **16**, 1685-1706, (2004).

[2] S. A. Maier and H. A. Atwater, H. A., The Journal of Applied Physics **98**, 011101 (2005).

[3] A. V. Zayats, I. I. Smolyaninov, and A. A. Maradudin, Physics Reports **408**, 131-314 (2005).

[4] W. L. Barnes and W. A. Murray, Advanced Materials **19**, 3771-3782 (2007).

[5] N. J. Halas, Nano Letters **10**, 3816-3822 (2010).

[6] M.I.Stockman, Optics Express, **19**, 22029-22106 (2011).

[7] M. Pelton, J. Aizpurua, and G. Bryant, Laser and Photonics Reviews **2**, 136-159 (2008).

[8] M. A. Noginov, G. Zhu, A. M. Belgrave, R. Bakker, V. M. Shalaev, E. E. Narimanov, S. Stout, E. Herz, T. Suteewong, and U. Wiesner, Nature **460**, 1110-1112 (2009).

[9] N. Liu, L. Langguth, T. Weiss, J. Kastel, M. Fleischhauer, T. Pfau, and H. Giessen, Nature Materials **8**, 758-762 (2009).

[10] A. K. Sarychev and V. M. Shalaev, *Electrodynamics of metamaterials* (World Scientific, Singapore, 2007).

[11] R. Quidant and V. P. Drachev, Optical Materials Express **1**, 1139-1140 (2011).

[12] O. Hess, J. B. Pendry, S. A. Maier, R. F. Oulton, J. M. Hamm, and K. L. Tsakmakidis, Nature Materials **11**, 573-584 (2012).

[13] M. I. Stockman, New Journal of Physics **10**, 025031 (2008).

[14] A. Yurtsever and A. H. Zewail, Nano Letters **12**, 3334-3338 (2012).

[15] K. R. Catchpole, K. R. and A. Polman, A., Optics Express **16**, 21793-21800 (2008).

[16] A. Pors, A. V. Uskov, M. Willatzen, and I. E. Protsenko, Optics Communications **284**, 2226-2229 (2011).

[17] E. D. Mammo, J. Marques-Hueso, and B. S. Richards, Proceedings of the SPIE **8438**, 84381M (2012).

[18] M. G. Reuter, M. Sukharev, and T. Seideman, Physical Review Letters **101**, 208303 (2008).

[19] V. Giannini, A. I. Fernandez-Dominguez, Y. Sonnefraud, T. Roschuk, R. Fernandez-Garcia, S. A. Maier, Small **6**, 2498-2507 (2010).

[20] M. Artamonov and T. Seideman, Nano Letters **10**, 4908-4912 (2010).

[21] J. Homola, Analytical and Bioanalytical Chemistry **377**, 528-539 (2003).

[22] M. Delcea, N. Sternberg, A. M. Yashchenok, R. Georgieva, H. Baumler, H. Mohwald, and A. G. Skirtach, ACS Nano **6**, 4169-4180 (2012).

[23] T. Sannomiya and J. Voros, Trends in Biotechnology **29**, 343-351 (2011).

[24] F. Eftekhari, C. Escobedo, J. Ferreira, X. B. Duan, E. M. Girotto, A. G. Brolo, R. Gordon, and D. Sinton, Analytical Chemistry **81**, 4308-4311 (2009).

[25] S. K. Gray and T. Kupka, Physical Review B **68**, 045415 (2003).

[26] J. Yelk, M. Sukharev, and T. Seideman, The Journal of Chemical Physics **129**, 064706 (2008).

[27] A. Coomar, C. Arntsen, K. A. Lopata, S. Pistinner, and D. Neuhauser, The Journal of Chemical Physics **135**, 084121 (2011).

[28] A.-I. Henry, J. M. Bingham, E. Ringe, L. D. Marks, G. C. Schatz, and R. P. Van Duyne, The Journal of Physical Chemistry C **115**, 9291-9305 (2011).

[29] J. M. McMahon, S. Li, L. K. Ausman, and G. C. Schatz, The Journal of Physical Chemistry C **116**, 1627-1637 (2012).

[30] J. Zuloaga, E. Prodan, and P. Nordlander, Nano Letters **9**, 887-891 (2009).

[31] S. M. Morton, D. W. Silverstein, and L. Jensen, Chemical Review **111**, 3962-3994 (2011).

[32] M. Sukharev and A. Nitzan, Physical Review A **84**, 043802 (2011).

[33] D. L. Jeanmaire and R. P. Van Duyne, The Journal of Electroanalytical Chemistry **84**, 1-20 (1977).

[34] S. Nie and S. R. Emory, Science **275**, 1102-1106 (1997).

[35] J. Zhang, Y. Fu, M. H. Chowdhury, and J. R. Lakowicz, Nano Letters **7**, 2101-2107 (2007).

[36] Z. Ioffe, T. Shamai, A. Ophir, G. Noy, I. Yutsis, K. Kfir, O. Cheshnovsky, and Y. Selzer, Nature Nanotechnology **3**, 727-732 (2008).

[37] D. R. Ward, N. J. Halas, J. W. Ciszek, J. M. Tour, Y. Wu, P. Nordlander, and D. Natelson, Nano Letters **8**, 919-924 (2008).

[38] S. W. Wu, G. V. Nazin, and W. Ho, Physical Review B **77**, 205430 (2008).

[39] H. P. Yoon, M. M. Maitani, O. M. Cabarcos, L. Cai, T. S. Mayer, and D. L. Allara, Nano Letters **10**, 2897-2902 (2010).

[40] D. R. Ward, D. A. Corley, J. M. Tour, and D. Natelson, Nature Nanotechnology **6**, 33-38 (2011).

[41] K. Lopata and D. Neuhauser, The Journal of Chemical Physics **130**, 104707 (2009).

[42] K. Lopata and D. Neuhauser, The Journal of Chemical Physics **131**, 014701 (2009).

[43] C. Arntsen, K. Lopata, M. R. Wall, L. Bartell, and D. Neuhauser, The Journal of Chemical Physics **134**, 084101 (2011).

[44] A. Salomon, R. J. Gordon, Y. Prior, T. Seideman, and M. Sukharev, Physical Review Letters **109**, 073002 (2012).

[45] Y. Gao and D. Neuhauser, The Journal of Chemical Physics **137**, 074113 (2012).

[46] J. Mullin and G. C. Schatz, The Journal of Physical Chemistry A **116**, 1931-1938 (2012).

[47] M. Galperin and A. Nitzan, Physical Chemistry Chemical Physics **14**, 9421-9438 (2012).

[48] B. D. Fainberg, M. Sukharev, T.-H. Park, and M. Galperin, Physical Review B **83**, 205425 (2011).

[49] M. Sukharev and M. Galperin, Physical Review B **81**, 165307 (2010).

[50] B. Lukýanchuk, N. I. Zheludev, S. A. Maier, N. J. Halas, P. Nordlander, H. Giessen, and C. T. Chong, Nature Materials **9**, 707-715 (2010).

[51] G. Li, M. S. Shishodia, B. D. Fainberg, B. Apter, M. Oren, A. Nitzan, and M. A. Ratner, Nano Letters **12**, 2228-2232 (2012).

[52] U. Peskin and M. Galperin, The Journal of Chemical Physics **136**, 044107 (2012).

[53] T.-H. Park and M. Galperin, Europhysics Letters **95**, 27001 (2011).

[54] T.-H. Park and M. Galperin, Physical Review B **84**, 075447 (2011).

[55] L. X. Wang and V. May, The Journal of Physical Chemistry C **114**, 41794185 (2010).

[56] G. Q. Li, B. D. Fainberg, A. Nitzan, S. Kohler, and P. Hanggi, Physical Review B **81**, 165310 (2010).

[57] M. Galperin, M. A. Ratner, and A. Nitzan, The Journal of Chemical Physics **130**, 144109 (2009).

[58] J. K. Viljas, F. Pauly, and J. C. Cuevas, Physical Review B **77**, 155119 (2008).

[59] B. D. Fainberg, M. Jouravlev, and A. Nitzan, Physical Review B **76**, 245329 (2007).

[60] J. K. Viljas, F. Pauly, and J. C. Cuevas, Physical Review B **76**, 033403 (2007).

[61] M. Galperin and A. Nitzan, The Journal of Chemical Physics **124**, 234709 (2006).

[62] S. Kohler, J. Lehmann, and P. Hanggi, Phys. Rep. **406**, 379-443 (2005).

[63] A.-P. Jauho, N. S. Wingreen, and Y. Meir, Physical Review B **50**, 5528-5544 (1994).

[64] H. Haug and A.-P. Jauho, *Quantum Kinetics in Transport and Optics of Semiconductors* (Springer-Verlag, Berlin, 2008).

[65] G. D. Mahan, *Many-Particle Physics* (Plenum Press, New York, 1990).

[66] M. Galperin and S. Tretiak, The Journal of Chemical Physics **128**, 124705 (2008).

[67] A. Taflove and S. C. Hagness, Susan C., *Computational electrodynamics: the finite-difference time-domain method* (Artech House, 2005).

[68] http://plasmon.poly.asu.edu

[69] A. Manjavacas, F. J. G. d. Abajo, and P. Nordlander, Nano Letters **11**, 2318-2323 (2011).

[70] A. J. White, B. Fainberg, and M. Galperin, The Journal of Physical Chemistry Letters **3**, 2738-2743 (2012)

[71] J. M. Mullin, J. Autschbach, and G. C. Schatz, Computational Theoretical Chemistry **987**, 32-41 (2012).

Chapter 6

Collective plasmon-molecule excitations in nanojunctions: Quantum consideration

Alexander J. White[1], Boris D. Fainberg[2] and Michael Galperin[1]

[1]Department of Chemistry and Biochemsitry, University of California at San Diego, La Jolla CA 92093, USA

[2]Faculty of Sciences, Holon Institute of Technology, Holon 58102, Israel

Reprinted with permission from *The Journal of Physical Chemistry Letters* **3**, 2738-2743 (2012).

We present a pseudoparticle nonequilibrium Green function formalism as a tool to study the coupling between plasmons and excitons in nonequilibrium molecular junctions. The formalism treats plasmon-exciton couplings and intra-molecular interactions exactly, and is shown to be especially convenient for exploration of plasmonic absorption spectrum of plexitonic systems, where combined electron and energy transfers play an important role. We demonstrate the sensitivity of the molecule-plasmon Fano resonance to junction bias and intra-molecular interactions (Coulomb repulsion and intra-molecular exciton coupling), and compare our predictions for non-linear optical effects to previous

studies. Our study opens a way to deal with strongly interacting plasmon-exciton systems in nonequilibrium molecular devices.

6.1 Introduction

Recent progress in nanofabrication techniques and advances in laser technologies opened new directions in research of plasmonic materials at nanoscale.[1,2] Nanoplasmonics finds its application in optical devices,[3–6] photovoltaics,[7–9] and biology.[10–13] In particular, field enhancement by surface plasmons at nanoscale allows the detection of optical response in current carrying molecular junctions.[14] Plasmon coupling to molecular excitations[15] is studied by a field of research named plexcitonics.[16] Such couplings yield a possibility for coherent control of molecular systems[17,18] and are utilized in molecular photodevices.[19–21]

Advances in experimental techniques has caused a surge of theoretical research in the areas of nanoplasmonics and plexcitonics. Usually plasmon excitations are studied utilizing the laws of classical electrodynamics,[22–26] while the molecular system is treated quantum-mechanically.[27–32] We used a similar scheme to study transport in molecular junctions driven by surface plasmons.[33,34] Recently, quantum descriptions of plasmonic excitatitons started to appear. For example, time-dependent density functional theory was employed to simulate plasmon excitations in relatively small metallic clusters in Refs.[35–38] while Ref.[39] utilized a quantum master equation to study the effect of plasmonic excitations on the current.

The observation of Fano resonances[40] in plasmonic nanostructures[41] gave impetus to a quantum description of excitations. Such considerations have been done for quantum dot-metal nanoparticle system, where the metal nanoparticle was studied classically while oscillations of the quantum dot were treated within a density matrix approach.[42–44] Recently a fully quantum description of the model was reported in Ref.[45] Finally, a mean-field quantum study of the dips in the absorption spectrum of a molecule between a pair of metallic spheres was presented in Ref.,[46] within an equilibrium Green function formalism. It relies on the factorization of the collective excitations into separated plasmonic and molecular contributions. In this respect, it is well to bear in mind that the dips discussed in Ref.[46] can arise from both Fano-like interference and hybridization of a molecule dipole and the plasmon resonances.[47] Strong hybridization is related to the physics of avoided crossing of diabatic states corresponding to the molecular resonance and plasmon, and gives rise to a new quasiparticle - the polariton.[48–50] Thus, the mean-field

type factorization of the molecular and plasmon excitations is not safe in the case of strong plasmon-exciton coupling.

Here we consider collective plasmon-molecule excitations in a junction, where a molecule (M) is placed between two nanoparticles (L and R), each representing a contact. The molecule, modeled as a chain of D two-level systems, exchanges electrons and energy with the contacts. Energy exchange is modeled as exciton-plasmon coupling within the dipole approximation. Both the molecule and plasmons are treated quantum mechanically. We employ a pseudoparticle nonequilibirum Green function formalism (NEGF), described in details in our recent publication.[51] The formalism allows us to generalize the consideration of Ref.[46] to a nonequilibrium, finite temperature, situation, and to treat the system part (molecule and plasmons) exactly. The latter is important in the case of strong plasmonic coupling to molecular excitations. We evaluate the absorption spectrum of the junction, and discuss the influence of bias and intra-molecular interactions (Coulomb repulsion, U, and exciton hopping, J) on the spectrum.

6.2 Model

The Hamiltonian of the junction is (here and below $\hbar = 1$)

$$\hat{H} = \hat{H}_M + \hat{H}_P + \hat{V}_{MP} + \sum_{K=L,R,rad} \left(\hat{H}_K + \hat{V}_K \right) \tag{6.1}$$

Here $\hat{H}_M$ is the molecular Hamiltonian

$$\begin{aligned} \hat{H}_M = & \sum_{c=1}^{D} \left[\sum_{s=g,e} \varepsilon_s \hat{c}_{cs}^\dagger \hat{c}_{cs} + \frac{U}{2} \hat{N}_c (\hat{N}_c - 1) \right] \\ & + \sum_{c=1}^{D-1} \left[- \sum_{s=g,e} t_s \hat{c}_{cs}^\dagger \hat{c}_{(c+1)s} + J \hat{b}_c^\dagger \hat{b}_{c+1} + H.c. \right], \end{aligned} \tag{6.2}$$

$\hat{H}_P$ models plasmonic excitations in the nanoparticles as two coupled dipoles, L and R,[1]

$$\hat{H}_P = \sum_{K=L,R} \Omega_K \hat{b}_K^\dagger \hat{b}_K - \Big(\Delta_{PP} \hat{b}_R^\dagger \hat{b}_L + H.c.\Big) \tag{6.3}$$

and $\hat{V}_{MP}$ describes the exciton-plasmon coupling

$$\hat{V}_{MP} = -\sum_{c=1}^{D} \sum_{K=L,R} \Big(\Delta_{cK} \hat{b}_c^\dagger \hat{b}_K + H.c.\Big) \tag{6.4}$$

The contacts L and R are modeled as reservoirs of free electrons

$$\hat{H}_K = \sum_{\kappa \in K} \varepsilon_\kappa \hat{c}_\kappa^\dagger \hat{c}_\kappa \qquad (K = L, R), \tag{6.5}$$

and $\hat{H}_{rad}$ introduces the radiation field

$$\hat{H}_{rad} = \sum_\alpha \omega_\alpha \hat{a}_\alpha^\dagger \hat{a}_\alpha \tag{6.6}$$

$\hat{V}_K$ $(K = L, R)$ and $\hat{V}_{rad}$ describe the electron transfer between the molecule and contacts, and the plasmons and molecular excitations coupling to the radiation field, respectively

$$\hat{V}_K = \sum_{\substack{\kappa \in K \\ s=g,e}} \Big(V_{\kappa s}\, \hat{c}_\kappa^\dagger \hat{c}_{c_K s} + H.c.\Big) \tag{6.7}$$

$$\hat{V}_{rad} = \sum_{\alpha; K \in \{L,1,\ldots,D,R\}} \Big(W_{\alpha K}\, \hat{a}_\alpha^\dagger \hat{b}_K + H.c.\Big) \tag{6.8}$$

where $c_K = 1$ (D) for $K = L$ (R).

In eqs 6.2-6.8 $\hat{c}_{cs}^\dagger$ $(\hat{c}_{cs})$ and $\hat{c}_\kappa^\dagger$ $(\hat{c}_\kappa)$ are creation (annihilation) operators for an electron in the molecular orbital s, at the site c of the chain, and contact state κ, respectively, $\hat{a}_\alpha^\dagger$ $(\hat{a}_\alpha)$ is the creation (annihilation) operator for a photon in mode α of the radiation field. $\hat{b}_K^\dagger(\hat{b}_K)$ creates (destroys) plasmons in a nanoparticle $(K = L, R)$ or excitons at a site $c = 1, \ldots, D$ of the molecule. $(K = c,\ \hat{b}_c^\dagger \equiv \hat{c}_{ce}^\dagger \hat{c}_{cg})$. $\hat{N}_c \equiv \sum_{s=g,e} \hat{c}_{cs}^\dagger \hat{c}_{cs}$ is the total charge of the site c.

[1]For simplicity we ignore the quadrupole mode of the plasmons described in Ref.[46] This simplifications does not influence the physics of the Fano resonance discussed below (see Supporting Information).

Below we consider molecular chains of one ($D = 1$) and two ($D = 2$) sites. The first model is used to extend the consideration of Ref.[46] to nonequilibrium and beyond the mean-field type of treatment. The second allows us to consider influence of intramolecular energy exchange on the absorption spectrum of the junction. In particular we examine features of exciton compensation of the Coulomb blockade[52] in the plasmon spectrum. Note that, in principle, the model (eqs 6.1-6.8) is capable of describing the optical spectrum features related to Kondo physics. However, such consideration requires going beyond the lowest order in the system-bath coupling (the non-crossing approximation) employed below, and is not presented here.

6.3 Theory

Following Ref.[46] we seek to calculate the correlation function

$$P(\tau, \tau') = -i\langle T_c \, \hat{D}(\tau) \, \hat{D}^\dagger(\tau')\rangle \tag{6.9}$$

of the bonding dipolar mode, $\hat{D} = \hat{b}_L + \hat{b}_R$, which implies the two nanoparticles absorb photons in the same phase.[2] Since we consider a nonequilibrium situation, the Green function in eq 6.9 is defined on the Keldysh contour. τ and τ' are contour variables, and T_c is the contour ordering operator.

We assume that only one mode of the radiation field, ω_0, pumps the system. All the other modes of the radiation bath are empty. Moreover the pumping mode is coupled to the bonding dipolar mode, eq 6.9, direct coupling to the molecule is neglected. Absorption at the laser frequency, ω_0, is given by a photon influx into the system, which at steady state is (see Supporting Information)[53]

$$I_{abs}(\omega_0) = -\int_0^\infty \frac{d\omega}{2\pi}\gamma(\omega)\, N_{\omega_0}(\omega)\, \mathrm{Im}\, P^{>}(\omega) \tag{6.10}$$

where $\gamma(\omega) = \sum_{K=L,R}\gamma_K(\omega) \equiv 2\pi \sum_{K=L,R}\sum_\alpha |W_{K\alpha}|^2 \; \delta(\omega - \omega_\alpha)$ is the total plasmon

[2]This is appropriate when assuming the incident photon field is perpendicular to the nanoparticle dimer axis.[46]

dissipation rate,

$$N_{\omega_0}(\omega) \equiv N_0 \frac{1}{\pi} \frac{\delta^2}{(\omega - \omega_0)^2 + \delta^2} \tag{6.11}$$

is the laser induced mode population (δ is the laser bandwidth), and $P^{>}(\omega)$ is the Fourier transform of the greater projection of $P(\tau, \tau')$, eq 6.9.

Here we briefly outline the pseudoparticle approach for energy and electron transfer in junctions. For an in depth description see e.g. Ref.[51] and references therein. The total Hamiltonian, ref 6.1, is separated into the system, eqs 6.2-6.4, and bath, eqs 6.5 and 6.6, parts. The system Hamitonian is represented in a basis of many-body states $\{|m\rangle\}$,[3] thus all interactions in the system subspace are treated exactly. Every creation $\hat{O}_\nu^\dagger$ (annihilation $\hat{O}_\nu$) operator in the system is expressed in terms of *pseudoparticles* via spectral decomposition

$$\hat{O}_\nu^\dagger \equiv \sum_{m_1, m_2} O^\nu_{m_1 m_2} \hat{d}^\dagger_{m_1} \hat{d}_{m_2} \tag{6.12}$$

where $O^\nu_{m_1 m_2} \equiv \langle m_1 | \hat{O}_\nu^\dagger | m_2 \rangle$. The pseudoparticle operator $\hat{d}^\dagger_m$ creates the many-body state $|m\rangle = \hat{d}^\dagger_m |0\rangle$ ($|0\rangle$ is vacuum state). These operators follow the usual boson/fermion commutation relations within an extended Hilbert space. To specify the physical subspace, the constraint

$$\hat{Q} = \sum_m \hat{d}^\dagger_m \hat{d}_m = 1 \tag{6.13}$$

must be applied. In the extended Hilbert space the pseudoparticle Green's function,

$$G_{mm'}(\tau, \tau') = -i \langle T_c \, \hat{d}_m(\tau) \, \hat{d}^\dagger_{m'}(\tau') \rangle \tag{6.14}$$

satisfies the usual Dyson equation, $\mathbf{G} = \mathbf{g} + \mathbf{g}\mathbf{\Sigma}\mathbf{G}$, where $\mathbf{\Sigma}$ is the pseudoparticle self-energy due to the coupling to the baths, eqs 6.7 and 6.8 (see Supporting Information for details).

The Green function in eq 6.9 is obtained utilizing eq 6.12. We need its greater

[3] This may be the eigenbasis of the system, or any other complete set of many-body states in the system subspace

projection to calculate the absorption spectrum in eq 6.10. The explicit expression is

$$P^{>}(\omega) = \sum_{\substack{K,K'\in\{L,R\} \\ m_1,m_1',m_2,m_2'\in M}} \overset{*}{\chi}{}^{K}_{m_1m_2}\, \chi^{K'}_{m_1'm_2'}\, \zeta_{m_2} \times \int_{-\infty}^{\infty} dE \frac{-1}{\pi} \mathrm{Im}\left[G^{r}_{m_1m_1'}(E+\omega)\right]\, G^{<}_{m_2'm_2}(E) \tag{6.15}$$

where $\chi^{K}_{m_1m_2} \equiv \langle m_1|\hat{b}^{\dagger}_{K}|m_2\rangle$, and $\zeta_m = 1$ (-1) if state $|m\rangle$ is bosonic (fermionic), and $G^{r(<)}$ are the retarded (lesser) projections of the pseudoparticle Green function, eq 6.14.

6.4 Numerical Results

Here we present the results of numerical simulations for the model, eq 6.1, which demonstrate the effect of electron transport on the plasmon absorption spectrum, and in particular, on the Fano resonance.[40] Following Ref.[46] most of the calculations below are performed in the optical linear response regime,[4] with nonlinear optical effects shown in Figure 6.2.

To make our calculations representative of a realistic junction we use the parameters proposed in Ref.[46] Unless otherwise specified, the parameters are $T = 300$ K, $\varepsilon_e = -\varepsilon_g = 1.6$ eV, $U = 1$ eV, $\Omega_L = \Omega_R = 3.49$ eV, and $\Delta_{PP} = 125$ meV. Below for $D = 1$ we follow Ref.[46] taking $\Delta_{1L} = \Delta_{1R} = 20$ meV. For molecular dimer ($D = 2$) this parameter represents coupling to the closest plasmon, $\Delta_{1L} = \Delta_{2R} = 20$ meV. To estimate the coupling to the other plasmon, we take into consideration that the electric field created by the dipole plasmon varies as $\sim 1/r^3$ (r is the distance from the center of the sphere).[54] Then, for the parameters of Ref.[46] and taking the distance between the molecules in the dimer ~ 1 nm, we get $\Delta_{1R} = \Delta_{2L} = 15.75$ meV. The electron escape rate to the contacts is $\Gamma^{K}_{c_K s} = 1$ meV ($K = L, R$, $s = g, e$), the dissipation rates are $\gamma_L = \gamma_R = 86$ meV for the plasmons and $\gamma_M = 4$ meV for the molecular exciton(s). The laser bandwidth is $\delta = 1$ meV. The Fermi energy is chosen at the origin, $E_F = 0$, and bias V_{sd} shifts the chemical potentials in the contacts as $\mu_L = E_F + \eta V_{sd}$ and $\mu_R = E_F - (1-\eta)V_{sd}$. Here η is the voltage division factor. Below we consider

[4] Optical linear response corresponds to disregarding effect of laser on the system.

symmetric, $\eta = 0.5$, and asymmetric, $\eta = 1$, bias divisions.

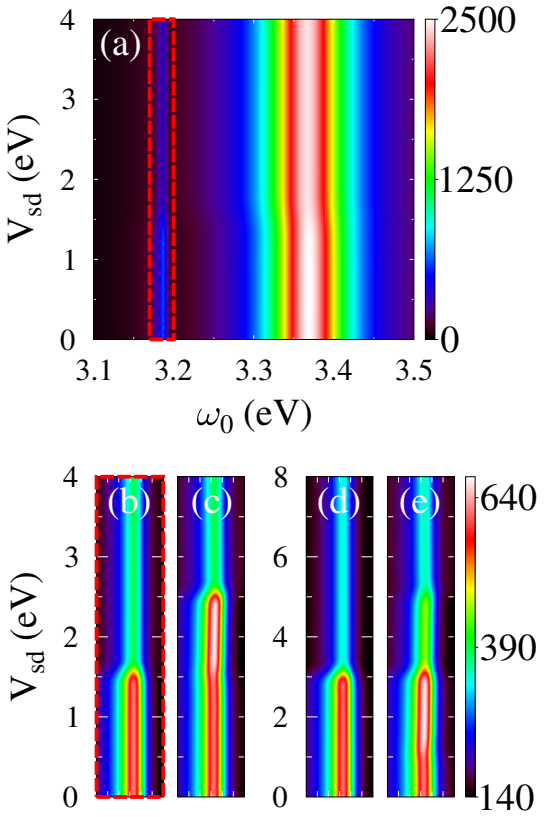

Figure 6.1: Plasmon absorption spectrum $I_{abs}(\omega_0)/\gamma N_0 \delta$, eq 6.10, as a function of bias V_{sd} (a) and close-up of the Fano resonance (b)-(e). Calculations with asymmetrically applied bias, $\eta = 1$, are performed with $U = 0$ in (a),(b) and $U = 1$ eV in (c). Results for symmetrically applied bias, $\eta = 0.5$, are shown in (d) $U = 0$ and (e) $U = 1$ eV. See text for other parameters.

6.4.1 Single molecule (D=1)

We work in the basis of many-body states $|S_M, P_L, P_R\rangle$ characterized by the states of the molecule $S_M \in \{0, g, e, 2\}$ and excitation states of the plasmons $P_{L,R} \in \{0, 1, 2, \ldots\}$. At equilibrium, the principle optical transition which controlls the absorption spectrum is between the ground state, $|g, 0, 0\rangle$ and two excited plasmon states, $|g, 1, 0\rangle$ and $|g, 0, 1\rangle$. The coupling, Δ_{MP}, between $|g, 1, 0\rangle$ ($|g, 0, 1\rangle$) and $|e, 0, 0\rangle$ is the origin of the Fano resonance in the absorption spectrum.

Figure 6.1 shows the effect of bias on the Fano resonance. For asymmetrically ap-

plied bias, $\eta = 1$, and in the absence of Coulomb repulsion, $U = 0$, both neutral, $|g, 0, 0\rangle$, and anion, $|2, 0, 0\rangle$, molecular states become equally populated above the threshold, $\mu_L = \varepsilon_e$. Since the anion state cannot exchange energy with the plasmons, the Fano resonance decreases to $\sim 50\%$ relative to its equilibrium value (see Figure 6.1b).

Finite Coulomb repulsion causes this transition to shift by U to higher biases (see Figure 6.1c). Moreover, in the region $\varepsilon_e < \mu_L < \varepsilon_e + U$ the Fano resonance increases. This is due to a partial blocking of the virtual transition from $|g, 1, 0\rangle$ ($|g, 0, 1\rangle$) via $|e, 0, 0\rangle$ to $|0, 0, 0\rangle$ by the Fermi distribution in the left contact. The blocking renormalizes the local density of the $|g, 1, 0\rangle$ and $|g, 0, 1\rangle$ states, which are responsible for the Fano resonance. Note that this is a combined electron/energy transfer mechanism, which is readily accounted for by the pseudoparticle NEGF formalism.[5]

We next consider a symmetrically coupled junction, $\eta = 0.5$. In the absence of Coulomb repulsion, $U = 0$, reaching the threshold results in equal population for all molecular states: cation $|0, 0, 0\rangle$, neutral ground $|g, 0, 0\rangle$, neutral excited $|e, 0, 0\rangle$, and anion $|2, 0, 0\rangle$. This would imply reduction in Fano resonance to $\sim 25\%$ of its equilibrium height. The observed reduction of $\sim 40\%$ (see Figure 6.1d) is due to the energy transfer between molecule and plasmon (and strong dissipation of the plasmon) which causes quick relaxation of the molecular exciton $|e, 0, 0\rangle$, thus increasing the population of to the neutral ground state $|g, 0, 0\rangle$.

Finite U reveals 4 distinct Fano resonance regions (see Figure 6.1e): 1. Below threshold $V_{sd} < \varepsilon_e - \varepsilon_g - 2U$ Fano resonance has its equilibrium appearance; 2. For $\varepsilon_e - \varepsilon_g - 2U < V_{sd} < \varepsilon_e - \varepsilon_g$ the virtual transition from $|g, 1, 0\rangle(|g, 0, 1\rangle)$ via $|e, 0, 0\rangle$ to $|2, 0, 0\rangle$ is blocked from the right contact, since $\mu_R - \varepsilon_g < U$. This results in an increase in the Fano resonance due to a local density of states renormalization by an electron/energy transfer mechanism (similar to that discussed in Figure 6.1c); 3. For $\varepsilon_e - \varepsilon_g < V_{sd} < \varepsilon_e - \varepsilon_g + U$ three molecular states (cation $|0, 0, 0\rangle$, neutral ground $|g, 0, 0\rangle$, and neutral excited $|e, 0, 0\rangle$) become accessible. Quick relaxation of the molecular exciton, $|e, 0, 0\rangle \to |g, 0, 0\rangle$, results in a population of the neutral ground state $\sim 2/3$, leading to a corresponding decrease in the Fano resonance relative to its equilibrium value (see discussion of Figure 6.1d); 4. For $V_{sd} > \varepsilon_e - \varepsilon_g + U$ all four molecular states

[5]Note that in the standard NEGF formalism a 4^{th} order perturbation theory is required to take the effect into account.

are accessible, and the Fano resonance reduces to $\sim 40\%$ of its equilibrium value.

Thus Figure 6.1 demonstrates sensitivity of the Fano resonance to nonequilibrium conditions, which renormalize the local molecular density of states resulting in measurable consequences for the absorption spectrum of the system. Note that the effect requires taking into account coherently coupled electron and energy transfer processes in an open nonequilibrium molecular system. The pseudoparticle NEGF is a convenient tool for such studies.

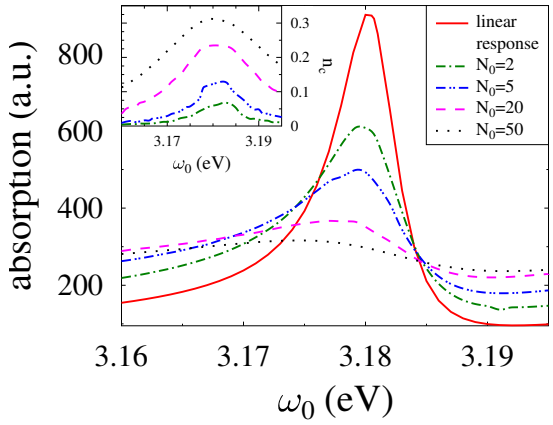

Figure 6.2: Nonlinear effects in the plasmon absorption: $I_{abs}(\omega_0)/\gamma N_0 \delta$, eq 6.10, for different intensities of laser field. Inset shows the population, n_c, of the molecular excited state $|e, P_L, P_R\rangle$. See text for parameters.

Figure 6.2 presents simulation beyond the optical linear response regime. Calculations are done at $V_{sd} = 0$, other parameters are as in Figure 6.1. Here the laser field is fully taken into account. Increase in the intensity of the laser results in population of the excited state of the molecule (see inset) and suppression of Fano resonance. Note however that contrary to predictions of Ref.[46] the Fano resonance is suppressed already for $n_c = 0.3$. The reason is additional broadening of the resonance due to coupling to the pumping mode, disregarded in earlier treatment. Moreover, since population of the excited state is different at different frequencies of the laser, the slope of the Fano resonance also depends on the intensity of the laser field. So, utilizing linear response theory in studies of optical spectrum of molecular junctions, where hot spots yield strongly enhanced local fields, is not always justified.

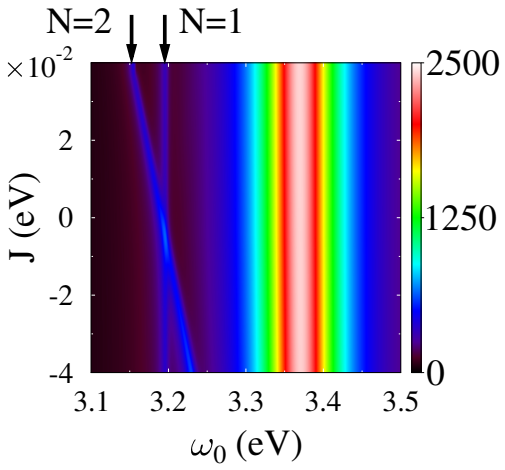

Figure 6.3: Plasmon absorption apectrum $I_{abs}(\omega_0)/\gamma N_0\delta$, eq 6.10, as a function of J at symmetrically applied bias of $V_{sd} = 6$ eV. Arrows indicate the Fano resonances attributed to the $N = 1$ and $N = 2$ charge blocks of the system. See text for parameters.

6.4.2 Molecular dimer (D=2)

A molecular dimer allows for the comparison of two energy transfer mechanisms: the intra-molecular and molecule-plasmon. Here the many-body states are $|S_1, S_2, P_L, P_R\rangle$, where S_1 and S_2 describe states of the first and second molecule. We use the following parameters: $t_e = t_g = 5$ meV, and $U = 2$ eV. Other parameters are as in Figure 6.1.

Figure 6.3 demonstrates the effect of intramolecular exciton coupling, J,[6] on the absorption spectrum at large symmetric bias, $\eta = 0.5$ and $V_{sd} = 6$ eV. With these parameters U is large enough to prevent double occupancy of either molecule, and the spectrum demonstrates two Fano resonances. The first does not change with J, and is a result of the plasmon coupling to transition between the singly occupied ($N = 1$) molecular states with an electron on either site of the dimer: $|g, 0, 1, 0\rangle$ ($|g, 0, 0, 1\rangle$) $\rightarrow$ $|e, 0, 0, 0\rangle$ or $|0, g, 1, 0\rangle$ ($|0, g, 0, 1\rangle$) $\rightarrow$ $|0, e, 0, 0\rangle$. The second peak is attributed to the plasmon coupling to transition between doubly occupied ($N = 2$) states with both sites populated by one electron: $|g, g, 1, 0\rangle$ ($|g, g, 0, 1\rangle$) $\rightarrow |e, g, 0, 0\rangle$ ($|g, e, 0, 0\rangle$). These excited molecular states ($|e, g, 0, 0\rangle$ and $|g, e, 0, 0\rangle$) are coupled by J, which results in a linear

[6]Generally, the energy transfer coupling J is controlled by electromagnetic environment that makes it complex-valued.[52] Here we consider J as independent parameter for the sake of simplicity.

dependence of the Fano resonance on the intramolecular excitonic coupling. Note that such absorption signatures may provide direct measurement of J in molecular dimers.

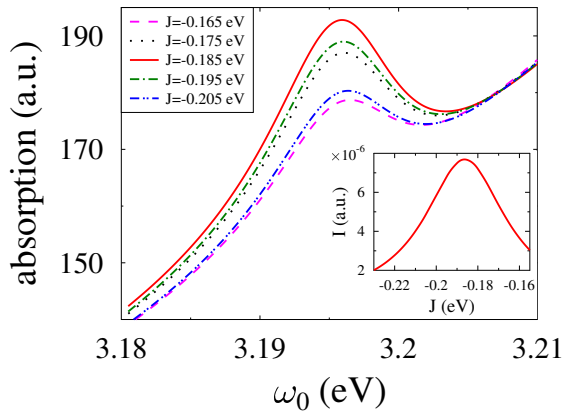

Figure 6.4: Fano resonance of the plasmon absorption spectrum $I_{abs}/\gamma N_0 \delta$, eq 6.10, for different values of J. Inset shows current I vs. J. See text for parameters.

6.4.3 Exciton Compensation for Coulomb Blockade

Recently, Li *et.al.*[52] demonstrated exciton compensation of the Coulomb blockade for a dimer system. Figure 6.4 shows how this physical phenomena affects the plasmon absorption spectrum. Parameters of the calculation are $t_e = t_g = 1$ meV, $U = 0.2$ eV, and $\Gamma^K_{c_K s} = 2$ meV ($K = L, R$; $s = g, e$). Other parameters as in Figure 6.3. The Coulomb blockade is lifted when $-J \sim U$, as was discussed in Ref.[52] (see inset). One sees that similar behavior is observed for the Fano resonance. The cause of enhancement of absorption spectrum is the same as for the transport, and is related to unblocking (reducing population) of the $|2, 0, P_L, P_R\rangle$ state ($E \approx \varepsilon_g + \varepsilon_e + U$), when it comes into resonance with an eigenstate of the $|g, e, P_L, P_R\rangle$ and $|e, g, P_L, P_R\rangle$ pair ($E \approx \varepsilon_g + \varepsilon_e \pm J$). Thus the absorption spectrum measurements can be used as a source of information on transport regime of the junction.

6.5 Conclusion

In conclusion, we have presented a pseudoparticle NEGF approach to study the optical properties of plasmonic systems interacting with a molecule in a current carry-

ing junction. The formalism is exact in its description of the model plasmon-exciton and intra-molecular interactions, so that collective plasmonic-molecular excitations in the strong coupling regime are treated properly. The method is an invaluable tool in describing combined electron and energy transfer processes in the system. The latter are shown to play important role in understanding the plasmon absorption spectrum at nonequilibrium. We demonstrated the ability to alter the Fano resonance intensity by changing the junction bias. We further discussed nonlinear effects in the spectrum and compared our results to the mean-field equilibrium study of Ref.[46] For a molecular dimer we showed the sensitivity of the Fano resonances to the intra-molecular exciton coupling, and discussed the possibility of revealing information on intra-molecular interactions from plasmonic absorption spectrum. Finally, we showed that the effect of exciton compensation of Coulomb blockade, introduced recently in Ref.[52] for transport through the junction, can also be measured in the absorption spectrum. Practical implementation of the developed approach based on its combination with consistent electrodynamical calculations of the corresponding parameters will be published elsewhere.

Supporting Information

A discussion of the pseudoparticle NEGF approach and its application to the problem of plasmon-molecule excitations in nanojunctions is discussed. Also an extra figure related to definition of the model, and derivation of eqs 6.10 and 6.15 are provided. This material is available free of charge via the Internet http://pubs.acs.org.

Acknowledgements

We gratefully acknowledge support by the Department of Energy (MG, Early Career Award, DE-SC0006422) and the US-Israel Binational Science Foundation (BF and MG, grant No. 2008282). Chapter 6, in full, is a reprint of the material as it appears in The Journal of Physical Chemistry Letters 2012. White, Alexander J.; Fainberg, Boris D.; Galperin, Michael, American Chemical Society 2012. The dissertation author was the primary investigator and author of the paper.

6.6 Supporting Information

6.6.1 Fluxes in terms of physical Green functions

Single particle Green functions are expressed as correlation functions of elementary excitations. For nonequilibirum systems these correlations are considered on the Keldysh contour[55]

$$R_{\nu\nu'}(\tau,\tau') = -\,i\langle T_c\,\hat{c}_\nu(\tau)\,\hat{c}^\dagger_{\nu'}(\tau')\rangle \tag{6.16}$$

$$P_{KK'}(\tau,\tau') = -\,i\langle T_c\,\hat{b}_K(\tau)\,\hat{b}^\dagger_{K'}(\tau')\rangle \tag{6.17}$$

where R and P are fermion and boson Green functions, T_c is the contour ordering operator, τ,τ' are contour variables, and $\hat{f}^\dagger_\nu$ ($\hat{f}_\nu$) and $\hat{b}^\dagger_K$ ($\hat{b}_K$) are creation (annihilation) operators for fermionic excitation in the orbital ν and bosonic excitation in the mode K, respectively. Projections of the contour correlation functions, eqs 6.16 and 6.17, to real time axis provide physical information about a nonequilibrium state of the system: interacting local density of states, form of the nonequilibrium distribution, etc.[56]

Fluxes between the nonequilibrium system and baths are introduced as rates of change of the populations in the baths. At steady state fermion and boson fluxes are (here and below $\hbar = 1$)[55,57]

$$I_K^{Fermi} = \int_{-\infty}^{+\infty} \frac{dE}{2\pi}\,\mathrm{Tr}\left[c^{K<}(E)\,R^{>}(E) - c^{K>}(E)\,R^{<}(E)\right] \tag{6.18}$$

$$I_B^{Bose} = -\int_{0}^{+\infty} \frac{d\omega}{2\pi}\,\mathrm{Tr}\left[f^{B<}(\omega)\,P^{>}(\omega) - f^{B>}(\omega)\,P^{<}(\omega)\right] \tag{6.19}$$

where $R^{>/<}(E)$ and $P^{>/<}(\omega)$ are Fourier transforms of the greater/lesser projections of the correlation functions, eqs 6.16 and 6.17, K and B indicate system-bath interface (e.g. $K = L, R$ for left and right contacts of the junction, and B may represent a thermal or radiation bath), Tr[...] is the trace over system excitations (fermi excitations for 6.18,

and bose excitations for 6.19), and

$$c^{K<}_{\nu\nu'}(E) = i\Gamma^{K}_{\nu\nu'}(E) f_K(E) \tag{6.20}$$

$$c^{K>}_{\nu\nu'}(E) = -i\Gamma^{K}_{\nu\nu'}(E)[1 - f_K(E)] \tag{6.21}$$

$$f^{B<}_{KK'}(\omega) = -i\gamma_{KK'}(\omega) N(\omega) \tag{6.22}$$

$$f^{B>}_{KK'}(\omega) = -i\gamma_{KK'}(\omega)[1 + N(\omega)] \tag{6.23}$$

are the (lesser and greater projections of) excitation self-energies due to coupling to the baths. Here

$$\Gamma^{K}_{\nu\nu'}(E) = 2\pi \sum_{\kappa \in K} V_{\nu\kappa} V_{\kappa\nu'} \delta(E - \varepsilon_\kappa) \tag{6.24}$$

$$\gamma_{KK'}(\omega) = 2\pi \sum_{\alpha} W_{K\alpha} W_{\alpha K'} \delta(\omega - \omega_\alpha) \tag{6.25}$$

are matrices characterizing the fermion escape rate to contact K and the boson dissipation to bath B (in our case K represents the contacts, and B is the radiation bath). In the wide-band approximation the two matrices become energy-independent quantities. Also we assume them to be diagonal, thus disregarding bath induced system correlations (this is a reasonable approximation, when energy separation between levels is bigger than corresponding diagonal elements of the matrices, eqs 6.24 and 6.25). Finally, $f_K(E)$ in eqs 6.20 and 6.21 and $N(\omega)$ in eqs 6.22 and 6.23 are population distributions in the baths. In our study we assume an equilibrium Fermi-Dirac population distribution for the contacts, $f_K(E) = [e^{(E-\mu_K)/T} + 1]^{-1}$ (μ_K is the electro-chemical potential of the contact K, and T is its temperature), and a laser induced population in a narrow band around the laser frequency, ω_0, (see eq 11 of the paper) for the radiation bath.

Note that in eqs 6.18 and 6.19 terms with $c^{K<}$ and $f^{B<}$ correspond to in-scattering processes (flux from a bath to the system), while those with $c^{K>}$ and $f^{K>}$ describe out-scattering fluxes (from system to baths). We use eq 6.18 to calculate electronic current in the inset of Figure 4. In-scattering part of eq 6.19 is used to characterize the absorption spectrum of the exciton-plasmon system (see eq 10 of the paper). Note that at equilibrium (and disregarding plasmons interactions with both radiation field and molecular exciton) eq 10 of our paper reduces to eq 6 from the Supporting Information

of Ref.[46]

6.6.2 System characteristics in terms of pseudoparticles

The pseudoparticle nonequilibrium Green function formalism utilizes a mapping of the physical space onto an extended Hilbert space. Within the formalism, many-body states of the system are described as *pseudoparticles*, similar to excitations in the physical Hilbert space, and it can be shown that corresponding many-body field operators follow usual commutation relations: Fermi or Bose depending on the character of the corresponding state (for detailed discussion see e.g. Ref.[51] and references therein). Operators of system excitations, which enter the definitions of the physical Green functions in eqs 6.16 and 6.17, are related to pseudoparticle creation, $\hat{d}^\dagger_m$, and annihilation, $\hat{d}_m$, operators via spectral decomposition (see eq 12 of the paper). In particular,

$$\hat{c}^\dagger_\nu = \sum_{m_1,m_2} \xi^\nu_{m_1 m_2}\, \hat{d}^\dagger_{m_1}\, \hat{d}_{m_2} \tag{6.26}$$

$$\hat{b}^\dagger_K = \sum_{m_1,m_2} \chi^K_{m_1 m_2}\, \hat{d}^\dagger_{m_1}\, \hat{d}_{m_2} \tag{6.27}$$

where sums are over many-body states $\{|m\rangle\}$ of the plasmon-exciton system, and

$$\xi^\nu_{m_1 m_2} \equiv \langle m_1|\hat{c}^\dagger_\nu|m_2\rangle \tag{6.28}$$

$$\chi^K_{m_1 m_2} \equiv \langle m_1|\hat{b}^\dagger_K|m_2\rangle \tag{6.29}$$

Transition to pseudoparticles accounts for all the interactions within the system exactly. The price to pay is the necessity to work in the extended Hilbert space, where pseudoparticle Green function $G_{mm'}(\tau,\tau')$ can be defined on the Keldysh contour similar to eqs 6.16 and 6.17 (see eq 14 of the paper).

Contrary to the usual Green function techniques, where perturbation theory is used to take into account interactions within the system, while quadratic coupling to baths (see eqs 7 and 8 of the paper) is treated exactly, the pseudoparticle Green functions formulation is exact in terms of system interactions but accounts for system-bath coupling perturbatively.[7] To establish a connection between physical and pseudoparti-

[7]Note that contrary to the quantum master equation formulations the pseudoparticle NEGF is con-

cle Green functions one utilizes eqs 6.26 and 6.27 in eqs 6.16 and 6.17. In particular, in the lowest order in the system-bath coupling (the non-crossing approximation) this connection is[58]

$$R_{\nu\nu'}(\tau,\tau') = i \sum_{\substack{m_1,m_1' \\ m_2 m_2'}} \zeta_{m_2} \overset{*}{\xi}{}^{\nu}_{m_1 m_2} \xi^{\nu'}_{m_1' m_2'} G_{m_1 m_1'}(\tau,\tau') G_{m_2' m_2}(\tau',\tau) \tag{6.30}$$

$$P_{KK'}(\tau,\tau') = i \sum_{\substack{m_1,m_1' \\ m_2 m_2'}} \zeta_{m_2} \overset{*}{\chi}{}^{\nu}_{m_1 m_2} \chi^{\nu'}_{m_1' m_2'} G_{m_1 m_1'}(\tau,\tau') G_{m_2' m_2}(\tau',\tau) \tag{6.31}$$

where $\zeta_m = 1$ (-1) if state $|m\rangle$ is bosonic (fermionic). Thus for the Fourier transforms of the projections used in eqs 6.18 and 6.19 one gets

$$R^{>/<}_{\nu\nu'}(E) = i \sum_{\substack{m_1,m_1' \\ m_2 m_2'}} \zeta_{m_2} \overset{*}{\xi}{}^{\nu}_{m_1 m_2} \xi^{\nu'}_{m_1' m_2'} \int_{-\infty}^{+\infty} \frac{dE'}{2\pi} G^{>/<}_{m_1 m_1'}(E+E') G^{</>}_{m_2' m_2}(E') \tag{6.32}$$

$$P^{>/<}_{KK'}(\omega) = i \sum_{\substack{m_1,m_1' \\ m_2 m_2'}} \zeta_{m_2} \overset{*}{\chi}{}^{\nu}_{m_1 m_2} \chi^{\nu'}_{m_1' m_2'} \int_{-\infty}^{+\infty} \frac{dE'}{2\pi} G^{>/<}_{m_1 m_1'}(E+E') G^{</>}_{m_2' m_2}(E') \tag{6.33}$$

6.6.3 Equations-of-motion for pseudoparticle Green functions

In the extended Hilbert space pseudoparticle Green functions for nonequilibrium systems follow the usual NEGF formulation. The Green function satisfy the Dyson equation, which at steady-state takes the form

$$\mathbf{G}(E) = \mathbf{g}(E) + \mathbf{g}(E)\,\Sigma(E)\,\mathbf{G}(\mathbf{E}) \tag{6.34}$$

Here $\mathbf{G}$ is the pseudoparticle Green function, $\mathbf{g}$ is the Green function of the isolated system, and Σ is self-energy introducing coupling between the system and baths. Note that matrix representation in 6.34 is in both contour variables and many-body states of the system.[59] For example,

$$\mathbf{G}(E) = \begin{bmatrix} \mathbf{G}^{c}(E) & \mathbf{G}^{<}(E) \\ \mathbf{G}^{>}(E) & \mathbf{G}^{\tilde{c}}(E) \end{bmatrix} \tag{6.35}$$

sistent in treating this coupling.[51]

where $\mathbf{G}^{c,<,>,\tilde{c}}(E)$ are Fourier transforms of the casual, lesser, greater, and anti-casual projections of the pseudoparticle Green function represented only in the basis of many-body states of the system.

The physically relevant subspace of the formulation is introduced by the normalization condition (see eq 13 of the paper). Technically this constraint is imposed by either a Lagrange multiplier[60,61] or an operator delta function.[58,62] In the physical subspace, equations of motion (EOMs) for the lesser and greater projections of the pseudoparticle Green function are decoupled with $G^{>}$ and $G^{<}$ restricted to $Q = 0$ and $Q = 1$ subspaces, respectively. As a result Green functions of the physical properties, eqs 6.32 and 6.33, belong to physical subspace, as it should be. Also this constraint leads to[58]

$$\mathbf{G}^{>}(E) = 2i\,\mathrm{Im}\,[\mathbf{G}^{r}(E)] \tag{6.36}$$

Below we treat the system-bath coupling in the non-crossing approximation, which corresponds to effective (dressed) second order in this interaction, and enforces additive structure of the self-energy in coupling to different baths.

At nonequilibrium steady-state one has to calculate two independent contour projections of a Green function to get full information on the state of the system. We employ retarded and lesser projections the pseudoparticle Green function (see eq 14 of the paper). After enforcing the physical subspace constraint (see eq 13 of the paper) Fourier transform of the Dyson equation, eq 6.34, for the two projections is[8]

$$\mathbf{G}^{r}(E) = [E\mathbf{I} - \mathbf{H}_M - \Sigma^{r}(E)]^{-1} \tag{6.37}$$

$$\mathbf{G}^{<}(E) = \mathbf{G}^{r}(E)\,\Sigma^{<}(E)\,\mathbf{G}^{a}(E) \tag{6.38}$$

[8] In eqs 6.37 and 6.38 Hamiltonian, Green functions and self-energy are matrices in the system many-body basis $\{|m\rangle\}$.

where

$$\Sigma^{r/<}_{mm'}(E) = \int_{-\infty}^{+\infty} \frac{dE_1}{2\pi} \sum_{m_1,m_2} G^{r/<}_{m_1m_2}(E_1)\times$$
$$\Bigg[\sum_{K=L,R} \Big(\Xi^K_{mm_1,m'm_2} F_K^{>/<}(E-E_1) + \Xi^K_{m_2m',m_1m} F_K^{</>}(E_1-E) \Big)$$
$$+\Phi_{mm_1,m'm_2} B^{>/<}(E-E_1) + \Phi_{m_2m',m_1m} B^{</>}(E_1-E) \Bigg] \tag{6.39}$$

are retarded/lesser projections of the self-energy. Here

$$\Xi^K_{m_1m_2,m_1'm_2'}(E) \equiv \sum_{s_1,s_2\in\{g,e\}} \xi^{c_Ks_1}_{m_1m_2} \Gamma^K_{c_Ks_1,c_Ks_2}(E) \overset{*}{\xi}{}^{c_Ks_2}_{m_1'm_2'} \tag{6.40}$$

$$\Phi(E) \equiv \sum_{K_1,K_2\in\{L,R,M\}} \chi^{K_1}_{m_1m_2} \gamma_{K_1K_2}(E) \overset{*}{\chi}{}^{K_2}_{m_1'm_2'} \tag{6.41}$$

describe coupling to the contacts (eq 7 of the paper) and the radiation bath (eq 8 of the paper). $\xi^{c_Ks}_{m_1m_2}$ and $\chi^K_{m_1m_2}$ are defined in eq 12 of the paper with $\hat{O}_\nu = \hat{c}_{c_Ks}$ and $\hat{b}_K$, respectively,

$$\Gamma^K_{c_Ks_1,c_Ks_2}(E) \equiv \sum_{\kappa\in K} V_{s_1\kappa}\, V_{\kappa s_2} \delta(E-\varepsilon_\kappa) \tag{6.42}$$

$$\gamma_{K_1K_2}(E) \equiv \sum_\alpha W_{K_1\alpha} W_{\alpha K_2} \delta(|E|-\omega_\alpha) \tag{6.43}$$

are matrices introducing escape rates into the contacts and dissipation.[9] $F^<_K(E) = f_K(E)$ and $F^>_K(E) = 1 - f_K(E)$ are defined by the Fermi distribution of electrons in the contacts $f_K(E) \equiv [e^{(E-\mu_K)/T}+1]^{-1}$; $B^<(E) = N_{\omega_0}(E)$ and $B^>(E) = 1 + N_{\omega_0}(E)$ (here $E > 0$, for $E < 0$ $B^{>/<}(E) = B^{</>}(-E)$) are defined by the laser induced mode population, (see eq 11 of the paper). Eqs 6.37 and 6.38 have to be solved self-consistently, since the pseudoparticle self-energies depends on the pseudoparticle Green's functions.

Detailed derivations of the expressions presented in eqs 6.37-6.39 can be found in Appendixes A and B of Ref.[51]

[9] Following Ref.[46] below we employ a wide band approximation for which Γ and γ do not depend on energy. We also assume the matrices to be diagonal.

6.6.4 Quadrupole contribution to plasmonic absorption spectrum

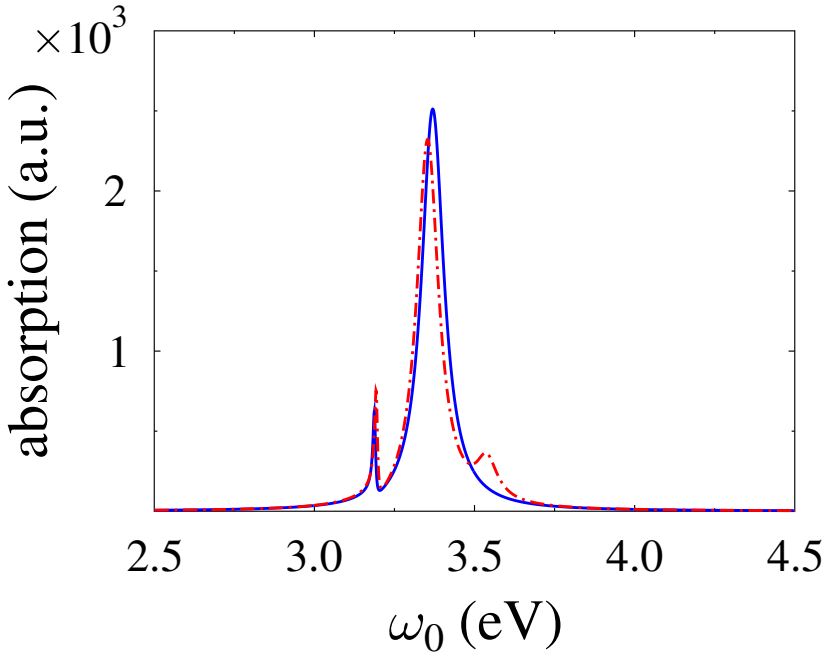

Figure 6.5: Plasmon absorption spectrum $I_{abs}(\omega_0)/\gamma N_0 \delta$ (see Eq.(10) of the paper), at equilibrium with (dash-dotted line, red) and without (solid line, blue) quadrupole contribution. Calculations use parameters of Ref.[46]

6.5 compares the plasmonic absorption spectrum, calculated for the parameters utilized in the paper within the pseudoparticle NEGF formalism, with (dash-dotted line) and without (solid line) quadrupole contribution. One sees that the main difference between the two spectra is the appearance of an additional feature to the right of the plasmonic dipole resonance. The Fano factor, whose physics we study, is almost not affected. Thus for simplicity we do not include the quadrupole contribution in calculations performed in the paper.

Chapter 6 References

[1] Halas, N.J. Nano Lett. **10**, 3816 (2010)

[2] Stockman, M.I. Opt. Express **19**, 22029 (2011)

[3] Gramotnev, D.K. and Bozhevolnyi, S.I. Nat Photon **4**, 83 (2010)

[4] Schuller, J.A.; Barnard, E.S.; Cai, W.; Jun, Y.C.; White, J.S. and Brongersma, M.L. Nat Mater **9**, 193 (2010)

[5] Hill, M.T. J. Opt. Soc. Am. B **27**, B36 (2010)

[6] Juan, M.L.; Righini, M. and Quidant, R. Nat Photon **5**, 349 (2011)

[7] Atwater, H.A. and Polman, A. Nat Mater **9**, 205 (2010)

[8] Pillai, S. and Green, M. Solar Energy Materials and Solar Cells **94**, 1481 (2010)

[9] Catchpolea, K.R.; Mokkapatia, S.; Becka, F.; Wanga, E.C.; McKinleya, A.; Bascha, A. and Lee, J. MRS Bulletin **36**, 461 (2011)

[10] Aslan, K.; Lakowicz, J.R. and Geddes, C.D. Current Opinion in Chemical Biology **9**, 538 (2005)

[11] Sannomiya, T. and Voeroes, J. Trends in Biotechnology **29**, 343 (2011)

[12] Hinterdorfer, P.; Garcia-Parajo, M.F. and Dufrene, Y.F. Acc. Chem. Res. **45**, 327 (2012)

[13] Zheng, Y.B.; Kiraly, B.; Weiss, P.S. and Huang, T.J. Nanomedicine **7**, 751 (2012)

[14] Galperin, M. and Nitzan, A. Phys. Chem. Chem. Phys. **14**, 9421 (2012)

[15] Zhang, Q.; Atay, T.; Tischler, J.R.; Bradley, M.S.; Bulovic, V. and V., N. Nat Nano **2**, 555 (2007)

[16] Fofang, N.T.; Park, T.H.; Neumann, O.; Mirin, N.A.; Nordlander, P. and Halas, N.J. Nano Lett. **8**, 3481 (2008)

[17] Wiederrecht, G.P.; Wurtz, G.A. and Hranisavljevic, J. Nano Lett. **4**, 2121 (2004)

[18] Wurtz, G.A.; Evans, P.R.; Hendren, W.; Atkinson, R.; Dickson, W.; Pollard, R.J.; Zayats, A.V.; Harrison, W. and Bower, C. Nano Lett. **7**, 1297 (2007)

[19] Eisele, D.M.; Knoester, J.; Kirstein, S.; Rabe, J.P. and Vanden Bout, D.A. Nat Nano **4**, 658 (2009)

[20] Walker, B.J.; Dorn, A.; Bulovic, V. and Bawendi, M.G. Nano Lett. **11**, 2655 (2011)

[21] Zheng, Y.B.; Kiraly, B.; Cheunkar, S.; Huang, T.J. and Weiss, P.S. Nano Lett. **11**, 2061 (2011)

[22] Zhang, S.; Wei, H.; Bao, K.; Håkanson, U.; Halas, N.J.; Nordlander, P. and Xu, H. Phys. Rev. Lett. **107**, 096801 (2011)

[23] Coomar, A.; Arntsen, C.; Lopata, K.A.; Pistinner, S. and Neuhauser, D. J. Chem. Phys. **135**, 084121 (2011)

[24] Henry, A.I.; Bingham, J.M.; Ringe, E.; Marks, L.D.; Schatz, G.C. and Van Duyne, R.P. J. Phys. Chem. C **115**, 9291 (2011)

[25] Li, S.; Gao, Y. and Neuhauser, D. J. Chem. Phys. **136**, 234104 (2012)

[26] McMahon, J.M.; Li, S.; Ausman, L.K. and Schatz, G.C. The Journal of Physical Chemistry C **116**, 1627 (2012)

[27] Lopata, K. and Neuhauser, D. J. Chem. Phys. **130**, 104707 (2009)

[28] Lopata, K. and Neuhauser, D. J. Chem. Phys. **131**, 014701 (2009)

[29] Masiello, D.J. and Schatz, G.C. J. Chem. Phys. **132**, 064102 (2010)

[30] Arntsen, C.; Lopata, K.; Wall, M.R.; Bartell, L. and Neuhauser, D. J. Chem. Phys. **134**, 084101 (2011)

[31] Sukharev, M. and Nitzan, A. Phys. Rev. A **84**, 043802 (2011)

[32] Mullin, J. and Schatz, G.C. J. Phys. Chem. A **116**, 1931 (2012)

[33] Sukharev, M. and Galperin, M. Phys. Rev. B **81**, 165307 (2010)

[34] Fainberg, B.D.; Sukharev, M.; Park, T.H. and Galperin, M. Phys. Rev. B **83**, 205425 (2011)

[35] Zuloaga, J.; Prodan, E. and Nordlander, P. Nano Lett. **9**, 887 (2009)

[36] Morton, S.M.; Silverstein, D.W. and Jensen, L. Chem. Rev. **111**, 3962 (2011)

[37] Song, P.; Nordlander, P. and Gao, S. J. Chem. Phys. **134**, 074701 (2011)

[38] Mullin, J.M.; Autschbach, J. and Schatz, G.C. Comput. Theor. Chem. **987**, 32 (2012)

[39] Zelinskyy, Y. and May, V. Nano Lett. **12**, 446 (2012)

[40] Fano, U. Phys. Rev. **124**, 1866 (1961)

[41] Luk'yanchuk, B.; Zheludev, N.I.; Maier, S.A.; Halas, N.J.; Nordlander, P.; Giessen, H. and Chong, C.T. Nat Mater **9**, 707 (2010)

[42] Zhang, W.; Govorov, A.O. and Bryant, G.W. Phys. Rev. Lett. **97**, 146804 (2006)

[43] Artuso, R.D. and Bryant, G.W. Nano Lett. **8**, 2106 (2008). PMID: 18558787

[44] Artuso, R.D. and Bryant, G.W. Phys. Rev. B **82**, 195419 (2010)

[45] Ridolfo, A.; Di Stefano, O.; Fina, N.; Saija, R. and Savasta, S. Phys. Rev. Lett. **105**, 263601 (2010)

[46] Manjavacas, A.; Abajo, F.J.G.D. and Nordlander, P. Nano Lett. **11**, 2318 (2011)

[47] Wu, X.; Gray, S.K. and Pelton, M. Opt. Express **18**, 23633 (2010)

[48] Haug, H. and Koch, S.W. *Quantum Theory of the Optical and Electronic Properties of Semiconductors* (World Scientific, 2009) (2009)

[49] Agranovich, V.M.; Litinskaia, M. and Lidzey, D.G. Phys. Rev. B **67**, 085311 (2003)

[50] Salomon, A.; Gordon, R.J.; Prior, Y.; Seideman, T. and Sukharev, M. Phys. Rev. Lett. **109**, 073002 (2012)

[51] White, A.J. and Galperin, M. Phys. Chem. Chem. Phys. **14**, 13809 (2012)

[52] Li, G.; Shishodia, M.S.; Fainberg, B.D.; Apter, B.; Oren, M.; Nitzan, A. and Ratner, M.A. Nano Lett. **12**, 2228 (2012)

[53] Galperin, M. and Nitzan, A. J. Chem. Phys. **124**, 234709 (2006)

[54] Novotny, L. and Hecht, B. *Principles of Nano-Optics* (Cambridge University Press, Cambridge, 2011) (2011)

[55] Haug, H. and Jauho, A.P. *Quantum Kinetics in Transport and Optics of Semiconductors*. Springer Series in Solid-State Sciences (Springer-Verlag, Berlin Heidelberg, 1996) (1996)

[56] Kadanoff, L.P. and Baym, G. *Quantum Statistical Mechanics*. Frontiers in Physics (W. A. Benjamin, Inc., New York, 1962) (1962)

[57] Galperin, M.; Nitzan, A. and Ratner, M.A. Phys. Rev. B **75**, 155312 (2007)

[58] Wingreen, N.S. and Meir, Y. Phys. Rev. B **49**, 11040 (1994)

[59] Park, T.H. and Galperin, M. Phys. Rev. B **84**, 205450 (2011)

[60] Coleman, P. Phys. Rev. B **29**, 3035 (1984)

[61] Oh, J.H.; Ahn, D. and Bubanja, V. Phys. Rev. B **83**, 205302 (2011)

[62] Bickers, N.E. Rev. Mod. Phys. **59**, 845 (1987)

Chapter 7

Raman scattering in molecular junctions: A pseudoparticle formulation

Alexander J. White[1], Sergei Tretiak[2] and Michael Galperin[1]

[1]Department of Chemistry and Biochemsitry, University of California at San Diego, La Jolla CA 92093, USA

[2]Theoretical Division, Center for Nonlinear Studies (CNLS), and Center for Integrated Nanotechnologies (CINT), Los Alamos National Laboratory, Los Alamos, NM 87545, USA

We present a formulation of Raman spectroscopy in molecular junctions, based on a many-body state representation of the molecule. The approach goes beyond the previous effective single orbital formalism, and provides a convenient way to incorporate computational methods and tools proven for equilibrium molecular spectroscopy into the realm of current carrying junctions. The presented framework is illustrated by first principle simulations of Raman response in a three-ring oligophenylene vinylene terminating in amine functional groups (OPV3) junction. The calculated shift in Stokes lines

and estimate of vibrational heating by electric current agree with available experimental data. In particular our results suggest that participation of the OPV3 cation in Raman scattering under bias may be responsible for the observed shift, and that the direction of the shift depends on renormalization of normal modes. This work is a step toward atomistic quantum *ab initio* modeling of the optical response of nonequilibrium electronic dynamics in molecular junctions.

7.1 Introduction

Molecular electronics promises to harness electronic functionality over an area of no more than a few molecules thus approaching the fundamental size limit of molecular electronic devices.[1] Our progress in this field is subject to the availability of advanced fabrication technologies and experimental capabilities to precisely characterize the structure and monitor the underlying fundamental electronic dynamics. The first observation of Raman spectroscopy enhancement for molecules chemisorbed on metal surfaces (SERS),[2,3] has manifested an important optical tool for single molecule detection.[4,5] Since then the field has progressed rapidly.[6–9] SERS is known to be dominated by *hot spots* (areas of particularly strong electromagnetic field enhancement).[10] The ability to produce nanometer scale gaps in metal junctions[11–13] paved the way for the application of SERS in molecular electronics as diagnostic and control tool.[14–16] In particular, Raman spectroscopy was used to estimate bias induced vibrational and electronic heating in molecular junctions,[17–19] to reveal the structure of single-molecule junctions,[20–23] and to estimate orientation of a molecule in junction.[24,25] Correlations between the Raman signal and conductance, due to junction dynamics, suggest the possibility to characterize electronic dynamics by optical means.[18,26,27]

Experimental advances have driven theoretical interest in this field. Several theoretical approaches have been put forward to analyze and explain existing data as well as to propose future experiments.[15,28] In particular, in our previous publications we combined a nonequilibrium Green's function description of quantum transport with a generalized scattering theory of the Raman flux, thus providing the first theoretical description of Raman scattering in such systems. Within simple models we applied the theory to study bias induced vibrational[29,30] and electronic[31,32] heating, charge transfer contribution to SERS,[33] and time-dependent correlations between conductance and Stokes signal.[26,34–36]

To this point existing studies of Raman scattering under nonequilibrium electronic conditions have utilized a noninteracting orbital-based approach (a single-electron mean-field picture), which becomes inadequate in the presence of strong interactions (e.g. molecule-plasmon coupling) in the system.[37] On the other hand only *ab inito* simulations based on equilibrium theory of Raman scattering, were reported in the literature for

molecules adsorbed on metal surfaces[21,38–44] and in junctions.[45–47] This necessitates the need for theoretical techniques enabling modeling of optical response of nonequilibrium electronic system in molecular junctions using advanced quantum-chemical methods able to describe the underlying many-body physics.

Here we present a pseudoparticle nonequilibrium Green function (PP-NEGF) formulation for Raman scattering probes in current carrying molecular junctions, and apply it to first principle simulations of Raman scattering in an OPV3 junction (see Figure 7.1). This molecular system has been used in Raman spectroscopy experiments.[19] The study is the first attempt of *ab initio* simulation within a nonequilibrium theory of Raman scattering. Our eventual goal is a realistic description of optical response in junctions, where the PP-NEGF molecular Raman scattering (presented here) should be accompanied by PP-NEGF description of interactions with plasmon excitations in the contacts (as presented in ref.[37]).

We stress that the PP-NEGF (many-body states) approach introduced here is fundamentally different from the quasiparticles (single-particle orbitals) considerations in our previous publications [26,29-36]. As a formulation based on the many-body states representation, the PP-NEGF allows one to account for all the intramolecular interactions exactly. It also provides a possibility of formulation in the language of vibronic (dressed) states. Note that while standard (Redfield) quantum master equation in principle can also account exactly for the intramolecular interactions, it is applicable only in the unphysically low temperature regime ($k_BT \ll \Gamma$)[48] and in the absence of degeneracies in the system.[49] It also completely misses hybrydization between molecule and contacts,[50] which results in qualitative failures.[51] The PP-NEGF approach to Raman scattering is an important theoretical advancement, because it provides a convenient way to incorporate tools of quantum chemistry and equilibrium molecular spectroscopy (traditionally formulated in the language of many-body states of an isolated molecule) into the realm of current carrying junctions.

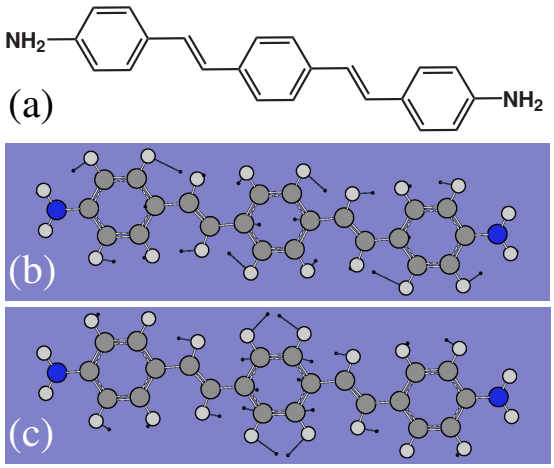

Figure 7.1: A three-ring oligophenylene vinylene terminating in amine functional groups (OPV3) molecule. Shown are (a) molecular structure and normal modes of neutral OPV3 at frequencies (b) 1199 cm^{-1} and (c) 1608 cm^{-1}. Created by GaussView 5.

7.2 Model and Method

We consider a molecule, M, bridging two metal electrodes, and subjected to an external laser radiation, rad. The electrodes act as electronic, L and R, and thermal, B, reservoirs, each at its own equilibrium. The Hamiltonian of the junction is

$$\hat{H} = \hat{H}_M + \sum_{K=L,R,B,rad} \left(\hat{H}_K + \hat{V}_K \right) \tag{7.1}$$

Here we represent the molecular Hamiltonian $\hat{H}_M$ in terms of many-body states $|S\rangle$ of the molecule

$$\hat{H}_M = \sum_{S_1,S_2 \in M} H^{(M)}_{S_1 S_2} \hat{X}_{S_1 S_2} \tag{7.2}$$

while the Hamiltonians of the baths are expressed within second quantization

$$\begin{aligned} \hat{H}_{L(R)} = \sum_{k \in L(R)} \varepsilon_k \hat{c}^\dagger_k \hat{c}_k, \quad \hat{H}_B = \sum_{\beta \in B} \omega_\beta \hat{b}^\dagger_\beta \hat{b}_\beta, \\ \hat{H}_{rad} = \sum_\alpha \nu_\alpha \hat{a}^\dagger_\alpha \hat{a}_\alpha, \end{aligned} \tag{7.3}$$

where $\hat{X}_{S_1S_2} \equiv |S_1\rangle\langle S_2|$ is a Hubbard (projection) operator, and $\hat{c}_k^\dagger$ ($\hat{c}_k$), $\hat{b}_\beta^\dagger$ ($\hat{b}_\beta$), and $\hat{a}_\alpha^\dagger$ ($\hat{a}_\alpha$) create (annihilate) an electron in the contacts L and R, phonon in the thermal bath B, and photon of radiation field rad, respectively. Finally, $\hat{V}_{L(R)}$, $\hat{V}_B$, and $\hat{V}_{rad}$ in Eq.(7.1) describe single electron, phonon, and photon transitions between the molecule and baths

$$\hat{V}_K = \sum_{\substack{S_1,S_2\in M \\ q\in K}} \left(V^{(K)}_{S_1S_2,q}\, \hat{X}^\dagger_{S_1S_2} \hat{O}_q + H.c. \right) \tag{7.4}$$

Here $\hat{O}_q = \hat{c}_k$, $\hat{b}_\beta$, and $\hat{a}_\alpha$ for $K = L(R)$, B, and rad, respectively. Below we utilize molecular vibronic states $|S_m\rangle = |e_m, v^{(m)}_\nu\rangle \approx |e_m\rangle\, |v^{(m)}_\nu\rangle$ as many-body basis, so that $H^{(M)}_{S_1S_2} = \delta_{S_1,S_2}\, E_{S_1}$, $V^{(L(R))}_{S_1S_2,k} = V_{e_1e_2,k}\, \langle v^{(1)}_{\nu_1}|v^{(2)}_{\nu_2}\rangle$, $V^{(B)}_{S_1S_2,\beta} = \delta_{e_1,e_2} W_{\nu_1^{(1)}\nu_2^{(1)},\beta}$, and $V^{(rad)}_{S_1S_2,\alpha} = -\vec{\mu}_{e_1,e_2}\vec{\mathcal{E}}_\alpha\, \langle v^{(1)}_{\nu_1}|v^{(2)}_{\nu_2}\rangle$. Here $\vec{\mu}_{e_1,e_2}$ is the electronic transition dipole moment, $\vec{\mathcal{E}}_\alpha$ is amplitude of the radiation field mode α, and $\langle v^{(1)}_{\nu_1}|v^{(2)}_{\nu_2}\rangle$ are overlap integrals of the vibrational wave functions for electronic ($L(R)$) and optical (rad) transitions. Corresponding Franck-Condon factors are evaluated following the method by Ruhoff and Ratner.[52,53]

An expression for Raman scattering in current-carrying junctions was first derived considering an outgoing photon flux caused by a coherent photon scattering from an occupied initial, $\alpha = i$, to an empty final, $\alpha = f$, mode of radiation field.[30] The derivation was performed using a noninteracting orbital-based representation. Here we develop a desirable generalization to the many-body molecular basis $\{|S\rangle\}$ by invoking the PP-NEGF method.[54–57] Within this approach one can introduce pseudoparticle operator, $\hat{d}_S^\dagger$, that creates the molecular many-body state $|S\rangle$ by acting on vacuum state, $|S\rangle = \hat{d}_S^\dagger|0\rangle$. The methodology is identical to the second quantization. However, it is formulated in an extended Hilbert space, whose physically relevant subspace is defined by a normalization condition $\sum_S \hat{d}_S^\dagger \hat{d}_S = 1$. In the extended Hilbert space the nonequilibrium pseudoparticle Green function

$$G_{S_1S_2}(\tau_1,\tau_2) = -i\langle T_c\, \hat{d}_{S_1}(\tau_1)\, \hat{d}^\dagger_{S_2}(\tau_2)\rangle \tag{7.5}$$

satisfies the usual Dyson equation. Restricting the latter to the physical subspace results in a coupled system of equations for projections of the Green function (see e.g. ref.[56] for

details).

Following the line of argument of ref.[30] and assuming no charge transfer (CT) contribution, an expression for intramolecular Raman flux which starts in a ground molecular state $|g\rangle$ and proceeds via set of excited states $\{|x\rangle\}$, is given by (see Supporting information for derivation details) [1]

$$\begin{aligned} J(t) = 2\mathrm{Re} \sum_{\substack{g_i,x_1,x_2,g_f \\ \bar{g}_i,\bar{x}_1\bar{x}_2,\bar{g}_f}} \zeta_{g_i} \int_{-\infty}^{t} dt' \int_{-\infty}^{t} dt_1 \int_{-\infty}^{t'} dt_2 \\ \Pi^{<}_{g_i x_1,\bar{g}_i\bar{x}_1}(t_1 - t_2)\, \Pi^{>}_{g_f x_2,\bar{g}_f\bar{x}_2}(t' - t) \\ G^{>}_{\bar{x}_1\bar{x}_2}(t_2,t')\, G^{>}_{\bar{g}_f g_f}(t',t)\, G^{>}_{x_2 x_1}(t,t_1)\, G^{<}_{g_i\bar{g}_i}(t_1,t_2) \end{aligned} \tag{7.6}$$

where $\zeta_{g_i} = 1\ (-1)$ when state $|g_i\rangle$ is of Fermi (Bose) type, $G^{\gtrless}_{S_1S_2}(t_1,t_2)$ are greater/lesser projections of the Green function (7.5), $\Pi^{\gtrless}$ are greater/lesser projections of the self-energies due to coupling to radiation field. The Fourier transforms of the latter are[37]

$$\begin{aligned} \Pi^{>}_{gx,g'x'}(\omega) &\equiv -\, i\Omega_{gx,g'x'}(\omega)\,[1 + N(\omega)] \\ \Pi^{<}_{gx,g'x'}(\omega) &\equiv -\, i\Omega_{gx,g'x'}(\omega)\, N(\omega) \end{aligned} \tag{7.7}$$

where $\Omega_{gx,g'x'}(\omega) \equiv 2\pi \sum_\alpha V^{(rad)}_{gx,\alpha}\, V^{(rad)}_{\alpha,g'x'} \delta\left(\omega - \nu_\alpha\right)$ and $N(\omega) \equiv \frac{1}{\pi} \frac{\gamma^2}{(\omega-\nu_i)^2+\gamma^2}$ with ν_i being the frequency of the incoming laser radiation, γ - laser bandwidth, and $N(\omega)$ characterizing the laser resolution. Note that Eq.(7.6) is an expression for 'the normal Raman process' as discussed in refs.[29,30] Note also that it is a time-dependent generalizaton similar to the CT-Raman consideration of refs.[34,35] At steady-state Eq.(7.6) becomes

[1] Our consideration is an extension to nonequilibrium of the ideas of atomic limit formulations, where the starting point of treatment is an isolated system, and coupling between the system and baths in taken into account within a perturbation theory. Thus ground and excited states used in the formulation are the many-body states of the isolated molecule.

$J = \int \frac{d\omega_f}{2\pi} J(\omega_f)$ with

$$J(\omega_f) = -\sum_{\substack{g_i,x_1,x_2,g_f \\ \bar{g}_i,\bar{x}_1\bar{x}_2,\bar{g}_f}} \zeta_{g_i} \int \frac{d\omega_i}{2\pi} \int \frac{dE_i}{2\pi} \int \frac{dE_f}{2\pi} \tag{7.8}$$

$$2\pi\delta(\omega_i + E_i - \omega_f - E_f)\, \Pi^{<}_{g_i x_1, \bar{g}_i \bar{x}_1}(\omega_i)\, \Pi^{>}_{g_f x_2, \bar{g}_f \bar{x}_2}(\omega_f)$$
$$\int \frac{dE_{\bar{x}}}{2\pi} \int \frac{dE_x}{2\pi} \frac{G^{>}_{\bar{g}_f g_f}(E_f)\, G^{>}_{\bar{x}_1 \bar{x}_2}(E_{\bar{x}})\, G^{>}_{x_2 x_1}(E_x)\, G^{<}_{g_i \bar{g}_i}(E_i)}{[\omega_i + E_i - E_{\bar{x}} - i\eta][\omega_i + E_i - E_x + i\eta]}$$

where $\eta \to 0^+$ is an infinitesimal real number, $\delta(\ldots)$ is the Dirac delta function. Expression (7.8) is convenient to use for numerical simulations as described below.

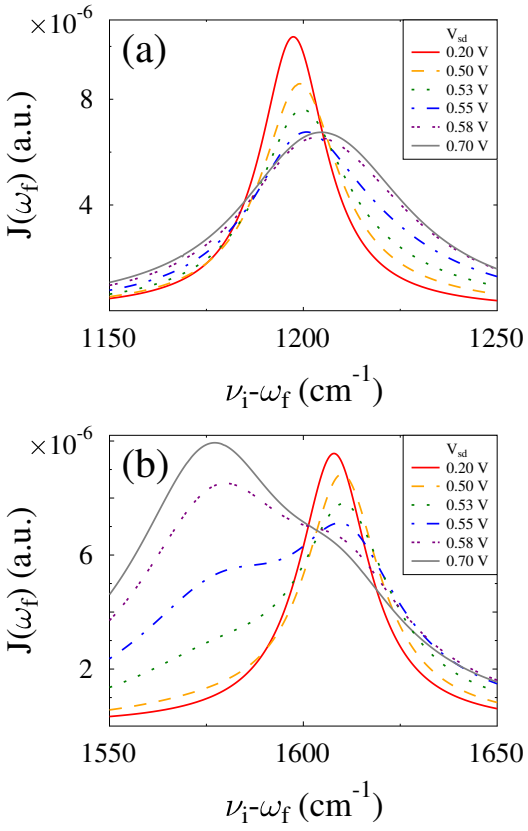

Figure 7.2: The Stokes peak, Eq.(7.8), versus Raman shift for several source-drain biases, V_{sd}. Shown are results for molecular vibrational modes at (a) 1199 and (b) 1608 cm^{-1}. See text for parameters used for simulations.

7.3 Numerical results

We apply the method introduced above to an OPV3 junction (see Figure 7.1a), which was the focus of recent Raman measurements.[19] We chose parameters to be representative of a realistic experimental situation. Following refs.[58–60] we assume that at low bias the main contribution to conductance comes from neutral (N) and cation (C) states of OPV3, and that $E_N^e - E_C^e - E_F = 0.05$ eV[61,62] (here E_N^e, E_C^e, and E_F are electronic energies of neutral and cation OPV3 species, and the Fermi energy, respectively). The electron escape rates to the contacts, $\Gamma_{L(R)} \equiv 2\pi \sum_{k\in L(R)} |V_{CN,k}|^2 \delta(E - \varepsilon_k)$, are taken as 15 meV in agreement with experimental estimate.[63] Molecular vibrations are modeled as harmonic oscillators (normal modes specific for cation and neutral molecule). The dissipation matrix for the vibrations due to coupling to thermal bath is assumed to be diagonal, $\Gamma^B_{v^{(m)}v^{(m)}+1,v^{(m)}v^{(m)}+1} \equiv 2\pi \sum_{\beta\in B} |W_{v^{(m)}v^{(m)}+1,\beta}|^2 \delta(\omega - \omega_\beta)$, and the rates are 2.5 meV. The laser field is assumed to be polarized along the principle axis of the OPV3 molecule. The intensity of the field is $\mathcal{E}_i \sim 10^{10}$ V/m, its frequency is $\nu_i = 1.4$ eV, and laser bandwidth $\gamma = 1$ meV. Temperature in the contacts is taken as 100 K.

Calculations were preformed on an adjustable energy grid.

Parameters of electronic and vibrational structure of the isolated molecule (ground and excited state electronic energies, normal mode frequencies and electronic transition dipole moments of neutral and cation species) were computed with Density Functional Theory (DFT) and Time Dependent DFT (TDDFT) methodologies.[64,65] For all calculations we use the B3LYP hybrid-functional with a 3-21+G basis set as implemented in the *Gaussian*'09 software package.[66]

Figure 7.2 shows the Stokes shift of two Raman active normal modes. For the neutral OPV3 these modes are at 1199 and 1608 cm^{-1} with displacements schematically shown in Figs. 7.1b and c. Oxidation of the molecule leads to shift of the modes to 1211 and 1577 cm^{-1}, respectively. Under finite bias both neutral and cation species contribute to the total Raman signal, with the latter contribution becoming more pronounced at higher bias. Correspondingly, the Stokes peak shifts to higher or lower frequencies for the two modes. Note that calculation in Figure 7.2a employs $\nu_i = 1.2$ eV as frequency of the laser field. Note also that the shift for the mode at 1608 cm^{-1} (see Figure 7.2b) was observed experimentally[16,19] and discussed theoretically within a perturbation theory

analysis of electron-vibration coupling.[67] At finite bias charge transfer between the molecule and contacts induces dissipation in the ground states of the neutral and cation species, which leads to broadening of the peaks. We note that the PP-NEGF approach is especially convenient for describing this system since it easily accounts for the different vibrational frequencies of the neutral and cation species while retaining information on mixture of molecular states with those of the contacts. This allows for high accuracy treatment of the electron-vibration coupling in junction which goes far beyond usual considerations within perturbation theory.[37,56]

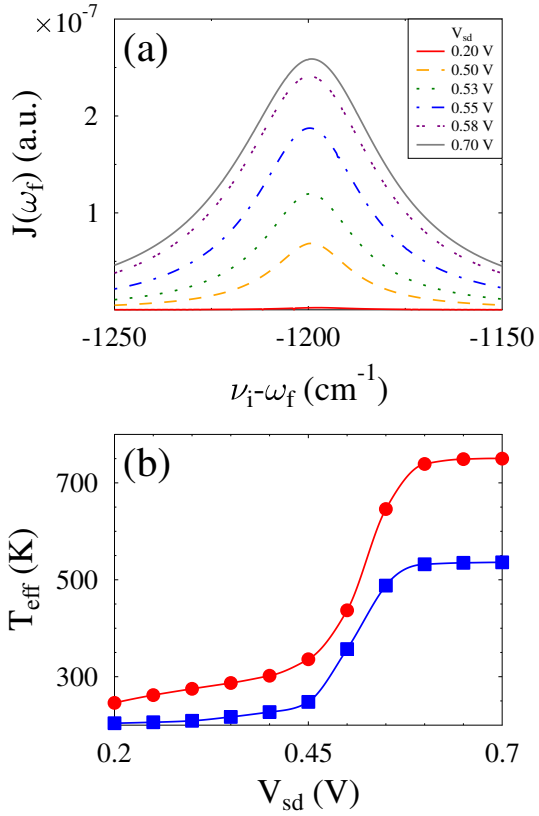

Figure 7.3: Bias induced vibrational heating. Shown are (a) the anti-Stokes peak, Eq.(7.8), of molecular vibration at 1199 cm^{-1} versus Raman shift for several source-drain biases, V_{sd}; (b) Effective temperature versus applied bias for molecular vibrational modes at 1608 cm^{-1} (squares, blue) and 1199 cm^{-1} (circles, red). See text for parameters used for simulations.

Dependence of the anti-Stokes peak on bias is shown in Figure 7.3a. In addition to the shift of the peak position, as discussed above, heating of the vibration by electric flux

results in an increase of the anti-Stokes peak amplitude at higher bias, as is observed in the experiment.[19] It is interesting to note that the shift in the anti-Stokes line is smaller than that of the Stokes peak. While in general there are a number of reasons for such shifts (for example, Stark effect or shift of the line induced by the molecule-contacts hybridization), here we argue that the main contribution comes from renormalization of molecular vibration under oxidation. Thus the shift under bias is defined by relative contributions from neutral molecule and cation to the total Raman signal. In a simplified way these contributions to Stokes and anti-Stokes lines are proportional to populations of the ground and excited states of the to species, respectively. Bias induced transfer of electronic population probability from vibronic states of neutral molecule to those of the cation is proportional to corresponding Franck-Condon factors. The latter are stronger for the ground state (see Supporting Information), which results in more pronounced shift in the Stokes line. We note that different shift of the Stokes and anti-Stokes lines with bias is consistent with the experimental data (see Figure 3b in ref.[19]).

While the temperature of nonequilibrium system is not defined, notion of "effective temperature" is often utilized in experiments to characterize extent of bias induced heating in the molecule.[17–19] In particular, effective vibrational temperature, describing the extent of vibrational excitation by electron flux, may be estimated from spectroscopic data utilizing ratio of anti-Stokes to Stokes peaks as

$$J(\nu_i + \omega_v)/J(\nu_i - \omega_v) \approx e^{-\hbar\omega_v/k_B T_{eff}} \tag{7.9}$$

(here ω_v is frequency of the normal mode of the neutral molecule). Figure 7.3b displays result of this estimate. Note that the calculated effective temperature is in agreement with the experimental data (compare with Figure 3a in ref.[19]).

7.4 Conclusion

In conclusion, we presented a pseudoparticle formulation for Raman spectroscopy in molecular junctions. This framework allows us to describe open nonequilibrium molecular system in the language of many-body states of the isolated molecule. The method treats all intramolecular interactions exactly, while also keeping the information on hy-

bridization between molecular states and those of the contacts, and on the nonequilibrium electronic population in the molecule. We further applied this methodology to simulate the Raman response of the OPV3 molecular junction under bias, where high quality experimental data recently became available. Parameters of the electronic and vibrational structure of the molecule were obtained from DFT and TDDFT quantum-chemical calculations and from experimental data. Our modeling results demonstrate a shift to lower frequencies and broadening of the Stokes line, reproducing the experimental trends. We argue that such a shift may be caused by the cation contribution to Raman scattering, and that in principle also a shift of the line to higher frequencies may be observable. Our estimate of vibrational heating caused by electric current is also in agreement with experimental data. Thus presented PP-NEGF methodology provides a convenient way to incorporate electronic information obtained for an isolated molecule in equilibrium with convectional quantum-chemical tools to simulate nonequilibrium dynamics of current carrying junctions. We believe that the developed method constitutes an important step towards full *ab initio* calculations of optical response in molecular junctions.

Supporting Information

Derivation of Eq. (7.6) and computational details (OPV3 chemical and electronic structure, and information on normal modes) are provided in the Supporting Information. This material is available free of charge via the Internet at http://pubs.acs.org.

Acknowledgements

We gratefully acknowledge support by the Department of Energy (M.G., Early Career Award, DE-SC0006422) and the Center for Integrated Nanotechnologies (CINT) at Los Alamos National Laboratory (LANL). LANL is operated by Los Alamos National Security, LLC, for the National Nuclear Security Administration of the U.S. Department of Energy under contract DE-AC5206NA25396. Chapter 7, in full, is a reprint of the material as it appears in Nano Letters, 2014. White, Alexander J.; Tretiak, Sergei; Galperin, Michael, American Chemical Society 2014. The dissertation author was the primary investigator and author of the paper.

7.5 Supporting Information

7.5.1 Derivation of the PP-NEGF expression for Raman flux

In the derivation of the expression we follow ref.[30] by separating the modes of the radiation field into initial (or pumping) and final (or absorbing) with the former being populated, while the latter empty. We note in passing that this is also the way expression for Raman spectroscopy is derived in the equilibrium molecular spectroscopy.[68] In reality both are the modes of the same radiation bath with the initial modes being those populated, while the final are the empty ones.

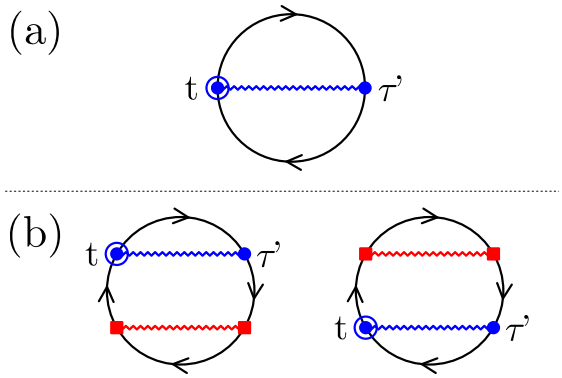

Figure 7.4: Flux diagrams. Shown are (a) general flux diagram and (b) possible flux diagrams in the fourth order perturbation theory in coupling to the radiation bath within the non-crossing approximation. Directed solid line (black) represents dressed pseudoparticle Green function, Eq.(6) of the paper. Non-directed zigzag lines stand for the self-energy due to coupling to radiation bath, Eq.(8) of the paper. Both directions have to be considered for the non-directed zigzag lines. We distinguish interactions with filled initial (red line, squares) and empty final (blue line, circles) modes of the field.

The starting point is writing an expression for the photon flux coming from the system into the empty final modes. The expression is written first by considering the total flux between system and radiation bath, and then keeping only the out-scattering (system to bath) part of it, i.e. the part given by the greater projection of the corresponding self-energy. The diagram responsible for the total flux between system and radiation bath is shown in Figure 7.4a (see ref.[56] for details).

Next we consider second order in coupling to the initial (filled) modes of the radiation field. Within the non-crossing approximation[56] the only two possible diagrams

are shown in Figure 7.4b. Note that only self-energies due to coupling to the radiation bath (wavy lines) are shown in the diagrams explicitly. In reality interactions with contacts and thermal bath also results in corresponding self-energies. The latter are not shown explicitly, and pseudoparticle Green functions (directed solid lines) are assumed to be dressed in these interactions. As usual, summation over all indices and integration over contour variables is assumes for every connection (circle or square) in the diagrams except the circled connection, where an assigned time t corresponds to the time at which the outgoing flux is calculated.

Finally, we are interested in the 'normal Raman' flux, that is the Raman scattering process which starts in a ground molecular state and proceeds via set of excited states. This is the main contribution to the Raman process in molecular junctions at low bias, when excited states cannot be populated by electron transfer from contacts. The contour projection relevant for the process is given in Figure8a of ref.[30] Also as discussed in ref.[54] when taking the projection we have to keep only contributions with single lesser pseudoparticle Green function. This guarantees that the resulting expression is bound to the physical subspace of the extended Hilbert space of the PP-NEGF. Projecting diagrams of Figure 7.4b within physical subspace, and keeping only greater projection for the self-energy due to coupling to final modes (blue line, circle) and lesser projection for the self-energy due to coupling to initial modes (red line, square) leads to Eq.(7) of the paper.

7.5.2 Computational details

Here we provide information on electronic structure calculations of the OPV3 molecule. Figure 7.5 shows atoms displacements related to the two normal modes, which were used in the Raman spectra analysis, and for which experimental data is available. Information on Raman active vibrational modes is provided in Table 7.1. Franck-Condon integrals between the states included in the calculations are listed in Table 7.2.

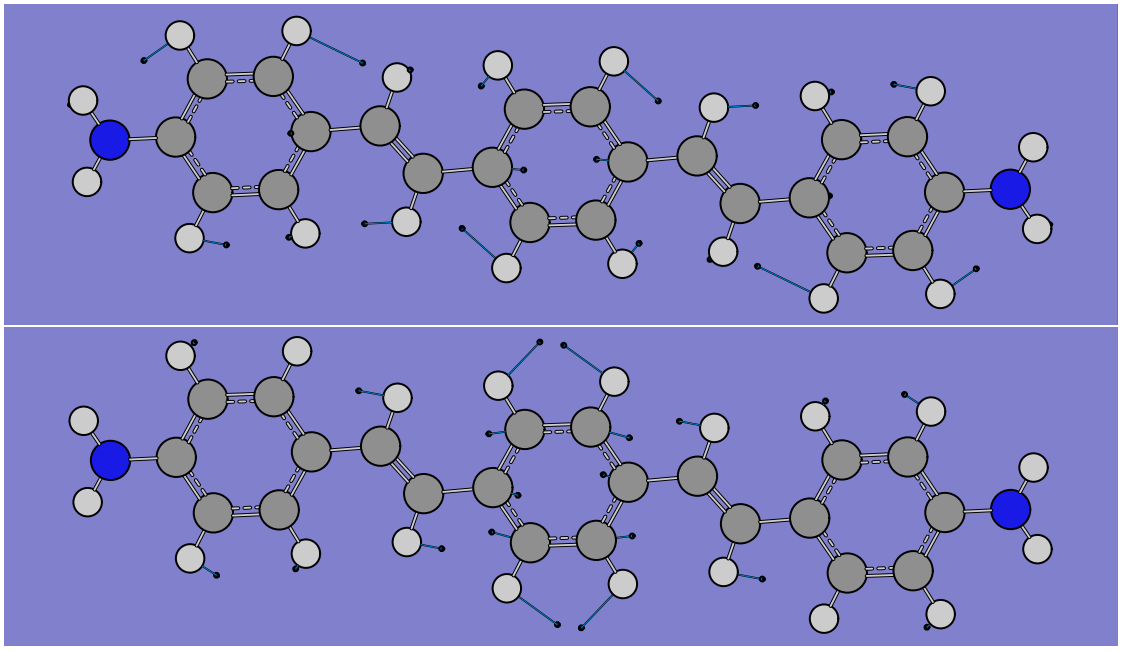

Figure 7.5: The normal modes of neutral OPV3 molecule at frequencies 1199 cm^{-1} (top) and 1608 cm^{-1} (bottom). Created by GaussView 5.

Table 7.1: Energies of the Raman active vibrational modes (cm^{-1})

Mode #	Neutral Ground	Cation Ground	Neutral Excited ($E_{ex} = 2.9$ eV) ($\mu_x = 5.2$ a.u.)	Cation Excited ($E_{ex} = 1.1$ eV) ($\mu_x = 4.6$ a.u.)
8	136	138	136	138
70	1174	1184	1171	1175
72	1199	1211	1214	1191
82	1316	1350	1326	1334
88	1398	1396	1390	1391
100	1609	1577	1573	1552
101	1630	1592	1609	1557
102	1637	1638	1622	1624
104	1673	1645	1634	1637

Table 7.2: Franck Condon Integrals of included states (cm^{-1})

Initial State	Final State	Franck-Condon Integral
Cation Ground	Neutral Ground	-
0	0	0.3087
0	$n_{72} = 1$	-0.1072
0	$n_{72} = 2$	0.0248
0	$n_{100} = 1$	-0.1320
0	$n_{100} = 2$	0.0416
$n_{72} = 1$	0	0.1157
$n_{72} = 1$	$n_{72} = 1$	0.2537
$n_{72} = 1$	$n_{72} = 2$	-0.1351
$n_{72} = 2$	0	0.0315
$n_{72} = 2$	$n_{72} = 1$	0.1449
$n_{72} = 2$	$n_{72} = 2$	0.2059
$n_{100} = 1$	0	0.1181
$n_{100} = 1$	$n_{100} = 1$	0.2216
$n_{100} = 1$	$n_{100} = 2$	-0.1486
$n_{100} = 2$	0	0.0298
$n_{100} = 2$	$n_{100} = 1$	0.1345
$n_{100} = 2$	$n_{100} = 2$	0.1548
Cation Ground	Cation Excited	-
0	0	0.9577
0	$n_{70} = 1$	0.0294
0	$n_{72} = 1$	0.0337
$n_{72} = 1$	0	-0.0312
$n_{72} = 1$	$n_{70} = 1$	0.4691
$n_{72} = 1$	$n_{72} = 1$	0.8024
$n_{72} = 2$	0	0.0062
$n_{72} = 2$	$n_{70} = 1$	-0.0214
$n_{72} = 2$	$n_{72} = 1$	-0.0368
$n_{100} = 1$	0	-0.0358
$n_{100} = 2$	0	-0.01073
Neutral Ground	Neutral Excited	-
0	0	0.4471
0	$n_8 = 1$	-0.3230
0	$n_{82} = 1$	0.0960
0	$n_{88} = 1$	-0.1333
0	$n_{101} = 1$	0.2132
0	$n_{102} = 1$	0.1336

Table 7.2 Continued: Franck Condon Integrals of included states (cm^{-1})

Neutral Ground	Neutral Excited	-
0	$n_{104} = 1$	0.1111
0	$n_8 = 2$	0.1689
0	$n_8 = 1$, $n_{82} = 1$	-0.0738
0	$n_8 = 1$, $n_{102} = 1$	-0.1009
0	$n_8 = 1$, $n_{104} = 1$	-0.0831
0	$n_{82} = 1$, $n_{101} = 1$	0.0545
0	$n_{101} = 1$, $n_{102} = 1$	0.0673
$n_{72} = 1$	0	-0.1764
$n_{72} = 1$	$n_8 = 1$	0.1345
$n_{72} = 1$	$n_{82} = 1$	0.3690
$n_{72} = 1$	$n_8 = 2$	-0.0725
$n_{72} = 1$	$n_8 = 1$, $n_{82} = 1$	-0.2706
$n_{72} = 1$	$n_{82} = 1$, $n_{101} = 1$	0.1873
$n_{100} = 1$	0	-0.2155
$n_{100} = 1$	$n_8 = 1$	0.1633
$n_{100} = 1$	$n_{88} = 1$	0.0858
$n_{100} = 1$	$n_{101} = 1$	0.0552
$n_{100} = 1$	$n_{102} = 1$	0.2456
$n_{100} = 1$	$n_{104} = 1$	0.1855
$n_{100} = 1$	$n_8 = 2$	-0.8744
$n_{100} = 1$	$n_8 = 1$, $n_{102} = 1$	-0.1792
$n_{100} = 1$	$n_8 = 1$, $n_{104} = 1$	-0.1356
$n_{100} = 1$	$n_{101} = 1$, $n_{102} = 1$	0.1677
$n_{72} = 2$	0	0.0468
$n_{72} = 2$	$n_8 = 1$	-0.0370
$n_{72} = 2$	$n_{82} = 1$	-0.2225
$n_{72} = 2$	$n_8 = 2$	0.0206
$n_{72} = 2$	$n_8 = 1$, $n_{82} = 1$	0.1688
$n_{72} = 2$	$n_{82} = 1$, $n_{101} = 1$	-0.0510
$n_{100} = 2$	0	0.0745
$n_{100} = 2$	$n_8 = 1$	-0.0579
$n_{100} = 2$	$n_{88} = 1$	-0.0367
$n_{100} = 2$	$n_{101} = 1$	-0.0754
$n_{100} = 2$	$n_{102} = 1$	-0.1946
$n_{100} = 2$	$n_{104} = 1$	-0.1486
$n_{102} = 1$	$n_8 = 2$	0.0318
$n_{100} = 2$	$n_8 = 1$, $n_{102} = 1$	0.1465
$n_{100} = 2$	$n_8 = 1$, $n_{104} = 1$	0.1121
$n_{100} = 2$	$n_{101} = 1$, $n_{102} = 1$	0.0329

Chapter 7 References

[1] Aviram, A. and Ratner, M.A. Chem. Phys. Lett. **29**, 277 (1974)

[2] Fleischmann, M.; Hendra, P. and McQuillan, A. Chem. Phys. Lett. **26**, 163 (1974)

[3] Jeanmaire, D.L. and Van Duyne, R.P. J. Electroanal. Chem. **84**, 1 (1977)

[4] Nie, S. and Emory, S.R. Science **275**, 1102 (1997)

[5] Kneipp, K.; Wang, Y.; Kneipp, H.; Perelman, L.T.; Itzkan, I.; Dasari, R.R. and Feld, M.S. Phys. Rev. Lett. **78**, 1667 (1997)

[6] Qian, X.M. and Nie, S.M. Chem. Soc. Rev. **37**, 912 (2008)

[7] Wustholz, K.L.; Brosseau, C.L.; Casadio, F. and Van Duyne, R.P. Phys. Chem. Chem. Phys. **11**, 7350 (2009)

[8] Sharma, B.; Frontiera, R.R.; Henry, A.I.; Ringe, E. and Duyne, R.P.V. Materials Today **15**, 16 (2012)

[9] Moskovits, M. Phys. Chem. Chem. Phys. **15**, 5301 (2013)

[10] Kleinman, S.L.; Frontiera, R.R.; Henry, A.I.; Dieringer, J.A. and Van Duyne, R.P. Phys. Chem. Chem. Phys. **15**, 21 (2013)

[11] Michaels, A.M.; Jiang, J. and Brus, L. J. Phys. Chem. B **104**, 11965 (2000)

[12] Ward, D.R.; Grady, N.K.; Levin, C.S.; Halas, N.J.; Wu, Y.; Nordlander, P. and Natelson, D. Nano Lett. **7**, 1396 (2007)

[13] Banik, M.; Nag, A.; El-Khoury, P.Z.; Rodriguez Perez, A.; Guarrotxena, N.; Bazan, G.C. and Apkarian, V.A. J. Phys. Chem. C **116**, 10415 (2012)

[14] Shamai, T. and Selzer, Y. Chem. Soc. Rev. **40**, 2293 (2011)

[15] Galperin, M. and Nitzan, A. Phys. Chem. Chem. Phys. **14**, 9421 (2012)

[16] Natelson, D.; Li, Y. and Herzog, J.B. Phys. Chem. Chem. Phys. **15**, 5262 (2013)

[17] Ioffe, Z.; Shamai, T.; Ophir, A.; Noy, G.; Yutsis, I.; Kfir, K.; Cheshnovsky, O. and Selzer, Y. Nature Nanotech. **3**, 727 (2008)

[18] Ward, D.R.; Halas, N.J.; Ciszek, J.W.; Tour, J.M.; Wu, Y.; Nordlander, P. and Natelson, D. Nano Lett. **8**, 919 (2008)

[19] Ward, D.R.; Corley, D.A.; Tour, J.M. and Natelson, D. Nature Nanotech. **6**, 33 (2011)

[20] Liu, Z.; Ding, S.Y.; Chen, Z.B.; Wang, X.; Tian, J.H.; Anema, J.R.; Zhou, X.S.; Wu, D.Y.; Mao, B.W.; Xu, X.; Ren, B. and Tian, Z.Q. Nat. Commun. **2**, 305 (2011)

[21] Jiang, N.; Foley, E.T.; Klingsporn, J.M.; Sonntag, M.D.; Valley, N.A.; Dieringer, J.A.; Seideman, T.; Schatz, G.C.; Hersam, M.C. and Van Duyne, R.P. Nano Lett. **12**, 5061 (2012)

[22] El-Khoury, P.Z.; Hu, D.; Apkarian, V.A. and Hess, W.P. Nano Lett. **13**, 1858 (2013)

[23] Matsuhita, R.; Horikawa, M.; Naitoh, Y.; Nakamura, H. and Kiguchi, M. J. Phys. Chem. C **117**, 1791 (2013)

[24] Banik, M.; El-Khoury, P.Z.; Nag, A.; Rodriguez-Perez, A.; Guarrottxena, N.; Bazan, G.C. and Apkarian, V.A. ACS Nano **6**, 10343 (2012)

[25] Zhang, R.; Zhang, Y.; Dong, Z.C.; Jiang, S.; Zhang, C.; Chen, L.G.; Zhang, L.; Liao, Y.; Aizpurua, J.; Luo, Y.; Yang, J.L. and Hou, J.G. Nature **498**, 82 (2013)

[26] Banik, M.; Apkarian, V.A.; Park, T.H. and Galperin, M. J. Phys. Chem. Lett. **4**, 88 (2013)

[27] Konishi, T.; Kiguchi, M.; Takase, M.; Nagasawa, F.; Nabika, H.; Ikeda, K.; Uosaki, K.; Ueno, K.; Misawa, H. and Murakoshi, K. J. Am. Chem. Soc. **135**, 1009 (2013)

[28] Chen, H.; Schatz, G.C. and Ratner, M.A. Rep. Prog. Phys. **75**, 096402 (2012)

[29] Galperin, M.; Ratner, M.A. and Nitzan, A. Nano Lett. **9**, 758 (2009)

[30] Galperin, M.; Ratner, M.A. and Nitzan, A. J. Chem. Phys. **130**, 144109 (2009)

[31] Galperin, M. and Nitzan, A. J. Phys. Chem. Lett. **2**, 2110 (2011)

[32] Galperin, M. and Nitzan, A. Phys. Rev. B **84**, 195325 (2011)

[33] Oren, M.; Galperin, M. and Nitzan, A. Phys. Rev. B **85**, 115435 (2012)

[34] Park, T.H. and Galperin, M. Europhys. Lett. **95**, 27001 (2011)

[35] Park, T.H. and Galperin, M. Phys. Rev. B **84**, 075447 (2011)

[36] Park, T.H. and Galperin, M. Phys. Scr. T **151**, 014038 (2012)

[37] White, A.J.; Fainberg, B.D. and Galperin, M. J. Phys. Chem. Lett. **3**, 2738 (2012)

[38] Jensen, L.; Aikens, C.M. and Schatz, G.C. Chem. Soc. Rev. **37**, 1061 (2008)

[39] Dieringer, J.A.; Wustholz, K.L.; Masiello, D.J.; Camden, J.P.; Kleinman, S.L.; Schatz, G.C. and Van Duyne, R.P. J. Am. Chem. Soc. **131**, 849 (2009)

[40] Morton, S.M. and Jensen, L. J. Am. Chem. Soc. **131**, 4090 (2009)

[41] Chen, H.; McMahon, J.M.; Ratner, M.A. and Schatz, G.C. J. Phys. Chem. C **114**, 14384 (2010)

[42] Zhao, L.B.; Huang, R.; Huang, Y.F.; Wu, D.Y.; Ren, B. and Tian, Z.Q. J. Chem. Phys. **135**, 134707 (2011)

[43] Payton, J.L.; Morton, S.M.; Moore, J.E. and Jensen, L. J. Chem. Phys. **136**, 214103 (2012)

[44] Mullin, J. and Schatz, G.C. J. Phys. Chem. A **116**, 1931 (2012)

[45] Zhao, L.L.; Jensen, L. and Schatz, G.C. Nano Lett. **6**, 1229 (2006)

[46] Spectrochim. Acta A Mol. Biomol. Spectrosc. **75**, 794 (2010)

[47] Mirjani, F.; Thijssen, J.M. and Ratner, M.A. J. Phys. Chem. C **116**, 23120 (2012)

[48] Leijnse, M. and Wegewijs, M. Phys. Rev. B **78**, 235424 (2008)

[49] Schultz, M. and von Oppen, F. Phys. Rev. B **80**, 033302 (2009)

[50] Esposito, M. and Galperin, M. Phys. Rev. B **79**, 205303 (2009)

[51] Esposito, M. and Galperin, M. J. Phys. Chem. C **114**, 20362 (2010)

[52] Ruhoff, P.T. Chem. Phys. **186**, 355 (1994)

[53] Ruhoff, P.T. and Ratner, M.A. Int. J. Quant. Chem. **77**, 383 (2000)

[54] Eckstein, M. and Werner, P. Phys. Rev. B **82**, 115115 (2010)

[55] Oh, J.H.; Ahn, D. and Bubanja, V. Phys. Rev. B **83**, 205302 (2011)

[56] White, A.J. and Galperin, M. Phys. Chem. Chem. Phys. **14**, 13809 (2012)

[57] Marbach, J.; Bronold, F.X. and Fehske, H. Phys. Rev. B **86**, 115417 (2012)

[58] Crljen, Ž.; Grigoriev, A.; Wendin, G. and Stokbro, K. Phys. Rev. B **71**, 165316 (2005)

[59] Stokbro, K. J. Phys.: Condens. Matter **20**, 064216 (2008)

[60] Bilić, A.; Crljen, Ž.; Gumhalter, B.; Gale, J.D.; Rungger, I. and Sanvito, S. Phys. Rev. B **81**, 155101 (2010)

[61] Hybertsen, M.S.; Venkataraman, L.; Klare, J.E.; Whalley, A.C.; Steigerwald, M.L. and Nuckolls, C. Journal of Physics: Condensed Matter **20**, 374115 (2008)

[62] Das, B. AIP Conference Proceedings **1349**, 951 (2011)

[63] Poot, M.; Osorio, E.; O'Neill, K.; Thijssen, J.M.; Vanmaekelbergh, D.; Walree, C.A.v.; Jenneskens, L.W. and van der Zant, H.S.J. Nano Lett. **6**, 1031 (2006)

[64] Parr, R.G. and Yang, W. *Density-Functional Theory of Atoms and Molecules* (Oxford University Press, 1989) (1989)

[65] Ullrich, C.A. *Time-Dependent Density-Functional Theory* (Oxford University Press, 2012) (2012)

[66] Frisch, M.J.; Trucks, G.W.; Schlegel, H.B.; Scuseria, G.E.; Robb, M.A.; Cheeseman, J.R.; Scalmani, G.; Barone, V.; Mennucci, B.; Petersson, G.A.; Nakatsuji, H.; Caricato, M.; Li, X.; Hratchian, H.P.; Izmaylov, A.F.; Bloino, J.; Zheng, G.; Sonnenberg, J.L.; Hada, M.; Ehara, M.; Toyota, K.; Fukuda, R.; Hasegawa, J.; Ishida, M.; Nakajima, T.; Honda, Y.; Kitao, O.; Nakai, H.; Vreven, T.; Montgomery, Jr., J.A.; Peralta, J.E.; Ogliaro, F.; Bearpark, M.; Heyd, J.J.; Brothers, E.; Kudin, K.N.; Staroverov, V.N.; Kobayashi, R.; Normand, J.; Raghavachari, K.; Rendell, A.; Burant, J.C.; Iyengar, S.S.; Tomasi, J.; Cossi, M.; Rega, N.; Millam, J.M.; Klene, M.; Knox, J.E.; Cross, J.B.; Bakken, V.; Adamo, C.; Jaramillo, J.; Gomperts, R.; Stratmann, R.E.; Yazyev, O.; Austin, A.J.; Cammi, R.; Pomelli, C.; Ochterski, J.W.; Martin, R.L.; Morokuma, K.; Zakrzewski, V.G.; Voth, G.A.; Salvador, P.; Dannenberg, J.J.; Dapprich, S.; Daniels, A.D.; Farkas, Ö.; Foresman, J.B.; Ortiz, J.V.; Cioslowski, J. and Fox, D.J. *Gaussian 09 Revision D.01.* Gaussian Inc. Wallingford CT 2009

[67] Kaasbjerg, K.; Novotný, T. and Nitzan, A. Phys. Rev. B **88**, 201405 (2013)

[68] Mukamel, S. *Principles of Nonlinear Optical Spectroscopy* (Oxford University Press, 1995) (1995)

Chapter 8

Conclusion

We introduced the pseudoparticle NEGF approach for calculating inelastic transport in molecular junctions. The PP-NEGF method is especially convenient when there is strong or nonlinear electron-vibration coupling. Our approach is a generalization of the exact-mapping technique bu Bonča and Trugman, when many-body character of the electronic system in the junction is fully taken into account. We demonstrate the ability of the method to go beyond the Born-Oppenheimer approximation regime. In particular, within simple models we study the interaction of a molecular vibration and conducing electron when the frequency of the vibration approaches intra-molecular Rabi frequency.

We compared approximate semi-classical, kinetic schemes with full quantum calculations for the dynamics of a model molecular redox junction. The redox junction consists of two conducting channels with vastly different coupling to electron reservoirs, one channel representing the redox site of the molecule, while the other models a current carrying channel. The two channels are coupled capacitively by Coulomb repulsion. We show that taking into account relative values of the intra-molecular and bath characteristic timescales, different semi-classical formulations are possible. These formulations work very well within their timescale regimesm and away from resonance. Absence of clear timescale separation at resonant tunneling (where electronic correlations are important) necessitates a fully quantum description of the model.

We study the role of coherence in correlated electronic energy and electron transfer of molecular junction systems. Correlation between electron and energy transfer is seen in a model bridge system with two interfering paths. The bridge is designed to max-

imize energy transfer due to constructive interference while minimizing electron transfer due to destructive interference. Introducing decoherence into the system initially increases current while decreasing energy transport. Surprizingly, further increase of decoherence rate to the order of the electronic hopping parameter results in an increase in energy transport. This effect may be due to competition between energy and charge transport on the same electronic population in the LUMO of the bridge molecule, where an increased localization of the charge in the LUMO increases the efficiency of incoherent energy transfer. We also discuss the possibility of charge-energy transport separation in a molecular switch, showing that by tuning the pumping laser field parameters the fluxes can be directed towards spatially separated terminals. This observation may be relevant to constructing low-heating molecular devices, which would require a technically similar consideration of propagation of vibrational excitation in junctions.

In the remaining chapters we focused on the continuing goal of calculating the optical response of molecular junctions. We use the method described in Sec 1.3 and consider a simple model of a molecular junction driven by an external chirped electromagnetic pulse. Using the finite difference time domain technique we calculate the local field of the junction resulting from surface plasmon-polaritons excitations of the contacts. We also take into account the molecular contribution to the local field. In particular, we show that for laser field frequencies shorter (longer) than the molecular excitation energy the local surface plasmon-polariton field is quenched (enhanced) by the molecular response. This results in significant changes to the transport properties of the junction, demonstrating that the molecular contribution to the formation of the local field is crucial for proper description.

The plasmon-enhanced electric field was considered to be completely classical, while the model molecule was treated quantum mechanically.We consider the case when the interaction between the surface plasmon-polaritons and the molecular excitations is strong and must be considered entirely quantum mechanically. We introduce system states of the molecule, dressed with the plasmonic excitations, whose interaction can be treated exactly within the PP-NEGF methodology. Within toy models of a single molecular excitation, or two interacting molecular excitations, interacting with two plasmonic nanoparticles we demonstrate the effect of electronic conduction on the plasmonic ab-

sorption spectrum. In particular we consider non-linear effects and suggest the possibility of direct measurement of intramolecular energy transfer rates in molecular dimers.

We apply the PP-NEGF method to nonequilibrium Raman scattering in molecular junctions. We demonstrate that the PP-NEGF approach is suitable for incorporating quantum chemistry calculations into the nonequilibrium Raman scattering calculations. We calculate the Raman spectrum for the OPV3 molecule as a function of bias and compare the results to experimental data. We argue that observed and calculated shift in Stokes peak is due to contribution of the cation OPV3 species to the Raman spectrum under bias. Additionally our estimate of current induced vibrational heating is also in agreement with the experimental results. This is an important first step towards full *ab initio* calculations of optical response in molecular junctions.

In the future atomistic, *ab initio*, calculations of the entire process of the optical response of the nonequilibrium electronic dynamics in molecular junctions may be required. This would involve combining the methods shown in chapters 5-7, or similar methods, *i.e.* the FDTD process to propagate surface plasmon-polariton excitations, with quantum description of the plasmon-molecular excitation interaction and optical scattering process. This would require development of a method for combining quantum mechanical fluxes with classical electrodynamics, i.e. an electric field, and partitioning of the problem into quantum and classical partitions. Additionally, generalization of the expression of the Raman scattering consideration in chapter 7 may be necessary to understand the role of coherent electron transfer-Raman scattering processes. Future *ab initio* calculations for Raman scattering in molecular junction should be improved to include metal atoms of the contacts, electric field due to bias, and more accurate electronic structure methods.